Biophysical characterisation of the mechanisms regulating sarcoplasmic reticulum K^+ channel gating

Fiona O'Brien

A dissertation submitted to the University of Oxford for award

of the degree of Doctor of Philosophy



Hertford College, Oxford

November 2015

Word count: 47,215

Abstract

Intracellular Ca^{2+}-release from the sarcoplasmic reticulum (SR) occurs through highly specialised Ca^{2+}-release channels called ryanodine receptors (RyR) in a process known as excitation-contraction coupling (EC-coupling) in striated muscle.

The RyR is the main ion-channel mediating Ca^{2+}-release from the SR but the SR also contains many other ion-channels and proteins, with many of unknown physiological role. For example, two SR K^+ channels, TRIC-A and TRIC-B, have recently been identified and are thought to play a key role in supporting intracellular Ca^{2+} movements across the SR. The TRIC double knockout (DKO) mouse dies in embryonic heart failure and the TRIC-B knockout (KO) dies in respiratory failure immediately after birth, highlighting their important roles in different tissue types. The TRIC-A KO mouse survives until adulthood, however, there are SR structural abnormalities and compromised Ca^{2+} release.

I have focused on characterising and comparing the single-channel properties of the native SR K^+ channels from WT and TRIC-A KO mouse skeletal muscle. I have investigated if the SR K^+ channels can gate in a cooperative manner when multiple SR K^+ channels are present in the bilayer. Since TRIC and RyR channels are both located in high abundance in the junctional SR regions, I have examined whether the SR K^+ and RyR channels also gate in a cooperative manner when both are present in a bilayer. In addition to voltage-regulation of native SR K^+ channels, I have characterised the pH sensitivity of the SR K^+ channels from WT and TRIC-A KO tissue. Finally, I investigated if the mouse isoform of TRIC-A could be purified using the Wheat germ cell-free system and incorporated into bilayers without loss of function.

In summary, this thesis describes novel mechanisms of regulation of ion-channels that are involved in the process of Ca^{2+}-release from the SR. By focusing on the biophysical properties of SR K^+ channels, I have highlighted the complexity of the ionic fluxes that are thought to be required to maintain normal EC-coupling in striated muscle.

Acknowledgements

I would like to express my sincerest gratitude to my supervisor, Professor Rebecca Sitsapesan for giving me the opportunity to work on such an interesting project and for her valuable guidance, encouragement and enthusiasm throughout my entire PhD. Thank you to everybody in the Sitsapesan Lab, both present and past members, for the ongoing support and encouragement, and for the laughter and fun times, you made me smile every day.

I would also like to thank the laboratory of Professor Hiroshi Takeshima and Dr Miyuki Nishi in Japan. Thank you for providing the recombinant TRIC proteins and the TRIC-KO mice.

Thank you to my group of Cork girls, especially Ailish and Val. I would be lost without your support. Thanks girls for the many visits to Bristol and Oxford, the craic was always up to 90. A big thank you to Eoghan and Shane, for making it so easy for me to settle in the UK. You two are beyond amazing.

A special thank you to Seamus for his constant love and support, especially throughout my PhD. I will always be grateful to you for moving to the UK and for looking after me during the crazy write up period! I love you to pieces and I am looking forward to returning to 'normal' girlfriend duties.

I am forever indebted to my parents Anne and Richard, for their unwavering support and unconditional love. Thank you for always being such a strong influence in my life and for giving me every opportunity possible. I am eternally grateful for everything you both have done for me.

Thank you to my sister Kelly and my brothers Shane and Eoin for always being there for me. A special thank you to Kelly for the countless visits and chats on the phone. I am so lucky to have you as my best friend.

This thesis is dedicated to my late grandfather, Gerard O'Sullivan, I miss you always. I know this would have meant the world to you and you would have enjoyed reading it.

Go raibh mile maith agat

This work was supported by the British Heart Foundation.

Author declaration

I declare that the work in this dissertation was carried out in accordance with the requirements of the University's Regulations and Code of Practice for Research Degree Programmes and that it has not been submitted for any other academic award. Except where indicated by specific reference in the text, the work is the candidate's own work. Work done in collaboration with, or with the assistance of, others, is indicated as such. Any views expressed in the dissertation are those of the author

SIGNED……..... DATE…….....

Table of Contents

1 Introduction 1

1.1 Excitation-contraction coupling in striated muscle 1

1.1.1 RyR-mediated Ca^{2+}-release in cardiac muscle 2

1.1.2 RyR-mediated Ca^{2+}-release in skeletal muscle 2

1.1.3 Ca^{2+} reuptake in cardiac and skeletal muscle 3

1.1.4 Ultrastructural aspects at the junction of t-tubules and SR membranes 5

1.2 The Ryanodine Receptor 7

1.2.1 The permeation properties of the RyR 7

1.3 The skeletal SR K^+ channel 8

1.3.1 The cardiac SR K^+ channel 11

1.4 TRIC proteins 12

1.4.1 Proposed structure of TRIC-proteins 12

1.4.2 TRIC-proteins behave as functional K^+ channels 13

1.5 Cl^- channels in the cardiac and skeletal SR 15

1.5.1 Physiological significance of TRIC channels 16

1.5.1.1 TRIC channels and disease 17

1.6 Aims of this thesis 17

2 Methods 19

2.1 Isolation of SR membrane vesicles from skeletal muscle 19

2.1.1 Collection of mouse skeletal muscle tissue 19

2.1.2 Isolation of SR membrane vesicles 19

2.2 The planar lipid bilayer technique 20

2.2.1 The planar lipid bilayer workstation 21

2.2.1.1 The bilayer chambers 21

2.2.1.2 The electrical equipment 22

2.2.2 Grounding the workstation 23

2.2.3 Silver-silver chloride electrodes 23

2.3. Formation of stable bilayers suitable for electrophysiological recordings 24

2.3.1 Priming 24

2.3.2 Bilayer formation 24

2.4 The voltage-clamp technique and bilayer detection 26

2.4.1 The voltage-clamp technique....26
2.4.2 Bilayer measurement....27
2.5 Incorporation of SR vesicles....28
2.6 Analysis of single-channel recordings....29
2.6.1 Data Acquisition....29
2.6.2 Single-channel analysis....30
2.6.2.1 Current amplitude measurements....30
2.6.2.2 Idealisation and open probability....32
2.6.2.2.1 Pre-processing data....33
2.6.2.2.2 Idealisation....34
2.6.3 Life time analysis....40
2.6.4 Noise analysis....41
2.7 Measurement of free Ca^{2+}....42
2.8 Statistics....42
2.9 Chemical compounds....42
3 Comparison of the biophysical properties of the SR K^+ channels from TRIC-A KO and WT skeletal muscle....43
3.1 Introduction....44
3.2 Methods....46
3.2.1 Po-voltage relationships....46
3.3 Results....47
3.3.1 TRIC-A KO....47
3.3.2 Contribution of other lab members to the data in this chapter....48
3.3.3 The gating characteristics of SR K^+ channels from TRIC-A KO tissue....48
3.3.3.1 The conductance of the SR K^+ channels from TRIC-A KO tissue....50
3.3.3.2 The gating of the 'typical' SR K^+ channels from TRIC-A KO tissue....50
3.3.3.3 The voltage-dependence of the typical SR K^+ channels....52
3.3.3.4 Exploring the voltage-dependency of typical SR K^+ channels from TRIC-A KO tissue....54
3.3.3.5 Lifetime analysis of the SR K^+ channels from TRIC-A KO tissue....55
3.3.3.6 The effect of voltage on the mean open and closed times....56
3.3.3.7 Investigating the transition routes between the closed and fully open channel level in the 'typical SR K^+ channel from TRIC-A KO tissue....59

3.3.3.8 The 'non-typical' SR K^+ channels from TRIC-A KO tissue 60
3.3.3.8.1 The voltage-dependent SR K^+ channels that gate predominately in sub-conductance states 60
3.3.3.8.2 The voltage-independent SR K^+ channels 63
3.3.4 The gating characteristics of SR K^+ channels from WT mouse skeletal muscle... 66
3.3.4.1 The conductance of the SR K^+ channels from WT tissue 68
3.3.4.2 The voltage-dependence of the SR K^+ channels from WT tissue 69
3.3.4.2.1 The 'typical' SR K^+ channels 69
3.3.4.2.2 The 'non-typical' SR K^+ channel 70
3.4 Comparison of data from WT and TRIC-A KO tissue 72
3.5 Discussion 74
3.5.1 SR K^+ channels from WT and TRIC-A KO display equally variable gating characteristics 74
3.5.2 Are there subtle differences in the TRIC-A KO and WT preparations? 75
3.5.3 TRIC channels and specialised structures in skeletal muscle that facilitate Ca^{2+} -release 78
3.5.4 The complexity of the SR K^+ channel gating 80
4 Do SR K^+ channels gate in a cooperative manner? 82
4.1 Introduction 83
4.2 Methods 85
4.2.1 Po analysis when multiple channels were in the bilayer 85
4.2.2 Binomial distribution analysis 87
4.3 Results 88
4.3.1 Contribution by other members of the lab to experiments described in this chapter. 88
4.3.2 TRIC-A KO tissue 88
4.3.2.1 The gating characteristics of the SR K^+ channel when there were two channels gating in the bilayer. 88
4.3.2.2 The gating characteristics of the SR K^+ channels when three channels from TRIC-A KO tissue were gating in the bilayer. 91
4.3.2.3 The gating characteristics of the SR K^+ channels when four channels were gating in the bilayer 94
4.3.3 The effect of decamethonium on the SR K^+ channel from TRIC-A KO 99
4.3.4 Do SR K^+ channels from TRIC-A KO gate in a cooperative manner? 101

4.3.5 Do we alter the Po-voltage relationship of the SR K^+ channel from TRIC-A KO when multiple channels are present? 105

4.3.6 WT tissue 109

4.3.6.1 The gating characteristics of the SR K^+ channel from WT tissue when there were two channels gating in the bilayer. 109

4.3.6.2 The gating characteristics of the SR K^+ channels when three or four channels were gating in the bilayer. 113

4.3.7 Is the cooperative nature of the SR K^+ channels altered in preps that contain TRIC-A K^+ channels? 115

4.3.8 SR K^+ channels deviate from the binomial distribution prediction 119

4.4 Summary and Discussion 123

4.4.1 The Po of the SR K^+ channels increases as the number of channels gating in the bilayer increases 123

4.4.2 Po-voltage relationships when more than one channel is in the bilayer 126

4.4.3 The gating of the SR K^+ channels deviates from the binomial statistical prediction 126

4.4.4 Decamethonium block of the SR K^+ channel 129

5 Does cooperativity between RyRs and SR K^+ channels exist? 132

5.1 Introduction 133

5.2 Methods 134

5.2.1 Incorporation of SR vesicles containing an SR K^+ channel and a RyR 134

5.2.2 Distinguishing the current-fluctuations due to RyR from those of an SR K^+ channel 134

5.2.3 Choosing an optimal filtering level to analyse the current fluctuations when both a RyR and an SR K^+ channel were gating in the bilayer 137

5.2.4 Idealisation of traces that contained a RyR and an SR K^+ channel 139

5.2.5 Separating the Po of the SR K channel from the Po of the RyR 140

5.3 Results 143

5.3.1 Are the biophysical properties of the SR K^+ channels altered when there is a RyR present in the bilayer? 143

5.3.2 Does the conformation of the SR K^+ channel (open or closed) affect the gating properties of RyR? 147

5.3.3 The gating of a RyR *without* an SR K^+ channel gating in the bilayer 148

5.4 Summary 150

5.4.1 SR K^+ channels retain their biophysical properties when a RyR is gating in the bilayer 150

5.4.2 RyR gating when an SR K^+ channel is also in the bilayer.....151

6 Investigating the pH sensitivity of the SR K^+ channel.....153

6.1 Introduction.....154

6.2 Methods.....155

6.2.1 Mean open and closed durations.....155

6.2.1.1 Measurement of full open burst length.....155

6.2.1.2 Measurement of interburst interval length.....157

6.3 Results.....159

6.3.1 Contribution by other members of the lab to experiments described in this chapter. 159

6.3.2 Composition of the buffers used in this chapter.....159

6.3.3 Effect of cytosolic pH 6.2 on SR K^+ channels from TRIC-A KO.....159

6.3.3.1 Effect of cytosolic pH 6.2 on SR K^+ channel gating.....159

6.3.3.2 Investigating the time-dependence of the effect of cytosolic pH 6.2 on SR K^+ channel function.....165

6.3.3.3 The effect of cytosolic pH 6.2 on the mean open time of the full open state..166

6.3.3.4 Effect of cytosolic pH 6.2 on mean open channel noise in the full open state 167

6.3.3.5 Effect of cytosolic pH on the frequency of openings to the full open channel level at +30 mV.....168

6.3.3.6 Effect of cytosolic pH 6.2 on SR K^+ channel conductance.....169

6.3.3.7 Investigating whether cytosolic pH 6.2 altered the properties of the merged sub-conductance level.....171

6.3.4 Effect of luminal pH 6.2 on SR K^+ channels from TRIC-A KO.....173

6.3.4.1 Effect of luminal pH 6.2 on SR K^+ channel gating.....173

6.3.4.2 Investigating the time-dependence of the effect of luminal pH 6.2 on SR K^+ channel function.....179

6.3.4.3 The effect of luminal pH 6.2 on mean open duration of the full open level ...180

6.3.4.4 Effect of luminal pH on the frequency of openings to the full open channel level 182

6.3.4.5 Effect of luminal pH 6.2 on SR K^+ conductance.....183

6.3.5 Effect of pH 6.2 on SR K^+ channels from WT tissue.....184

6.3.6 Effect of symmetrical pH 6.2 on SR K^+ channel gating.....186

6.3.6.1 Are their distinct sites on the cytosolic and luminal side of the SR K^+ channel that are sensitive to acidic pH?.....186

6.3.6.2 The gating properties of the SR K^+ channel in symmetrical pH 6.2.....193

6.3.6.3 The conductance of the SR K^+ channel in symmetrical pH 6.2 197
6.3.7 Effect of pH 9.2 on SR K^+ channel function 198
6.3.7.1 The effect of alkaline pH 9.2 on the stability of the artificial membrane..... 199
6.3.7.2 Effect of cytosolic pH 9.2 on SR K^+ channel gating 200
6.3.7.3 The effect of cytosolic pH on the mean open duration of the full open channel level..... 203
6.3.8 Effect of luminal pH 9.2 on SR K^+ channel function 204
6.3.8.1 Effect of luminal pH 9.2 on SR K^+ channel gating 204
6.3.8.2 Effect of cytosolic or luminal pH 9.2 on the SR K^+ channel conductance..... 207
6.3.9 Comparison of the gating of the SR K^+ channel in pH 6.2 and pH 9.2 207
6.4 Discussion..... 209
6.4.1 The SR K^+ channel has more than one proton binding site 209
6.4.2 Alkaline pH increases SR K^+ channel activity 212
6.4.3 Mechanisms underlying the effects of changing pH on SR K^+ channel gating..... 213
6.4.4 Future work..... 216

7 Investigating the single-channel properties of purified TRIC-A channels 218

7.1 Introduction..... 219
7.2 Methods 221
7.2.1 Preparation of liposomes for protein purification..... 221
7.2.2 Wheat Germ cell-free protein synthesis kit 221
7.2.3 Transcription of plasmid DNA 222
7.2.4 Translation 223
7.2.5 Purification of proteoliposomes..... 224
7.2.6 Solubilisation of native SR 225
7.3 Results 227
7.3.1 Purified TRIC-A single-channel currents 228
7.3.1.1 Single-channel currents from purified TRIC-A..... 228
7.3.2 Recording native SR K^+ channels in gradient conditions..... 234
7.3.3 The effect of detergent on SR K^+ channel function..... 237
7.3.3.1 The voltage-dependence of the solubilised LSR K^+ channels..... 240
7.4 Discussion..... 241

7.4.1 Purified TRIC-A single-channel current fluctuations.....241
7.4.1.1 Can TRIC-A gate like TRIC-B?.....242
7.4.2 The gating of native SR K^+ channels is altered in gradient conductions.....243
7.4.3 CHAPS detergent alters the gating of the native SR K^+ channel 244
7.5 Future work.....245
8 Conclusion 247
References 250

Table of figures

Chapter 1

Figure 1.1 Schematic representation of EC-coupling in striated muscle 4
Figure 1.2 Model of RyR-lattice array..... 6
Figure 1.3 A simplification of the gating states of the SR K^+ channel described by Labarca *et al* (1981) (85). 10
Figure 1.4 A simplification of the gating states of the SR K^+ channel described by 12
Figure 1.5 Amino acid sequence alignments for mouse, rabbit and human TRIC-A proteins and mouse and human TRIC-B proteins. 13

Chapter 2

Figure 2.1 Schematic illustration of 20-40 % sucrose density gradient. 20
Figure 2.2 A schematic illustrating the two distinct compartments formed by the block and cup apparatus. 21
Figure 2.3 A schematic representation of the connections between the electrical components used for single-channel recording. 23
Figure 2.4 Schematic illustrating the forces involved in bilayer formation 25
Figure 2.5 Incorporation of ion-channels into planar lipid bilayers. 29
Figure 2.6 Illustration of model topologies used to idealise SR K^+ channel Po 34
Figure 2.7 Comparison of the idealisation of the single-channel recordings using model M1 and M2. 35
Figure 2.8 Single-channel event detection using SKM analysis. 37
Figure 2.9 A representative all-points histogram of the recording shown in Figure 2.8. 38

Chapter 3

Figure 3.1. A representative trace illustrating the typical gating properties of the SR K^+ channels from TRIC-A KO. 49
Figure 3.2 Current-voltage relationship of the full open channel level of the SR K^+ channel from TRIC-A KO tissue 50
Figure 3.3 Sub-conductance gating patterns observed in SR K^+ channel from TRIC-A KO tissue at +30 mV 52
Figure 3.4. The 'typical' SR K^+ channels from TRIC-A KO tissue are voltage-dependent ... 53
Figure 3.5 The contribution of Po_{FULL} to overall Po of SR K^+ channels from TRIC-A KO tissue 53
Figure 3.6 The Po-voltage relationship of the SR K^+ channel from TRIC-A KO tissue. 55
Figure 3.7 Lifetime distributions and probability density functions from a typical SR K^+ channel from TRIC-A KO tissue 56
Figure 3.8 The mean open and closed times of the SR K^+ channel from TRIC-A KO tissue as a function of voltage 58
Figure 3.9 Transitions between the full open and closed channel 59
Figure 3.10 Typical openings from the voltage-dependent SR K^+ channels that gate predominately in sub-conductance levels 61
Figure 3.11 The voltage-dependence of the SR K^+ channels from TRIC-A KO tissue that gate predominately in sub-conductance open states 62

Figure 3.12 The contribution of Po_{FULL} to overall Po of the voltage-dependent SR K^+ channels that gate predominately in a sub-conductance level. 63
Figure 3.13 Representative gating behaviour of voltage-independent SR K^+ channels 64
Figure 3.14 The Po of the voltage-independent SR K^+ channels from TRIC-A KO tissue. ... 65
Figure 3.15 The contribution of Po_{FULL} to overall Po of the voltage-independent SR K^+ channels. 66
Figure 3.16 A representative trace illustrating the typical gating properties of the SR K^+ channels from WT skeletal muscle. 67
Figure 3.17 Current-voltage relationship of the full open channel level of the SR K^+ channel from WT 68
Figure 3.18 SR K^+ channels from WT tissue are voltage-dependent 69
Figure 3.19 Representative gating behaviour of the voltage-dependent SR K^+ channels from WT tissue that gate predominately in sub-conductance states 71
Figure 3.20 Comparison of the Po of the SR K+ channels from TRIC-A KO and WT tissue 73
Figure 3.21 % of experiments containing a single SR K^+ channel in the bilayer in TRIC-A KO and WT tissue 80

Chapter 4

Figure 4.1 Single-channel event detection using our simplified 2 state Markov Model 86
Figure 4.2 The gating of the SR K^+ channels from TRIC-A KO tissue when there were two channels in the bilayer. 89
Figure 4.3 The voltage-dependence of the SR K^+ channels from TRIC-A KO tissue when two channels were gating in the bilayer 90
Figure 4.4 The contribution of Po_{FULL} to Po_{TOTAL} when two SR K^+ channels from TRIC-A KO tissue were present in the bilayer. 91
Figure 4.5 The gating of the SR K^+ channels when there were three channels in the bilayer. 92
Figure 4.6 The voltage-dependence of the SR K^+ channels from TRIC-A KO when three channels were gating in the bilayer 93
Figure 4.7 The contribution of Po_{FULL} to Po_{TOTAL} when three SR K^+ channels were present in the bilayer. 94
Figure 4.8 The gating of the SR K^+ channels from TRIC-A KO when four channels were gating in the bilayer. 95
Figure 4.9 Effect of Decamethonium on SR K^+ channels 97
Figure 4.10 The voltage-dependence of the SR K^+ channels from TRIC-A KO when four channels were gating in the bilayer 98
Figure 4.11 The effect of decamethonium on the function of the SR K^+ channels from TRIC-A KO tissue 100
Figure 4.12 Effect of decamethonium on the mean open time of the SR K^+ channel 101
Figure 4.13 The relationship between SR K^+ channel Po and the number of channels in the bilayer at ±30 mV. 103
Figure 4.14 The relationship between Po_{FULL}/Po_{SUB} and the number of channels in the bilayer at ±30 mV. 104
Figure 4.15 The gating of multiple SR K^+ channels from TRIC-A KO at +20 mV and +50 mV 106
Figure 4.16 The Po of the SR K^+ channels at +20 mV and +50 mV. 107

Figure 4.17 Comparing the closed and the open channel noise at holding potentials of +20 mV and +50 mV. 108
Figure 4.18 The effect voltage on Po_{SUB} 109
Figure 4.19 The gating of the SR K^+ channels from WT when there were two channels gating in the bilayer. 110
Figure 4.20 The gating properties of the SR K^+ channels from WT when two channels were gating in the bilayer 113
Figure 4.21 The gating properties of the SR K^+ channels from WT when three channels were gating in the bilayer 115
Figure 4.22 The voltage-dependence of the SR K^+ channels when four channels were gating in the bilayer 115
Figure 4.23 SR K^+ channels from WT tissue also gate in a cooperative manner 117
Figure 4.24 Combining data from TRIC-A KO and WT tissue to determine SR K^+ channel cooperativity 119
Figure 4.25 The gating of multiple SR K^+ channels in the bilayer deviates from the binomial distribution prediction 121
Figure 4.26 The average Po of the SR K^+ channels increases in a non-linear manner as the number of channels in the bilayer increases. 125
Figure 4.27 The binomial distribution prediction for SR K^+ channels with a higher Po than our single-channel experiments 128

Chapter 5

Figure 5.1 The current fluctuations that are observed when both an SR K^+ channel and a RyR are gating in the bilayer. 136
Figure 5.2 The effect of filtering on the current-fluctuations observed when both SR K^+ channel and RyR channel current-fluctuations are observed simultaneously. 138
Figure 5.3 Comparison of the Po of the SR K^+ and RyR channels at filtering levels of 1 kHz and 4 kHz 141
Figure 5.4 SR K^+ channels are voltage-dependent when a RyR is also gating in the bilayer 143
Figure 5.5 SR K^+ channels retain their cooperative gating behaviour when there is also a RyR present in the bilayer. 144
Figure 5.6 Comparison of the gating of the SR K^+ channel when a RyR was present in the bilayer 147
Figure 5.7 The effect of SR K^+ channel gating on RyR function 148
Figure 5.8 Single-channel current fluctuations observed when only a RyR was gating in the bilayer. 149

Chapter 6

Figure 6.1 Single-channel mean open time measurements using SKM idealisation 156
Figure 6.2 Single-channel mean closed time measurements using SKM idealisation 158
Figure 6.3. The effect of cytosolic pH 6.2 on SR K^+ channel gating. 161
Figure 6.4 The effect of cytosolic pH 6.2 on SR K^+ channel Po at +30 mV. 162
Figure 6.5. The effect of cytosolic pH 6.2 on the contribution of Po_{FULL} to Po_{TOTAL} at + 30 mV. 163
Figure 6.6. The effect of cytosolic pH 6.2 on SR K^+ channel Po at -30 mV. 163

Figure 6.7 The effect of cytosolic pH 6.2 on the contribution of Po_{FULL} to the overall Po at - 30 mV. 164
Figure 6.8 Time course of cytosolic pH 6.2 inhibition of the SR K channel. 165
Figure 6.9 Effect of cytosolic pH 6.2 on the SR K^+ channel mean open time at +30 mV. ...166
Figure 6.10 Effect of cytosolic pH 6.2 on the mean open time of the full open state at -30 mV. 167
Figure 6.11 Effect of cytosolic pH 6.2 on the open channel noise of the full open state at +30 mV. 168
Figure 6.12 Effect of cytosolic pH 6.2 on the frequency of full open level bursts at -30 mV 169
Figure 6.13. Effect of cytosolic pH 6.2 on the conductance of the SR K^+ channel.....170
Figure 6.14 The effect of cytosolic pH 6.2 on the parameters of the merged sub-conductance level at +30 mV.....172
Figure 6.15 The effect of luminal pH 6.2 on SR K^+ channel gating. 175
Figure 6.16 . The effect of luminal pH 6.2 on SR K^+ channel Po at +30 mV. 176
Figure 6.17 The effect of luminal pH 6.2 on the contribution of Po_{FULL} to Po_{TOTAL} at + 30 mV. 177
Figure 6.18. The effects of luminal pH 6.2 on SR K^+ channel Po at -30 mV. 178
Figure 6.19. The effects of luminal pH 6.2 on the contribution of Po_{FULL} to Po_{TOTAL} at -30 mV. 179
Figure 6.20 Time course of luminal pH 6.2 inhibition of the SR K^+ channel. 180
Figure 6.21 Effect of luminal pH 6.2 on the mean open time of the full open channel level at +30 mV. 181
Figure 6.22 Effect of luminal pH 6.2 on the mean open time of the full open channel level at -30 mV. 181
Figure 6.23 Luminal pH 6.2 appeared to reduce frequency at -30 mV 183
Figure 6.24. Effect of luminal pH 6.2 on the unitary conductance of the SR K^+ channel....184
Figure 6.25 Effect of pH 6.2 on SR K^+ channel gating from WT tissue 185
Figure 6.26 The effect of pH 6.2 on the contribution Po_{FULL} to Po_{TOTAL} at + 30 mV. 186
Figure 6.27. Effect of subsequent perfusion of both chambers with pH 6.2 (Cytosolic side first) at +30 mV. 188
Figure 6.28. Effect of subsequent perfusion of both chambers with pH 6.2 (Luminal side first) at +30 mV. 190
Figure 6.29 Effect of subsequent perfusion of both chambers with pH 6.2 191
Figure 6.30 Effect of pH 6.2 on the mean open time of the full open channel level at +30 mV. 192
Figure 6.31. The effect of pH 6.2 on SR K^+ channel gating.....194
Figure 6.32. Effect of symmetrical pH 6.2 on SR K^+ channel Po at +30 mV. 195
Figure 6.33 The effects of symmetrical pH 6.2 on the contribution of the full open channel level at + 30 mV.....196
Figure 6.34 Effect of symmetrical pH 6.2 on SR K_+ channel Po at -30 mV. 196
Figure 6.35. Effect of symmetrical pH 6.2 on SR K^+ channel conductance. 197
Figure 6.36. A representative example of the 'unanalysable' current observed in pH 9.2....199
Figure 6.37. Effect of cytosolic pH 9.2 on SR K^+ channel gating.....201
Figure 6.38. The effects of cytosolic pH 9.2 on SR K^+ channel Po. 202

Figure 6.39 The effects of cytosolic pH 9.2 on the contribution of Po_{FULL} to Po_{TOTAL} + 30 mV. 203
Figure 6.40 Effect of cytosolic pH 9.2 on the mean open time of the full open channel level at +30 mV. 204
Figure 6.41 Effect of luminal pH 9.2 on SR K^+ channel gating. 205
Figure 6.42 The effect of luminal pH 9.2 on SR K^+ channel Po. 206
Figure 6.43 The effects of luminal pH 9.2 on the contribution of Po_{FULL} to Po_{TOTAL} at + 30 mV. 207
Figure 6.44 Combined effect of cytosolic or luminal pH change on SR K^+ channel gating. 208
Figure 6.45 A simplified kinetic scheme illustrating the mechanisms underlying cytosolic or luminal pH 6.2 at +30 mV. 210
Figure 6.46 Simplified schematic of the structure an amino acid 214
Figure 6.47 Amino acid sequence for mouse TRIC-B proteins 216

Chapter 7

Figure 7.2 Purification of the proteoliposomes containing TRIC-proteins 224
Figure 7.3 A typical opening observed from a purified TRIC-A channel 229
Figure 7.4 TRIC-A gating in alkaline recording solutions after incubation in phosphorylation mixture 231
Figure 7.5 TRIC-A gating in alkaline solutions 233
Figure 7.6 Representative openings of native SR K^+ channels from WT tissue in gradient conditions 235
Figure 7.7 Current-voltage relationships of SR K^+ channels recorded in gradient conditions. 236
Figure 7.8 Representative trace illustrating the typical gating properties of the K^+ channels observed after incorporation of solubilised LSR into a bilayer. 239
Figure 7.9 The SR K^+ channels from solubilised LSR are voltage-independent 240
Figure 7.10 Amino acid sequence alignments and conserved motifs for mouse, rabbit and human TRIC-A proteins and for mouse and human TRIC-B proteins. 242

List of tables

Table 3-1. The various types of SR K^+ channel gating characteristics observed in single-channel recordings from TRIC-A KO tissue. 48

Table 3-2 Observed number of direct transitions between the full closed and full open conductance levels 60

Table 3-3 Comparison of the 'typical' SR K+ channels from WT and TRIC-A KO prep 73

Table 4-1 Individual experiments illustrating the voltage-dependence of the SR K+ channels when there were four channels in the bilayer 98

Table 4-2 Comparison of the two methods used to analyse the Po when four SR K^+ channels were gating in the bilayer. 99

Table 5-1 The 4 state Markov model used to idealise experiments containing one SR K^+ channel and one RyR 139

Table 6-1. Closed time durations at +30 mV 168

Table 6-2 Mean closed duration +30 mV. 182

Table 6-3. The mean data illustrating the decrease in Po in pH 6.2 as a % of control (symmetrical pH 7.2) 192

Table 7-1 Reagents used for the transcription mixture for the wheat germ cell free system 223

Table 7-2 Reagents used for solubilisation of native SR vesicles 226

List of Publications

Full papers

O'Brien, F., Venturi, E. & Sitsapesan, R. (2015). The ryanodine receptor provides high throughput Ca^{2+}-release but is precisely regulated by networks of associated proteins: A focus on proteins relevant to phosphorylation. *Biochem Soc Trans. 43(3):426-33*

Matyjaszkiewicz A, Venturi E, O'Brien F, Iida T, Nishi M, Takeshima H, Tsaneva-Atanasova K, Sitsapesan R. (2015). Sub-conductance gating and voltage-sensitivity of sarcoplasmic reticulum K^+ channels: a modelling approach. *Biophys.J. 109(2):265-76*

Venturi, E., Galfré, E., O'Brien, F., Pitt, S.J., Bellamy, S., Sessions R.B. & Sitsapesan, R. (2014). FKBP12.6 activates RyR1: investigating the amino acid residues critical for channel modulation. *Biophys J. 106, 824-33.*

Published abstract

O'Brien, F., Venturi, E., Galfrè, E., Matyjaszkiewicz, A., Yamazaki, D., Nishi, M., Takeshima, H., & Sitsapesan, R. (2014). H^+ inhibits TRIC-B channels derived from mouse TRIC-A knockout tissue. *Biophysical Society Meeting Abstracts. Biophys. J., Supplement, 106(3) pp. 763a*

Venturi, E., Matyjaszkiewicz, A., O'Brien, F., Nishi, M., Takeshima, H., & Sitsapesan, R. (2014). Critical role of TRIC-channels: What can be revealed by single-channel studies? *Proc Physiol Soc 31*

O'Brien, F., Galfrè, E., Venturi, E., Matyjaszkiewicz, A., Yamazaki, D., Nishi, M., Takeshima, H., & Sitsapesan, R. (2013). pH regulates the single-channel gating behaviours of TRIC-B channels derived from TRIC-A knockout tissue. *Proc 37th IUPS*

Venturi, E., Matyjaszkiewicz, A., O'Brien, F., Nishi, M., Yamazaki, D., Takeshima, H., & Sitsapesan, R. (2013). TRIC-B channels exhibit labile gating properties; evidence from TRIC-A knockout mice. *Biophysical Society Meeting Abstracts. Biophys. J., Supplement, 104(3) p105a*

Venturi, E., Pitt, S.J., Galfrè, E., O'Brien, F., Nishi, M., Takeshima, H., & Sitsapesan, R. (2012). The TRIC-A knockout mouse model provides insight into the labile gating nature of TRIC-B channels. *Proc Physiol Soc 28*

Abbreviations

POPC	1-Palmitoyl-2-oleoyl-*sn*-glycero-3-phosphocholine
POPE	1-Palmitoyl-2-oleoyl-*sn*-glycero-3-phosphoethanolamine)
CHAPS	3-[(3-Cholamidopropyl)dimethylammonio]-1-propanesulfonate
HEPES	5 mM N'-2-hydroxethylpiperazine-N'-2-ethanesulphonic acid
CICR	Ca^{2+}-induced Ca^{2+}-release
CK2	Casein Kinase 2
CHO	Chinese hamster ovary
S	coefficient of sedimentation
CFTR	cystic fibrosis transmembrane conductance regulator
DEPC	diethylpyrocarbonate
DTT	dithiothreitol
DKO	double knockout
ER	endoplasmic reticulum
EC-coupling	excitation-contraction coupling
HSR	heavy sarcoplasmic reticulum
HMM	hidden Markov model
HEK	embryonic kidney epithelial cells
pKa	ionization constant
pI	isoelectric point
KO	knockout
LSR	light sarcoplasmic reticulum
LTCC	L-type Ca^{2+}-channels

MG-23	Mitsugumin 29
MM	mixed membrane
HEPES	N'-2-hydroxethylpiperazine-N'-2-ethanesulphonic acid
NCX	Na^+/Ca^{2+} exchanger
DM	n-Decyl-β-D-maltopyranoside
DDM	n-Dodecyl-β-D-maltopyranoside (DDM)
pKA	negative log of the acid dissociation constant (pKa)
Po	occupancy probability
ANOVA	one way analysis of variance
OI	osteogenesis imperfecta
PMSF	phenylmethylsulfonyl fluoride
PBS	Phosphate-buffered saline
PE	phosphatidylethanolamine
pS	picoseimens
PIPES	piperazine-N,N'-bis [ethanesulfonic acid]
Pdf	probability density function
PKA	Protein Kinase A
PKC	Protein kinase C
RyR	ryanodine receptor
RyR1	RyR isoform 1
RyR2	RyR isoform 2
SM	sarcolemma membrane
SR	sarcoplasmic reticulum
SKM	segmental k-means
S	Siemens

SNP	single nucleotide polymorphisms
TRIC	trimeric intracellular cation channel
VICR	voltage induced Ca^{2+}-release
VDAC	voltage-dependent anion-channel
WT	wild type

1 Introduction

1.1 Excitation-contraction coupling in striated muscle

The process of converting electrical signals into mechanical contraction is termed excitation-contraction coupling (EC-coupling) (1-3). In cardiac and skeletal muscle, depolarisation of the sarcolemma membrane (excitation) is coupled to an increase in cytoplasmic Ca^{2+} (causing contraction) (4-7). There are specialised structures within cardiac and skeletal muscle cells that facilitate the EC-coupling process. These include the sarcoplasmic reticulum (SR) , an intracellular Ca^{2+}-storage unit that regulates the calcium ion concentration in the cytoplasm of striated muscle cells (8-10) and deep invaginations of the plasma membrane that extend down into the cell, termed the t-tubules (11). The portion of the SR that faces the T-tubule is termed the junctional SR (12-14). The T-tubule and the junctional SR form triads in skeletal muscle (15, 16) and dyads (17-20) in cardiac muscle. Triads and dyads form the basic EC-coupling units (11).

In addition to the T-tubule and the SR, there are many additional proteins that are associated with the SR that have been suggested to play a role in the structural organisation of the dyads and triads. Junctophilins are responsible for maintaining the close proximity of the t-tubule and the endoplasmic reticulum (ER)/SR in cardiac and skeletal muscle cells (21-24) . Integral membrane proteins such as triadin and junctin may help anchor the RyR complex into the SR membrane, and may also provide nearby binding space for potential effectors (24-26). Mitsugumin 29 (MG-29) is a 29 kDa protein located in the SR membrane of skeletal muscle cells (27, 28). Knock out models have shown that ablation of MG-29 causes swollen T-Tubule and misaligned triads as well as rapid SR Ca^{2+} content depletion and fatigue illustrating that MG-29 has a role in triad organisation, which is crucial for correct EC coupling (17, 29).

One of the significant differences between cardiac and skeletal muscle resides within the EC-coupling process (30). In both cardiac and skeletal muscle, the ryanodine receptor (RyR), a high molecular mass membrane spanning protein of the SR is the pathway for the rapid intracellular Ca^{2+}-release from the SR (31-35). However, the underlying mechanisms that cause RyR opening are different in cardiac and skeletal muscle tissue.

1.1.1 RyR-mediated Ca^{2+}-release in cardiac muscle

In cardiac muscle, the mechanism for EC-coupling is Ca^{2+}-induced Ca^{2+}-release (CICR) (2, 6, 7, 36-39). Figure 1.1 illustrates a very simplistic schematic diagram of some of the structures that are involved in EC-coupling in striated muscle. Depolarisation of the plasma membrane following an action potential activates the voltage-gated L-type Ca^{2+}-channels (LTCC). In a cardiac cell the $Ca_v1.2$ is the isoform of the LTCC that is present and the opening of this channel leads to a Ca^{2+}-influx into the cardiac cell (40). This small increase in cytosolic $[Ca^{2+}]$ is not enough to initiate contraction of the myofilaments (40), but it causes Ca^{2+}-release from the SR via the Ca^{2+} sensitive cardiac RyR (RyR2) isoform (31, 32, 40). This mechanism of CICR was first proposed by Fabiato in 1983 (40). From his experiments, conducted on skinned cardiac cells, he suggested the presence of a Ca^{2+}-channel in the SR that was activated by submicromolar cytosolic $[Ca^{2+}]$. It was later shown that extracellular Ca^{2+} is required for triggering Ca^{2+} release in cardiac ventricular cells by Nabauer *et al* (1989) (37).

1.1.2 RyR-mediated Ca^{2+}-release in skeletal muscle

In skeletal muscle, the mechanism for EC-coupling is based on the physical coupling of LTCC and RyR1 (41-44). Similar to the process in cardiac cells, depolarisation of sarcolemmal T-tubules activates the voltage sensitive $Ca_v1.1$ isoform of the LTCC (42-44).

The skeletal isoform of the (RyR), RyR1, is the pathway for the rapid intracellular Ca^{2+}-release from the SR (33-35).

In contrast to cardiac EC-coupling, skeletal muscle EC-coupling does not require extracellular Ca^{2+} and thus, it is termed voltage induced Ca^{2+}-release (VICR) (45). The LTCCs that are on the T-tubules are directly coupled to RyR1 channels on the SR (46) and it is thought that a movement of charges in the S4 voltage sensor of the LTCC causes opening of the LTCC. This conformational change induces conformational changes in RyR1 that bring about RyR1 channel opening (43, 44, 46).

Although voltage-gated Ca^{2+}-channels and RyR form essential components of EC-coupling in cardiac and skeletal muscle, there are many other ion-channels, membrane transporters, ATPases and accessory proteins that are involved in the complex regulation of this process. Figure 1.1 illustrates a very simplistic schematic diagram of some of the structures that are involved in EC-coupling in striated muscle.

1.1.3 Ca^{2+} reuptake in cardiac and skeletal muscle

After the contractile event, in both skeletal and cardiac muscles, basal intracellular [Ca^{2+}] is restored via the activity of the SR Ca^{2+}-ATPase to reload the SR for the next event (47, 48) and via Ca^{2+} extrusion from the cell by the Na^{+}/Ca^{2+} exchanger (NCX) (49, 50) and the sarcolemmal Ca^{2+}-ATPase (51, 52) (see Figure 1.1).

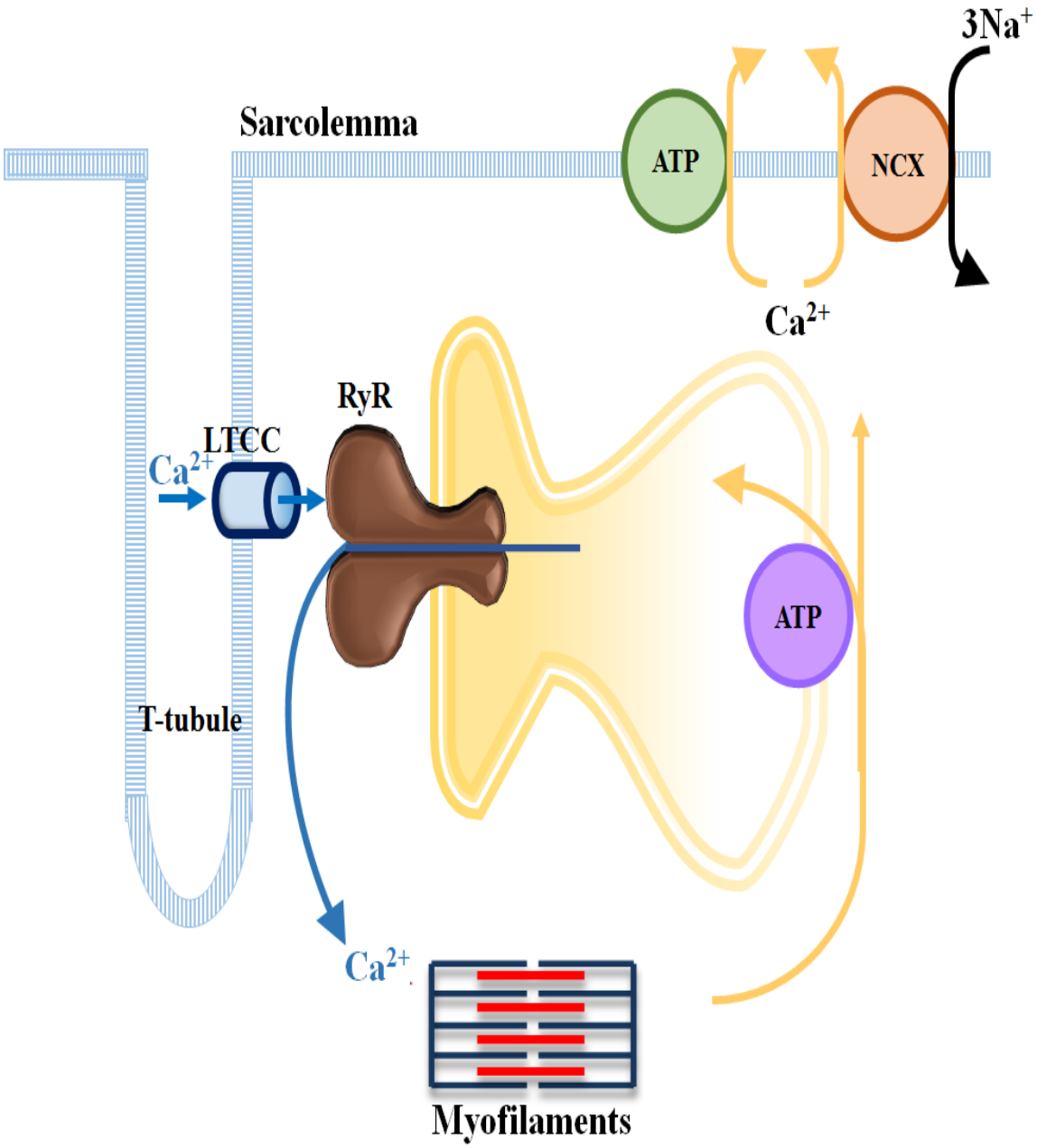


Figure 1.1 Schematic representation of EC-coupling in striated muscle
Depolarisation of the sarcolemma membrane activates voltage-sensitive L-type Ca^{2+}-channels (LTCC) located on the T-tubule region (blue channel). The localised rise in intracellular [Ca^{2+}] triggers the opening of cardiac RyR (CICR), while skeletal RyR are opened by a direct physical interaction with voltage-sensitive Ca^{2+}-channels (VICR) which forces a conformation change in RyR. The large Ca^{2+} flux through RyR channels enables movements of the cell myofilaments causing the contraction of the cell. After cell contraction, intracellular [Ca^{2+}] is restored to basal levels by the action of the SR Ca^{2+}-ATPase (purple), which enables refilling of the SR, and by Ca^{2+} flux out of the cell mediated by the the Ca^{2+}/Na^{+} exchanger (NCX) and the sarcolemmal Ca^{2+}-ATPase.

1.1.4 Ultrastructural aspects at the junction of t-tubules and SR membranes

As described earlier, intracellular junctional complexes, where the terminal cisternae of the SR lie in close proximity with the T-tubules, form the basic elements required for Ca^{2+}-release and Ca^{2+}-reuptake (see Figure 1.1). It is thought that interactions between the LTCC and the cytoplasmic domains of the RyR are thought to mediate communication between the plasma membranes/t-tubules and the transmembrane, ion-conducting region of the RyR in the SR (41-44). It has been illustrated that when the triadic complexes are isolated, the location of cytoplasmic regions of RyRs protrude from the SR and span the SR-plasma membrane junction in what has been described as ‘ feet structures’ (16, 53, 54).

These feet structures form unique lattices in striated muscle (55-58). In skeletal muscle, each RyR subunit is proximal to four adjacent particles at each corner that resemble the pattern observed on a checkerboard (55, 59-61), as illustrated in Figure 1.2. Purified RyR1 channels have been shown to form lattice structures (59), enabling researchers to suggest which RyR domains are possibly involved in physically connecting adjacent RyRs (62). It is thought that this intrinsic ability to form lattice arrangements underlies the RyR1 coupled gating that has been observed at the single-channel level (62, 63). In addition, in skeletal muscle, the LTCCs form distinct arrangements or tetrads consisting of four receptors in close proximity (46, 64). Close examination of overlaying arrays of LTCC tetrads and RyR lattices reveals that every alternate RyR is associated with a tetrad (four LTCCs) (64). For the RyR channels that are associated with a tetrad, each RyR1 monomer is coupled to a LTCC channel,

Similar to RyR1, when RyR2 is incorporated into artificial bilayers, coupled gating has been reported (65), leading to the assumption that RyR2 may also be arranged in a checkerboard lattice *in situ*. However, recent electron tomographic analysis of rat ventricular myocytes has shown RyR2 distributed in a combination of checkerboard and

side-by-side configurations with some isolated tetramers (57, 58). In addition, regular LTCC tetrads are not present in cardiac muscle, and so, it is thought that this tetrad is crucial for the VICR of skeletal muscle (64).

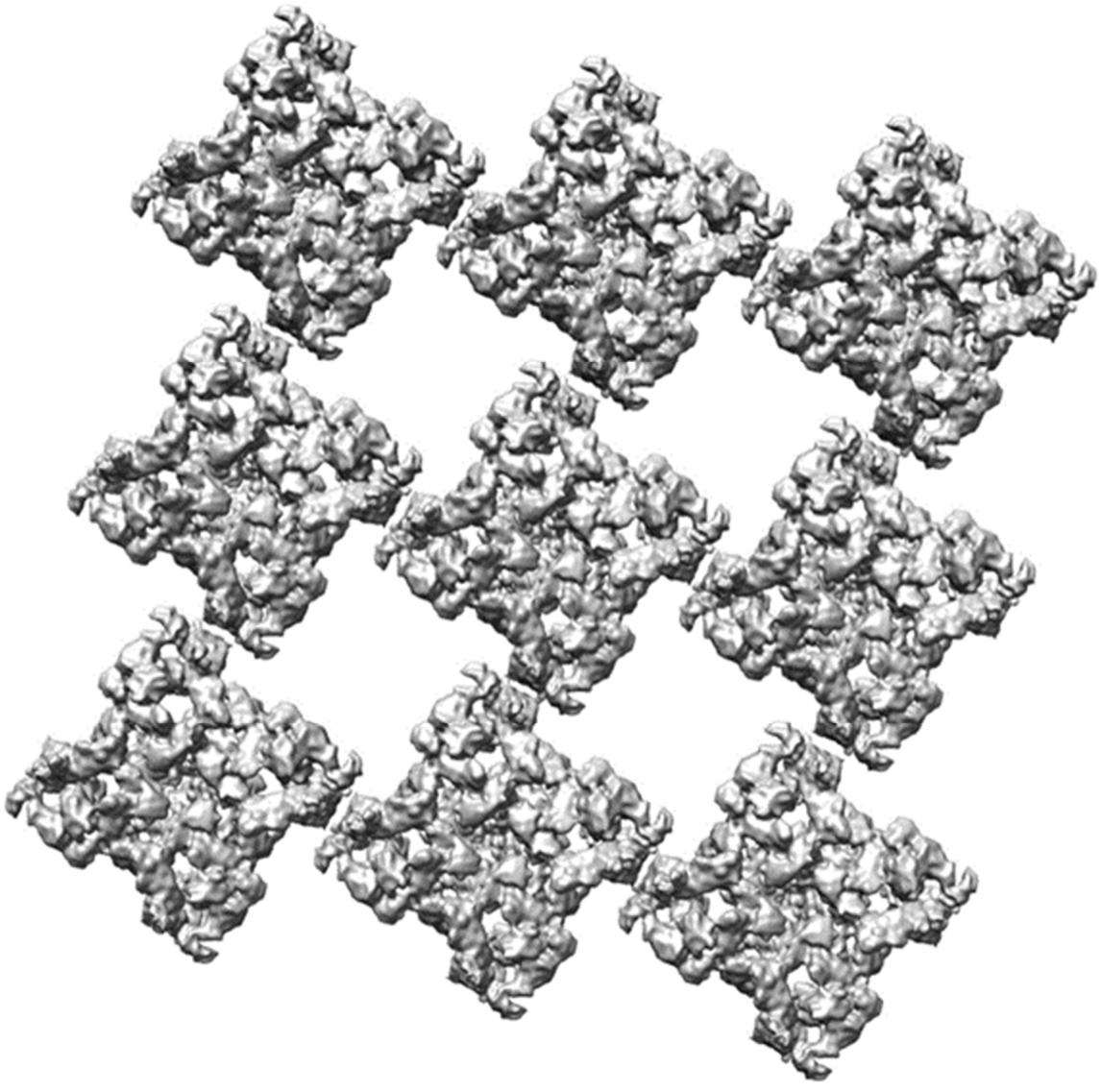


Figure 1.2 Model of RyR-lattice array
Model of the RyR checkerboard pattern was adapted from Van Petegem (61). The model was created using a RyR1 cryo-EM map (EMDB number 1607) with interactions that have been reported by Yin *et al* (57)

1.2 The Ryanodine Receptor

RyR isoform 1 (RyR1) are found at their highest concentration in skeletal muscles, RyR isoform 2 (RyR2) are expressed predominantly in cardiac and smooth muscle while RyR isoform 3 (RyR3) are found with a lower expression in many cell types, but are found at their highest in brain and diaphragm muscle (35, 66, 67). The term 'ryanodine receptor' derives from the high affinity of the plant alkaloid, ryanodine, for the RyR channels (68, 69). At the single-channel level, nanomolar ryanodine was demonstrated to lock the RyR channels into a low conductance, high probability open state (68, 69). RyRs are homotetramers with a molecular weight of 2.3 MDa, rendering them the largest known ion channel (70, 71). Each monomer is made up of approximately 5000 amino acids, with monomeric molecular weights of approximately 565 kDa (35, 66, 67). The large N-terminal cytosolic domain makes up approximately 80% of the protein mass, and its large cytosolic surface of roughly 120 Å serves as an interface with which many proteins and pharmacological agents interact, allowing them to regulate Ca^{2+} release from intracellular stores (72).

1.2.1 The permeation properties of the RyR

The planar lipid bilayer technique (described in detail in Section 2.2 of this thesis) is an invaluable tool to characterise the biophysical properties of the RyRs. Using this technique, it was shown that the RyR is selective for divalent cations over monovalent cations (73-75). For example, under bi-ionic solutions of Ca^{2+} and K^+, it was shown that the Ca^{2+}/K^+ permeability ratio was approximately 6, indicating that the RyR is 6 times more selective for Ca^{2+} than for K^+ (76, 77). In addition, RyRs have a smaller conductance in Ca^{2+} than K^+ suggesting that the affinity for divalent ions in the pore of the channels is higher than the affinity for monovalent cations (78, 79). Ion permeation though the RyR is ohmic,

meaning that the current produced due to channel openings is proportional to the holding membrane potential and the channel does not show rectification at the single-channel level at holding potentials between ± 100 mV (80)

1.3 The skeletal SR K^+ channel

In the 1970s, using a combination of radioactive flux measurements and voltage-sensitive dyes, McKinley and Meissner (1978) illustrated that fragments of rabbit skeletal SR were highly permeable to K^+ and Na^+, but not to $choline^+$ or $Tris^+$ (81). They inferred that there must be a specific mechanism or a pathway that mediates this monovalent cation permeability. A hypothesis started to emerge in concomitance with those studies that in order for sufficient Ca^{2+} to be released from the SR, any developing charge asymmetry across the SR needed to be compensated for (82-85). It was suggested that the movements of other ionic species such as Cl^- and K^+ could constitute the counter current mechanisms necessary to balance the SR Ca^{2+}-fluxes during Ca^{2+}-release and Ca^{2+}-uptake

The idea of a K^+ selective pathway across the SR membrane that McKinley and Meissner proposed (81) was supported by Miller in 1978 (87) when the SR from rabbit skeletal muscle was isolated and incorporated into planar lipid bilayers. Miller reported observing a voltage-sensitive current that was selective for small monovalent cations, particularly K^+ (87). Miller's group proceeded to study the selectivity and permeability properties of the SR K^+ channel and illustrated that the channel was ideally selective for K^+ and does not conduct Ca^{2+} (82). The open channel conductance measured in symmetrical conditions for different monovalent cations follows in decreasing order $K^+ > NH^+_4 > Rb^+ > Na^+ > Li^+ > Cs^+$ (82).

After this first study, many other reports followed that provided analysis of the biophysical properties of the SR K^+ channel (82, 88-93). Coronado and Miller (1979) reported that Cs^+ could block the K^+ flux from the SR K^+-channel (94). They suggested that a single Cs^+ ion, after entering the channel pore, remains bound to a particular site (within the pore) resulting in the reduction of K^+ flux through the channel (94). This theory of Cs^+ blockade was later revisited by Miller when he illustrated that the SR K^+-channel is, in fact, permeable to Cs^+ and that current fluctuations can be observed in symmetrical Cs^+ solutions (95). The Cs^+/K^+ permeability ratio was reported to be 0.7, suggesting that the SR K^+ channel is almost equally permeable Cs^+ and K^+, however, the conductance of the SR K^+ channel in Cs^+ is 16-fold smaller than it is in K^+ (95).

In addition, Coronado and Miller provided a first estimation of the conduction pathway of the SR K^+ channel from experiments utilising large organic cations such as ammonium and tetraethylammonium (88). Based on their experiments, they proposed that the conducting pathway of the SR K^+-channel is composed of a non-selective large 'mouth' of diameter 50 Å followed by a narrow constriction of diameter 20 Å (88). Coronado and Miller also characterised the blocking actions of decamethonium and hexamethonium on the single-channel gating of the SR K^+-channel (96). Decamethonium block was described to be voltage-dependent and the channel appeared to 'flicker' between the open and closed channel states. In contrast, hexamethonium block of the SR K^+ channel represented the appearance of lower conductance openings without the appearance of 'flicker' blocking events and thus, was described as a 'smooth blocker'. It was reported that the differences between the blocking agents derive from differences in the rate of dissociation of the drugs. For example, the slower rate of dissociation of decamethonium induces discrete flickering opening events ('flickery block') that can be resolved in the single-channel recording (96).

The gating features of the SR K^+ channels from frog skeletal SR in planar phospholipid bilayers were described by Labarca *et al* (1981) (85). In 100 mM K^+, three distinct conductance levels were observed; a zero-conducting closed state, a small 50 pS open state (termed α) and a larger 150 pS open state (termed β), as illustrated by the schematic in Figure 1.3. Although the two observed open levels differed in conductance, they were identical in ionic selectivity (85). It was suggested that because a 200 pS (α + β) level was never observed, both conductance levels originated from a single entity, and thus, the 50 pS level must be a sub-conductance open state, with the full level opening being 150 pS. In addition, transitions to the β-conductance level occurred via the α-conductance level. Fox supported this in 1985 when he described the gating of the SR K^+ channel from rabbit skeletal muscle. It was illustrated that the selectivity sequence of the full open channel level and the sub-conductance level were identical. However, in contrast to the 33 % sub-conductance level reported by Labarca *et al* (1981), in this paper, the sub-conductance level was described as being 60 % of the full open channel level (93).

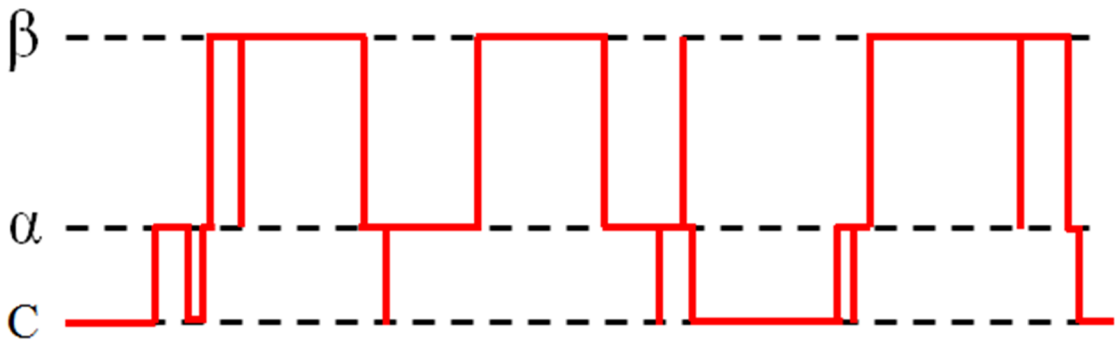


Figure 1.3 A simplification of the gating states of the SR K^+ channel described by Labarca *et al* (1981) (85).
The three states of the SR K channel included a zero-conducting closed state, a small 50 pS open state (termed α) and a larger 150 pS open state (termed β). C represents the zero current level.

Improvements in the resolution of the single-channel recordings and advancements in reconstitution techniques allowed for a more detailed characterisation and analysis of the sub-conductance open state of the skeletal SR K^+ channel. In two separate studies, one by Fox *et al* (1985) (93) and the other by Tomlins and Williams (1986) (90), the sub-conductance level of the skeletal SR K^+ channel was reported as 60-70% of the full open channel level, which in contrast to the 30% level observed by Labarca and Miller (1981) (85). However, in both reports, the channel opening to the sub-conductance state was characterised by substantial open channel noise and variability (90, 93).

1.3.1 The cardiac SR K^+ channel

Tomlins *et al* (1984) (97) first described the gating properties of the SR K^+ channel from cardiac muscle after permeability studies of Meissner and McKinley (1982) (98) on mammalian cardiac muscle. The cardiac SR K^+ channel isoform exhibited similar characteristics to the skeletal SR K^+-channel such as voltage-dependence, ionic selectivity and block by decamethonium (97). The cardiac SR K^+ channels were observed after both the 'heavy' and the 'light' SR fractions (see Section 2.1.2) were fused to artificial bilayers, suggesting that the K^+-channels are not contained in a specific region of the SR but are present in the whole SR network (97). The sub-conductance level of the SR K^+ channel was found to be approximately 60% of the fully open channel state, which, again, appeared to contrast to the sub-level of the K^+-channel observed by Labarca and Miller (sub-conductance state at 30% of the full open channel level). In addition, the cardiac SR K^+ channel studied by Tomlins *et al* (1984) (97) showed equal probability of transitions between the three states (fully open, sub-conductance and closed states).

.

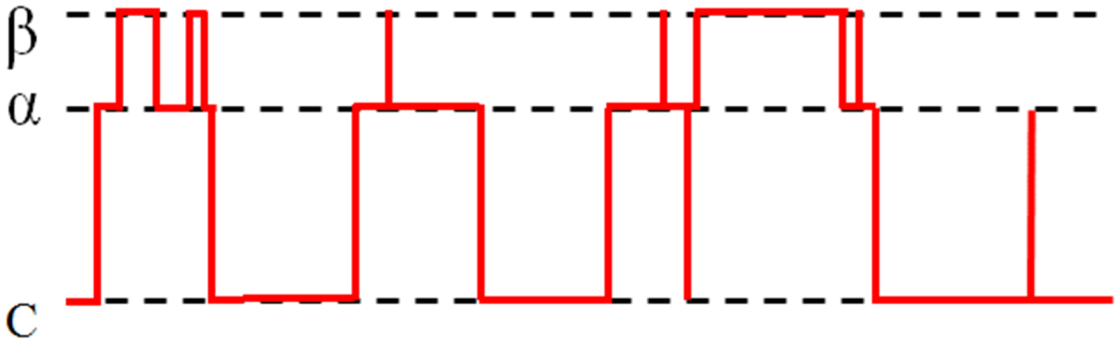


Figure 1.4 A simplification of the gating states of the SR K^+ channel described by Tomlins *et al* (1984) (97)
The three states of the SR K^+ channel included a zero-conducting closed state, a 100 pS open state (termed α) and a larger 150 pS open state (termed β). C represents the zero current level.

1.4 TRIC proteins

The work of Takeshima and colleagues in resolving the molecular identity of many SR junctional membrane proteins (23, 28, 99) led to the identification of a novel SR protein of 33 kDa (mitsugumin 33, subsequently named the trimeric intracellular cation channel (TRIC), subtype A)) and a second structural homologue (named TRIC-B) (100).

1.4.1 Proposed structure of TRIC-proteins

TRIC proteins are composed of approximately 300 amino acids (100). The amino acid sequences of the mouse, rabbit and human TRIC-A, and the mouse and human TRIC-B are shown in Figure 1.5. From the hydropathicity studies conducted by Yazawa *et al* (2007) (100) both TRIC-A and TRIC-B proteins are thought to have have three putative membrane-spanning domains (highlighted in the red boxes in Figure 1.5). Chemical crosslinking studies and EM particle imaging of recombinant TRIC-A proteins revealed a bullet-shaped homotrimeric structure for TRIC-A (100).



Figure 1.5 Amino acid sequence alignments for mouse, rabbit and human TRIC-A proteins and mouse and human TRIC-B proteins.
UniProtKB database identifiers for TRIC-A are Q3TMP8, A5A6S6 and Q9H6F2. TRIC-B UniProtKB database identifiers are Q9DAV9 and Q9NVV0. The three putative transmembrane segments identified by Yazawa *et al* (2007) (100) are illustrated by the red boxes.

1.4.2 TRIC-proteins behave as functional K^+ channels

It was thought that the SR K^+-channel was a single molecular entity until the more recent studies of Yazawa et *al* (2007) and Pitt *et al* (2010) suggested that it may have a dual identity (100, 101). When the TRIC-proteins were cloned, isolated, purified and then fused with artificial bilayers, both TRIC-A and TRIC-B behaved as functional K^+-selective ion-channels (101). When a gradient of KCl was added to the cytosolic side of the channels,

the reversal potential that was measured was that of the expected value for a channel selective for cations but impermeable to anions (101). The gating of the TRIC-A and TRIC-B proteins were voltage-dependent, with the Po of each isoform being higher at the holding potential of +30 mV compared to that at -30 mV (101). In addition, Pitt *et al* (2010), reported that the gating of TRIC-B was dependent on cytosolic and luminal [Ca^{2+}], with micromolar cytosolic [Ca^{2+}] activating TRIC-B and luminal [Ca^{2+}] inhibiting TRIC-B (101). Furthermore, both isoforms gated to sub-conductance levels. In 210 mM K^+, the purified TRIC-A gated to a full open channel conductance level of 192 pS in addition to a sub-conductance state that was 70% of this level whereas TRIC-B gated to a full open channel conductance level of 138 pS and in addition to two sub-conductance levels that were 40 % and 25 % of this level (101).

Pitt *et al* (2010) provided many reasons why previous reports failed to observe the gating of two distinct ion-channels. They suggested that this was because TRIC-A and TRIC-B channels are both permeable to K^+, impermeable to anions and show a similar type of voltage-dependent gating. In addition, the sub-conductance level detected in TRIC-A gating was indistinguishable from the TRIC-B full open level (101). Furthermore, they have suggested that the high levels of background noise of single-channel recordings and the necessity of applying high filtering levels in order to observe single-channel opening events (100-400 Hz), could explain why most of the transitions to a small conductance level such as the TRIC-B sub-conductance states were missed and also explained the inability to distinguish between TRIC-A sub-conductance gating and the TRIC-B full openings (101). The striking similarities that were observed in the gating properties of purified TRIC-A and TRIC-B channels make it extremely difficult to distinguish between a TRIC-A opening and TRIC-B opening when studying the biophysical properties of the native SR K^+ channels from cardiac or skeletal SR, thus, limiting the biophysical

information that can be obtained about each TRIC-subtype when studying native SR vesicles. As discussed in Chapter 3, the use of the TRIC-A KO mouse for single-channel reconstitution experiments has enabled the study of a more homogeneous SR K^+ channel population.

1.5 Cl^- channels in the cardiac and skeletal SR

When Miller first fused the SR of rabbit skeletal muscle to artificial bilayers, in addition to the K^+-selective channel that has been described in detail above, he also reported observing a Cl^- -selective channel (87). Several groups have characterised the Cl^- current-fluctuations that are observed when cardiac and skeletal SR is fused to artificial membranes (102-109). Several anion selective ion-channels have been reported to be present on the SR membrane although the exact number of distinct channels remains unclear as different groups have used varying ionic concentrations and different experimental protocols in single-channel measurements. In the majority of reports, it has been shown that the SR Cl^- channels that are observed at the single-channel level exhibit voltage dependent gating (102-109) behaviour and gate to sub-conductance open states. The number of sub-conductance states that have been reported for SR Cl^- channels varied from 2 in some reports (102, 106) up to 13 in another report (109).

To date, the SR Cl^- current-fluctuations that have been documented from native SR have not yet been linked to any protein identity. The cystic fibrosis transmembrane conductance regulator (CFTR) is a cAMP-regulated Cl^- channel that expressed on the apical surface of epithelial and recently, it was detected on the SR membrane of human skeletal muscle (110). However, CFTR exhibits a very small conductance of 6-10 pS (111) and thus, may not be responsible for the native Cl- currents that exhibit the much larger conductances that have been documented. Another anion channel that has been reported to be located in the

SR membrane is the voltage-dependent anion-channel, VDAC by Barmatz et *al* (1996) (112). It is thought that the physiological role of VDAC is charge compensation during Ca^{2+}-release, but also ATP transport into the SR lumen (112).

1.5.1 Physiological significance of TRIC channels

The expressional levels of TRIC-A and TRIC-B are slightly different; TRIC-A is expressed at high levels in excitable cells such as skeletal muscle and cardiac muscle cells, whereas TRIC-B is ubiquitously expressed at much lower levels (100). The physiological role of TRIC-channels is currently unknown, however, their importance is highlighted by the phenotype of the TRIC-knockout (KO) mice. Genetic deletion studies of both TRIC subtypes (double-KO, DKO) (100) and single TRIC-A (113) or TRIC-B (114), have indicated a major role of TRIC channels in supporting SR Ca^{2+}-release and uptake processes. The TRIC-DKO is embryonic lethal. The mice exhibit a weak heartbeat at embryonic day (E) 9.5 leading to embryonic cardiac failure by E10.5 (100). Electron microscopy revealed severely swollen SR/ER structures in TRIC-DKO cardiomyocytes and TRIC-DKO embryos with visible Ca^{2+} oxalate deposits (100). Amplitudes of spontaneous Ca^{2+} oscillations were markedly depressed in the TRIC-A KO cardiomyocytes, however, the caffeine evoked Ca^{2+} response was significantly larger, suggesting high levels of SR Ca^{2+} and illustrating that intracellular Ca^{2+} signalling is severely compromised. In this paper, the similarities between the TRIC-DKO and RyR2-knockout mice were highlighted. Both TRIC-DKO and RyR2-knockout mice display similar cardiac arrest phenotypes with the presence of swollen and over-loaded SR/ER in the embryonic cardiomyocytes (100, 115).

In addition to the DKO mouse, the single KO mice have also been characterised (113, 114, 116). The TRIC-B KO neonate dies immediately after birth in respiratory failure (114). In the alveolar epithelial cells devoid of TRIC-B, the IP_3R-mediated Ca^{2+} release was

markedly reduced and the intracellular stores showed evidence of Ca^{2+} overload (114). The TRIC-A KO mouse survives until adulthood, however, the mice develop hypertension due to vascular hypertonicity (116). In the vascular smooth muscle cells from TRIC-A KO, insufficient RyR-mediated Ca^{2+} sparks for inducing hyperpolarisation were detected (116). In addition, Ca^{2+} dysregulations have also been reported in the skeletal muscle of TRIC-A KO mice, with overloaded intracellular stores and compromised Ca^{2+} signalling (113).

1.5.1.1 TRIC channels and disease

The knock out mice models have been crucial to identify significant areas where TRIC-channels may play a pivotal role. Recently, there have been several links between TRIC-channels and human diseases. In a Japanese population-based study, comparing 1119 hypertensive and 1140 control subjects, it was found that single nucleotide polymorphisms (SNPs) in the TRIC-A gene were associated with the hypertensive subjects (117). In addition, deletion mutations in the TRIC-B gene have been associated with the autosomal recessive disease osteogenesis imperfecta (OI), a congenital bone disorder characterised by brittle bones and increased susceptibility to fractures. The pathophysiological mechanism linking TRIC-B channels and OI is currently not known.

1.6 Hypothesis and aims of this thesis

This thesis focuses on the single-channel properties of the SR K^+-selective channel of cardiac and skeletal muscle (82, 85, 87-89). The combined gating of TRIC-A and TRIC-B are suggested to underlie native SR K^+ channel openings (101), but the single-channel properties of purified TRIC-A and TRIC-B are very similar, and therefore, it would be difficult to distinguish TRIC-A gating events from TRIC-B gating when SR vesicles are incorporated into bilayers.

I hypothesise that TRIC-A KO mouse may be a suitable experimental model to investigate SR K^+ channel function without contamination from TRIC-A. This model may therefore enable investigation of the contribution TRIC B to overall SR K^+ current. The major aim of this thesis was therefore to characterise and compare the biophysical properties of the native SR K^+ channels that are observed when the SR from wild type (WT) and TRIC-A KO mouse skeletal muscle was fused to artificial bilayers. I have compared the voltage-dependence, conductance, gating characteristics, and pH sensitivity of the SR K^+ channels from both WT and TRIC-A KO preparations. In addition, I have explored whether, when multiple SR K^+ channels are gating in the bilayer, they gate in a cooperative manner.

As previously described, both the TRIC-channels and RyRs are thought to be located on the junctional regions of the SR and thus, I have investigated whether the single-channel properties of the SR K^+ channel or of the RyR were altered when both channels were gating together in a bilayer.

Finally, I have tried to improve the techniques for purifying TRIC-A so that channel function can be investigated more easily and in more detail and be related to structure.

The results from my experiments will provide new insights into physiological regulation and putative roles that these SR K^+ channels may play in different tissue types. This knowledge is important for understanding excitation-contraction coupling in cardiac and skeletal muscle cells in health and disease.

2 Methods

2.1 Isolation of SR membrane vesicles from skeletal muscle

2.1.1 Collection of mouse skeletal muscle tissue

In the laboratory of Hiroshi Takeshima, University of Kyoto, Japan, skeletal muscle from the hind leg from WT and TRIC-A KO mice was quickly extracted and collected in ice-cold Phosphate-buffered saline (PBS) solution (137 mM NaCl, 2.7 mM KCl, 10 mM Na_2HPO_4, 1.8 mM KH_2PO_4). The tissue was snap frozen and stored in liquid nitrogen until enough samples had been collected for shipment on dry ice to the UK.

2.1.2 Isolation of SR membrane vesicles

The procedure of isolating the sarcoplasmic reticulum was carried out in a cold room at 4 °C. The frozen tissue was ground to a powder with a mortar and pestle prior to homogenisation in 300 ml of solution containing 300 mM sucrose, 20 mM piperazine-N,N'-bis [ethanesulfonic acid] (PIPES), protease inhibitors (300 nM aprotinin, 1 µM leupeptin, 1 mM benzamidine, 1 mM phenylmethylsulfonyl fluoride (PMSF)), 2.5 mM dithiothreitol (DTT), pH 7.2. The mixture was centrifuged at 10,000 x g, for 20 min, at 4°C, in a Sorvall GSA rotor and the resulting supernatant was ultracentrifuged at 100,000 x g, for 1 h, at 4°C (in a Beckman Type 45i rotor). The resulting pellet contained the mixed membrane (MM) fraction. The heavy sarcoplasmic reticulum (HSR), light sarcoplasmic reticulum (LSR) and sarcolemma membrane (SM) were separated from each other using a discontinuous sucrose gradient. The gradient was prepared using three different concentrations of sucrose: 20 %, 30 %, and 40 % w/v. The solutions were layered on top of each other in a 32 ml Beckman tube, as shown in Figure 2.1, using a 10 ml glass syringe attached to a 10 cm needle with a 14 mm diameter. The MM pellet was resuspended in a solution containing 10 % sucrose and placed on top of the discontinuous sucrose gradient.

Following centrifugation at 100,000 x g, for 120 min, at 4°C, in a Beckman SW 32i rotor, the membranes had separated into three distinct fractions, as shown in Figure 2.1. The sarcolemma remained at the top of the tube , the LSR membranes sedimented to the 20-30% interface and the HSR membranes sedimented to the 30-40% interface (118). The LSR and HSR were collected, diluted in 400 mM KCl, 10 mM PIPES, pH 7.2 and ultracentrifuged at 100,000 x g, for 1 h, at 4°C (in a Beckman 45i rotor) to remove the excess sucrose. The final pellets were resuspended in a solution containing 400 mM sucrose, 5 mM N'-2-hydroxethylpiperazine-N'-2-ethanesulphonic acid (HEPES), titrated to pH 7.2 with Tris, aliquoted, snap frozen in liquid nitrogen, and stored at -80 °C.

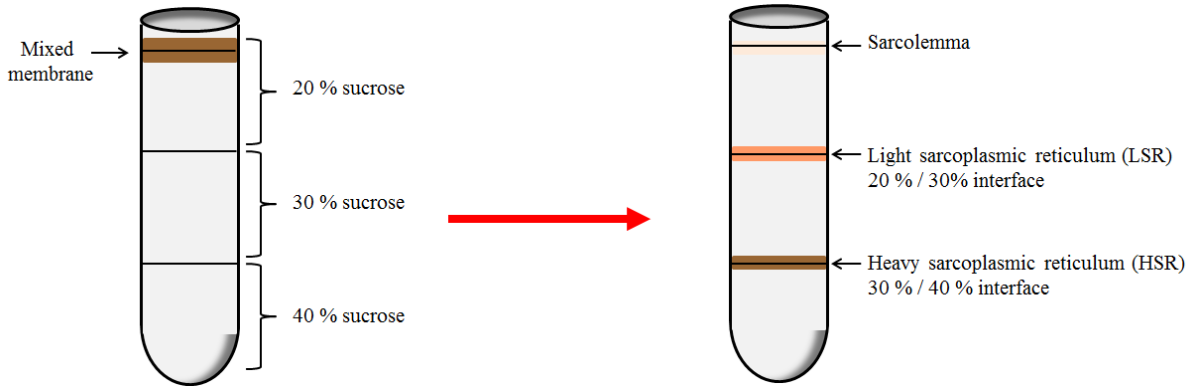


Figure 2.1 Schematic illustration of 20-40 % sucrose density gradient.
10 ml of 40 % sucrose, 30 % sucrose and 20 % sucrose were sequentially added to a Beckman tube. The MM, diluted in 10 % sucrose was layered on top (left). Following centrifugation (right) the LSR and HSR were detected at the 20%-30% and the 30%-40% (w/v) interfaces, respectively.

2.2 The planar lipid bilayer technique

The planar lipid bilayer technique, first described by Mueller et al (1962) (119), is a unique electrophysiological approach used to characterise the behaviour of ion-channels that cannot be accessed using a traditional patch pipette. It allows researchers to study ion-channels at the single molecule level and in a highly controlled environment.

2.2.1 The planar lipid bilayer workstation

2.2.1.1 The bilayer chambers

The bilayer chambers consisted of cup, with a 150 µm aperture, and a block, with a figure of 8 shaped cavity, made from Delrin (acetyl resin) (Warner Instrument, Hamden, USA) that were assembled together to form two distinct compartments, as illustrated in Figure 2.2. The compartment inside the cup was termed the *cis* chamber while the outer compartment was termed the *trans* chamber. On one side of the block, two small cavities, filled with 300 µl 3M LiCl, accommodated two silver-silver chloride electrodes and two agar bridges. The agar bridges were formed from glass capillaries bent into a U-shape over a Bunsen burner, filled with 3M LiCl and 2 % agar and stored in 3M LiCl.

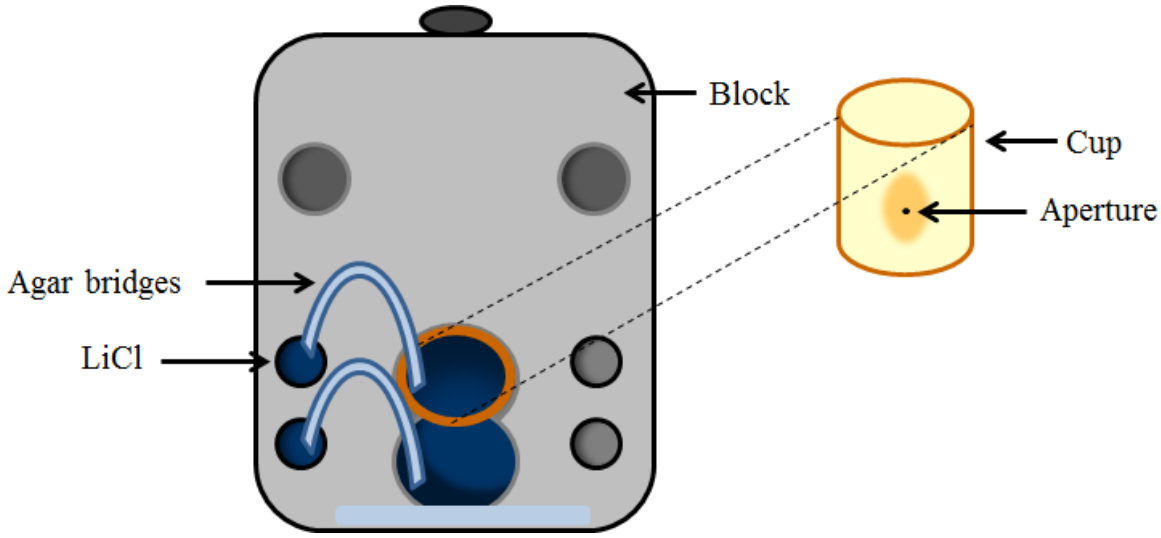


Figure 2.2 A schematic illustrating the two distinct compartments formed by the block and cup apparatus.
The block (grey) accommodates the cup (orange) to form two compartments separated by the aperture.

In order to mix the solutions in both recording chambers, the block was placed on a stir plate (Warner instruments, Hamden, USA) and the solutions were stirred using magnetic fleas. The entire bilayer apparatus was placed inside a Faraday cage to minimise electrical

noise and set on an anti-vibration table (Newport Corporation, Irvine, United States) to minimise mechanical noise.

A perfusion system was custom made from a peristaltic pump in the Electrical and Electronic Engineering Department, University of Bristol, and was used to change the experimental recording solutions without perturbing the bilayer. The perfusion system was located outside the Faraday cage in order to minimise electrical noise.

In our recording system, the *trans* chamber was held at ground, and the *cis* chamber was clamped at voltages relative to the ground.

2.2.1.2 The electrical equipment

In addition to the block and cup apparatus described above, the planar lipid bilayer workstation consisted of several electrical components outlined below:

- BC-535 bilayer clamp amplifier (Warner Instruments, Hamden, USA) and a headstage. The amplifier contained a 4-pole low pass Bessel filter which was used to filter the outgoing signal to the computer. In my experiments, a filter of 10 kHz was applied.
- InstruTECH ITC-18 Interface (HEKA, Elektronik Lambrecht/Pfalz, Germany), used to convert the analogue signal from the amplifier into a digital form that could be stored on the computer.
- A computer was used for data acquisition and analysis (Windows XP, 32 bit).
- A low pass 8-pole Bessel filter (Frequency Devices Inc, Ottawa, Canada) was used to filter the signal from the amplifier for real time visualisation of the single-channel current fluctuations

- An oscilloscope (Hitachi VC-6545, UK) was used to preview the data (filtered through the low pass 8-pole Bessel filter) during the acquisition.

The electrical components of the planar lipid bilayer workstation are illustrated in Figure 2.3.

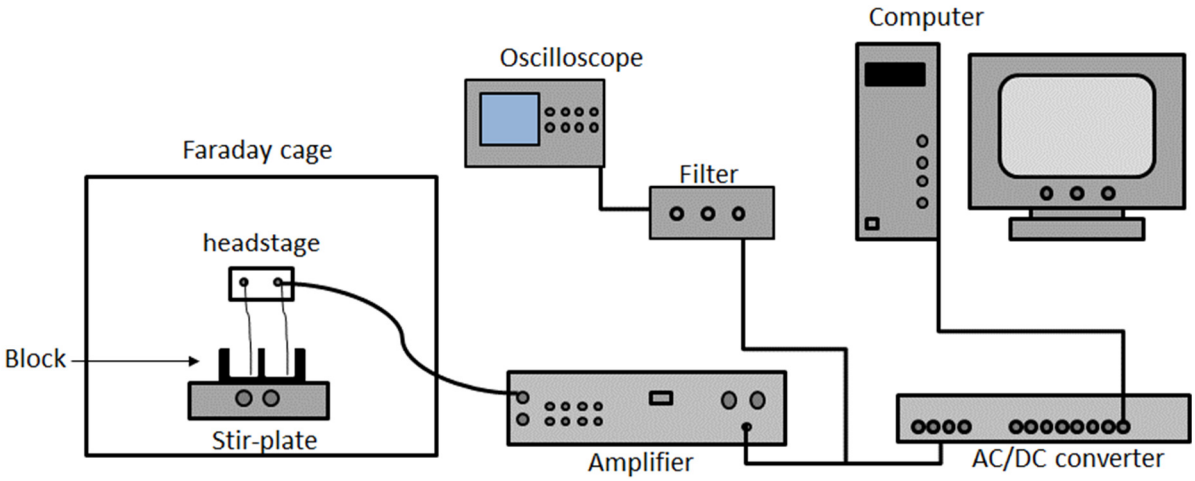


Figure 2.3 A schematic representation of the connections between the electrical components used for single-channel recording.

2.2.2 Grounding the workstation

Electrical noise is common in electrophysiology equipment, and the noise can contaminate the recordings and mask the signal. Each electrical device was grounded directly to the ground at the back of the amplifier.

2.2.3 Silver-silver chloride electrodes

Silver-silver chloride electrodes act as signal transducers by converting ionic currents in solution to an electric current within a wire. This is achieved by a reversible oxidation/reduction reaction between the electrode and the Cl^- in solution. The chemical reaction is

$$Cl^- + Ag \Leftrightarrow AgCl + e^-$$

The silver electrodes were chlorided by soaking them in bleach until a dark grey colour was observed.

2.3. Formation of stable bilayers suitable for electrophysiological recordings

Planar lipid bilayers were formed following the original method of Mueller (1962) (119). Neutrally charged bovine heart phosphatidylethanolamine (PE) (Avanti Polar Lipids, Alabama, USA) was used in our experiments. PE was stored in chloroform at -80 °C in a stock of 50 mg/ml. To prepare the lipids for electrophysiological recordings, the chloroform was evaporated using nitrogen gas, and the lipids were resuspended in a nonpolar solvent (n-decane) to a final concentration of 35 mg/ml. The final lipid suspension was kept on ice until needed.

2.3.1 Priming

Priming the cup consisted of pushing a small drop (< 0.5 µl) of the lipid suspension through the aperture of the cup from the inside. This was done using a 10 µl pipette with a tip attached. The tip was dipped into the lipid suspension and the liquid was allowed to naturally travel up a small portion of the tip without any manual intervention. The tiny drop of lipid in the tip was then manually pushed through the aperture. The lipids were left to dry and after 5 min, the cup was inserted into the block. The agar bridges and silver chloride electrodes were positioned, and the recording solutions were added to both chambers.

2.3.2 Bilayer formation

A layer of lipid was painted on the internal side of the cup using a plastic Pasteur pipette fashioned to a point at the tip. Initially the film of lipid is several micrometres thick,

however, it quickly begins to thin due to several driving forces (120-122). A schematic representation of the forces involved in formation of a stable bilayer is shown in Figure 2.4.

The forces involved in thinning the bilayer are:

1. The Plateau-Gibbs border suction, the pressure derived from the curvature of the torus (122). The pressure is greater in the thinner regions of the film, leading to the movement of the bulk solution towards the border and thinning of the membrane.
2. As the bilayer thins to a few hundred Angstroms, the Van der Waals forces become apparent between the aqueous phases on the two sides of the film (120).

As the bilayer continues to thin, it would not be stable unless the thinning forces were opposed by another set of forces. The steric repulsive force, which only operates over very short distances, opposes the Van der Waals forces. Additionally, as the bilayer thins, the solvent flows out from between the advancing surfaces. When the surfaces are very close, intermolecular attractive forces of the solvent work against this, making it difficult for solvent to pull away from its neighbours, helping to resist the thinning forces.

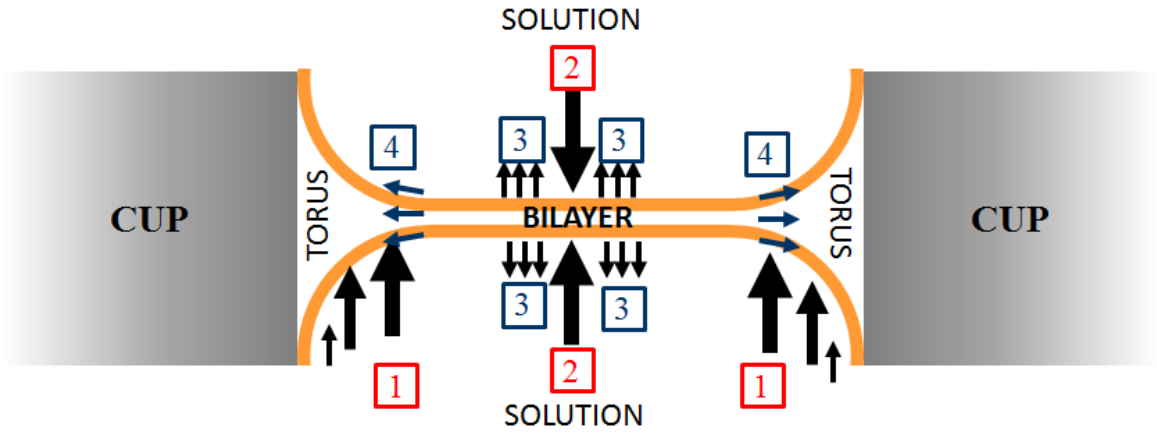


Figure 2.4 Schematic illustrating the forces involved in bilayer formation
The border of the cup is shown in grey which makes contact with the torus of the lipids surrounding the planar lipid bilayer (forming in the middle). The forces that are involved in thinning the bilayer are labelled in red, and forces that stabilise the bilayer by opposing the thinning forces are labelled in blue. The forces include the Plateau-Gibbs border suction

(1), van der Waals forces (2), steric repulsive forces (3) and viscous drag of solvent out of the forming bilayer (4).

2.4 The voltage-clamp technique and bilayer detection

2.4.1 The voltage-clamp technique

A planar lipid bilayer represents a capacitor that is capable of storing charge that builds up on either side of a dielectric medium (an insulator) in an electric field.

A steady-state charge on a capacitor is expressed as:

$$\boldsymbol{Q = V C}$$

Equation 1

which states that the amount of charge (**Q**) on a capacitor is dependent upon the potential difference (**V**) and is related to the specific capacitance (**C**).

When the voltage changes across the capacitor, a current is generated, since current (**I**) is defined as the change in charge (**Q**) with time:

$$\boldsymbol{I = C \frac{\Delta V}{\Delta t}}$$

Equation 2

An ion-channel acts as a resistor (R_m) [units of Gigaohms (GΩ)], or in inverse terms, as a conductor ($\rho_m = R_m^{-1}$) [units of picoseimens (pS)]. When an ion-channel is reconstituted in the bilayer, a current can flow through the open ion-channel, therefore, the total current of

the membrane is given by the sum of the currents across the bilayer ($C\ \frac{\Delta V}{\Delta t}$) and the current flowing through the ion-channel (I_i).

$$\boldsymbol{I\ =\ Ii + C\ \frac{\Delta V}{\Delta t}}$$

Equation 3

In our single-channel experiments, the membrane potential is voltage-clamped at 0 mV ($\frac{dV}{dt}\ =\ 0$) and, therefore, the current measured during our experiments is due to the ions flowing through the ion-channel only.

In order to voltage-clamp the artificial membrane, two electrodes were connected to the BC-535 bilayer clamp amplifier. One electrode measured the voltage input, and the other electrode passed a feedback current in order to maintain the voltage constant during current fluxes through the bilayer.

2.4.2 Bilayer measurement

The formation of the bilayer was monitored by measuring the membrane capacitance using the capacitance test (CAPTEST) function on the amplifier, to determine the size and quality of the artificial bilayer created.

The capacitance of the bilayer is directly proportional to its surface area and dielectric constant (**ε**), and is inversely proportional to the thickness of the bilayer (***d***):

$$\boldsymbol{C\ =\ \varepsilon\ \frac{A}{d}}$$

Equation 4

where, ε is the dielectric constant, d is the distance between the two sides of the plates and A is the area. Equation 2 can be expressed by taking the time derivative of the charge, thus

$$\boldsymbol{I = \varepsilon \frac{A}{d} \frac{\Delta V}{\Delta t}}$$

Equation 5

In our experiments, ε depends on the lipids used and d depends on the length of the lipid tails. During the formation of the bilayer, a triangular wave is applied to the membrane, therefore $\frac{\Delta V}{\Delta t}$ is also a constant (by definition, a triangular wave has a constant rate of voltage change). Thus we can express equation X as:

$$\boldsymbol{I = k A}$$

Equation 6

where k is a constant of proportionality and A is the area of the developing bilayer.

Under the experimental conditions described in this thesis, formation of a bilayer was characterised by a capacitance of 80 - 100 pF.

2.5 Incorporation of SR vesicles

A bilayer was painted in symmetrical 210 mM KPIPES, pH 7.2 and LSR vesicles were incorporated into the membrane by a combination of stirring and applying an osmotic gradient. A gradient of high salt solution was created by adding approximately 500 mM KCl to the *cis* chamber. In the osmotic gradient, the vesicles swelled and adhered to the bilayer. This led to the lysis of the vesicle and subsequent fusion with the membrane. Figure 2.5 illustrates the process. Following the incorporation of vesicles at this stage and in the

solutions above, it was possible to observe current fluctuations derived from Cl^- channels and/or K^+ channels.

After a fusion event, the *cis* chamber was perfused with 10 volumes of 210 mM KPIPES, pH 7.2, to ensure removal of the KCl gradient. There is evidence that SR vesicles incorporate into the lipid bilayers in a fixed orientation, so that the *cis* chamber corresponds to the cytosolic side of the incorporated channels and the *trans* chamber to the SR lumen (79).

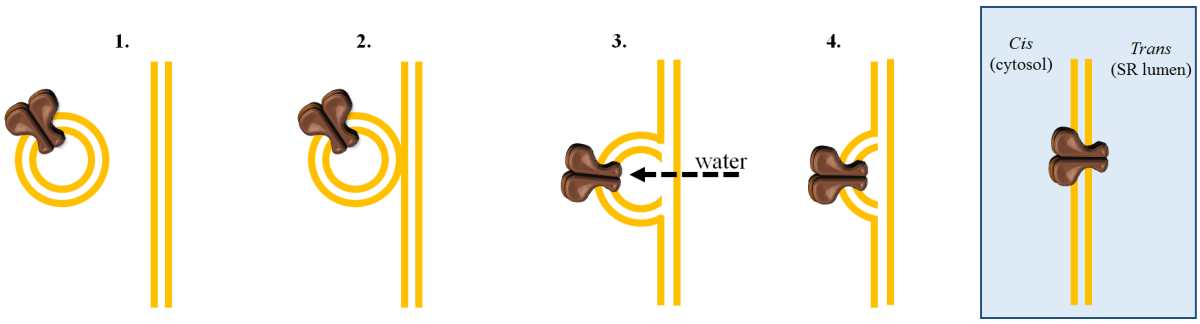


Figure 2.5 Incorporation of ion-channels into planar lipid bilayers.
Vesicles containing SR ion-channels were added into the *cis* compartment (1, 2). Due to an osmotic gradient the vesicles swell (3) and fuse with the membrane (4). SR ion-channels incorporate into the bilayer in a fixed orientation.

2.6 Analysis of single-channel recordings

2.6.1 Data Acquisition

To record single-channel events, the analogue signal from the amplifier was converted to digital form by the Instrutech ITC18 interface (HEKA, Elektronik Lambrecht/Pfalz, Germany). The signal was then resampled using the program WinEDRv3.05 (John Dempster, Strathclyde University, UK). During the digitisation process, it is important to select the optimum sample frequency (f_s) in order to reconstruct the signal accurately.

Failure to do so will result in the signal being distorted (termed aliasing). According to the Nyquist-Shannon Sampling Theorem, the optimal sampling frequency must be at least twice the frequency(B) of the original signal (123, 124).

$$f_s > 2B$$

Equation 7

We chose a sampling frequency that was 10 times greater than the filtered signal. The amplifier contained an internal low-pass 4-pole Bessel filter which filtered the data at 10 kHz, and therefore, our sampling frequency was 100 kHz. Sampling frequency is measured in sample per unit of time therefore, the optimal sample interval in our procedure was 0.01 msec.

$$f_s = \frac{1}{sec} = 10B$$

Equation 8

Following digitisation, the data were filtered further at 1 kHz using a low pass filter built into the WinEDRv3.3.1 software. This further filtering removed any high frequency noise to reduce the likelihood of mistaking background noise as single-channel events.

2.6.2 Single-channel analysis

2.6.2.1 Current amplitude measurements

An ion-channel, when incorporated into an artificial membrane, behaves as a conductor, providing a conductive pathway across the dielectric barrier formed by the lipid bilayer.

The ionic conductance is the rate of ions travelling through an ion-channel and depends on the permeability of the ion-channel to the particular ion. The conductance is measured in Siemens (S).

For electrophysiology, perhaps the most important law of electricity is Ohm's law. The potential difference between two points linked by a current path with a conductance **G** and a current **I**:

$$\boldsymbol{I = \frac{V}{R}}$$

Equation 9

The reciprocal of the resistance **R** is the conductance **G**, defined as:

$$\boldsymbol{G = \frac{I}{V}}$$

Equation 10

where ***I*** is the measured current flow through the channel and ***V*** is the voltage across the membrane.

Single-channel current amplitude measurements were performed using WinEDRv3.3.1. Cursers were manually positioned on the closed level (baseline) and on an opening to the fully open channel level that was longer than 20 ms and the difference between the two levels was noted.

Current-amplitude measurements were repeated at different holding potentials so that a current-voltage relationship could be constructed. The slope of the current-voltage

relationship, calculated using linear regression, corresponds to the conductance of the channel.

2.6.2.2 Idealisation and open probability

Typical single channel recordings in voltage-dependent K^+ channels show two simple conductance states: open or closed. When the channel is open, ions flow through the channel producing a current measured in PicoAmperes (pA); when the channel is closed there is no current through the channel. The duration of time that the channel spends in either state is called the 'dwell time'. The activity of a channel can be quantified by calculating the open probability (Po), defined as the fraction of time the channel remained in the open conformation.

The first step in calculating the Po of a channel is to idealise the recording, generating a train of closed and open events from the raw single-channel trace. Traditionally, when a channel only has two conductance levels, Po is calculated by half-amplitude threshold crossing. The 50 % threshold level is defined as half of the maximum current amplitude of the channel, and, any opening that reaches the 50 % threshold is detected and binned as an open event. This method of analysis has been used in our laboratory to study the gating of RyR with Ca^{2+} or K^+ as the permeant ion.

This simple two-conductance model of K^+ channels, described above, was experimentally challenged by Chapman et al (1997) (125) when they observed intermediate conductance levels in drk1 K^+ channels. They found that the subconductance levels were usually extremely short lived, and they could be interpreted as an artefact produced by very fast gating observed under a limited bandwidth. However, often they observed subconductance levels that were longer-lived, exceeding the rise time of the filter. They suggested that these

intermediate current levels were a result of the channel residing in a certain conformation that produced a current of a smaller conductance.

In our recordings of SR K^+ channels, we observed both types of sub-conductance gating; we saw short-lived flickery transitions between levels, and, longer lived dwellings in sub-conductance levels. We measured sub-conductance levels that had amplitudes less than 50 % of the full open channel level, and so, we concluded that Po analysis using the 50 % threshold method would not adequately analyse sub-conducting levels. To idealise recordings that contained subconductance levels, we used the segmental k-means (SKM) algorithm in the QuB software suite (www.*qub*.*buffalo*.edu).

The SKM algorithm uses a hidden Markov model (HMM) to infer the state transitions under an observed, noisy, signal. A HHM is a Markov model in which the system being modelled is assumed to be a Markov process with unobserved (*hidden*) states. A Markov process is a memoryless statistical process in which transitions between states are assumed to occur independently of previous states. A HMM consists of:

- A state/transition backbone that defines how many states there are and outlines the possible route transitions that can occur between states
- A set of probability distributions, one for each state, which specifies the distribution of events that have been assigned to that state

The SKM technique uniquely assigns each observation to one state given the assumptions provided above.

2.6.2.2.1 Pre-processing data

In order to prepare our traces for SKM analysis, we had to export the recordings from WinEDR as ABF files so they could be opened within the QuB software. In QuB, we resampled each file at 10 kHz and and applied a 1 kHz Gaussian digital filter to visualise

the trace. We visually inspected each recording and we excluded any electrical noise and/or capacitance spikes from the data before analysis.

2.6.2.2.2 Idealisation

The Po of the SR K^+ channel has been analysed in this laboratory using two different models outlined below:

- A six state Markov model (M1) consisting of the closed, fully open channel level and the four observed sub-conductance levels with full connectivity between all states (Venturi *et al* (2013)) (126)
- A three-state Markov model (M2) consisting of the closed, fully open level and a single 'merged' conductance level (Matyjaszkiewicz et al (2015)) (127)

Both models are shown in Figure 2.6.

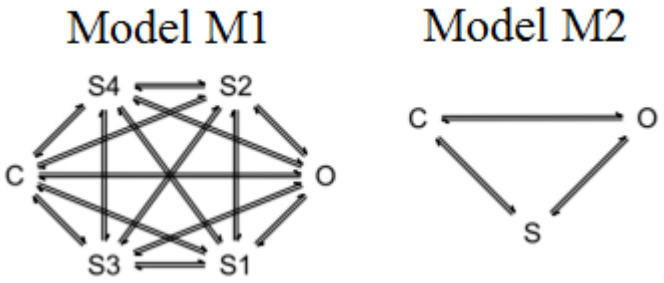


Figure 2.6 Illustration of model topologies used to idealise SR K^+ channel Po

In a recent paper, Matyjaszkiewicz *et al* (2015) (3) extensively described the ability of model M2 to accurately idealise the current fluctuations from SK K^+ channel openings. They directly compared the idealisation of each trace using M1 and M2, and concluded that model M2 provided an adequate idealisation of the recording, and that misclassifications of levels were rare. The comparison of the SR K^+ channel idealisation

produced by M1 and M2 is compared in Figure 2.7. The numerical value for the rate constants for models M1 and M2 are reported in Matyjaszkiewicz *et al* (2015) (3).

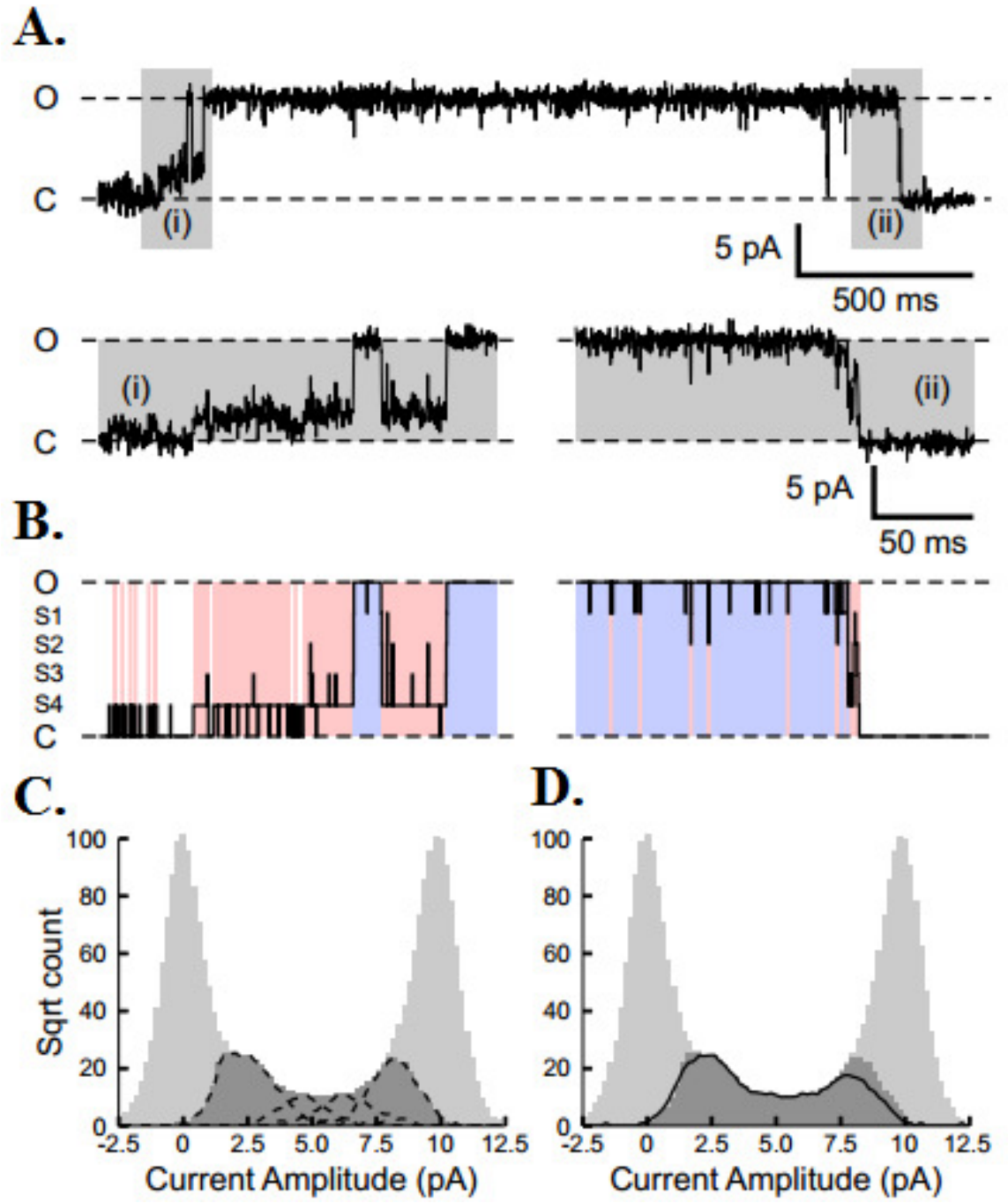


Figure 2.7 Comparison of the idealisation of the single-channel recordings using model M1 and M2.
The trace in (A) shows a representative opening burst at +50 mV after filtering at 1 kHz. O and C represent the fully open and closed levels, respectively. The grey boxes highlight typical subconductance events observed during the transition to (i) and from (ii) the full open channel level. In B, the opening and closing events highlighted in grey were idealised using models M1 and M2 for comparison. The solid black lines in (B) show the idealisation obtained using model M1, with the amplitudes of the sub-conductance levels labelled S1–

S4 on the left. Idealisation of the same data using model M2 is represented by colours, where pink regions are classified as subconductance levels and blue regions as the fully open level. The all point amplitude histograms compare the idealisation produced from Model M1 (C) or M2 (D). The light grey segments show the all-points amplitude distribution for the entire recording. The dashed lines in (C) show the amplitude distributions of data points classified as subconductance states in model M1. The solid line in (D) shows the amplitude distribution of subconductance states classified by model M2. This figure was adapted from Matyjaszkiewicz *et al* (2015) (3).

In this thesis, because we had experiments that contained more than one channel gating in the bilayer, we analysed all recordings using the M2 model, unless otherwise stated. We now outline the specific process used to idealise our data using the M2 model.

The three-state Markov model M2 consisted of the closed, open and one merged sub-conductance states using our initial estimates of the current amplitudes of the conductance states. The closed and the full conductance level were highlighted manually on the recording in QuB, and the parameters of the highlighted sections were applied to state 1 (the closed state) and state 3 (the fully open state), respectively, using the QuB software.

After building the model, the Viterbi algorithm [2, 5] was applied in order to estimate the best fit to our data based on the log-likelihood function value. The parameters of the model were then used to plot amplitude probability density functions which were superimposed on the all-points amplitude histogram. The idealisations obtained with the SKM method were also superimposed on the single-channel traces to visually examine the accuracy of the method.

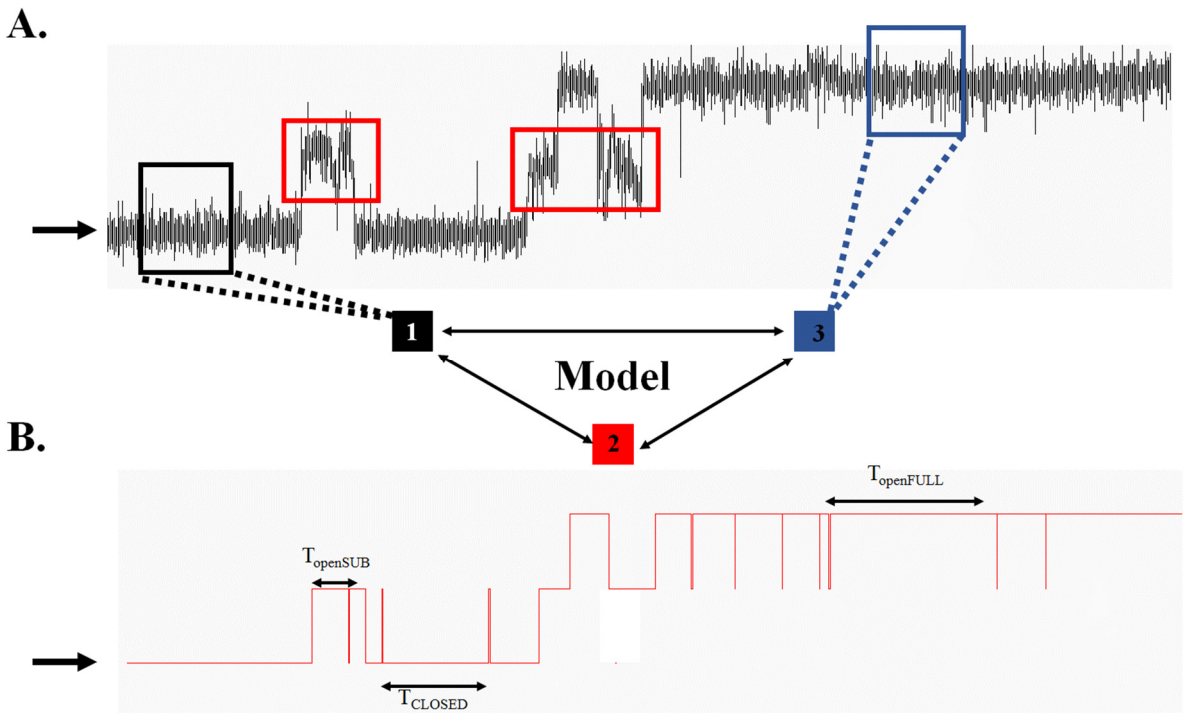


Figure 2.8 Single-channel event detection using SKM analysis.
A. Panel A shows a typical single SR K^+ channel recording after filtering at 1 kHz. The zero current level is specified with the black arrows. The closed and the full open channel levels of the channel are indicated by the black and blue box, respectively. Subconductance gating is highlighted by the red boxes. The model below, consisted of three levels. Level 1 and level 3 were 'grabbed' from the recording (using the 'grab' feature in QuB) as shown by the red and blue dotted lines. The parameters of level 2 were manually entered. The result of the SKM analysis is an idealised trace shown in **B.** T_{closed}, $T_{openSUB}$ and $T_{openFULL}$ represent the time that the channel spends in the closed, a sub-conductance level and the full open channel level, respectively.

The idealised conductance levels were represented by Gaussian fits to single-channel current amplitude distributions according to the equation

$$f(I) = \frac{Po}{\sqrt{2\pi\sigma^2}} exp\left(\frac{-(I-\mu)^2}{2\sigma^2}\right)$$

Equation 11

where I is the current, *Po* is the channel occupancy probability in a given state, μ is the mean current amplitude for the given state and σ is its open channel noise (standard deviation of the current).

The Gaussian fits for each state of the model were superimposed on an all-points amplitude histogram of the recording to visualise the fitting. An example of the all points histogram is shown in Figure 2.9 . To further examine the fit of the model to the data, we visually inspected the trace to ensure all levels were correctly assigned to the appropriate model state.

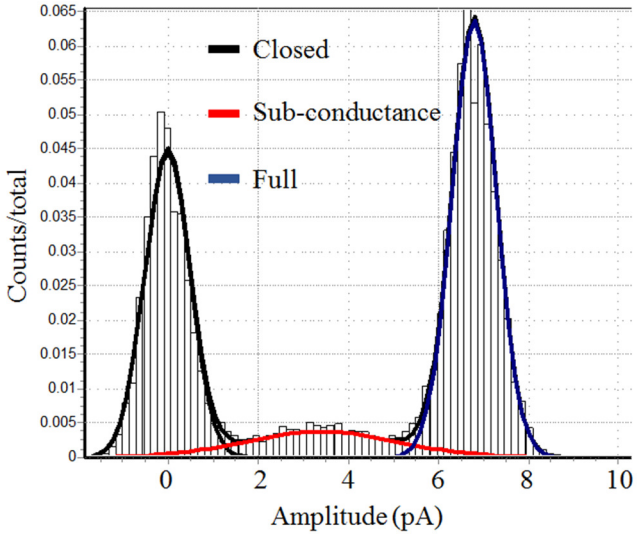


Figure 2.9 A representative all-points histogram of the recording shown in Figure 2.8.
Gaussian distributions were computed using the SKM algorithm for the closed, the open and the sub-conductance states. The thick black trace represents the sum of the Gaussians (the combined fit of the model's state amplitudes to the filtered data).

From the idealisation, occupancy probability (Po) for each conductance class of the model was calculated using the formula below

$$Po = \frac{T_{\text{openFULL}} + T_{\text{openSUB}}}{T_{\text{total}}}$$

Equation 12

Where T_{openFULL} is the time that the channel spends in the full open channel level, T_{openSUB} is the time that the channel spends in a substate, and T_{total} is the total length of the trace.

The overall Po can be split into the Po in the full open channel level (Po_{FULL}) and the Po in the subconductance states (Po_{SUB}). Po values were calculated using the formulas below

$$\boldsymbol{Po_{\text{FULL}} = \frac{T_{\text{openFULL}}}{T_{\text{total}}}}$$

Equation 13

$$\boldsymbol{Po_{\text{SUB}} = \frac{T_{\text{openSUB}}}{T_{\text{total}}}}$$

Equation 14

This formula is appropriate *only* in the case where a single channel is gating in the bilayer. When multiple channels are present it is necessary to calculate the average Po of *n* channels using the formula

$$\boldsymbol{Po = \frac{\sum_1^n nT_{open(n)}}{nT_{total}}}$$

Equation 15

for example, for three channels gating simultaneously,

$$\boldsymbol{Po = \frac{T_{open1} + 2T_{open2} + 3T_{open3}}{3T_{total}}}$$

Equation 16

2.6.3 Life time analysis

An ion-channel is thought to exist in an infinite number of conformations, however only a limited number of these are stable enough for us to detect in our recordings. Although Po analysis can tell us about overall changes in ion-channel gating, it is only a simplified approximation of the channel behaviour. By performing additional analysis, termed 'lifetime analysis' we can extract further details about the gating of the channel. Lifetime analysis can be carried out when only a single-channel is gating in the bilayer.

We now outline our procedure for performing lifetime analysis on SR K^+ channels. Recordings were idealised in QuB using model M2, and events shorter than 0.6 ms were stripped from the idealisation. We exported the idealised event sequences from QuB to Clampfit, where lifetime analysis was performed.

The durations that the channel spent in each state was visualised by arranging the events in histograms and plotting the events on a logarithmic scale for the abscissa and a square root scale for the ordinate (128). The *y* axis of the histograms was divided into intervals (bins) of event durations while the *x* axis represented the dwell time durations.

The histograms were fit with with one or more exponentials and the dwell time distributions corresponded to the sum of the different exponentials. A probability density function (pdf) was then be used to fit the data.

The pdf of a single exponential is represented by:

$$f_{(t)} = \frac{1}{\tau} \exp\left(\frac{-t}{\tau}\right)$$

Equation 17

where $f_{(t)}$ is the probability that the channel will be in a dwell time of duration t, τ is the time constant equal to the mean of the durations within the distribution.

When the dwell time distributions required more than one exponential, a sum of exponential pdfs is necessary according to the equation

$$f_{(t)} = \sum_{i=1}^{n} \frac{a_i}{\tau_i} \exp\left(\frac{-t}{\tau_i}\right)$$

Equation 18

where a is the relative area corresponding to the time constant (τ).

The fitting of an exponential pdf was first done manually and the values of the manual fit were used as the starting point to estimate the "most likely" pdf for a distribution of open or closed events for a specified number of exponentials using 'maximum likelihood' fitting (129). The parameters a and τ of the model were modified in order to reach the optimum likelihood, L. The number of exponentials that best fit the distribution was determined using the likelihood ratio test (130).

2.6.4 Noise analysis

Noise analysis is a type of analysis most commonly applied to whole cell currents, however, it can be used in single-channel recordings to estimate channel activity, especially when there is more than one channel gating in the bilayer. We used the noise analysis application in the WinEDR software to calculate the mean current that flows through the bilayer over the length of the recording. In brief, current fluctuations across the bilayer

were subdivided into multiple segments in time, with each segment containing **N** samples. The mean current for each sample was calculated using the formula

$$\boldsymbol{I}_{\mathbf{mean}} = \frac{\sum_{i=1}^{n} \boldsymbol{I}(\boldsymbol{i})}{\boldsymbol{N}}$$

Equation 19

where *I(i)* is the amplitude of the *i*th of the N samples in the segment. The mean current samples are then plotted against time.

2.7 Measurement of free Ca^{2+}

The free [Ca^{2+}] and pH of the bilayer recording solutions were measured using a Ca^{2+}-selective electrode (Orion 93-20) and a Ross-type pH electrode (Orion 81-55). Experiments were carried out at room temperature (22 ± 2 °C).

2.8 Statistics

Data were expressed as mean ± SD (standard deviation) where n=3 and mean ± SEM (standard error) when $n \geq 4$. Statistical comparisons between groups were performed with a two-tailed Student's T-test. Differences between mean values were considered statistically significant when $p < 0.05$. For comparison of three or more groups, a one way analysis of variance (ANOVA) test was performed, followed by a Bonferroni paired test.

2.9 Chemical compounds

Chemical compounds used in this thesis, were purchased from Sigma Aldrich Company Ltd (Gillingham, UK) if not otherwise stated.

3 Comparison of the biophysical properties of the SR K^+ channels from TRIC-A KO and WT skeletal muscle

3.1 Introduction

As described previously, when native SR vesicles are fused to artificial bilayers, it is thought that the SR K^+ current fluctuations that are observed may result from distinct openings of TRIC-A and TRIC-B (101). When purified TRIC-A and TRIC-B were incorporated into bilayers, it was shown that the biophysical properties of both channels were so similar, that it would be almost impossible to distinguish the gating of TRIC-A from the gating of TRIC-B when native SR vesicles are fused to bilayers (101). The use of purified TRIC-proteins is therefore required to fully characterise the gating of each isoform in isolation. Obtaining purified TRIC-proteins has proved difficult however, partly because high yield preparations are obtained with detergents such as n-Decyl-β-D-maltopyranoside (DM) or n-Dodecyl-β-D-maltopyranoside (DDM) and trace levels of these detergents can lead to artefacts in the bilayer. Using detergents such as 3-[(3-Cholamidopropyl)dimethylammonio]-1-propanesulfonate (CHAPS) yield low levels of proteins and infrequent incorporations into the bilayer for characterisation (unpublished observations).

The viability of the TRIC-A KO mouse has enabled researchers to study SR K^+ channels in the absence of TRIC-A. The TRIC-A KO mouse appears normal and can survive until adulthood however, there are SR structural abnormalities and Ca^{2+} release is compromised (113). The SR appears swollen with visible concentrated Ca^{2+} deposits (113). Moreover, isolated TRIC-A KO skeletal muscle often displayed "alternans" behaviour reflected by the transient and alternate increases of contractile force during fatigue stimulations (113).

The first description of the K^+ channels that were observed when the SR from TRIC-A KO tissue was fused with artificial membranes was provided by Venturi *et al* (2013) (126) and later in another paper by Matyjaszkiewicz *et al* (2015) (127). Both papers described a multi-conductance K^+ channel with a maximum conductance of approximately 200 pS and at

least 4 observable sub-conductance levels. In addition, most channels were voltage-dependent with the Po higher at +30 mV compared to -30 mV (126, 127).

Venturi *et al* (2013) postulated that the SR K^+ channels that were observed were likely to be TRIC-B channels since TRIC-A was not present in the preparations (126). They suggested that the higher conductance observed in TRIC-B channels (200 pS) compared to the purified TRIC-B channel (138 pS) could be caused by damage to the purified TRIC-B channels during isolation, purification and reconstitution into bilayers (126). This seemed likely because the apparent full conductance (138 pS) of the purified TRIC-B protein was identical to the a main sub-conductance level of both the native SR K^+ channels from TRIC-A KO tissue and the purified TRIC-A proteins (101). The complex gating of the native SR K^+ channels from TRIC-A KO tissue that have not been exposed to detergent or subjected to lengthy purification protocols and that were reported in both papers, reiterates the complications that appear to result when the TRIC-isoforms are purified

The aim of this chapter was therefore to characterise and compare the biophysical properties of the SR K^+ channels from TRIC-A KO and WT tissue, by incorporating the LSR into artificial bilayers to record the current fluctuations that were observed.

3.2 Methods

3.2.1 Po-voltage relationships

To investigate the effect of voltage on the gating of ion-channels, usually Po is plotted against increments of holding voltage. When plotted, for voltage-dependent channels, these experiments can show a sigmoidal voltage dependence and is typically characterized by fitting to a single Boltzmann equation (131-134). For such a curve, the chemical free energy difference between the open and the closed state is defined by ∆G, which is characterized by two parameters: *z*, the Boltzmann slope, and $V_{1/2}$, the voltage that elicits the half-maximal response. This free energy difference is also referred to as the free energy of channel opening at zero voltage.

In our experiments, we recorded SR K^+ channels over a range of voltages and calculated Po according to section 2.6.2.2. We fitted Po_{FULL} by a Boltzmann equation according to the formula:

$$\boldsymbol{Po(V) = PoMAX\left\{1 + \exp\left(\frac{[\triangle\, G + zFV]}{RT}\right)\right\} - 1}$$

Equation 20

Where ∆G is the internal free energy of opening, z is the effective gating charge, Po_{MAX} is the maximum Po, R is the universal gas constant, T is temperature in °K and F is the Faraday constant.

3.3 Results

3.3.1 TRIC-A KO

Venturi *et al* (2013) (126) characterised the K^+ fluctuations that were observed when the LSR from TRIC-A KO was incorporated into artificial membranes. They described a multi-conductance K^+ channel that exhibited variable gating properties. In the majority of experiments (6/8 single-channel recordings), Venturi *et al* (2013) observed a voltage-dependent K^+ channel that opened predominately in the full open channel level. The remaining 2/8 single-channel recordings gated predominately in sub-conductance states, with only brief openings to the full open channel level. Of the 2 experiments that gated primarily in sub-conductance levels, one experiment was voltage-dependent and the other was voltage independent. For Po analysis, particularly when investigating voltage-dependent behaviour of ion-channels, this paper highlighted the importance of separating the voltage-dependent channels from the voltage-independent channels.

In this chapter, I present 17 single-channel recordings from TRIC-A KO mice that were obtained from 5 preparations. The skeletal muscle from 10 mice was used for each SR membrane vesicle preparation.

It is worth noting that the 17 recordings in this chapter do not include the 8 single-channel recordings that appeared in Matyjaszkiewicz *et al* (2015) (127).

The various gating patterns observed in the 17 experiments are outlined in Table 3-1.

N NUMBER	VOLTAGE-DEPENDENT OR VOLTAGE-INDEPENDENT?	PREDOMINATELY FULL OPEN LEVEL OR SUB-CONDUCTANCE LEVELS?
12	Voltage-dependent	Full open
3	Voltage-dependent	Sub-conductance
2	Voltage-independent	Sub-conductance

Table 3-1. The various types of SR K^+ channel gating characteristics observed in single-channel recordings from TRIC-A KO tissue.

In this thesis, and in publications from this laboratory (126, 127), the voltage-dependent SR K^+ channel that gated predominately in the full open channel level was observed most frequently. Considering that this gating pattern has also been heavily documented in the literature by other groups (82, 85, 89-92, 94, 135) , I refer to this type of channel as the 'typical' SR K^+ channel.

3.3.2 Contribution of other lab members to the data in this chapter.

In this chapter, I compared the gating of the SR K^+ channels from TRIC-A KO and WT tissue. The 24 single-channel traces (17 experiments from TRIC-A KO and 7 experiments from WT tissue) were all recorded and analysed by myself.

3.3.3 The gating characteristics of SR K^+ channels from TRIC-A KO tissue

I monitored the current fluctuations observed when LSR vesicles, isolated from the skeletal muscle of TRIC-A KO mice, were incorporated into artificial bilayers in symmetrical solutions of 210 mM KPIPES, pH 7.2. As outlined in section 3.3.1, in agreement with Venturi *et al* (2013) (126), I observed SR K^+ channels that opened to multiple conductance levels with variable channel gating. However, irrespective of the gating pattern, the dwell times in the full open channel level could be easily identified. A typical recording, as shown in Figure 3.1, illustrates the key gating characteristics of the SR K^+ channels that were most commonly observed (12/17 experiments).

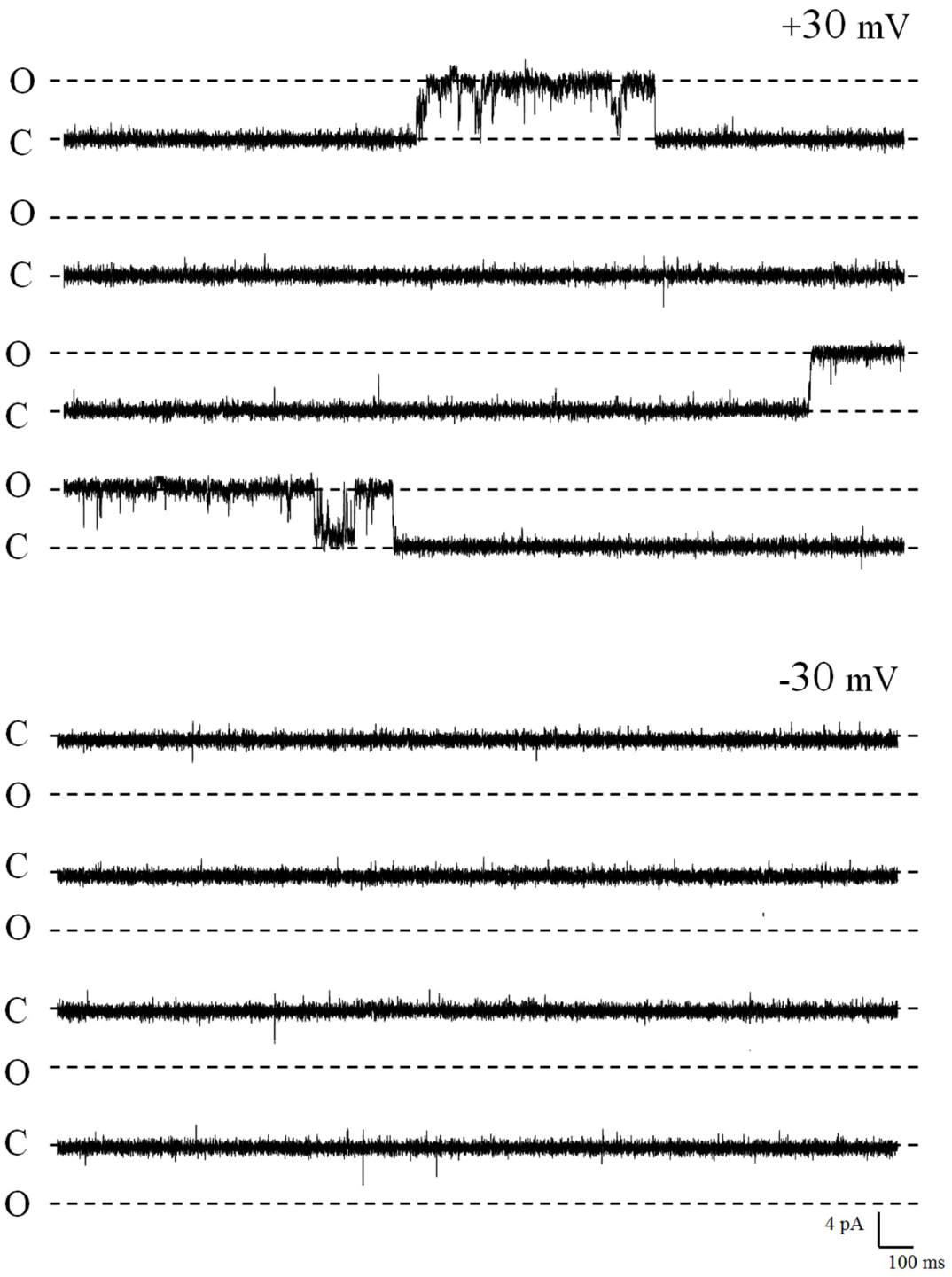


Figure 3.1. A representative trace illustrating the typical gating properties of the SR K^+ channels from TRIC-A KO.
The traces show the single-channel activity at +30 mV (top traces) and at -30 mV (bottom traces). O and C indicate the full open and closed levels, respectively. The recording was low pass filtered at 1 kHz.

3.3.3.1 The conductance of the SR K^+ channels from TRIC-A KO tissue

We obtained current-amplitude measurements over a range of voltages for the full open channel level. The resulting current-voltage relationship is shown in Figure 3.2.

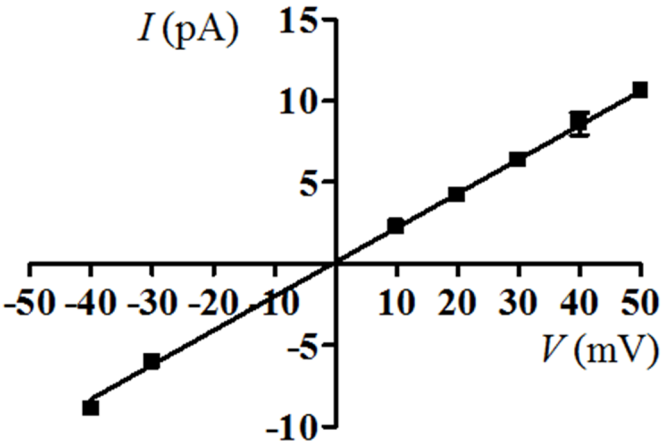


Figure 3.2 Current-voltage relationship of the full open channel level of the SR K^+ channel from TRIC-A KO tissue Linear regression of the current–voltage relationships for the full open channel level yields a conductance of 209 ± 0.003 pS (n=16, SEM). Error bars are within the symbol if not visible

3.3.3.2 The gating of the 'typical' SR K^+ channels from TRIC-A KO tissue

A representative trace illustrating the key gating properties of the 'typical' SR K^+ channels is shown in Figure 3.1. The majority of openings consisted of long-lived dwell times in the full open channel level that occurred via sub-conductance events. Although the sub-conductance gating of the channels appeared complex, there were certain gating patterns that we observed. As illustrated in Figure 3.3, sub-conductance gating often appeared as a very noisy singular level approximately 50 % of the full open channel amplitude (panel A). However, when openings were viewed on an expanded timescale, we could easily identify sub-conductance levels and gating patterns. We observed transitions that occurred between sub-conductance levels that were extremely short-lived (iii and iv) and 'flickery' in appearance and impossible to resolve as individual events. However, we also observed sub-

conductance gating events that appeared to dwell in particular levels for longer periods of time (i, ii, and v) and the current-amplitude could be easily measured from these openings.

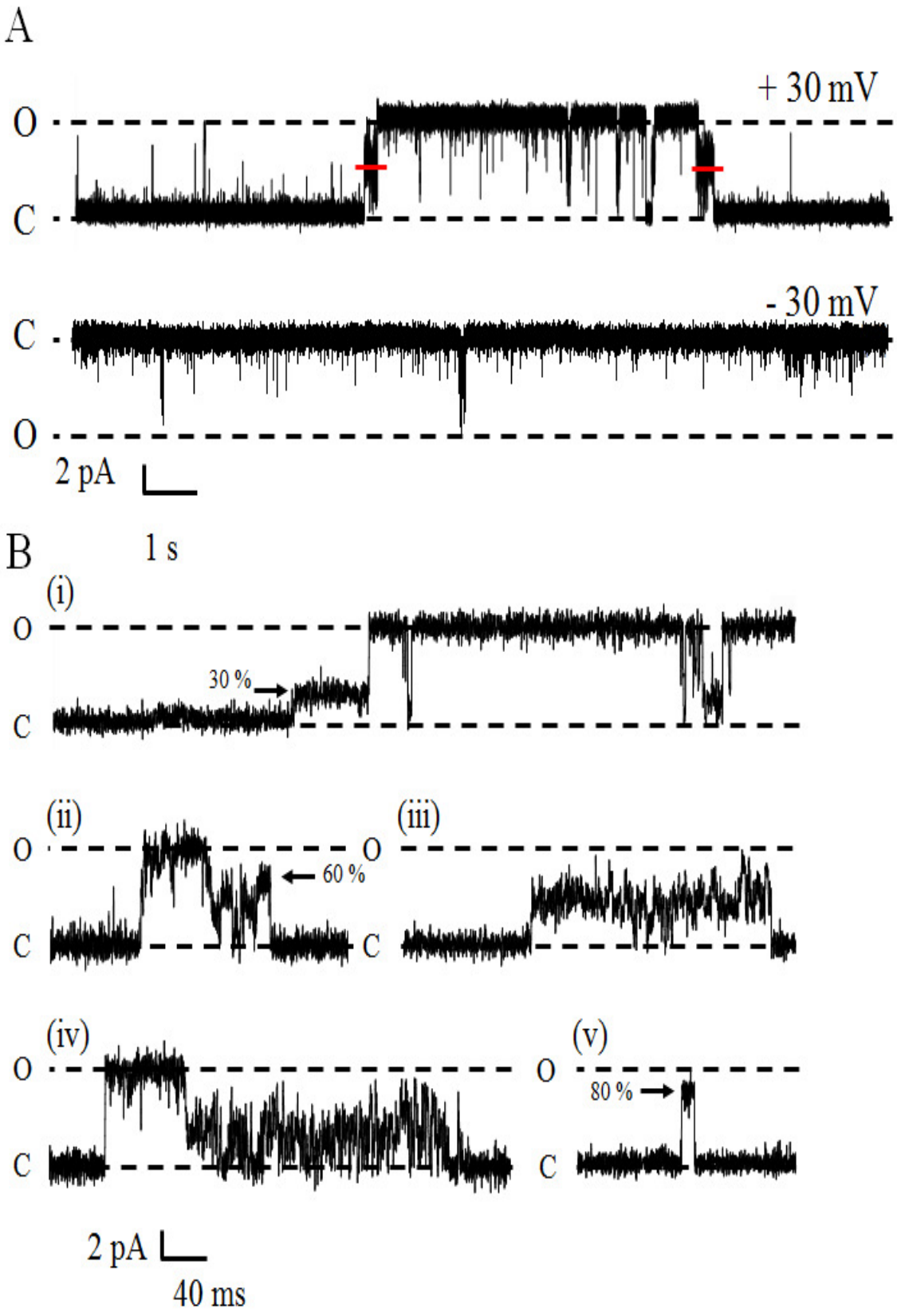


Figure 3.3 Sub-conductance gating patterns observed in SR K^+ channel from TRIC-A KO tissue at +30 mV
A representative single-channel opening burst at +30 mv is shown in A. The red lines illustrate the average current level of the subconductance gating (53 % of the full open level). O and C represent the full open and closed levels respectively. Expanded openings in B. demonstrate typical subconductance gating behaviour. The black arrows indicate sub-conductance gating events that dwelled for long periods of time. This figure has been adapted from Matyjaszkiewicz *et al* 2015 (127), which was originally made using my single-channel recordings.

3.3.3.3 The voltage-dependence of the typical SR K^+ channels

The gating of the SR K+ channel was recorded over 3 min continuous recording at +30 mV and -30 mV. The mean data shown in Figure 3.4 highlights the voltage-dependence of these typical SR K^+ channels from TRIC-A KO tissue. The channels were significantly voltage-dependent, with the Po_{TOTAL} higher at +30 mV compared to -30 mV (***p<0.001). When the Po_{TOTAL} was subdivided into Po_{FULL} and Po_{SUB}, Po_{FULL} was significantly voltage dependent (***p<0.001) and, although the data was not significant for Po_{SUB}, it did appear that the possibility of dwelling in a sub-conductance state was also reduced at -30 mV.

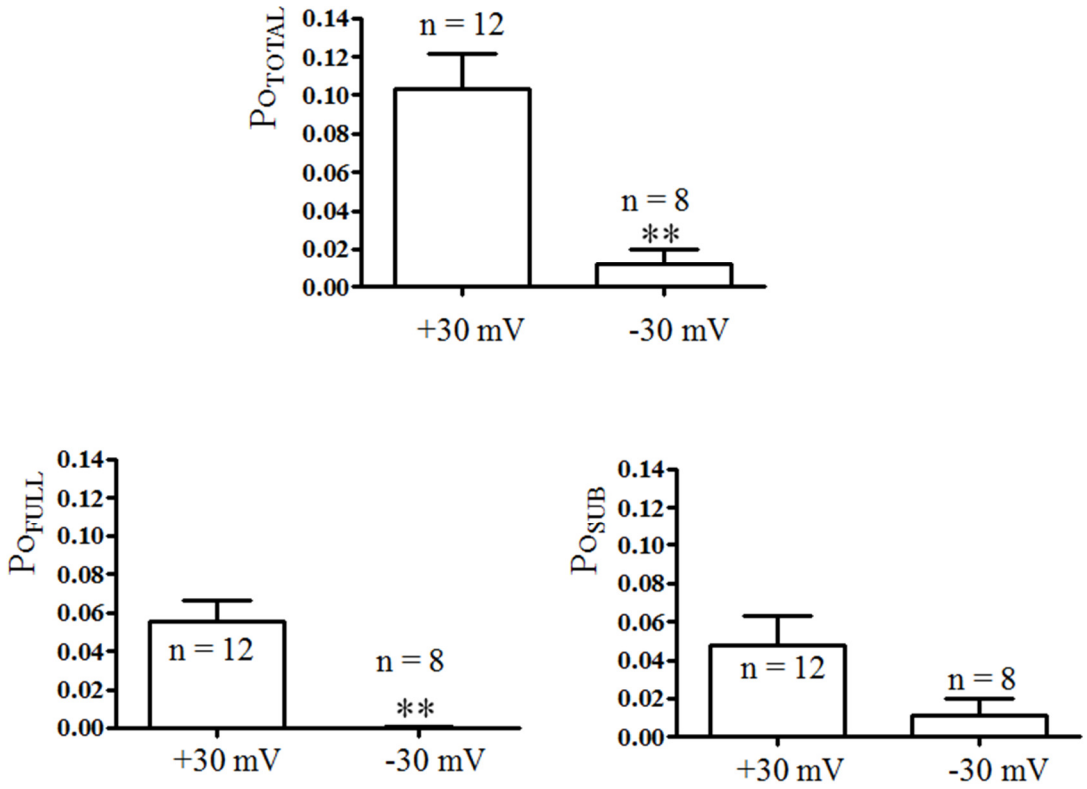


Figure 3.4. The 'typical' SR K^+ channels from TRIC-A KO tissue are voltage-dependent
The Po of the SR K^+ channel at holding potentials of +30 mV and -30 mV is shown. Data are presented as mean ± SEM.

As shown in Figure 3.5 the contribution of Po_{FULL} to the overall Po was significantly greater at +30 mV compared to -30 mV (***p<0.001).

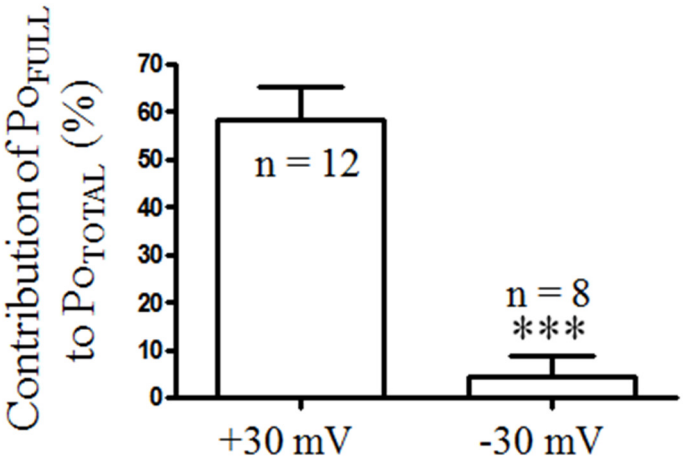


Figure 3.5 The contribution of Po_{FULL} to overall Po of SR K^+ channels from TRIC-A KO tissue
Data are presented as mean ± SEM.

3.3.3.4 Exploring the voltage-dependency of typical SR K^+ channels from TRIC-A KO tissue

To examine voltage-dependence further, we performed additional experiments and voltage-clamped the bilayer at various holding potentials (-40 mV to + 50 mV) to monitor Po. Po was plotted against the holding potential, as shown in Figure 3.6.

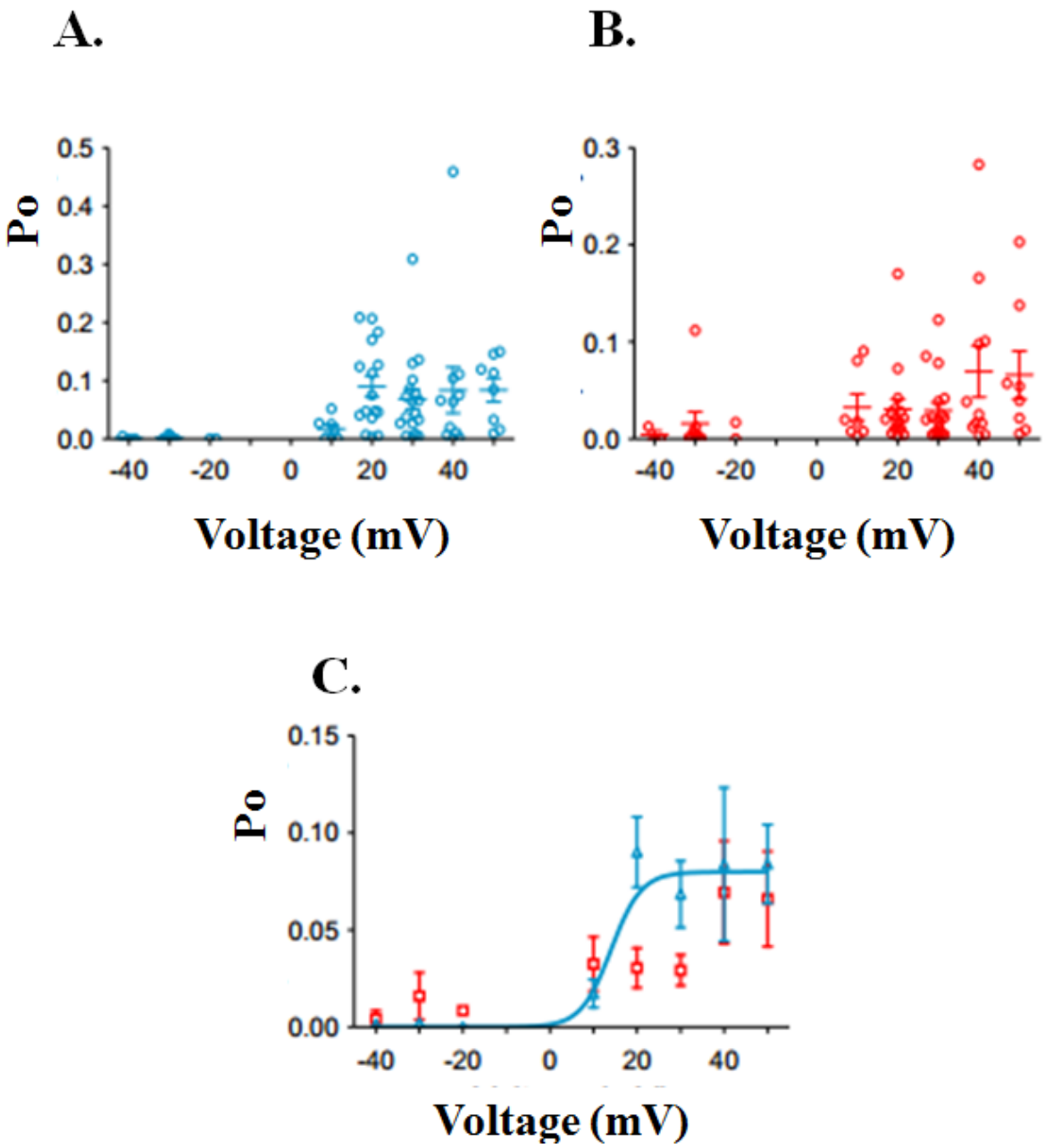


Figure 3.6 The Po-voltage relationship of the SR K^+ channel from TRIC-A KO tissue.
Individual Po values are shown for full (A) and sub-conductance (B) openings as a function of voltage. In C, the mean data illustrates the Po-voltage relationship for Po_{FULL} (blue) and Po_{SUB} (red). The fitted line corresponds to a Boltzmann fit to Po_{FULL} according to the equation in section 3.2.1. The negative z value indicates that negative charge moves in the luminal to cytosolic direction or that positive gating charge moves in the opposite direction as voltage was increased from 0 to +20 mV. The following number of recordings were used at each voltage: -40 mV (3),-30 mV (8),-20 mV (2), 10 mV (7), 20 mV (12), 30 mV (17), 40 mV (10), and 50 mV (8). These recordings were obtained by myself and Elisa Venturi and the figures were made by Antoni Matyjaszkiewicz. This figure was adapted from Matyjaszkiewicz *et al* 2015 (127)

3.3.3.5 Lifetime analysis of the SR K^+ channels from TRIC-A KO tissue

The lifetime durations of the full open and full closed levels were assessed using Model M1 at +30 mV. There were not enough events at -30 mV to perform lifetime analysis. Figure 3.7 shows the lifetime histograms from a representative SR K^+ channel from TRIC-A KO at +30 mV for the full open and closed levels.

At +30 mV, in 4 out of 8 experiments, the events were best fit by three exponentials to the closed lifetime distribution and two exponentials to the open lifetime distribution, indicating at least three closed states and two open gating states, respectively. In the remaining 4 experiments, four closed states and three open states were observed.

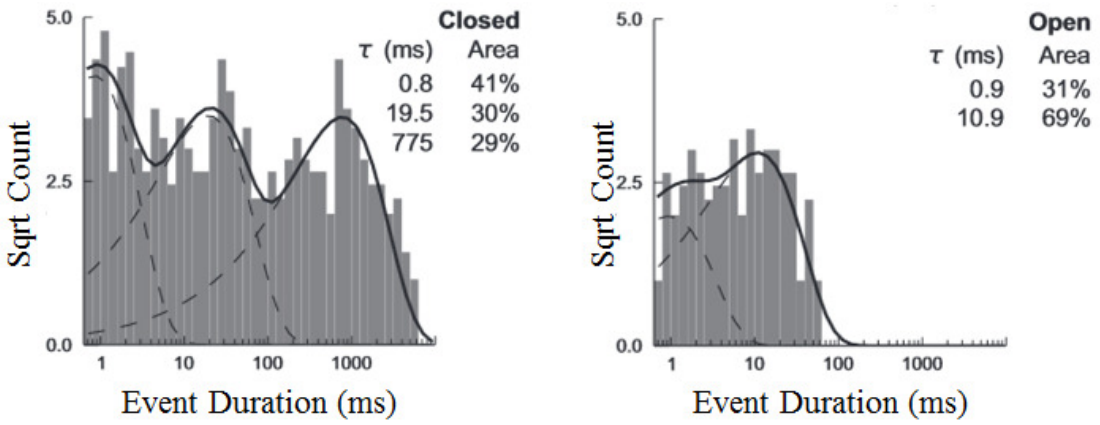


Figure 3.7 Lifetime distributions and probability density functions from a typical SR K^+ channel from TRIC-A KO tissue
Representative lifetime distributions are shown for events from a single-channel recording, idealised using model M1. The histogram on the left shows the closed lifetimes, while the histogram on the right shows the open lifetimes. The best fits to the data were obtained using maximum likelihood fitting. The time constants and percentage areas are shown to the right of each histogram. The experiment was recorded by myself and the analysis performed by Mr. Antoni Matyjaszkiewicz. This figure was adapted from Matyjaszkiewicz *et al* (2015) (127).

3.3.3.6 The effect of voltage on the mean open and closed times

We wanted to investigate whether the mean open or mean closed times change with increments of voltage. For each idealised trace, the event lifetimes in QuB was exported to Microsoft excel. Event durations were grouped into columns based on their assigned state (closed, full open or sub-conductance) and the average dwell time of each column was calculated. We plotted the values for the closed, the full and the sub-conductance states against the holding potential, as illustrated in Figure 3.8. There was no change in the mean open time of the sub-conductance open channel level as the voltage was increased. This was not unexpected since the duration of these events was always close to or less than the minimum resolvable duration. Mean closed time decreased with increasing voltage and we have demonstrated that this is the main mechanism why which voltage regulates Po (127). No significant increases in mean open time was observed although longer open times were

observed at the higher positive potentials (≥ +20 mV). In fact, it is difficult to tease out the significant changes here because although there may be an increase in burst length, the open bursts are truncated by very brief closings.

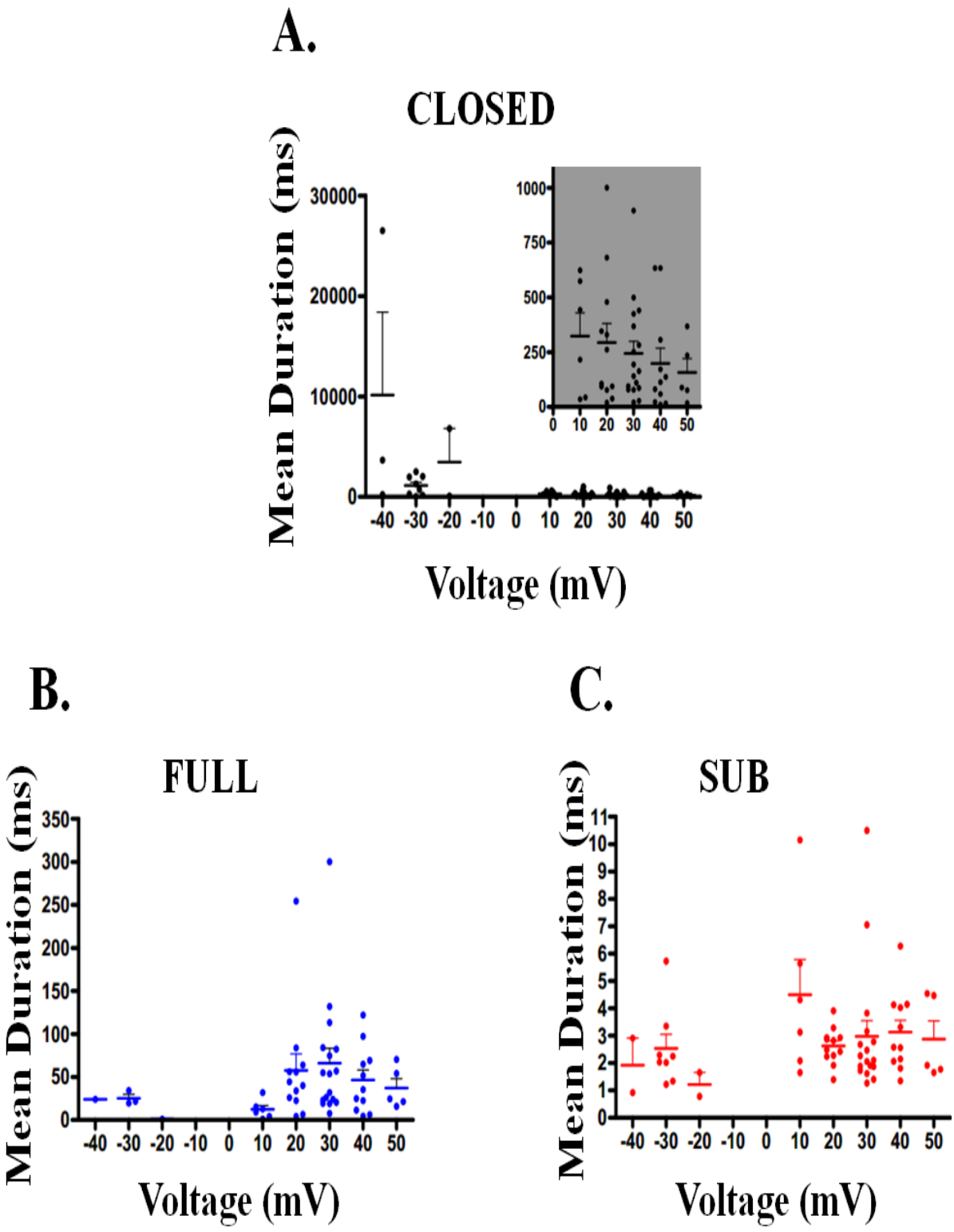


Figure 3.8 The mean open and closed times of the SR K^+ channel from TRIC-A KO tissue as a function of voltage

Mean durations are shown for the closed (A), full open level (B) and sub-conductance levels (C) over a range of voltages. The following number of recordings were used at each voltage: -40 mV (3),-30 mV (8),-20 mV (2), 10 mV (7), 20 mV (12), 30 mV (17), 40 mV (10), and 50 mV (8). These recordings were obtained by myself and Elisa Venturi and analysis was done by Antoni Matyjaszkiewicz.

3.3.3.7 Investigating the transition routes between the closed and fully open channel level in the 'typical SR K^+ channel from TRIC-A KO tissue

As we discussed in Section 3.3.3.2 , transitions between the full closed and the full open channel level appeared to occur via the sub-conductance levels. In rare occasions, we observed a transition that did not appear to go through a sub-conductance level. However, when we increased the cut off frequency of the filter, as shown in Figure 3.9, we found evidence for possible sub-conductance levels.

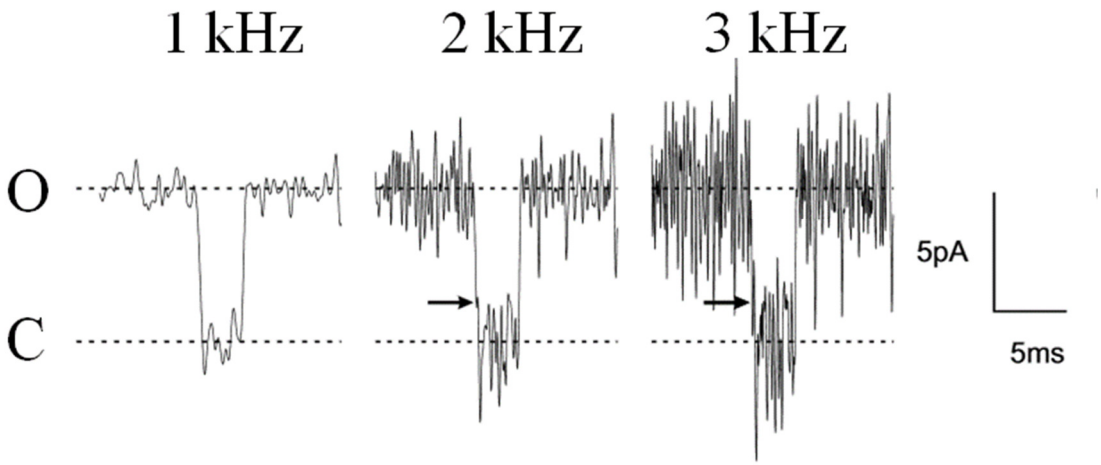


Figure 3.9 Transitions between the full open and closed channel
Arrows indicate the possible sub-conductance levels that emerge as the filtering level is altered from 1 kHz (left), to 2 kHz (middle) and 3 kHz (right). The holding potential was +30 mV. This figure was adapted from in Matyjaszkiewicz et al (2015) (127).

The total number of detected transitions, and the number of direct transitions between the fully open and the fully closed states were calculated for the 8 voltage-dependent experiments that were used in Matyjaszkiewicz et al (2015) (127). The data are shown in Table 3-2.

	TOTAL NUMBER OF TRANSITIONS	DIRECT OPEN-CLOSED TRANSITIONS	PERCENTAGE OF TOTAL
MODEL M1	90839	12	0.013 %
MODEL M2	63538	7	0.011 %

Table 3-2 Observed number of direct transitions between the full closed and full open conductance levels
Each experiment was idealised with Models M1 and M2 (both shown in Figure 2.6). Only roughly 0.01 % of all transitions were potentially direct transitions (not occurring via sub-conductance states). This table is adapted from Matyjaszkiewicz et al (2015) (127). The experiments were recorded by myself and Dr. Elisa Venturi and the analysis was done by Mr. Antoni Matyjaszkiewicz.

3.3.3.8 The 'non-typical' SR K^+ channels from TRIC-A KO tissue

3.3.3.8.1 The voltage-dependent SR K^+ channels that gate predominately in sub-conductance states

In accordance with Venturi *et al* (2013) (126), we recorded SR K^+ channels that were voltage-dependent but gated predominately in sub-conductance open states (3/17 recordings). As the Po of these recordings was quite low, in Figure 3.10, we have shown representative openings (instead of long stretches of data) to illustrate the observed opening events.

We did observe rare 'typical opening bursts' within these recordings (openings that entered and exited the long-lived full open channel level via sub-conductance gating periods, as shown in Figure 3.10 (i)), however, the majority of openings fell into two main categories, outlined below :

- Opening bursts characterised by long periods of sub-conductance gating with brief transitions to the full open state (ii, iii, iv, v).
- Bursts of sub-conductance level gating that occurred without resolvable openings to the full open channel level (vi, vii, viii).

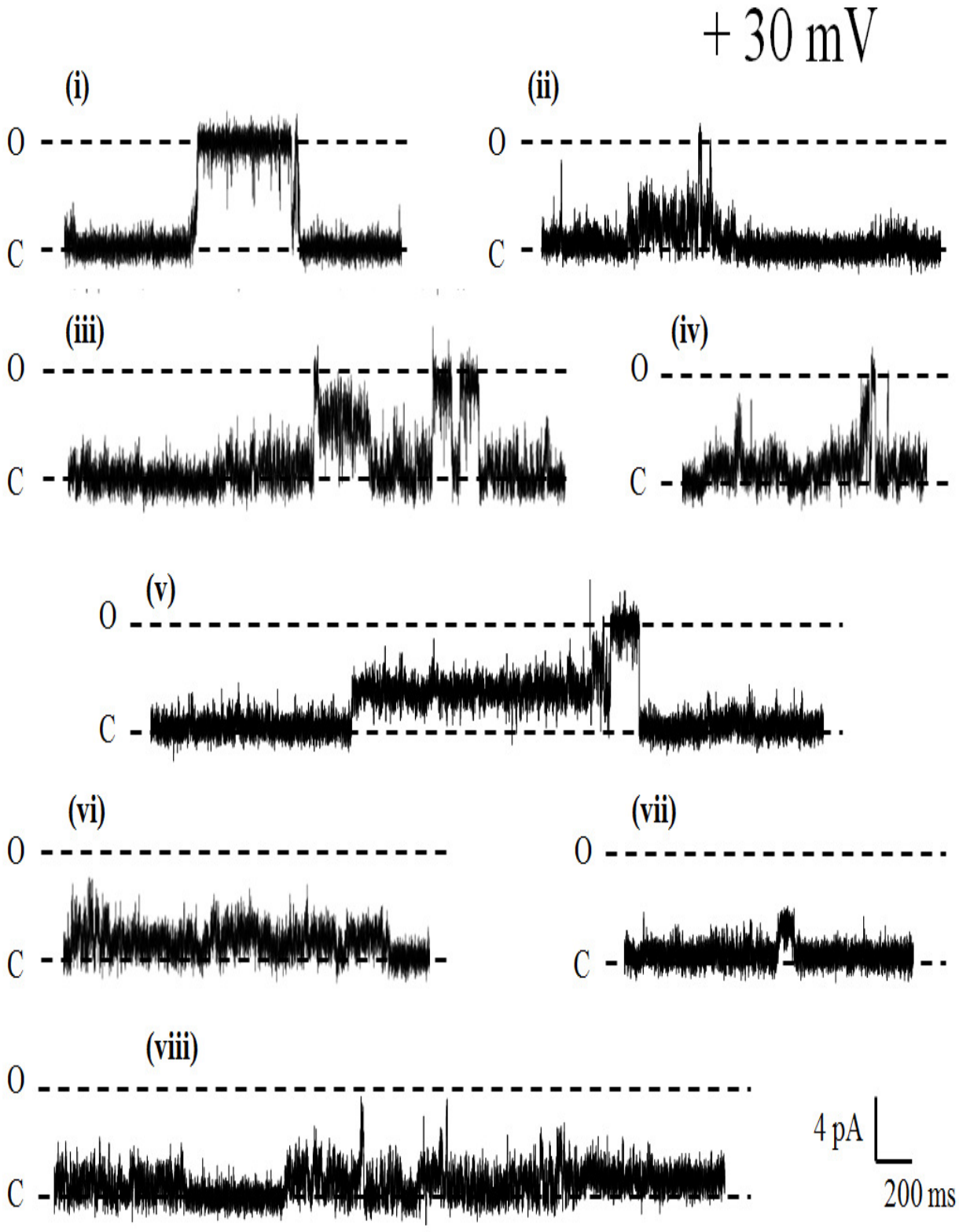


Figure 3.10 Typical openings from the voltage-dependent SR K^+ channels that gate predominately in sub-conductance levels
O and C represent the full open and closed channel levels, respectively.

The mean data, shown in Figure 3.11, illustrates the voltage-dependence of the SR K^+ channels that gate mainly in sub-conductance levels. Although not significant, the channels appeared to be voltage-dependent, with very little channel activity at -30 mV compared to +30 mV (n=3, SD). The overall voltage-dependence of these channels bears gross similarity to that of the 'typical' voltage-dependent channels.

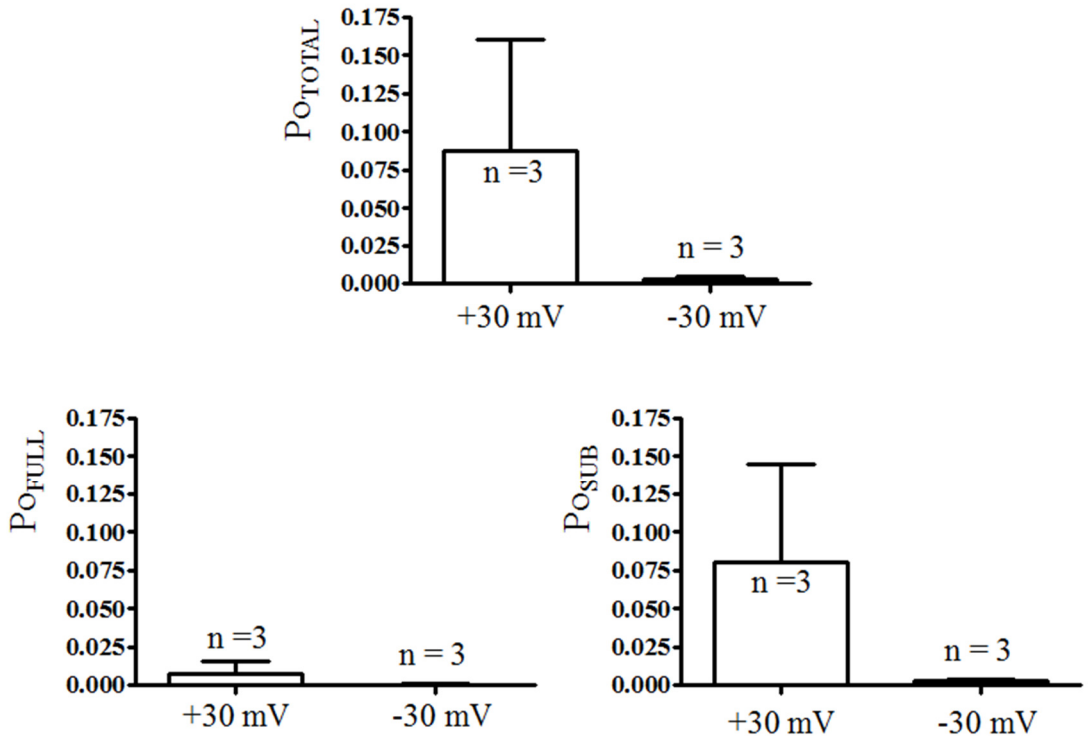


Figure 3.11 The voltage-dependence of the SR K^+ channels from TRIC-A KO tissue that gate predominately in sub-conductance open states
The bar charts show the Po_{TOTAL}, Po_{FULL} and Po_{SUB} of the SR K^+ channels that gate predominately in sub-conductance states. Data are presented as Mean ± SD.

As shown in Figure 3.12, the contribution of Po_{FULL} to the overall Po was extremely low in the voltage-dependent SR K^+ channels that gate mainly in sub-conductance levels. In addition, there was no change in the contribution of Po_{FULL} at +30 mV compared to -30 mV.

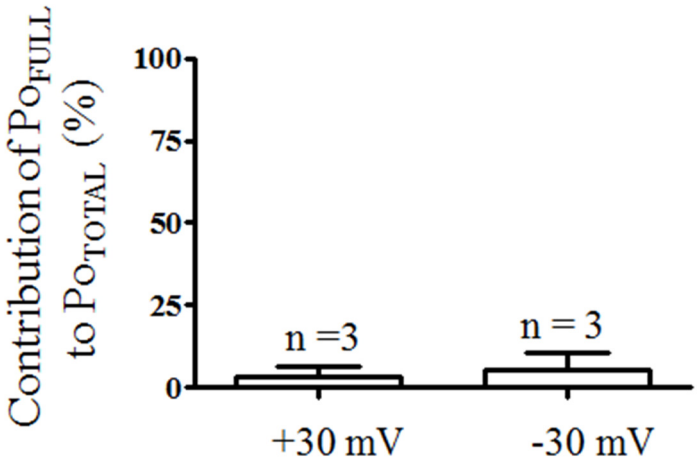


Figure 3.12 The contribution of Po_{FULL} to overall Po of the voltage-dependent SR K^+ channels that gate predominately in a sub-conductance level.
Data are presented as Mean ± SD.

3.3.3.8.2 The voltage-independent SR K^+ channels

2/17 experiments from TRIC-A KO were voltage-independent. The gating in both of these recordings was predominately in sub-conductance levels, with the channels rarely opening to the full open channel level. Representative gating behaviour is illustrated in

Figure 3.13.

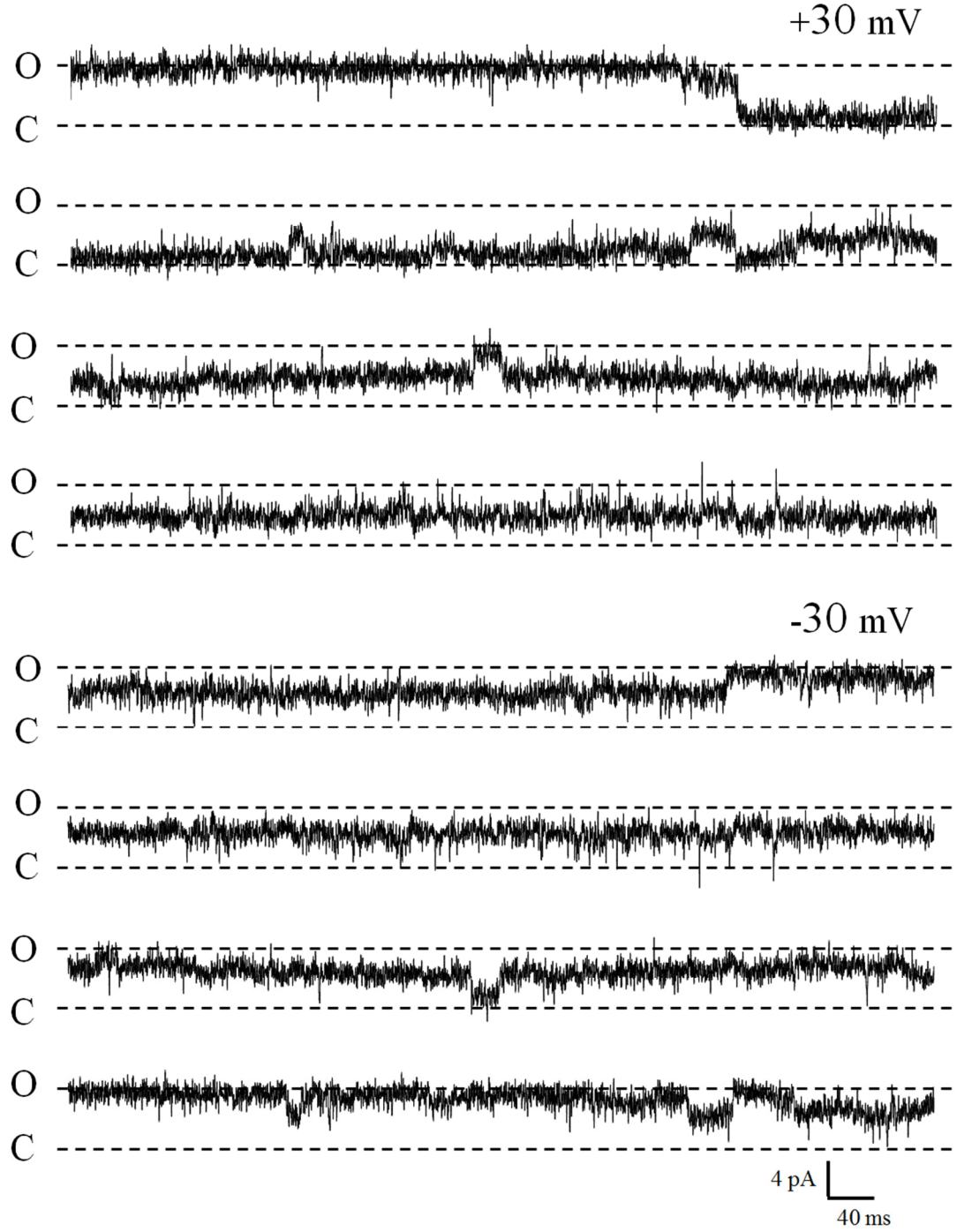


Figure 3.13 Representative gating behaviour of voltage-independent SR K^+ channels
The traces show the single-channel activity at +30 mV (top traces) and at -30 mV (bottom traces). O and C indicate the full open and closed levels, respectively. The recording was low pass filtered at 1 KHz.

The mean data illustrating the Po of the voltage-independent channels from TRIC-A KO tissue is shown in Figure 3.14.

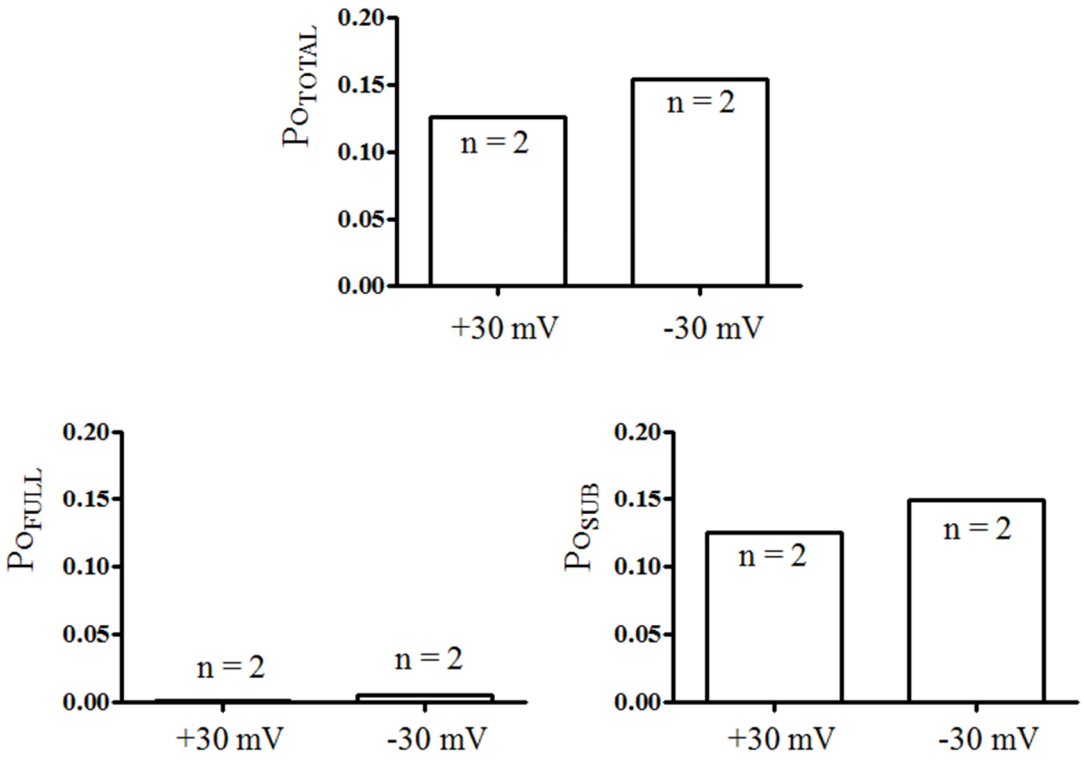


Figure 3.14 The Po of the voltage-independent SR K^+ channels from TRIC-A KO tissue.
The bar charts show the mean Po_{TOTAL}, Po_{FULL} and Po_{SUB} of the SR K^+ channels that gate predominately in sub-conductance states.

As seen in Figure 3.15 the contribution of the full open channel level in the voltage-independent channels is low at ±30 mV. It is possible that these channels have incorporated into the bilayer in the opposite orientation. However, if this was the case then it would be expected that Po_{TOTAL} and Po_{FULL} would be higher at -30 mV.

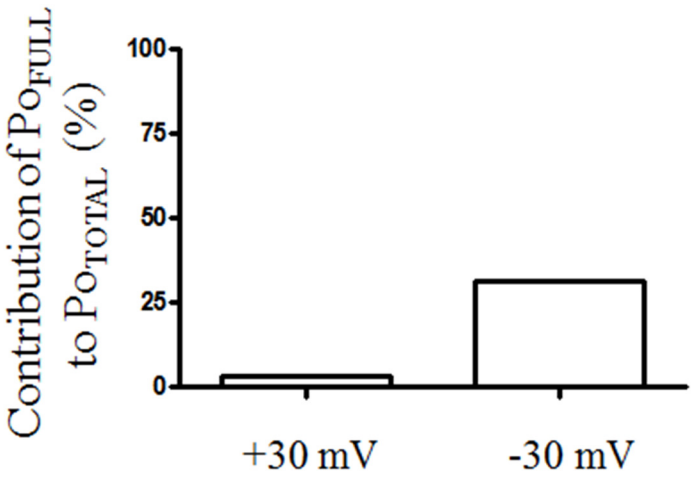


Figure 3.15 The contribution of Po_{FULL} to overall Po of the voltage-independent SR K^+ channels.
The mean data from 2 experiments are shown.

3.3.4 The gating characteristics of SR K^+ channels from WT mouse skeletal muscle

We incorporated LSR from WT mice of identical strain and age as those used in KO experiments, into artificial membranes and recorded the single-channel current fluctuations in symmetrical solutions of 210 mM KPIPES, pH 7.2.

As seen in Figure 3.16, the gating characteristics of the typical SR K^+ channels observed most frequently from WT skeletal muscle were similar to those observed in TRIC-A KO tissue.

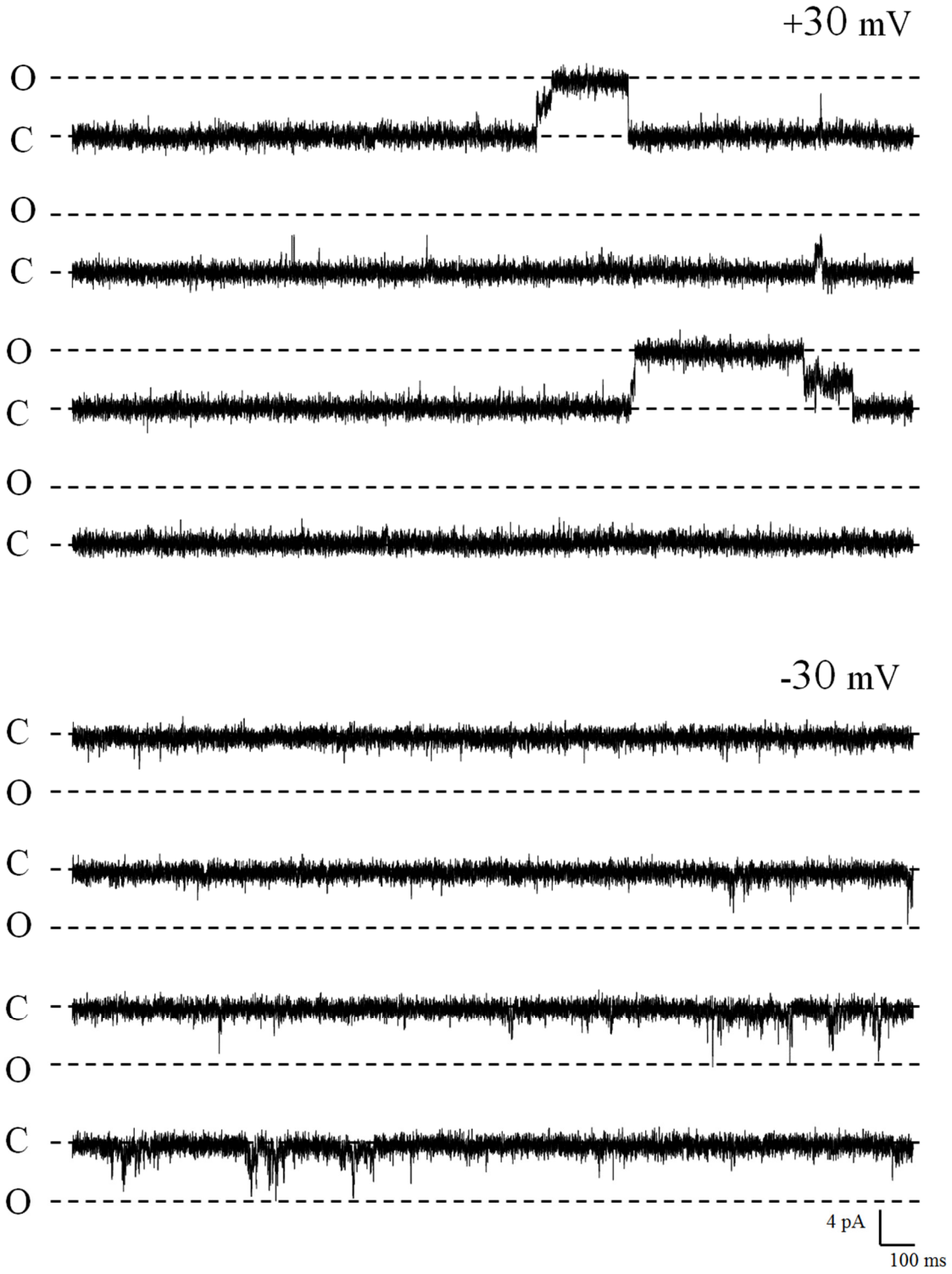


Figure 3.16 A representative trace illustrating the typical gating properties of the SR K^+ channels from WT skeletal muscle.
The traces show the single-channel activity at +30 mV (top traces) and at -30 mV (bottom traces). O and C indicate the full open and closed levels, respectively. The recording was low pass filtered at 1 kHz.

3.3.4.1 The conductance of the SR K^+ channels from WT tissue

Amplitude measurements were obtained over a range of voltages (±50) for the full open channel level only. The resulting current-voltage relationship is shown in Figure 3.17. The current–voltage relationships for the channel yields a conductance of 210 pS for the full open channel level.

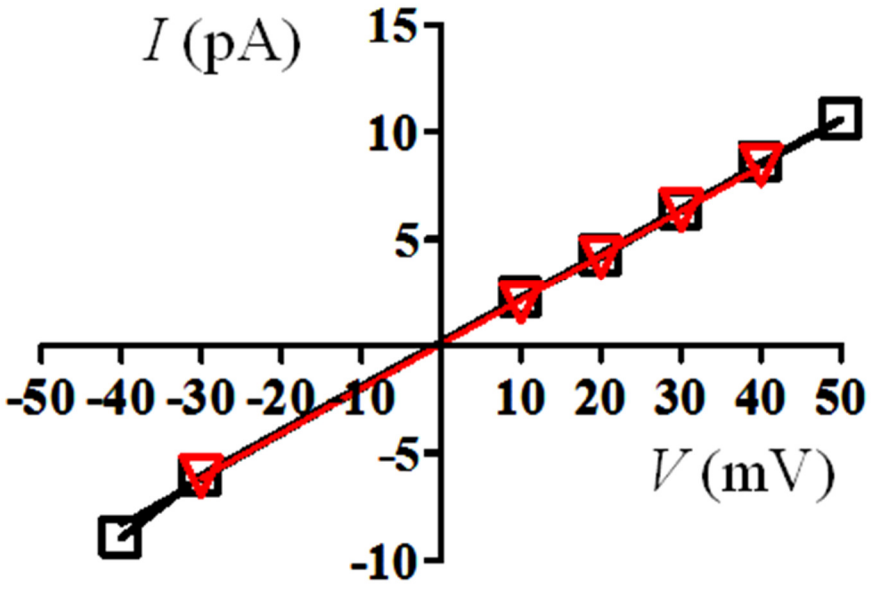


Figure 3.17 Current-voltage relationship of the full open channel level of the SR K^+ channel from WT
The conductance of the SR K^+ channel from WT tissue is shown in red, and from TRIC-A KO is shown in black. Where errors bars are not shown, they lie within the symbol. (n=6 recording obtained from WT and n=12 recordings obtained from TRIC-A KO.

3.3.4.2 The voltage-dependence of the SR K^+ channels from WT tissue

3.3.4.2.1 The 'typical' SR K^+ channels

Seven single-channel experiments from WT skeletal muscle were obtained. In 6 out of 7 experiments, the 'typical' voltage-dependent SR K^+ channels, similar to the channels observed from TRIC-A KO tissue (that gated predominately in the full open channel level) were observed. In 1 out of 7 a voltage-dependent SR K^+ channel that gated primarily in sub-conductance states was observed. I did not observe any voltage-independent channels, however, this may be due to low n numbers obtained from WT tissue (n=7 from WT compared to n=17 from KO).

The mean data shown in Figure 3.18 compared the voltage-dependence and the contribution of Po_{FULL} of the typical SR K^+ channels from WT tissue (red) compared to those recorded from TRIC-A KO tissue (white).

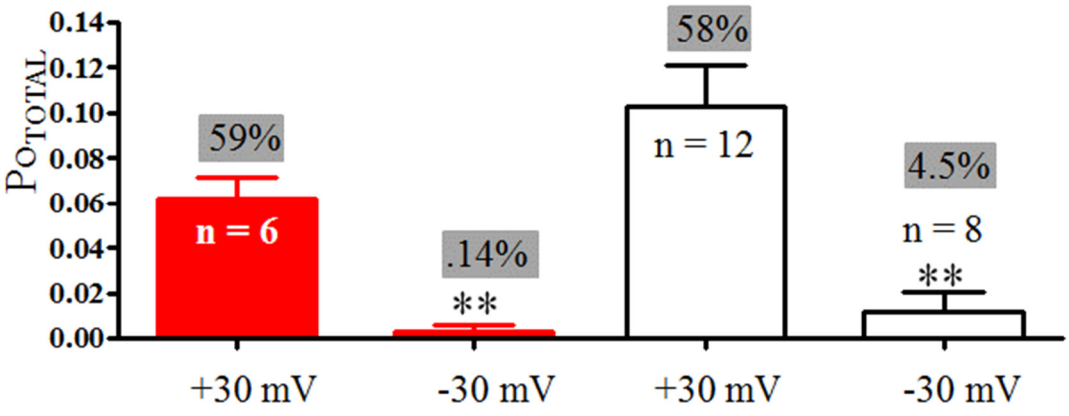


Figure 3.18 SR K^+ channels from WT tissue are voltage-dependent
The Po of the SR K^+ channel at holding potentials of +30 mV and -30 mV for WT (red) and TRIC-A KO (white) is shown. The contribution of Po_{FULL} to Po_{TOTAL} is indicated above each column in a grey box. Data are presented as mean ± SEM. (**$p < 0.01$).

3.3.4.2.2 The 'non-typical' SR K^+ channel

In our recordings from WT, 1/7 SR K^+ channels were voltage-dependent but gated primarily in sub-conductance open states with brief transitions to the fully open channel level. Representative openings from this recording is shown in Figure 3.19. This channel had a $P_{O_{TOTAL}}$ of 0.80 at +30 mV and 0.42 at -30 mV. The contribution of $P_{O_{FULL}}$ was extremely low in this channel (3.8 % at +30 mV and 0 % at -30 mV)

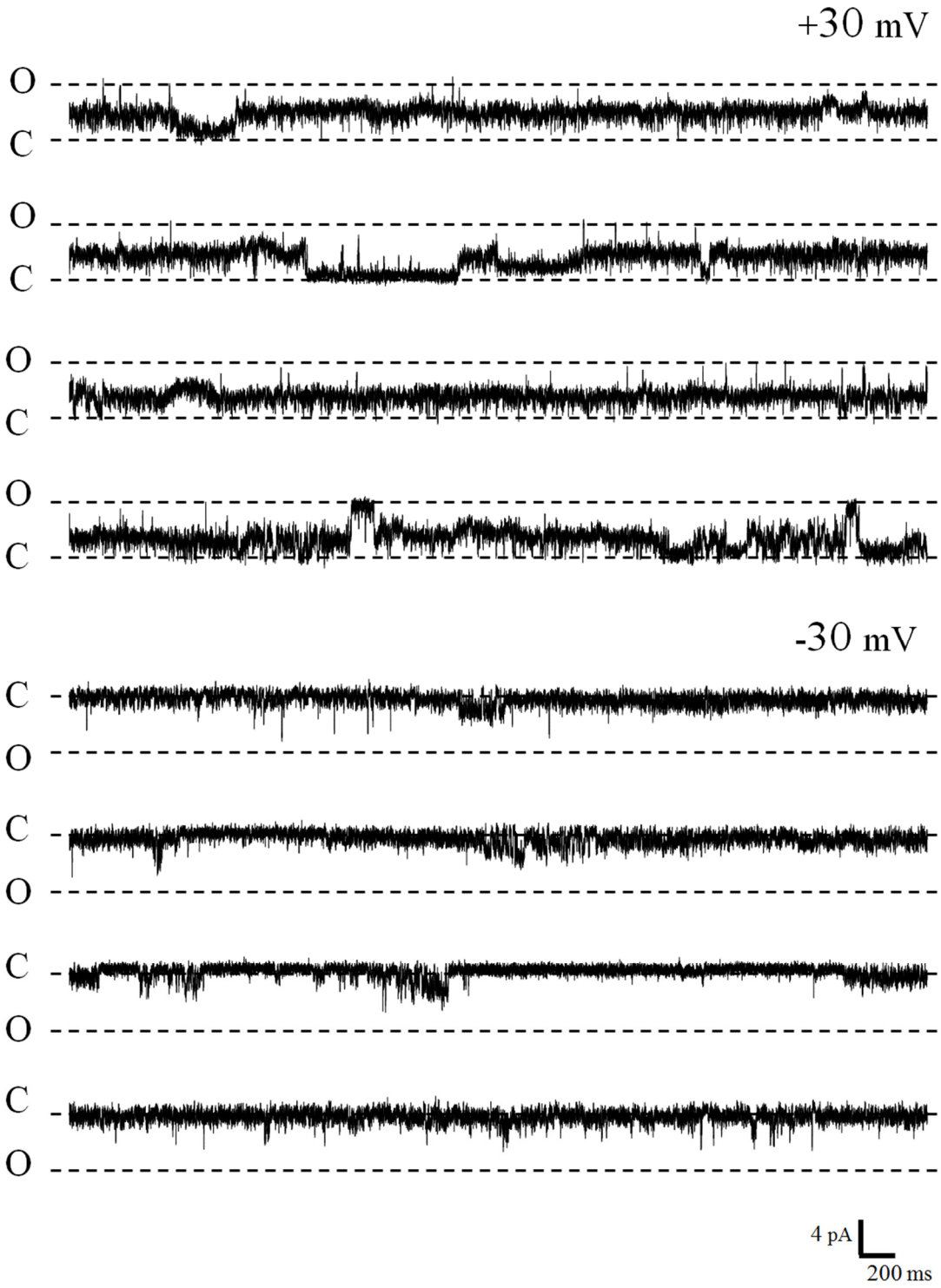


Figure 3.19 Representative gating behaviour of the voltage-dependent SR K^+ channels from WT tissue that gate predominately in sub-conductance states
The traces show the single-channel activity at +30 mV (top traces) and at -30 mV (bottom traces). O and C indicate the full open and closed levels, respectively. The recording was low pass filtered at 1 KHz.

3.4 Comparison of data from WT and TRIC-A KO tissue

The aim of this study was to characterise the single-channel K^+ fluctuations that were observed when the LSR from either TRIC-A KO or WT tissue was fused with artificial membranes. The SR K^+ channels observed in both preparations had wide variability in channel gating, which has been described extensively in Venturi *et al* (2013) (126) and Matyjaszkiewicz *et al* (2015) (127) for the SR K^+ channels from TRIC-A KO tissue. In agreement with these publications, we observed three distinct gating patterns, outlined below:

- Voltage-dependent SR K^+ channels (more open at +30 mV compared to -30 mV), which gate primarily in the full open channel level. This behaviour was observed in 70% of recordings from TRIC-A KO tissue and 85% of recordings from WT tissue.
- Voltage-dependent SR K^+ channels (more open at +30 mV compared to -30 mV), which gated predominately in sub-conductance open states. This behaviour was observed in 18 % of recordings from TRIC-A KO tissue and 15 % of recordings from WT tissue.
- Voltage-independent SR K^+ channels that gated predominately in sub-conductance open states. This behaviour was observed in 12 % of recordings from TRIC-A KO tissue and was not observed in the seven experiments from WT tissue.

Since the typical SR K^+ channel gating is most frequently observed in both preparations, it is the only gating behaviour where there are sufficient observations for a direct comparison between the KO and WT. The table below highlights the similarities of these SR K^+ channels observed in both WT and TRIC-A KO tissue.

	Conductance (pS)	Po at + 30 mV	Po at - 30 mV	% contribution of Po_{FULL} (+30 mV)
TRIC –A KO *(N=12)*	209 ± 0.003	0.10 ± 0.018	0.01 ± 0.008	58 ± 7 %
WT *(n=6)*	210 ± 0.004	0.06 ± 0.009	0.003 ± 0.003	59 ± 8 %

Table 3-3 Comparison of the 'typical' SR K^+ channels from WT and TRIC-A KO prep

From the table above it appears that the Po of the SR K^+ channels from KO tissue at +30 mV may be higher than that of channels from WT tissue. Closer inspection of the individual data points, as shown in Figure 3.20 illustrates the individual Po values. Further insight into possible differences will require more experiments, especially from channels derived from WT tissue.

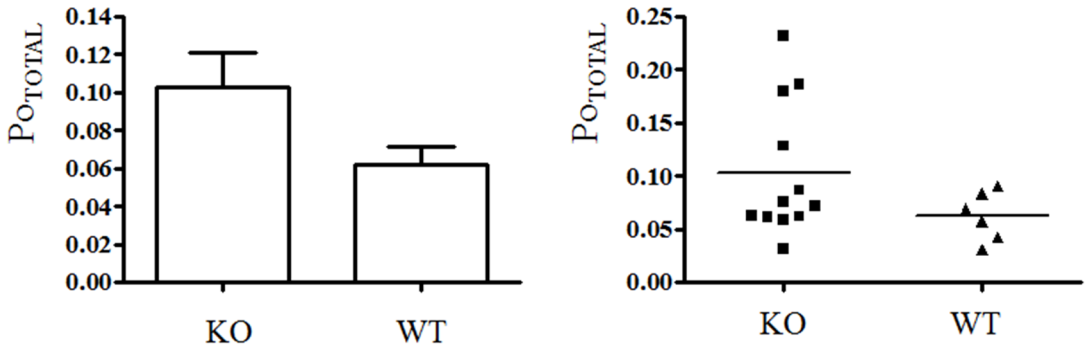


Figure 3.20 Comparison of the Po of the SR K+ channels from TRIC-A KO and WT tissue
The bar chart on the left illustrates the mean Po of the SR K^+ channels from TRIC-A KO and WT at +30 mV. On the right, the individual Po values are shown for comparison.

3.5 Discussion

The objective of this study was to investigate if there were any differences in the single-channel properties of the SR K^+ channels from TRIC-A KO and WT tissue. It is thought that the current-fluctuations that are produced by the combination of gating events from TRIC-A and TRIC-B may underlie the gating of the SR K^+ channel and thus, it was postulated that there may be noticeable differences in the single-channel gating events observed when the native SR K^+ channels from WT and TRIC-A KO tissue were compared.

3.5.1 SR K^+ channels from WT and TRIC-A KO display equally variable gating characteristics

It was presumed that when a K^+ channel that is located on the SR membrane (TRIC-A) was deleted, the resulting SR K^+ channel population would be more homogeneous. We thought that this increased homogeneity in the TRIC-A KO tissue might be detected at the single-channel level and thus, we might observe distinct gating characteristics in the WT preparation that were not observed in the TRIC-A KO preparation. However, in our experimental conditions and when only a single SR K^+ channel was gating in the bilayer, as illustrated in this chapter, this was not the case. In both WT and TRIC-A KO tissue we observed SR K^+ channels that had apparently similar gating characteristics, although, the gating in both cases was extremely variable in nature (refer to Section 3.4 for a summary). The extreme variability in the gating of the SR K^+ channels from mouse TRIC-A KO tissue have been described in previous publications (126, 127) and, thus, we were not surprised that the SR K^+ channels from the WT preparations still exhibited very variable gating behaviour and that no significant differences were observed at the single-channel level. Perhaps additional n numbers (we only recorded 6 single-channel experiments from WT preparations) may be required to identify any obvious differences in SR K^+ channel gating.

3.5.2 Are there subtle differences in the TRIC-A KO and WT preparations?

When SR vesicles from TRIC-A KO tissue were fused to artificial bilayers, we know that the SR K^+ single-channel current fluctuations that were observed could not be due to TRIC-A. Since the gating of the SR K^+ channels from WT tissue were similar to the gating of the SR K^+ channels from TRIC-A KO tissue, one possibility is that the TRIC-B isoform was the channel that was usually observed in the bilayer in experiments from WT preparations. However, in skeletal muscle, the expression level of TRIC-A is approximately 10 fold higher level than the expression level of TRIC-B (101, 113). Therefore, when the SR is isolated from WT skeletal muscle, the resulting SR vesicles are likely to contain significantly more TRIC-A than TRIC-B. Both purified TRIC-A and TRIC-B have been reported to behave as functional K^+ channel when incorporated into bilayers with similar gating properties (101), and therefore, it would be extremely surprising if we did not observe any TRIC-A single-channel events when the SR from WT preparations was fused to artificial bilayers.

As illustrated in Figure 3.20, when we compared the individual Po values from the single-channel experiments in WT and TRIC-A KO tissue, there were several channels from the KO preparation that had a higher Po than those from WT tissue. Additional experiments are required to quantify this observation, but nevertheless it may be of significant importance. If the SR K^+ channel activity is higher in TRIC-A KO preps, there are a number of reasons why this could be. I speculate below.

1. ***TRIC-A has a lower Po than TRIC-B***

When the SR from WT tissue is fused with artificial bilayers, we assume that the SR K^+ channel current fluctuations that are observed are more likely to be from TRIC-A gating than TRIC-B gating, given the high abundance of TRIC-A in skeletal muscle. If we recorded mostly TRIC-A channels from WT tissue (and TRIC-B from TRIC-A KO tissue)

, and if the Po of TRIC-A was lower than the Po of TRIC-B, we would expect the Po of the SR K^+ channels from WT to be lower than those observed from TRIC-A KO mice.

Pitt *et al* (2010) (101) reported that the Po of purified TRIC-A was in fact, greater than the Po of TRIC-B. However, if TRIC-B was damaged so that it was only gating in a sub-conductance level then the Po values may not predict native behaviour. At +30 mV, the Po of TRIC-A was 0.71 and at +50 mV, the Po of TRIC-B was 0.24 (101). While these Po values may be representative of the basic gating properties of the TRIC-channels, it is important to remember that these proteins were purified using detergent and the high Po gating that was observed could be, in part, due to damage to the proteins. For example, when RyRs are purified from HSR (to separate RyR channels from SR K^+ and SR Cl^- channels) and the proteoliposomes containing RyR channels are reconstituted into artificial membranes, the gating observed can occasionally be Ca^{2+}-insensitive, even when the native RyR from the same isolation are Ca^{2+}-sensitive. Sub-conducting levels in RyRs can also be observed in purified preparations.

2. ***Native TRIC-A does not open***

If TRIC-A channels simply gated with an extremely low Po under our experimental conditions, so low that we *never* observed any TRIC-A gating events, we would simply be observing TRIC-B gating events in both the WT and TRIC-A KO preparations. Given the high abundance of TRIC-A in skeletal muscle, the SR vesicles that are incorporated into the bilayers are likely to contain TRIC-A channels, however, these channels may not open (or have very few openings). It is important to remember that just because a particular ion-channel has been shown to be located on the SR membrane, does not imply that this channel will be repeatedly observed in native SR preparations. For example, Mitsugumin 23 (MG23) is a 23 kDa transmembrane protein that has been shown to be localised to the

SR/ER and nuclear membranes in a wide variety of cells (99, 136). When MG23 was purified and incorporated into artificial bilayers, in solutions of 260 mM KPIPES, pH 7.2, a single-channel conductance of 82 ± 2.9 pS was obtained (136). However, in my studies, I have not observed single-channel recordings with this conductance.

If we were simply observing current-fluctuations that were produced by TRIC-B channel gating in both the WT and TRIC-A KO preparations, it would still be apparent that several TRIC-B channels gate with a higher Po in the TRIC-A KO preparation.

3. TRIC-A inhibits TRIC-B

If TRIC-A simply does not open in native preparations, and we therefore do not observe TRIC-A gating events, it may be that the presence of TRIC-A inhibits TRIC-B function. As part of a larger study, we are comparing the biophysical properties of other ion-channels that are located on the SR, such as the RyR and the SR Cl^- channels in WT and TRIC-A KO tissue. Although the data is preliminary, we have found that RyR1 function is dampened at the single-channel level in TRIC-A KO preparations, with the RyR channels gating in a lower Po in the presence of activating ligands (unpublished). It is possible that other ion-channels on the SR (such as TRIC-B/Cl-) may be indirectly affected by the presence of TRIC-A channels, even if TRIC-A gating events are rarely or never observed.

4. The molecular identity of the SR K^+ channel is separate to the molecular identity of TRIC-A and TRIC-B

The similar gating characteristics of the SR K^+ channels that were observed in both preparations raises the question of whether the molecular identity of the SR K^+ channel is separate to the identity of the TRIC-channels. The two TRIC isoforms have been shown to behave as functional ion-channels when incorporated into artificial bilayers in the literature

(and in ongoing projects in the lab) (101), and thus, if the TRIC channels were separate entities to the SR K^+ channel, we would still expect to see differences in the K^+ channel population from the SR of WT and TRIC-A KO. This question cannot be truly answered until we develop a successfully purification method to study the gating of both TRIC-isoforms in isolation, which will be discussed in Chapter 7

3.5.3 TRIC channels and specialised structures in skeletal muscle that facilitate Ca^{2+}-release

Knocking out TRIC-A and TRIC-B have detrimental effects on intracellular Ca^{2+} release, and so, it is important that we try to connect what is known about the TRIC-channels to what is known about the specialised intracellular structures in striated muscle that facilitate Ca^{2+} release. It has been reported that there is a higher abundance of both TRIC-isoforms in the HSR fraction compared to the LSR fraction (100), suggesting that TRIC-channels are located on junctional SR membrane (the portion of the SR that faces the T-tubule). As discussed previously, there is approximately 10 times more TRIC-A than TRIC-B in skeletal muscle (101) and in addition, it has also been reported that there are 5 times more TRIC-A than RyR (113). Therefore, in skeletal muscle HSR, we can estimate that for every TRIC-B channel, there are 2 RyR1 channels and 10 TRIC-A channels.

Evidence suggests that TRIC-channels form homotrimeric structures (100). As reported by Yazawa *et al* (2007), when recombinant TRIC-A purified from bacteria and native TRIC-A purified from skeletal muscle was treated with several chemical cross linkers, products with sizes corresponding to dimeric and trimeric assemblies were generated (100). In addition, when purified TRIC-A was labelled with colloidal-gold-conjugated Fab fragments, electron microscopy detected antigen–antibody complexes carrying three immunogold particles that protruded at near equal angular intervals, again suggesting the formation of a homotrimeric complex (100). Although the formation of TRIC-A/TRIC-B

heterotrimers have not been detected (100), we cannot rule out the possibility that TRIC-A homotrimers and TRIC-B homotrimers interact or communicate with each other in a cell.

It is thought that TRIC-A may associate with the RyR channel and TRIC-B may associate with the IP_3R channel to modulate the overall SR and ER Ca^{2+} homeostasis (137). As previously described, in skeletal muscle, RyR1 has been reported to form distinct structural lattice arrays in the junctional regions of the the SR (55, 56, 58, 111) where each RyR subunit is proximal to four adjacent particles at each corner, resembling the pattern observed on a checkerboard (59). Given the high abundance of TRIC-channels that are present in junctional regions of skeletal SR, we wonder if these TRIC-channels would be somehow intertwined within the RyR1 lattice arrays, and thus, perhaps knocking out TRIC-A could alter the arrangement of the RyR lattices.

While gathering n numbers for this study, I found it that it was easier to obtain recordings where only a single SR K^+ channel was gating in the bilayer in the TRIC-A KO preparations compared to the WT preparations. As illustrated in Figure 3.21, 62 % of all recordings obtained from TRIC-A KO tissue contained only one channel in the bilayer (34 out of 55 total recordings) whereas only 27 % of all recordings obtained from WT tissue contained only one channel gating in the bilayer (6 out of 22 total recordings).

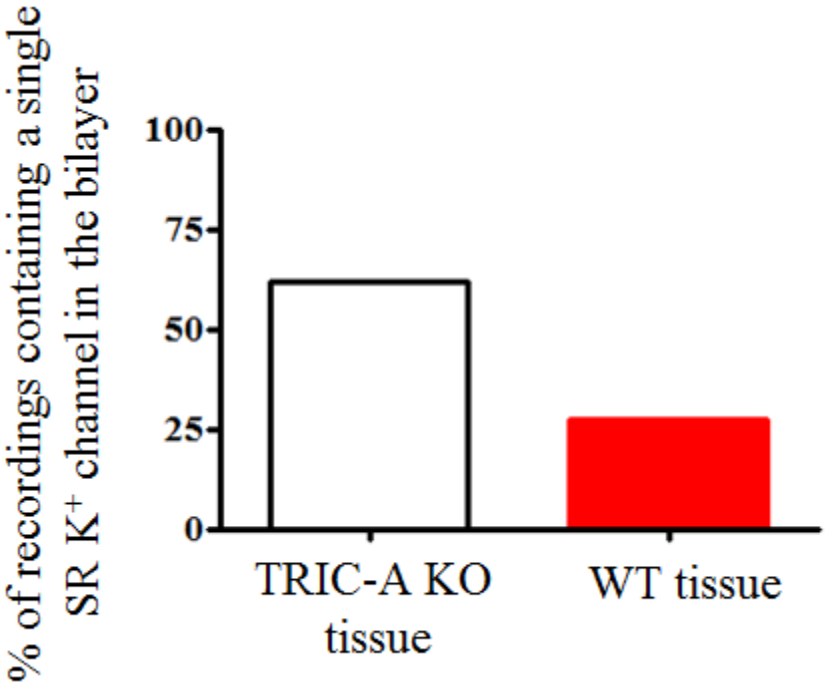


Figure 3.21 % of experiments containing a single SR K^+ channel in the bilayer in TRIC-A KO and WT tissue
In TRIC-A KO tissue, 34 out of a total 55 experiments contained a single SR K+ channel gating in the bilayer whereas only 6 out of a total 22 experiments from WT tissue contained a single SR K+ channel gating in the bilayer.

As previously mentioned, there is approximately 10 times more TRIC-A than TRIC-B in HSR (101) and we do not know if the TRIC-channels are arranged in a particular array in the junctional SR. Presumably, knocking out TRIC-A causes the SR vesicles to form differently during an SR membrane preparation since there is a normally abundant protein missing. Perhaps knocking out TRIC-A causes TRIC-B and other ion-channels and proteins to separate from each other thus increasing the number of experiments where only a single SR K^+ channel is present in a vesicle which fuses with the bilayer.

3.5.4 The complexity of the SR K^+ channel gating

The SR K^+ channels from TRIC-A KO and WT tissue exhibited extreme variability and the complexity of the gating behaviour has been extensively described in publications from this laboratory (126, 127) and is outlined in Section 3.3.1. The complexity of the SR K^+

channel gating is further affirmed when we investigate the effect of voltage on the mean open time of the full open channel bursts (see Figure 3.8). By visual examination of the traces where an SR K^+ channel was gating, it was evident that the mean open time of a full open burst was greater at + 30 mV compared to -30 mV. However, in the mean data from the lifetime analysis, there appeared to be no difference in the mean open time of a full open burst at +30 mV compared to -30 mV. This was because during an open channel burst there were many extremely short lived transitions from the full open level to lower conductance levels that truncated the idealised data trace. I have discussed this further in Chapter 6. The results from our lifetime analysis highlight how important it is to *always* refer back to the single-channel recordings after any method of analysis to be certain that the obvious gating-characteristics have been captured. The presence of a voltage-insensitive SR K^+ channel merely adds to complexity. We do not know the physiological significance of the voltage-insensitive gating pattern, but, because these channels exhibit high Po we can speculate that they will be gating when the SR membrane potential is near 0 mV thus equilibrating K^+ at all times. Another possibility is that the voltage insensitive channels gate in this manner because they have been damaged during isolation and do not represent a physiologically relevant channel. However, this could be a pattern of gating that occurs under a pathological situation, for example ischemia, if it is the result of oxidation, phosphorylation or enzymatic degradation.

4 Do SR K^+ channels gate in a cooperative manner?

4.1 Introduction

In Chapter 2, I compared the biophysical properties of the SR K^+ channels from TRIC-A KO and WT tissue when a single channel was gating in the bilayer. In experimental recording solutions of 210 mM KPIPES, pH 7.2, I could not detect any significant differences in the gating of the SR K^+ channels from both preparations at the single channel level. Therefore, I expanded my study to investigate how the gating of SR K^+ channels may be regulated, and, how physiological and pharmacological regulation of the SR K^+ channels may differ in TRIC-A KO and WT tissue. Apart from voltage, we do not know of any other known regulators of the native SR K^+ channels from TRIC-A KO and WT tissue. Therefore, I investigated whether the biophysical properties (outlined in Chapter 3) of the SR K^+ channels from TRIC-A KO and WT tissue were altered when more than one channel was present in the bilayer. Increasing the number of channels in the bilayer in each experiment would ultimately increase the total population of SR K^+ channels that were studied in both preparations, and therefore, it may be possible to detect differences in channel gating that were not observed when only a single-channel was gating in the bilayer. In addition, this study would provide the opportunity to investigate whether SR K^+ channels can gate in a cooperative manner.

Cooperative gating describes a process in which, when two channels are gating together, each channel affects the gating of the other channel. This may be observed as inhibition or stimulation of channel openings. At the cellular level, cooperative gating may serve a purpose to enhance channel mediated signalling. Ion-channels that are located on the SR have been shown to gate in a cooperative manner. For example, coupled gating (synchronous openings and closures) of RyR1, was first described by Marx *et al* (1998) (63). It was later shown that the coupled gating of RyR1 could be modulated by cytosolic and luminal Ca^{2+} concentrations and Mg^{2+}/ATP by Porta *et al* (2012) (62). A similar

phenomenon of gating behaviour for RyR2 has also been described (65). Although the mechanisms that governs the coupled gating nature of the RyR channel is not known, it is assumed that physical interaction between the RyRs occur (59).

As described previously, RyR channels have been shown to form distinct lattice structures that resemble the pattern observed on a checkerboard (55, 56, 58) and it is thought that the intrinsic ability of purified RyR channels to form this lattice assembly mediates their coupled gating behaviour (59). For example, coupling of purified RyR1 was only found to occur in fractions with a coefficient of sedimentation (S) ≥60, which represent enriched fractions in RyR1 channels that remain associated as dimers or larger (110). Coupled gating was not observed after reconstitution of purified RyR1s from the 30S fraction that mainly contains a single RyR channel (110). It is worth noting that synchronous opening and closing events do not need to occur for ion-channels to gate in a cooperative manner. For example, the cooperative gating behaviour of P2X2 receptors was studied using kinetic analysis in addition to Po analysis (138). Ding *et al* (2002) illustrated that the mean open time of single-channel patches was shorter than that of multiple-channel patches, suggesting that the closing rate is influenced by positive coupling (138).

TRIC-channels have been shown to be located in high abundance in the HSR (100), and therefore, it is possible that they are arranged in a particular array or pattern, and gate in a coupled manner. In this chapter, we fused the LSR isolated from TRIC-A KO and WT skeletal muscle in artificial bilayers, and we recorded the SR K^+ channel behaviour when there was up to four channels gating in the bilayer.

4.2 Methods

4.2.1 Po analysis when multiple channels were in the bilayer

In the recordings that contained 1-3 channels, Po was calculated as previously described in this thesis (Section 2.6.2.2).

In the recordings that contained four channels in the bilayer, due to the complexity of the SR K^+ channel gating, the idealisation protocol was simplified to calculate Po. A simple 2 state Markov model was used that consisted of the closed and the fully open channel level. As illustrated in Figure 4.1, the closed and the full conductance level were highlighted manually on the recording in QuB, and the parameters of the highlighted sections were applied to state 1 (the closed state) and state 2 (the full open state), respectively, using the QuB software. The data were idealised using the SKM application in the QuB software and Po was calculated using the formula in Equation 16.

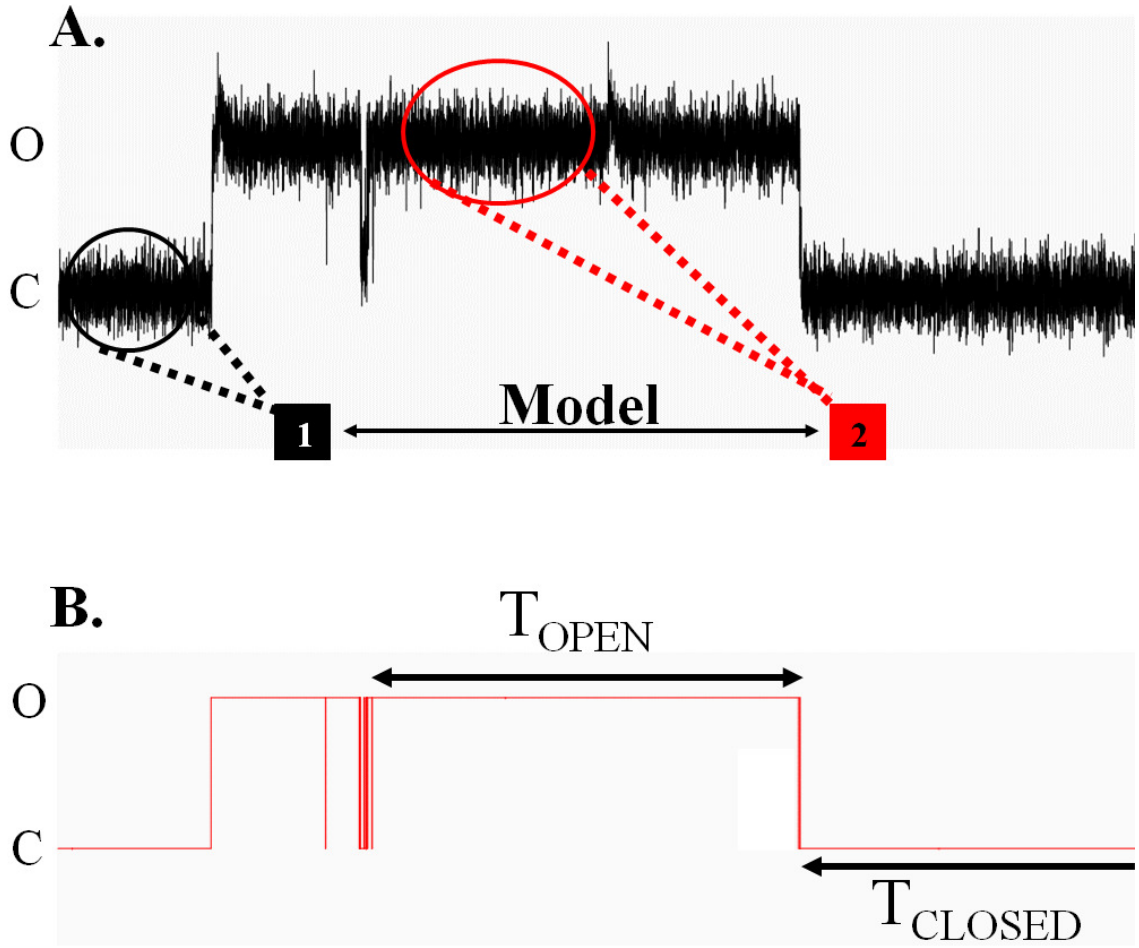


Figure 4.1 Single-channel event detection using our simplified 2 state Markov Model Panel A shows a typical single SR K^+ channel opening at +30 mV after filtering at 1 kHz. O and C indicate the full open and full closed levels, respectively. The model below, consisted of two levels (level 1 and level 2). Levels C and O were highlighted on the trace in QuB (as indicated by the red and black circles) and the parameters were 'grabbed' and applied to the appropriate level of the model (using the grab feature in QuB), as indicated by the black and red dotted lines, respectively. The result of the SKM analysis is an idealised trace shown in B. An example of a duration that the channel spends in the closed state and a duration in the open state is illustrated by T_{closed} and T_{open}, respectively.

To provide a coarse estimate of channel Po, we performed noise analysis on the trace using the noise analysis feature in WinEDR. As explained in section 2.6.4, noise analysis can be used to calculate the average current that flows through multiple ion-channels gating in a bilayer. We divided the mean current by the number of observed channel levels. We then

divided this number by the amplitude of the full open channel level in order to obtain a Po measurement.

It is difficult to accurately 'count' the number of channels in each bilayer when there are more than 3 channels present since a leaky bilayer could appear as additional channels. We therefore used 1 mM cytosolic decamethonium to aid in counting the channels. Decamethonium blocks the channels in a manner that enables us to count the channels in the bilayer and determine the zero current level.

4.2.2 Binomial distribution analysis

The gating of more than one identical and independent ion-channels in a bilayer is expected to follow a binomial distribution that is similar to the pattern observed when a coin is flipped multiple times. However, if channels are non-identical in their open probabilities or gate non-independently, the experimental data will deviate from the binomial distribution prediction.

If there are *N* identical channels in a membrane, each with a probability p of being open, and, if the channels gate independently, the probability of k channels being in the open state simultaneously is given by the binomial distribution

$$P(k)_{binomial} = \binom{N}{k} p_o{}^k (1-p_o)^{N-k}$$

Equation 21

4.3 Results

4.3.1 Contribution by other members of the lab to experiments described in this chapter.

In this chapter, we investigated whether the single-channel properties of the SR K^+ channels from TRIC-A KO and WT tissue, described in Chapter 2 of this thesis, were altered when there was more than one channel gating in the bilayer. Some experiments that are included in the mean data were performed by Dr. Elisa Venturi and Mr. David Eberhardt. Their exact contribution to the mean data is indicated under the each figure.

4.3.2 TRIC-A KO tissue

SR K^+ channel currents were recorded from TRIC-A KO tissue under control conditions (210 mM KPIPES, pH 7.2) and the experiments were grouped based on the number of channels that were observed over 3 min of continuous recording at +30 mV. To check the number of channels in the bilayer, the bilayer was held at a high holding potential (> 50 mV) to maximally activate channels and count the number of channels that were present.

4.3.2.1 The gating characteristics of the SR K^+ channel when there were two channels gating in the bilayer.

A representative example of the gating observed when two SR K^+ channels from TRIC-A KO tissue were gating is shown in Figure 4.2.

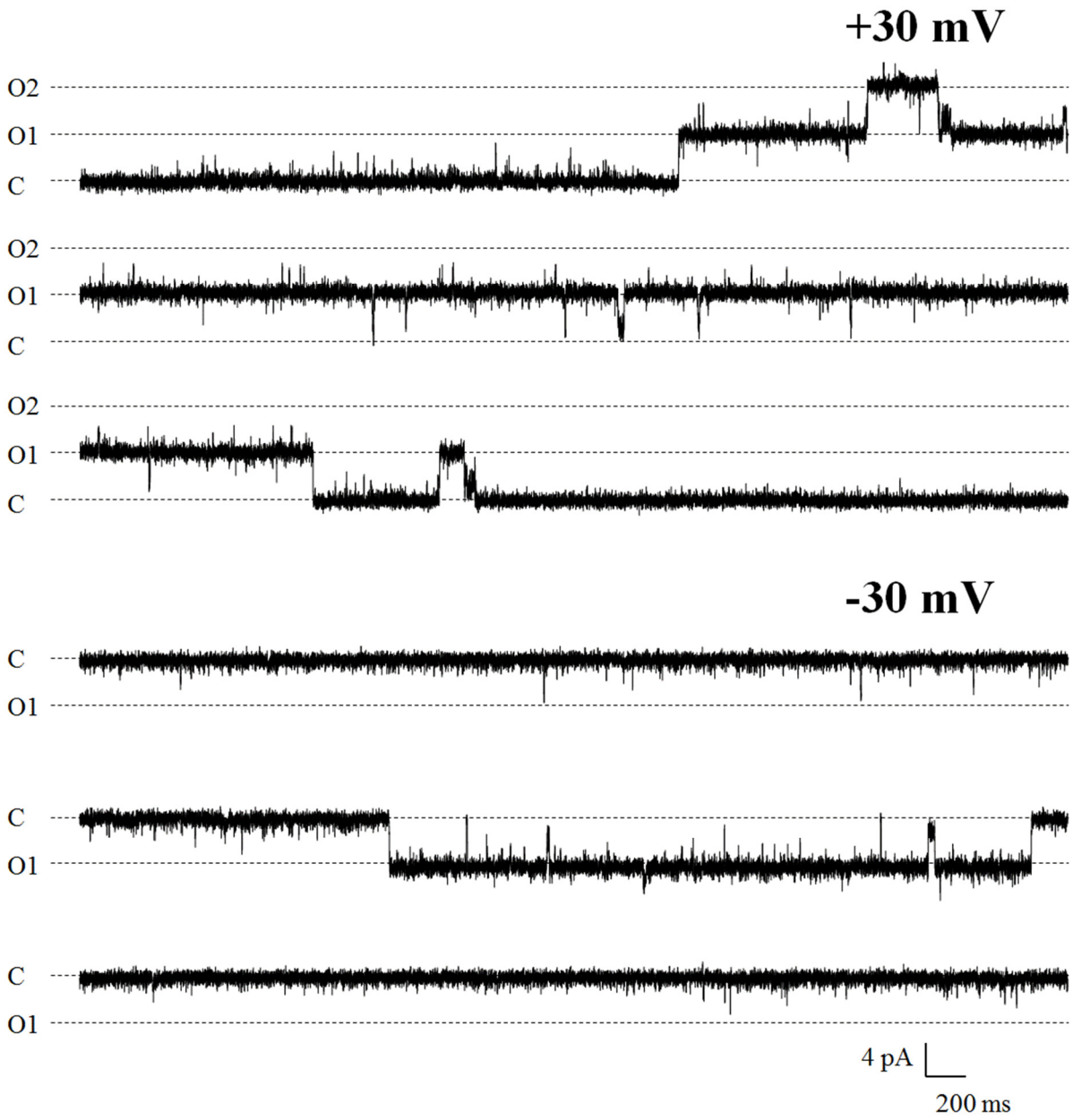


Figure 4.2 The gating of the SR K^+ channels from TRIC-A KO tissue when there were two channels in the bilayer.
A representative trace at +30 mV (above) and -30 mV (below) when there were two SR K^+ channels gating in the bilayer in 210 mM KPIPES, pH 7.2 is shown. O1 and O2 indicate the channel levels for one and two SR K^+ channels opening, respectively, and C indicates the zero current level. The recording was low pass filtered at 1 KHz.

The mean data shown in Figure 4.3 illustrates the voltage-dependence of the SR K^+ channels from TRIC-A KO tissue when there were two channels gating in the bilayer. The channels were significantly voltage dependent, with the $P_{O_{TOTAL}}$ of each channel being

higher at +30 mV compared to -30 mV (n=12, ***p<0.001). When Po_{TOTAL} was subdivided into Po_{FULL} and Po_{SUB}, as observed when only one channel was present in the bilayer (Chapter 3), again both parameters were significantly voltage dependent (n=12, **p<0.01).

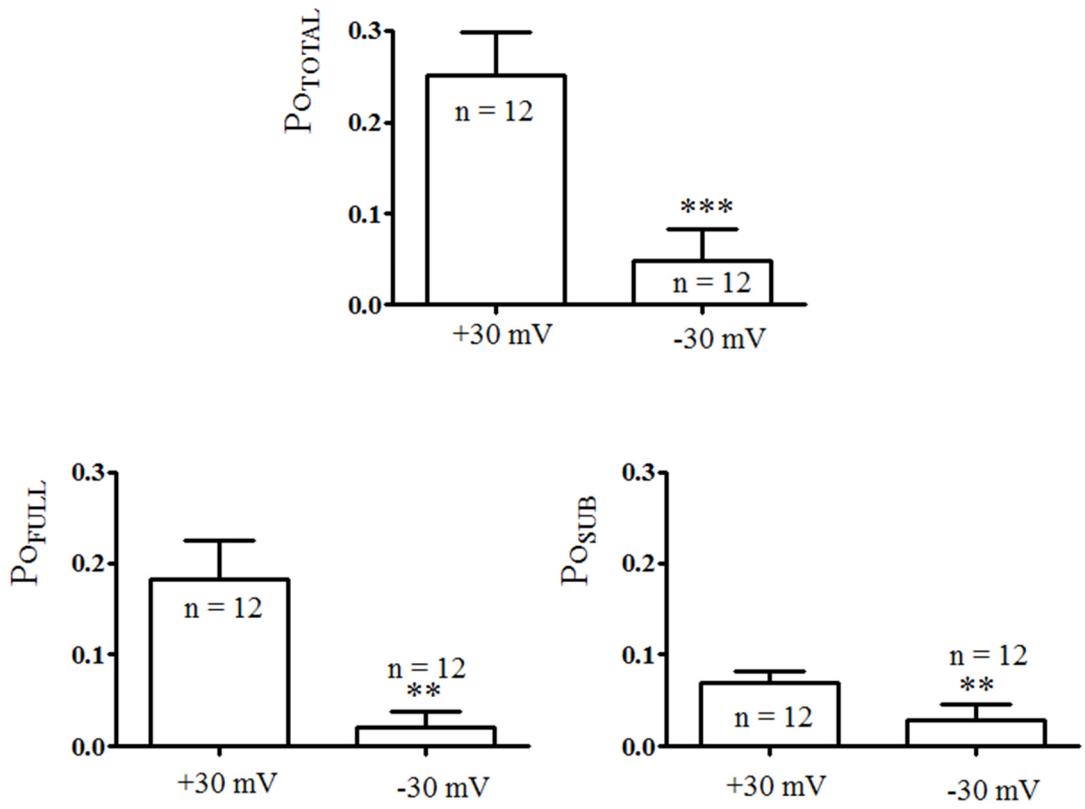


Figure 4.3 The voltage-dependence of the SR K^+ channels from TRIC-A KO tissue when two channels were gating in the bilayer
The bar charts show the average Po when 2 SR K^+ channels were gating in the bilayer. The data are presented as mean ± SEM (**p<0.01, ***p<0.001). This set of experiments was performed by Dr. Elisa Venturi and myself. I analysed the traces.

The contribution of Po_{FULL} to Po_{TOTAL} was significantly higher at +30 mV compared to -30 mV when there were two SR K^+ channels gating in the bilayer, as shown in Figure 4.4

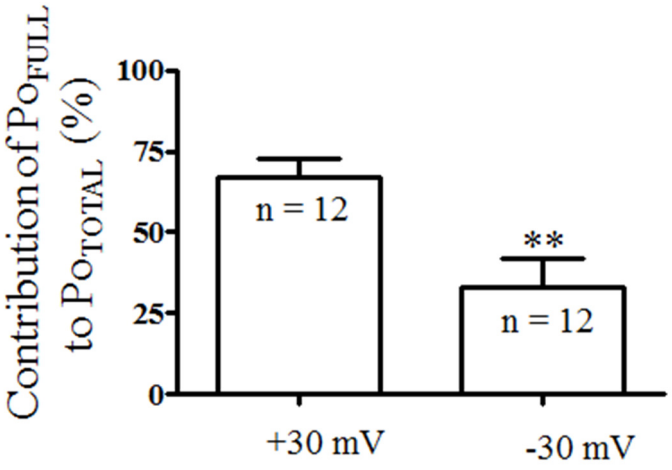


Figure 4.4 The contribution of $P_{O_{FULL}}$ to $P_{O_{TOTAL}}$ when two SR K^+ channels from TRIC-A KO tissue were present in the bilayer.
The mean data ± SEM is shown (**p<0.01)

4.3.2.2 The gating characteristics of the SR K^+ channels when three channels from TRIC-A KO tissue were gating in the bilayer.

A representative example of the gating observed when three SR K^+ channels from TRIC-A KO tissue were in the bilayer is shown in Figure 4.5.

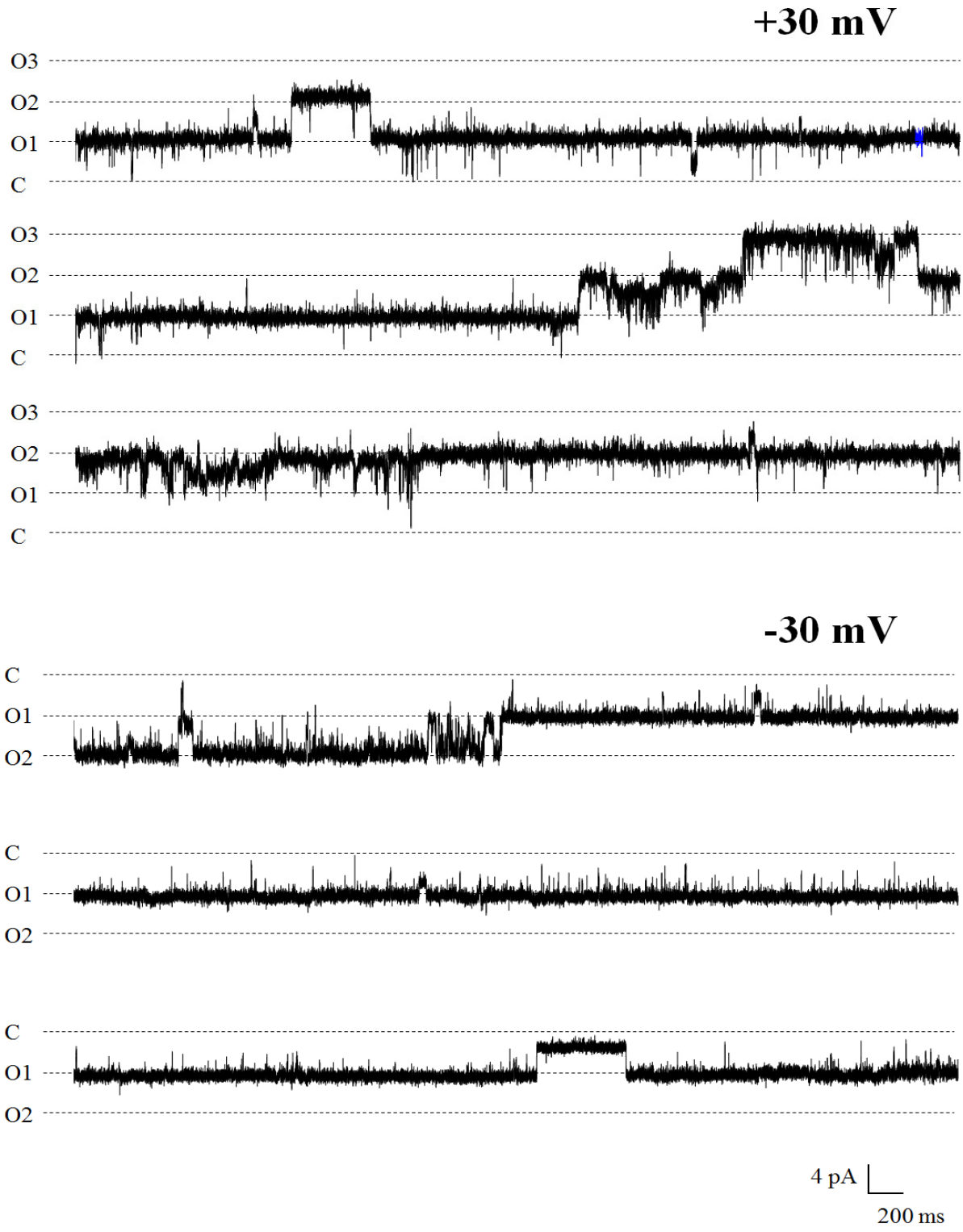


Figure 4.5 The gating of the SR K^+ channels when there were three channels in the bilayer.
A representative single-channel trace at +30 mV (above) and -30 mV (below) when there were three SR K^+ channels gating in the bilayer in 210 mM KPIPES, pH 7.2 is shown. O1, O2 and O3 indicate the open channel levels for one, two and three SR K^+ channels opening, respectively, and C indicates the zero current level. The recording was low pass filtered at 1 kHz

The mean data shown in Figure 4.6 illustrates the voltage-dependence of the SR K^+ channels when there were three channels gating in the bilayer. The SR K^+ channels were significantly voltage-dependent, with the average Po being higher at +30 mV compared to -30 mV (n=6, $*p<0.05$). When the $P_{O_{TOTAL}}$ was subdivided into $P_{O_{FULL}}$ and $P_{O_{SUB}}$, $P_{O_{FULL}}$ was significantly voltage dependent (n=6, $**p<0.01$).

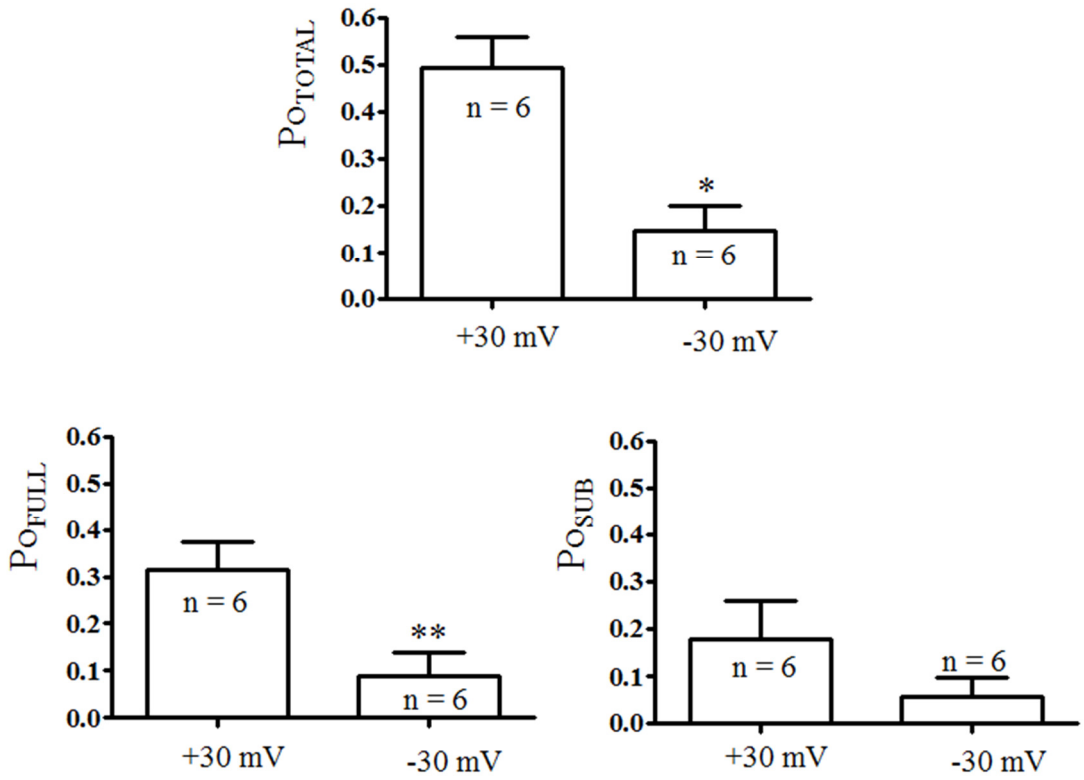


Figure 4.6 The voltage-dependence of the SR K^+ channels from TRIC-A KO when three channels were gating in the bilayer
The bar charts show the average Po when three SR K^+ channels were present in the bilayer. The data are presented as mean ± SEM ($*p<0.05$, $**p<0.01$)

The contribution of $P_{O_{FULL}}$ to the overall Po was not significantly different +30 mV compared to -30 mV when there were three SR K^+ channels gating in the bilayer, as shown in Figure 4.7.

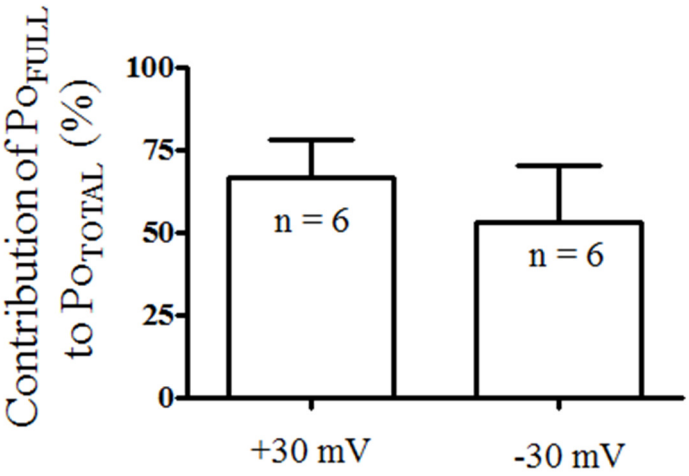


Figure 4.7 The contribution of Po_{FULL} to Po_{TOTAL} when three SR K^+ channels were present in the bilayer.
The data is presented as mean ± SEM.

4.3.2.3 The gating characteristics of the SR K^+ channels when four channels were gating in the bilayer

A representative experiment when four SR K^+ channels were gating in the bilayer is shown in Figure 4.8.

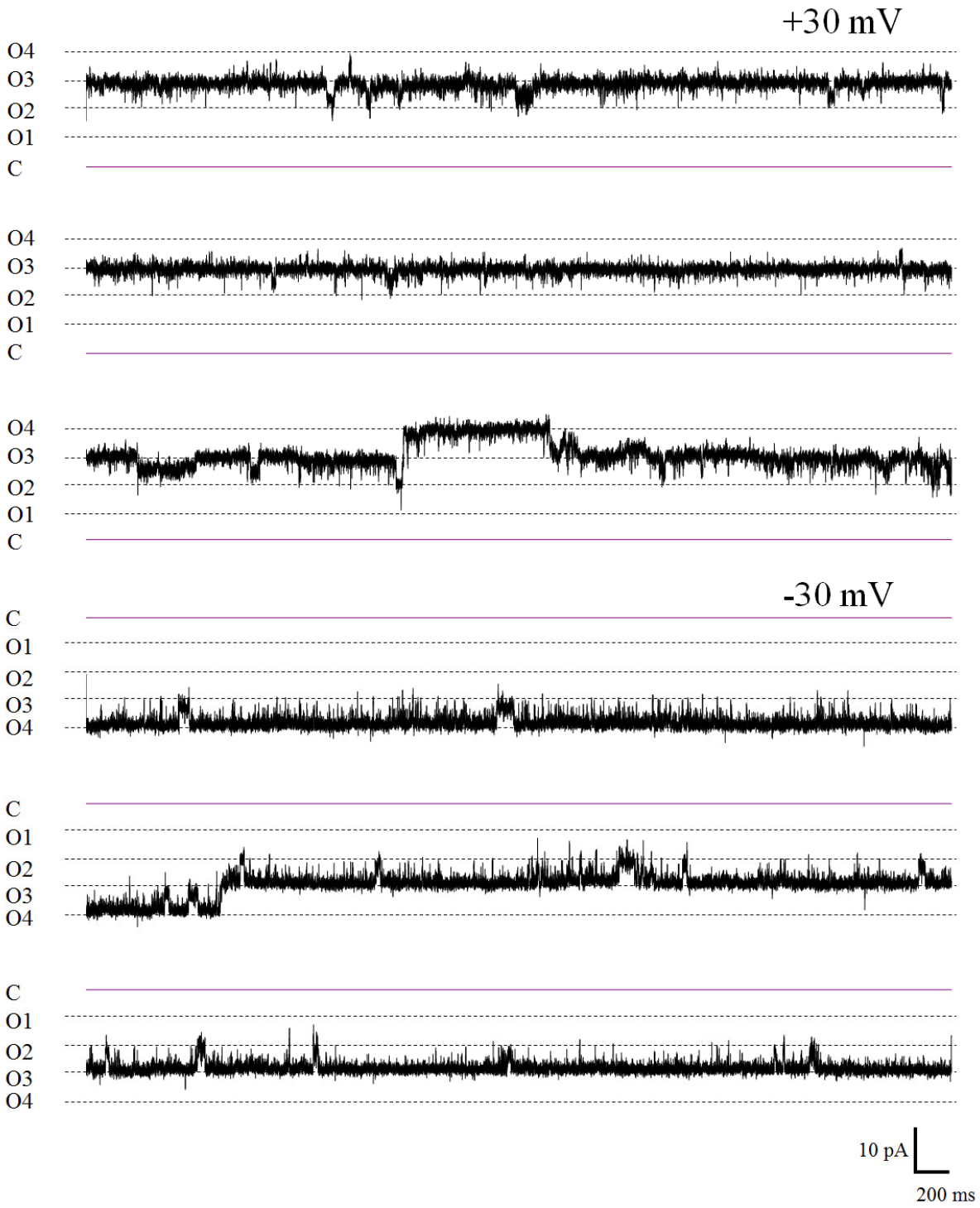


Figure 4.8 The gating of the SR K^+ channels from TRIC-A KO when four channels were gating in the bilayer.

A representative single-channel trace at +30 mV (above) and -30 mV (below) when there was four SR K^+ channels gating in the bilayer in 210 mM KPIPES, pH 7.2 is shown. O1, O2, O3 and O4 indicate the channel levels for one, two, three and four SR K^+ channels opening, respectively C indicates the zero current level, and is marked on the trace by a purple line. The recording was low pass filtered at 1 kHz

In the three experiments that contained four SR K^+ channels gating in the bilayer, although individual opening and closing events were observed, there was never a period when all four channels were closed at the same time. Without knowing where the zero current level was, it was very difficult to distinguish whether the channels were gating in a high Po, or, whether there was a leak in the bilayer. 1 mM decamethonium was added to the cytosolic side of the channel to induce closings that reached the zero current level, as described on page 85. A representative experiment is shown in Figure 4.9.

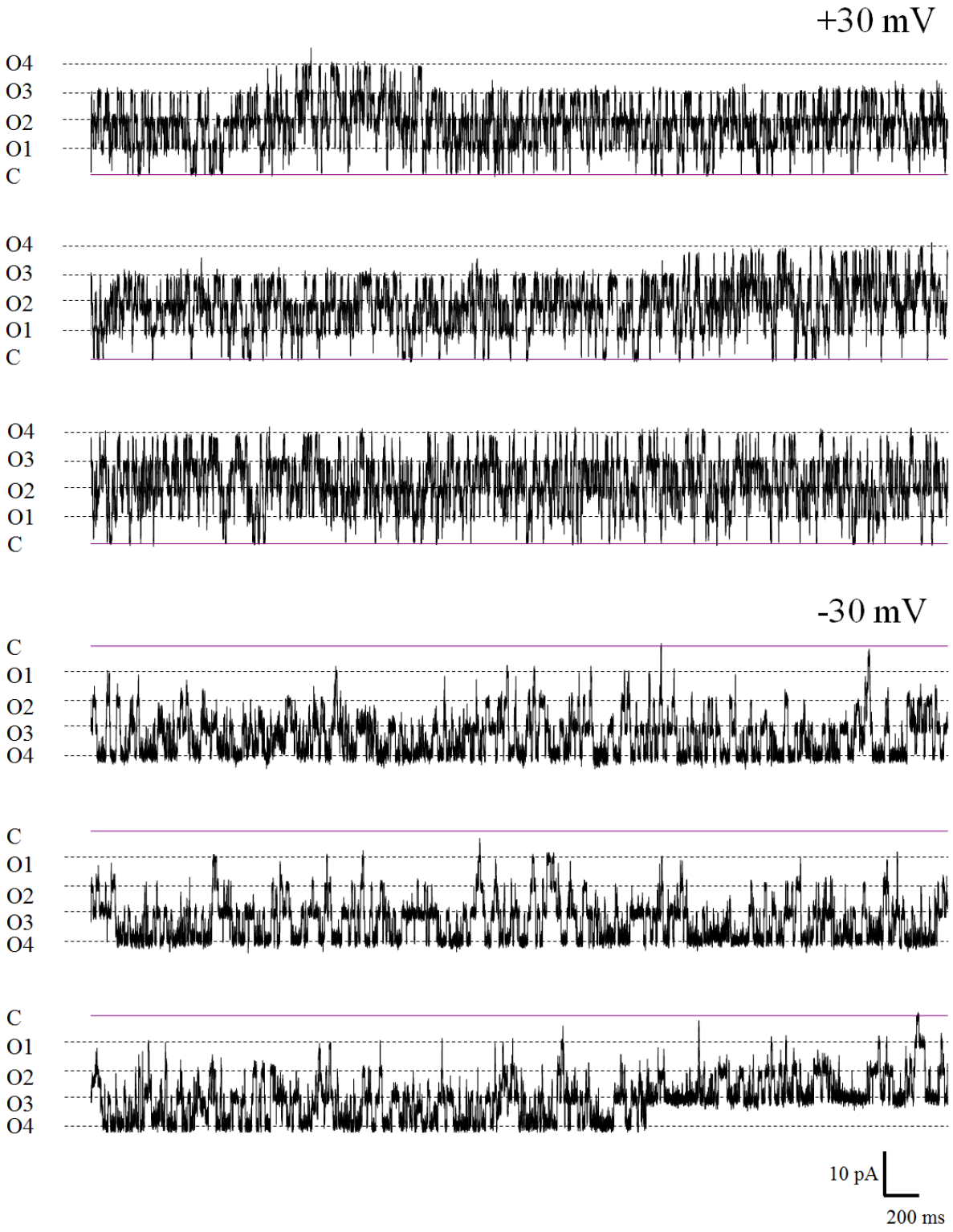


Figure 4.9 Effect of Decamethonium on SR K^+ channels
A representative single-channel trace at +30 mV (above) and -30 mV (below) after 1 mM decamethonium was added to the cytosolic chamber. The corresponding control trace is shown in Figure 4.8. O1, O2, O3 and O4 indicate the open channel levels for one, two, three and four SR K^+ channels, respectively. C and the purple line indicate the zero current level. The recording was low pass filtered at 1 kHz

In the three experiments that contained four SR K^+ channels, after the addition of 1 mM decamethonium to the cytosolic side of the channel, we observed closing events to the zero current level, as seen in Figure 4.9. After establishing that there was no leak in the bilayer, we were able to return to our previously recorded control traces (Figure 4.8) and idealise the recordings using our simplified 2 state Markov model. The mean data illustrating the Po when four SR K^+ channels were in the bilayer is shown in Figure 4.10.

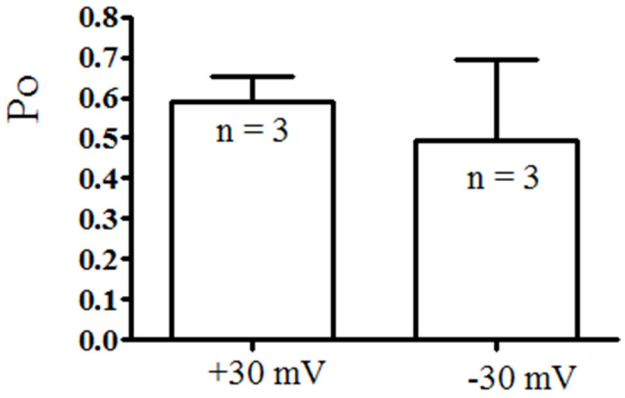


Figure 4.10 The voltage-dependence of the SR K^+ channels from TRIC-A KO when four channels were gating in the bilayer The mean data ± SD is shown.

Surprisingly, the mean data suggested that the SR K^+ channels were relatively voltage-independent when four channels were in the bilayer. However, when we looked at the individual Po values in Table 4-1, it appeared that 2 out of the 3 experiments did have a higher Po at +30 mV compared to -30 mV. Interestingly, one experiment had a higher Po at -30 mV compared to +30 mV.

Po at + 30 mV	Po at -30 mV
0.56	0.27
0.71	0.89
0.51	0.32

Table 4-1 Individual experiments illustrating the voltage-dependence of the SR K^+ channels when there were four channels in the bilayer

In addition to the method outlined above, we analysed the 3 experiments using the noise analysis method. Both methods of Po analysis are compared in Table 4-2. The two methods have weaknesses. Both provide only an estimate of channel Po and do not distinguish openings to the full open channel level from openings to sub-conductance levels. However, I decided to use the simplified 2 state Markov model in QuB for the analysis, because, by using the QuB software, I could control the analysis more. The idealisation could be visually inspected in close detail and it was possible to manually ignore any capacitance spikes and/or noisy events. In addition, adjustment for drift in the baseline could be made. In contrast, the noise analysis feature in WinEDR does not allow removal of any capacitance/noise spikes or rectification of baseline drift, and so, if these events are present in a recording, they will be included as single-channel events.

	Po at +30 mV	**Po at -30 mV**
SKM	0.59 ± 0.10	0.49 ± 0.35
NOISE ANALYSIS	0.64 ± 0.12	0.49 ± 0.36

Table 4-2 Comparison of the two methods used to analyse the Po when four SR K^+ channels were gating in the bilayer.

4.3.3 The effect of decamethonium on the SR K^+ channel from TRIC-A KO

As outlined above, decamethonium was used to enable counting of the number of channels gating in the bilayer by inducing closings to the zero current level, as illustrated in Figure 4.9. The mean data illustrating the effect of 1 mM cytosolic decamethonium on conductance and Po is shown in Figure 4.11.

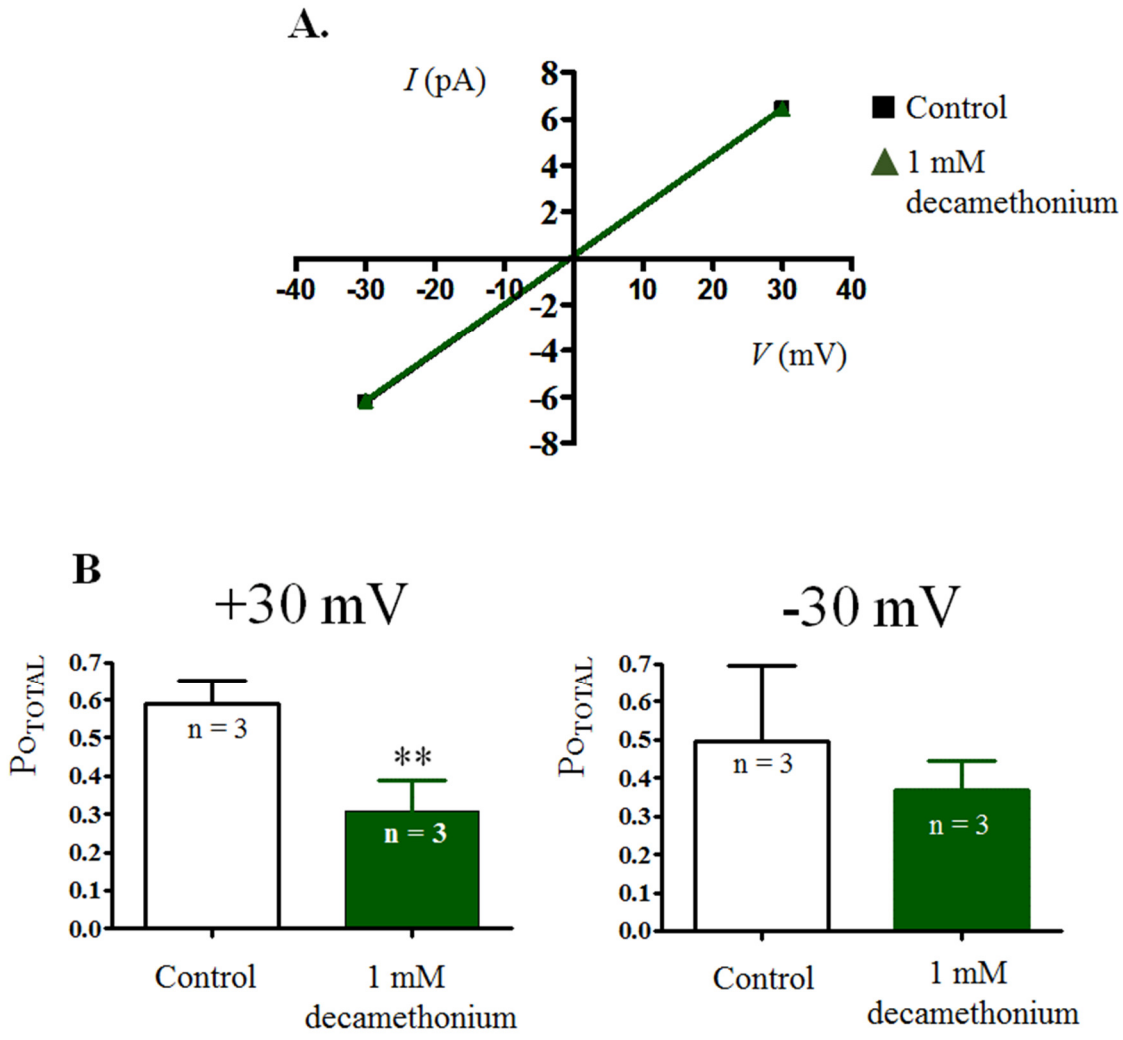


Figure 4.11 The effect of decamethonium on the function of the SR K^+ channels from TRIC-A KO tissue

In A, the current-voltage relationship was 211 ± 0.002 pS in control conditions (black squares) and 210.5 ± 0.004 pS in 1 mM decamethonium (green squares). Where error bars are not shown, they are within the symbol. In B, the bar charts show the decrease in SR K^+ channel Po after 1 mM decamethonium (shown in green) was added to the cytosolic side of the channel. The data are presented as mean ± SD (**p<0.01)

As illustrated in Figure 4.9, the blocking events induced by cytosolic decamethonium were pronounced at +30 mV. However, at – 30 mV, there also appeared to be an increase in the number of closing events. Where possible, we measured the mean open time by measuring the stretches of data where only one channel was opening and closing in control conditions and in 1 mM decamethonium. Mean closed time could not be obtained from any of these

traces. As shown in Figure 4.12, there was trend towards a reduction in the mean open time at both +30 mV and -30 mV (as expected by visually inspecting the traces).

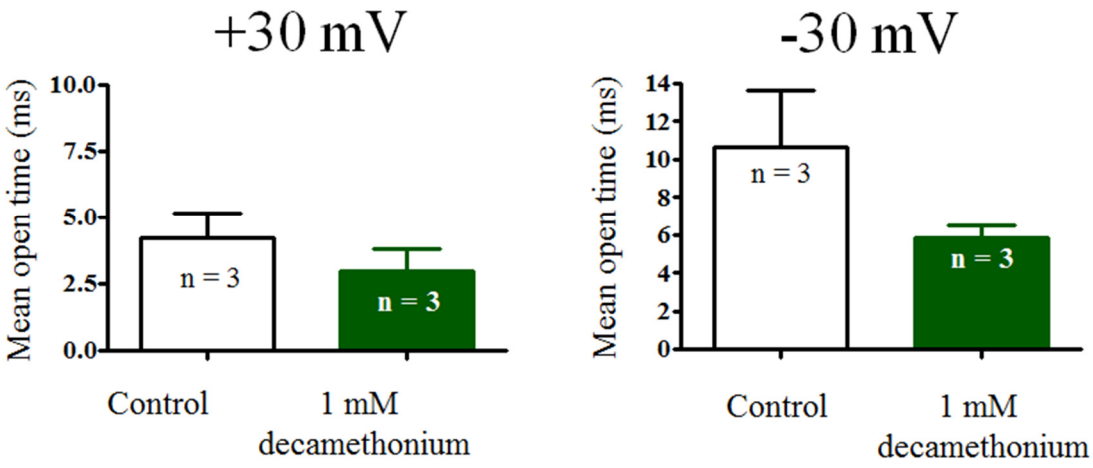
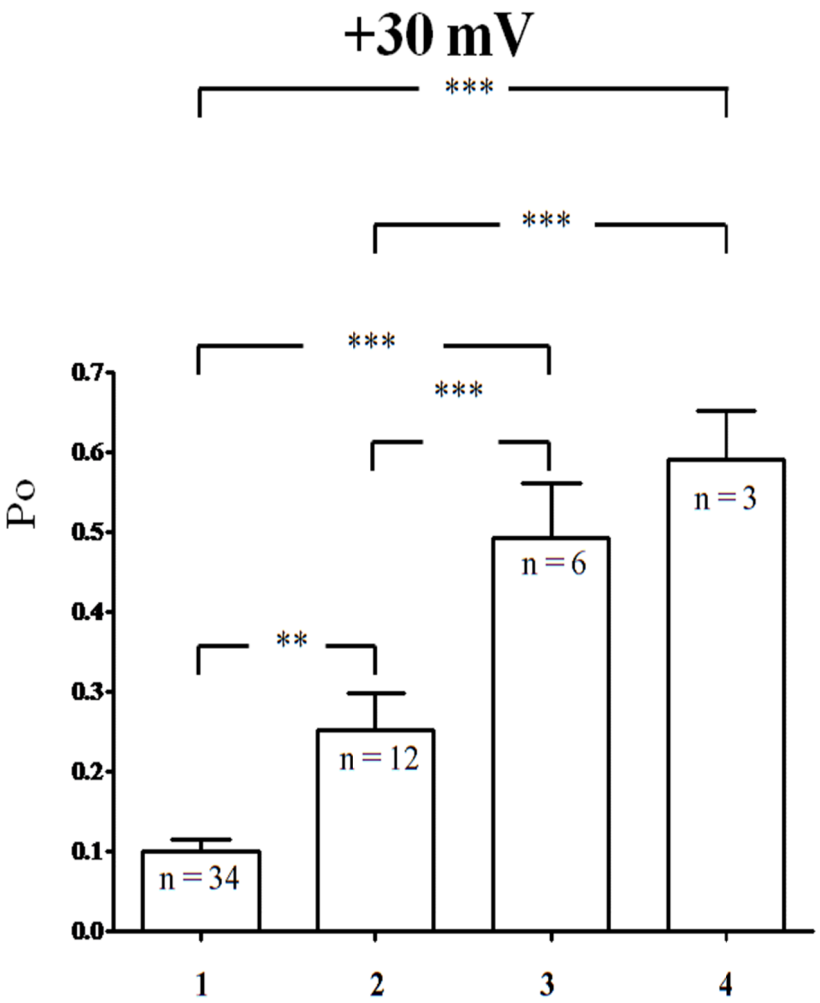


Figure 4.12 Effect of decamethonium on the mean open time of the SR K^+ channel
The mean open time of the SR K^+ channel in control conditions (white) and in 1 mM cytosolic decamethonium (green) at +30 mV (left) and -30 mV (right) is shown. Data are presented as mean ± SEM for n=3.

4.3.4 Do SR K^+ channels from TRIC-A KO gate in a cooperative manner?

We compared the Po of the SR K^+ channels from TRIC-A KO tissue when one, two, three or four channels were gating in the bilayer at +30 mV and -30 mV. To increase the n numbers, I included the eight single-channel recordings from Matyjaszkiewicz *et al* (2015) (127). The mean data highlighting the relationship between Po and the number of channels gating in the bilayer at +30 mV is shown in Figure 4.13. The data illustrates that the Po of the SR K^+ channels from TRIC-A KO increased as the number of channels in the bilayer increased (***p<0.001), suggesting that the channels may gate in a cooperative manner.


+30 mV
***
***
***
***
**
Po
0.7
0.6
0.5
0.4
0.3
0.2
0.1
0.0
n = 34
n = 12
n = 6
n = 3
1
2
3
4

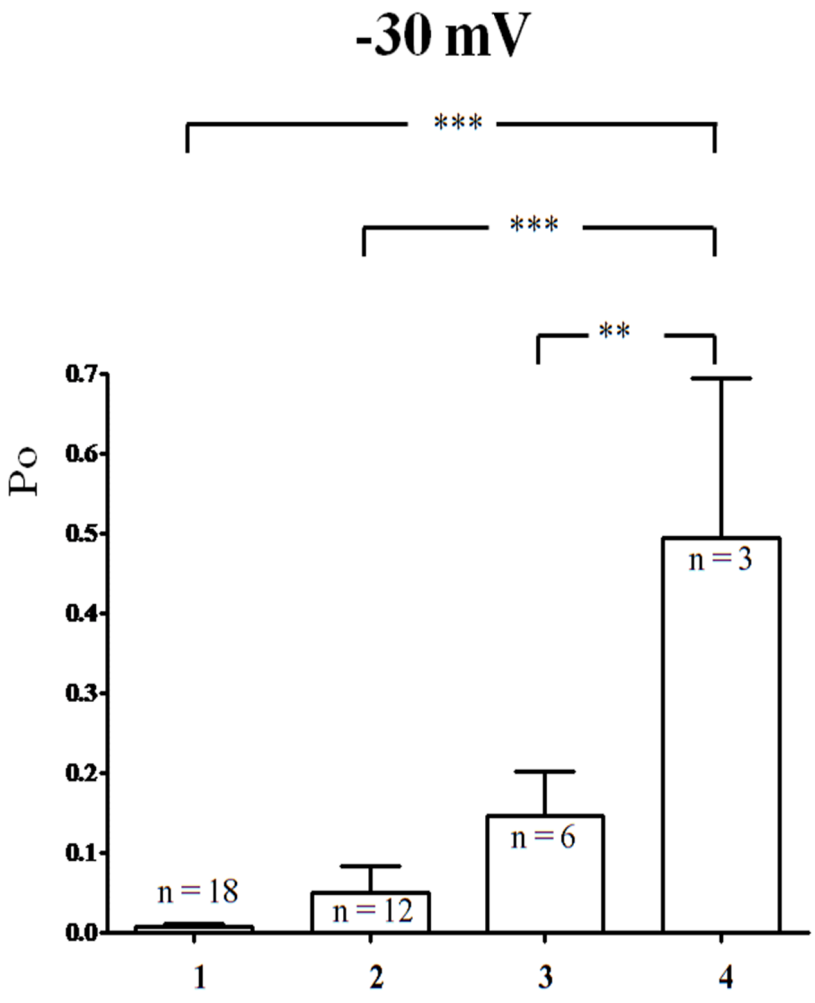

-30 mV
***
***
**
Po
0.7
0.6
0.5
0.4
0.3
0.2
0.1
0.0
n = 18
n = 12
n = 6
n = 3
1
2
3
4

Figure 4.13 The relationship between SR K^+ channel Po and the number of channels in the bilayer at ±30 mV.
The bar chart illustrates the changes in the Po of SR K^+ channels from TRIC-A KO tissue as the number of channels in the bilayer increases. The holding potential is indicated on the graph. The data are presented as mean ± SEM for n ≥ 4 and mean ± SD for n=3 (**p<0.01, ***p<0.001).

We wanted to investigate whether the cooperative gating observed was associated with the full open channel level or the sub-conductance levels, or a combination of both. When we separated the Po into Po_{FULL} and Po_{SUB}, we had to exclude the experiments where 4 channels were gating in the bilayer, as we had used the simplified 2 state Markov model, which does not account for sub-conductance states. The mean data illustrating the relationship between Po_{FULL}/Po_{SUB} and the number of channels in the bilayer is shown in Figure 4.14 for +30 mV (column A) and -30 mV (column B). When we looked at the contribution of Po_{FULL} to Po_{TOTAL} as the number of channels present in the bilayer increased (Figure 4.14 (iii)), we observed a marked effect at -30 mV (*p<0.05). As the number of channels in the bilayer increased, so did the contribution of the full openings to overall Po.

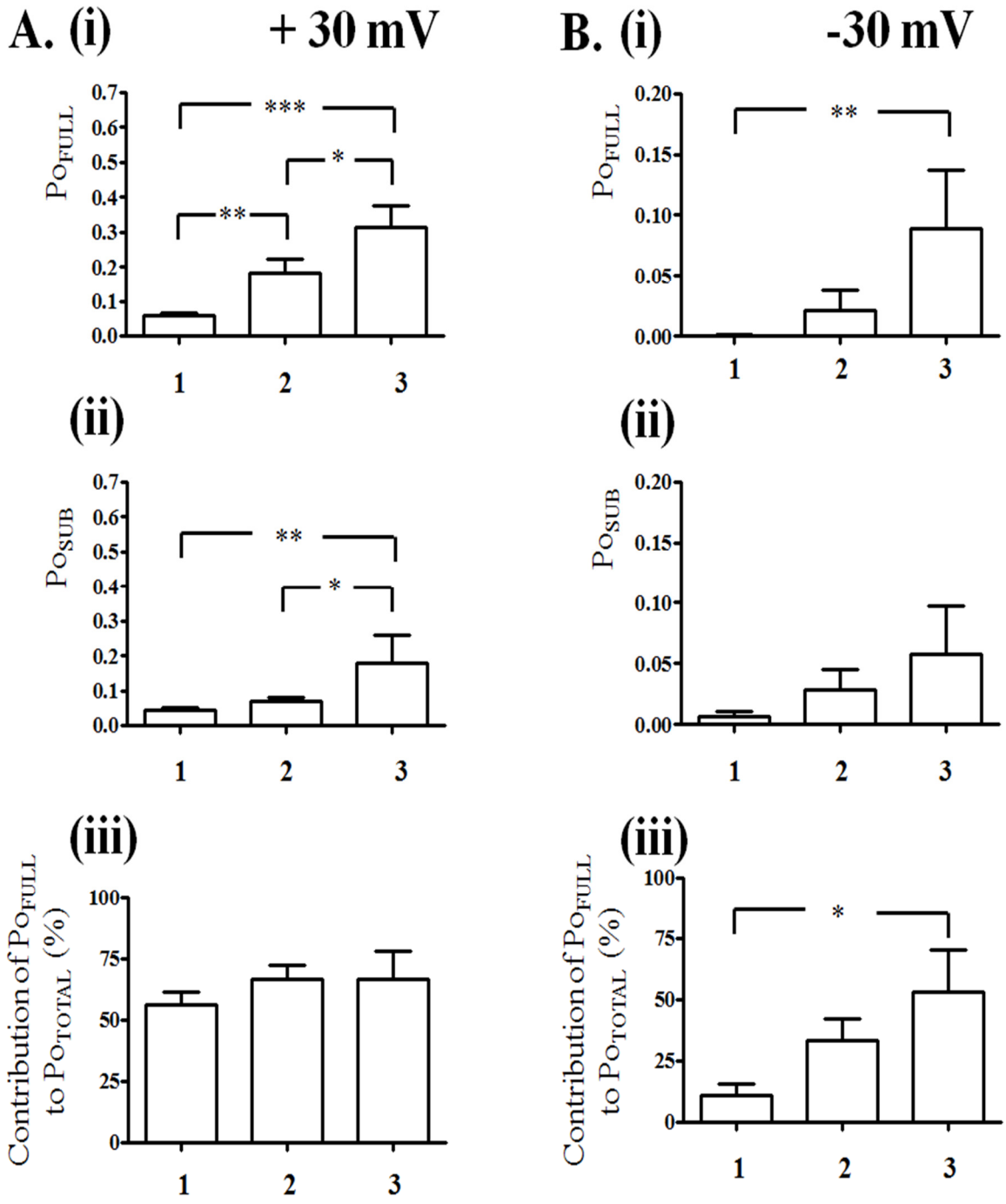


Figure 4.14 The relationship between Po_{FULL}/Po_{SUB} and the number of channels in the bilayer at ±30 mV.

The bar chart illustrates the change in SR K^+ channel Po_{FULL} (i), Po_{SUB} (ii) and the contribution of Po_{FULL} to Po_{TOTAL} (iii) at holding potentials of +30 mV (column A) and -30 mV (column B) as the number of channels in the bilayer increases. The data are presented as mean ± SEM for n ≥ 4 and mean ± SD for n=3 (*p<0.05, **p<0.01, ***p<0.001).

4.3.5 Do we alter the Po-voltage relationship of the SR K^+ channel from TRIC-A KO when multiple channels are present?

As illustrated in figure Figure 3.6, when we study the Po-voltage relationship of single SR K^+ channels from TRIC-A KO tissue, the voltage-dependence of the full open channel level is pronounced. The channels rarely visit the full open channel level at negative potentials, but, when the voltage becomes more positive, we begin to see openings at +10 mV and the channel seems to be gating to a maximum Po at +20 mV. At higher positive holding potentials, no further increments in channel Po are observed.

With more than one SR K^+ channel gating in the bilayer, ideally, I would have liked to replicate this Po-voltage plot to investigate if the nature of the voltage-dependence was altered. For example, is the relationship simply shifted to the left? However, due to time limitations (a good experiment frequently lasts <20 min), I decided to record the gating of multiple SR K^+ channels at potentials of +20 mV and +50 mV. A representative experiment illustrating the gating of the SR K^+ channels from TRIC-A KO at +20 mV and +50 mV when multiple channels were in the bilayer is shown in Figure 4.15.

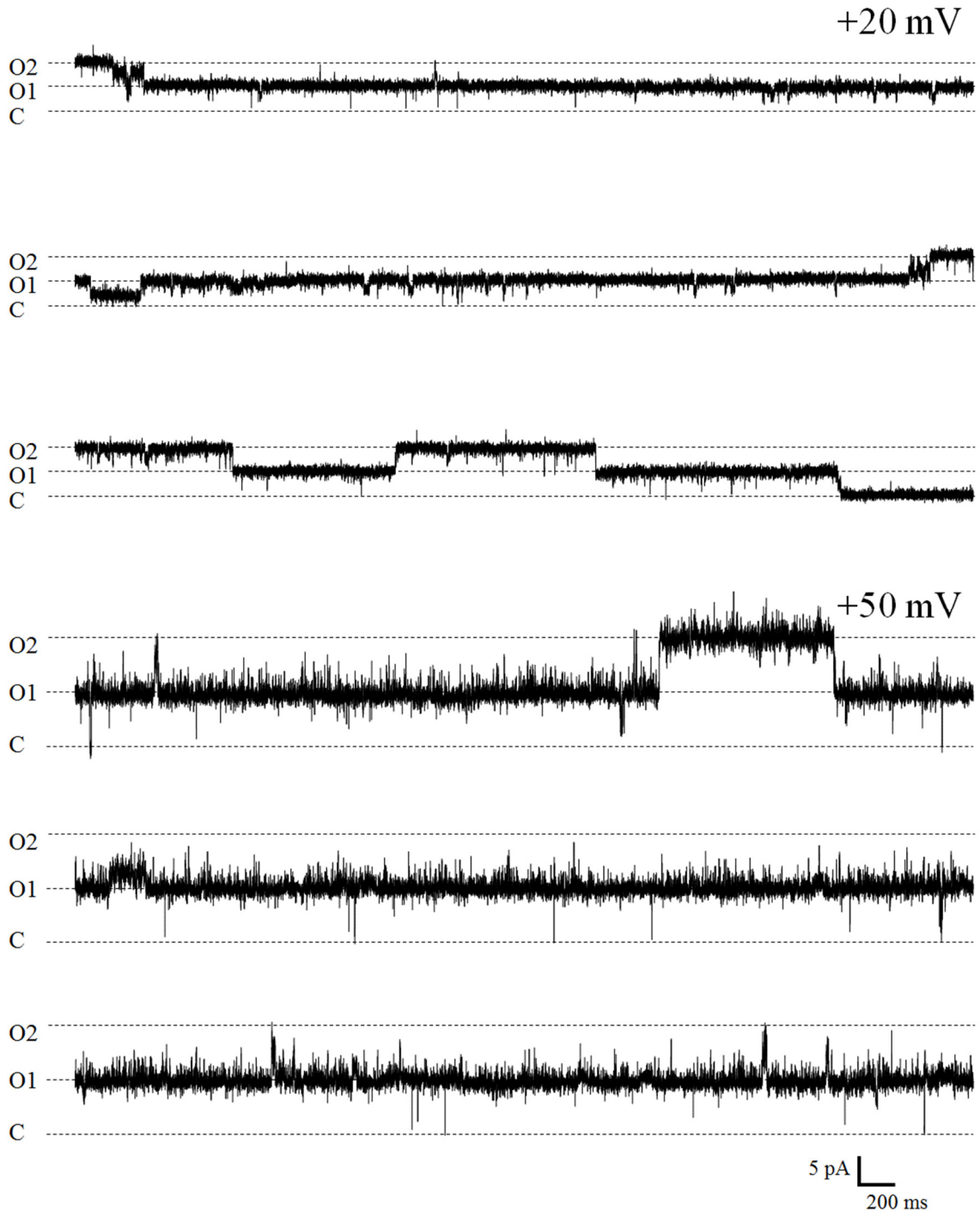


Figure 4.15 The gating of multiple SR K^+ channels from TRIC-A KO at +20 mV and +50 mV

A representative trace at +20 mV (above) and +50 mV (below) when there were two SR K^+ channels gating in the bilayer in 210 mM KPIPES, pH 7.2 is shown. O1 and O2 indicate the channel levels for one and two SR K^+ channels opening, respectively, and C indicates the zero current level. The recording was low pass filtered at 1 kHz.

At these voltages, I recorded 5 experiments that contained between 2 and 5 SR K^+ channels gating in the bilayer. Each experiment was analysed according to the simplified 2 state Markov model to calculate Po. The mean Po of the SR K^+ channels was smilar at +20 mV and +50 mV, as shown in Figure 4.16 (n=5, SEM).

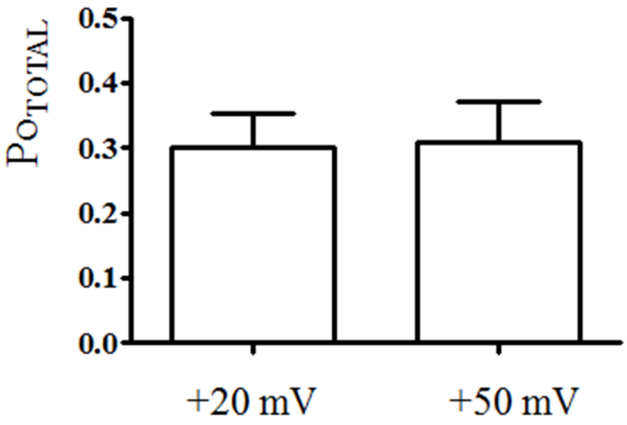


Figure 4.16 The Po of the SR K^+ channels at +20 mV and +50 mV. No change in Po was observed when the holding potential was increased from +20 mV to +50 mV. Data are presented as mean ± SEM for n=5.

Since the Po did not appear to change when holding voltage was increased from +20 mV to +50 mV, I assumed that the plateau feature of the Po-voltage plot (as shown in Figure 3.6) remained even when there was more than one channel in the bilayer. However, as seen in Figure 4.15, I noticed that the traces at +50 mV appeared more 'noisy' than the corresponding traces at +20 mV. There also appeared to be an increase in the frequency of very short-lived transitions from the closed level or fully open level to sub-conductance levels. To quantify this, the noise (which was the equivalent of the standard deviation in QuB) of the closed level (level 1) and the open channel level (level 2) were compared. As shown in Figure 4.17, an increase in both the closed current level noise and the full open channel level noise were observed when the holding voltage was increased from +20 mV to +50 mV (n=5,**p<0.01).

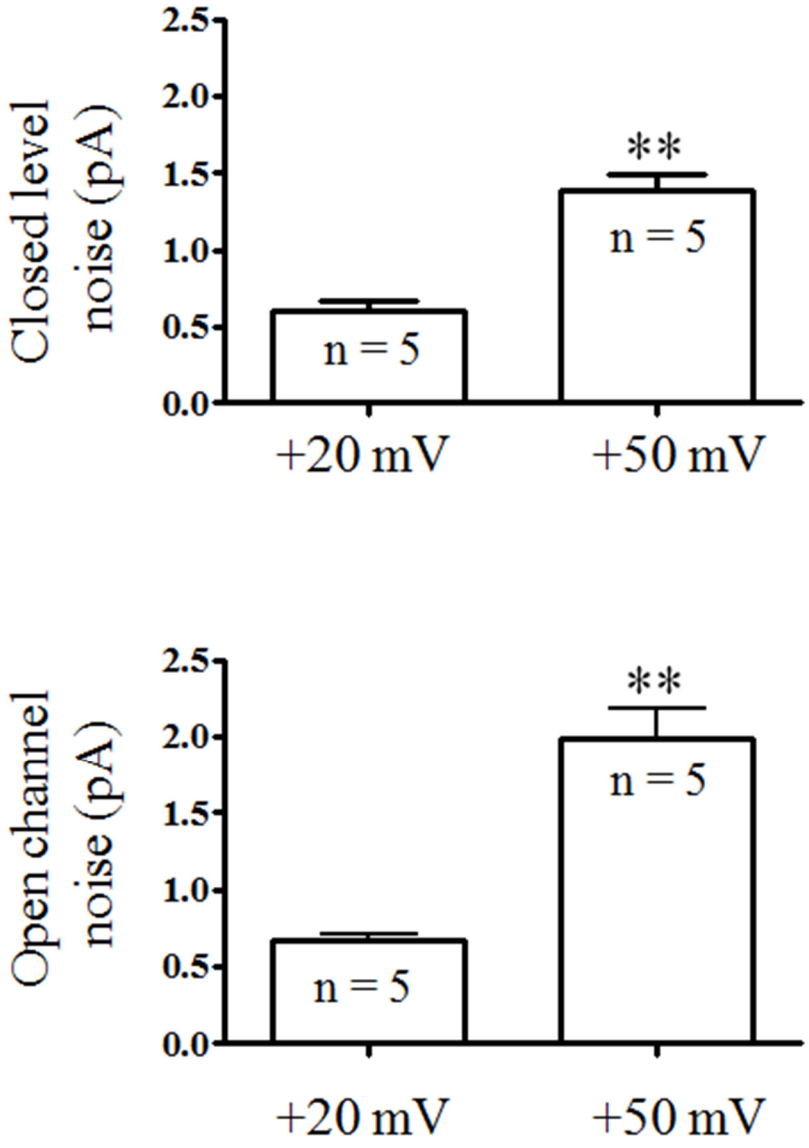


Figure 4.17 Comparing the closed and the open channel noise at holding potentials of +20 mV and +50 mV.
The bar charts show the noise of the fully closed level (above) and the full open channel level (below) of the SR K^+ channels from TRIC-A KO tissue at holding potentials of +20 mV and +50 mV (**p<0.01).

The Po_{SUB} at +20 mV and +50 mV when only one channel was gating in the bilayer was extracted from the Po-voltage plot in Figure 3.6 and presented in isolation in Figure 4.18. The small increment in Po_{SUB} at +50 mV compared to +20 mV could explain the increase in the closed and fully open level channel noise that we report in this thesis.

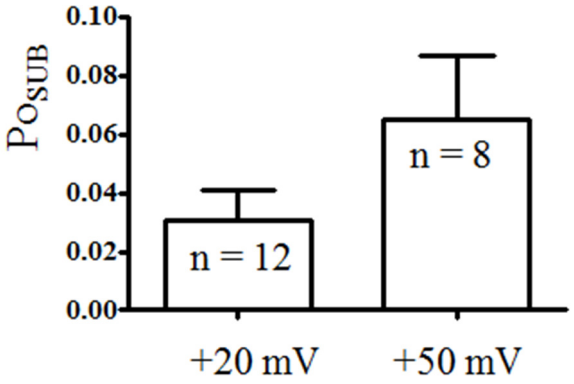


Figure 4.18 The effect voltage on Po_{SUB} Data are presented as mean ± SEM for Po_{SUB} values that were adapted from Matyjaszkiewicz et al (2015) (127).

4.3.6 WT tissue

In chapter 2, the single-channel properties of the SR K^+ channels from TRIC-A KO and WT tissue were compared. It was concluded that no differences between the gating of channels derived from WT or TRIC-A KO tissue could be identified under control conditions (210 mM KPIPES, pH 7.2). In this chapter, I have described a novel regulatory feature of the SR K^+ channels from the TRIC-A KO tissue. The channels appear to gate in a cooperative manner, with the Po of each channel increasing as the number of channels in the bilayer increases. My next aim was to investigate whether this cooperative gating phenomenon was also present in channels from WT tissue, as the SR K^+ channel population might be expected to be more heterogeneous.

4.3.6.1 The gating characteristics of the SR K^+ channel from WT tissue when there were two channels gating in the bilayer.

A representative example of the gating observed when two SR K^+ channels from WT tissue were gating in the bilayer is shown in Figure 4.19.

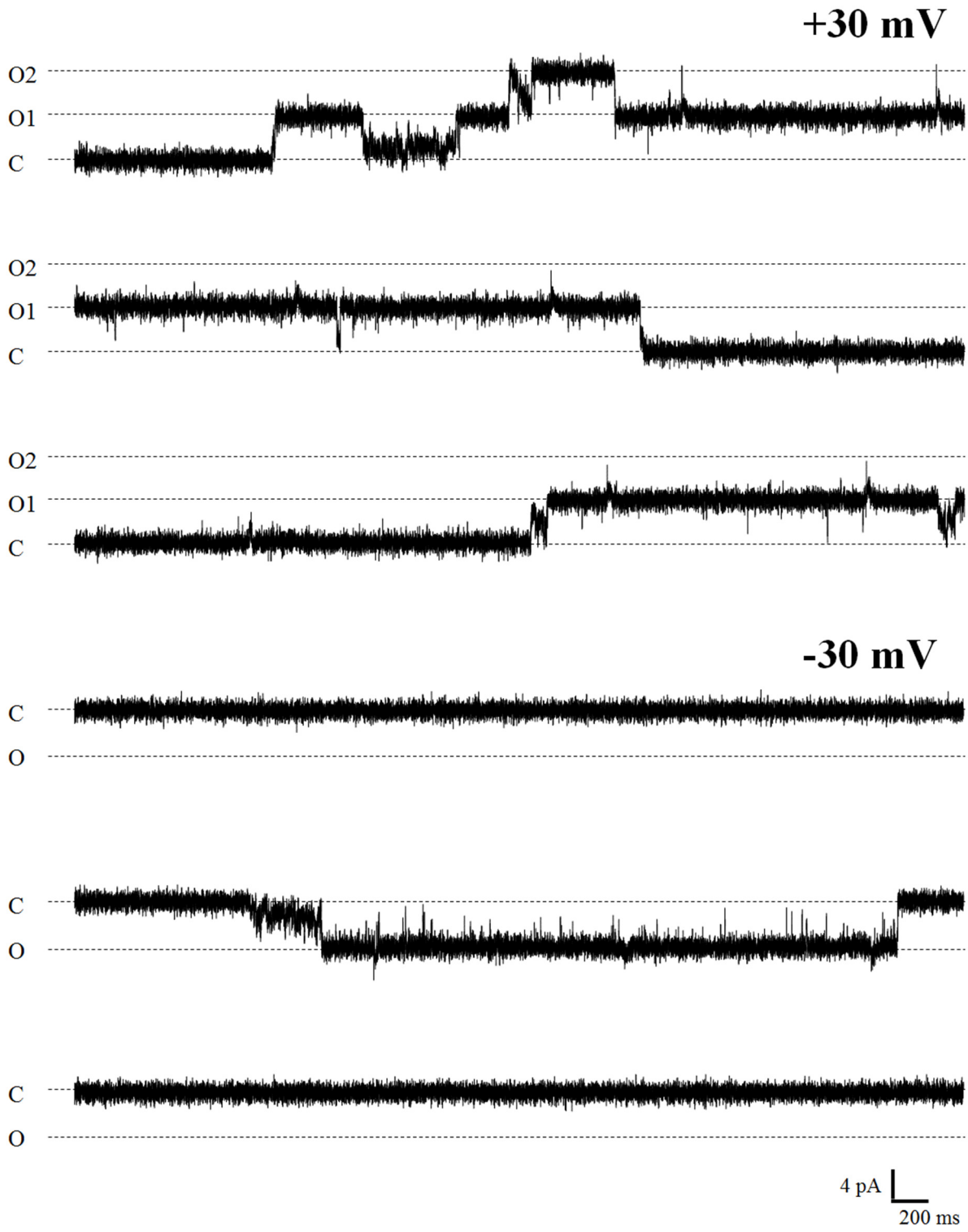


Figure 4.19 The gating of the SR K^+ channels from WT when there were two channels gating in the bilayer.
A representative single-channel trace at +30 mV (above) and -30 mV (below) when there were two SR K^+ channels gating in the bilayer in 210 mM KPIPES, pH 7.2 is shown. O1 and O2 indicate the channel levels for one and two SR K^+ channels opening, respectively, and C indicates the zero current level. The recording was low pass filtered at 1 kHz.

The mean data shown in Figure 4.20 compares the voltage-dependence and the contribution of $P_{O_{FULL}}$ to $P_{O_{TOTAL}}$ of the SR K^+ channels from WT tissue and TRIC-A KO tissue when two channels were present in the bilayer (*p<0.05, **p<0.01, ***p<0.001). There does not appear to be any difference between the KO and WT data

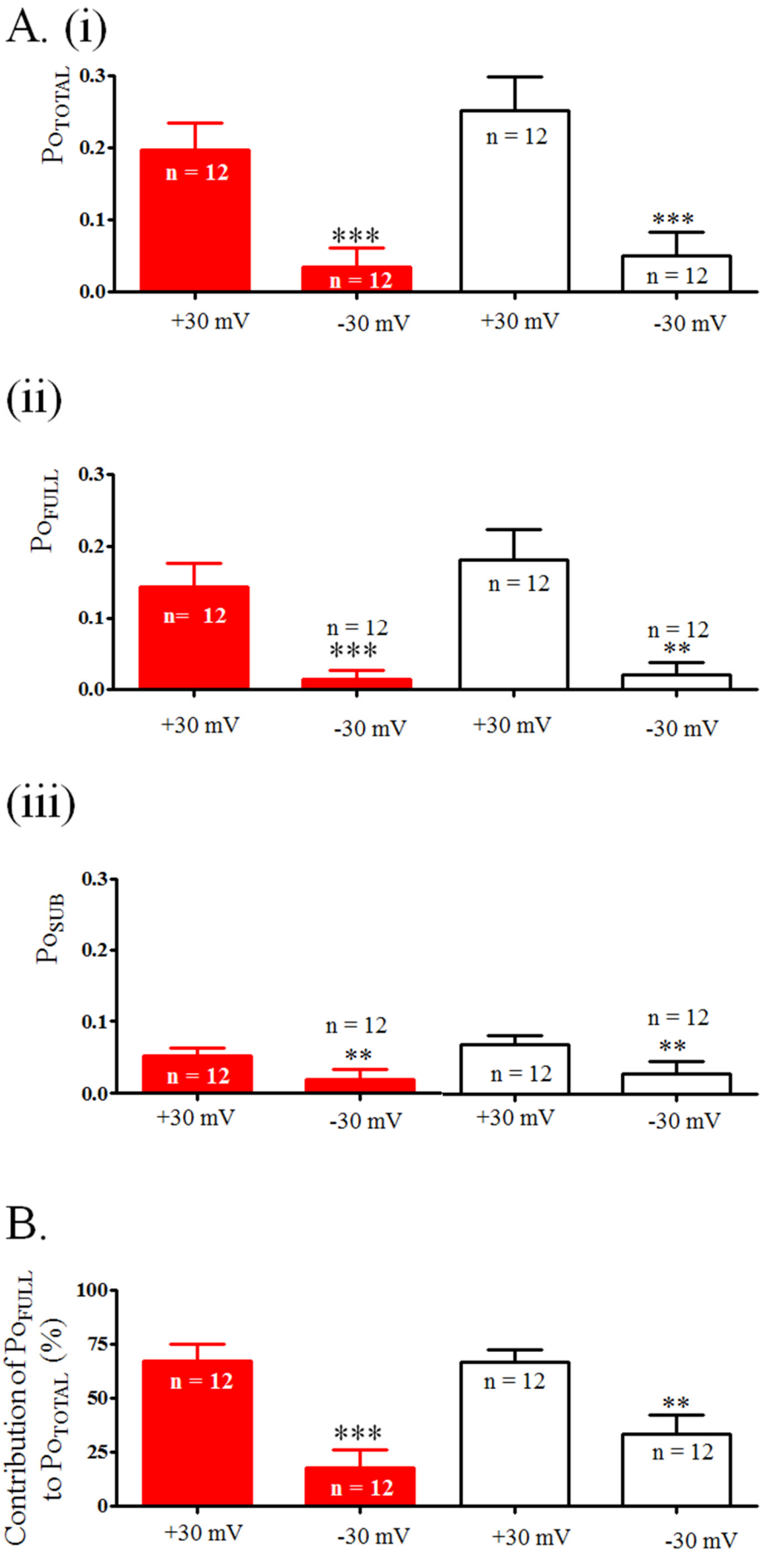

A. (i)
Po_{TOTAL}
0.3
0.2
0.1
0.0
n = 12
***
n = 12
n = 12
***
n = 12
+30 mV
-30 mV
+30 mV
-30 mV
(ii)
Po_{FULL}
0.3
0.2
0.1
0.0
n= 12
n = 12
***
n = 12
n = 12
**
+30 mV
-30 mV
+30 mV
-30 mV
(iii)
Po_{SUB}
0.3
0.2
0.1
0.0
n = 12
n = 12
**
n = 12
n = 12
**
+30 mV
-30 mV
+30 mV
-30 mV
B.
Contribution of Po_{FULL} to Po_{TOTAL} (%)
100
75
50
25
0
n = 12
***
n = 12
n = 12
**
n = 12
+30 mV
-30 mV
+30 mV
-30 mV

Figure 4.20 The gating properties of the SR K^+ channels from WT when two channels were gating in the bilayer
In A, the bar chart illustrates the Po of the SR K^+ channels from WT (red) compared to TRIC-A KO (white) when two channels were present in the bilayer. In B, the contribution of Po_{FULL} to Po_{TOTAL} is shown for WT (red) and TRIC-A KO (white). Data are presented as mean ± SEM (*p<0.05, **p<0.01, ***p<0.001).

4.3.6.2 The gating characteristics of the SR K^+ channels when three or four channels were gating in the bilayer.

Figure 4.21 compares the voltage-dependence and the contribution of Po_{FULL} to Po_{TOTAL} of the SR K^+ channels from WT tissue and TRIC-A KO tissue when three channels were present in the bilayer (*p<0.05, **p<0.01). Again, the Po of channels from WT and KO did not appear to differ in relation to the cooperative nature of gating.

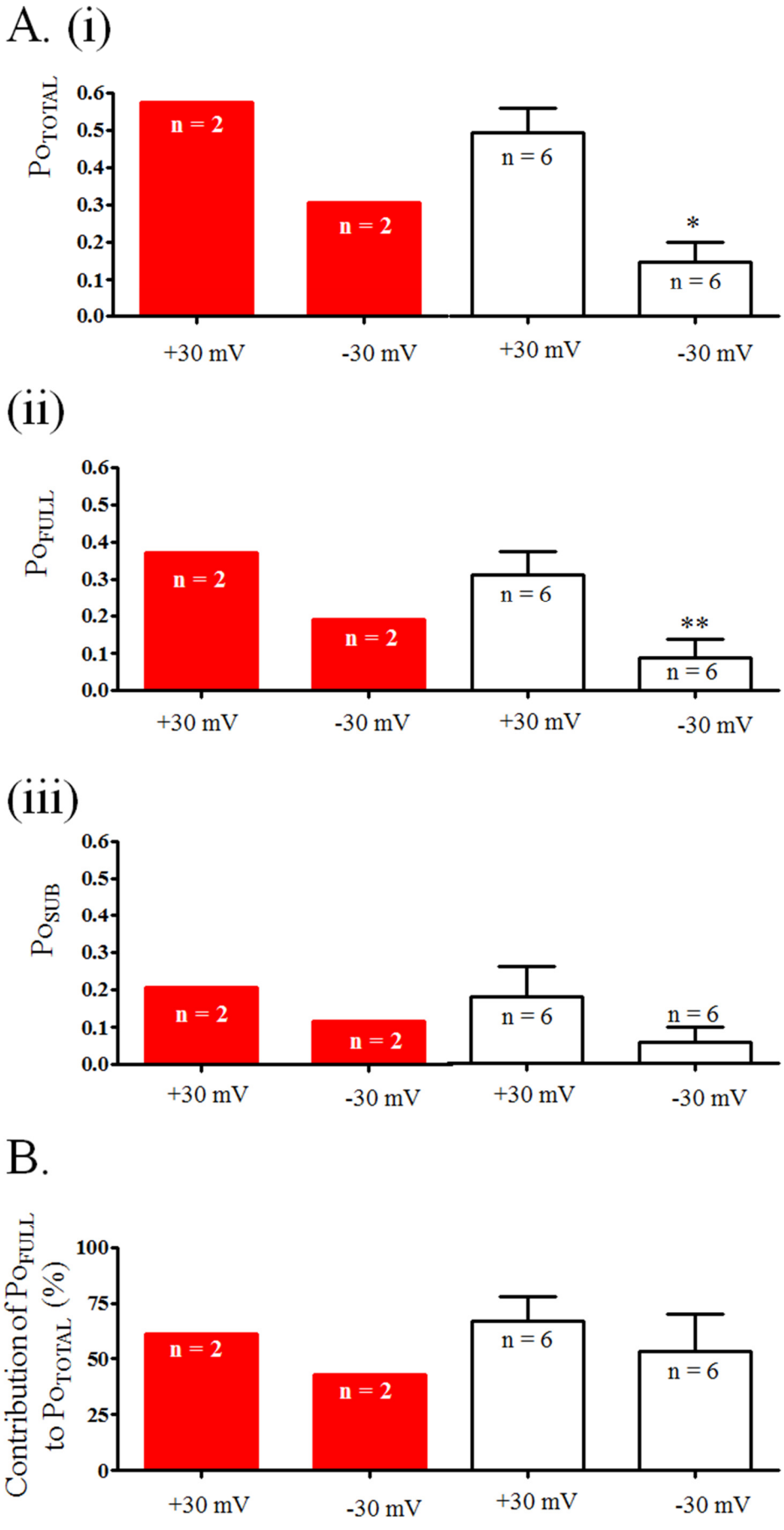

A. (i)
Po_{TOTAL}
0.6
0.5
0.4
0.3
0.2
0.1
0.0
n = 2
n = 2
n = 6
*
n = 6
+30 mV
-30 mV
+30 mV
-30 mV
(ii)
Po_{FULL}
0.6
0.5
0.4
0.3
0.2
0.1
0.0
n = 2
n = 2
n = 6
**
n = 6
+30 mV
-30 mV
+30 mV
-30 mV
(iii)
Po_{SUB}
0.6
0.5
0.4
0.3
0.2
0.1
0.0
n = 2
n = 2
n = 6
n = 6
+30 mV
-30 mV
+30 mV
-30 mV
B.
Contribution of Po_{FULL} to Po_{TOTAL} (%)
100
75
50
25
0
n = 2
n = 2
n = 6
n = 6
+30 mV
-30 mV
+30 mV
-30 mV

Figure 4.21 The gating properties of the SR K^+ channels from WT when three channels were gating in the bilayer
In A, the bar chart compares the Po_{TOTAL} (i), Po_{FULL} (ii) and Po_{SUB} (iii) at ± 30 mV from WT (red) and TRIC-A KO (white). In B, the contribution of Po_{FULL} to Po_{TOTAL} is shown for WT (red) and TRIC-A KO (white). The mean is shown for n=2, and mean ± SEM for n=6 (*p<0.05, **p<0.01).

Figure 4.22 compares the Po of the SR K^+ channels from WT (red) and TRIC-A KO (white) when four channels were present in the bilayer. There could be some differences in the Po at -30 mV between channels from TRIC-A KO and WT tissue, but higher n numbers are required to establish this.

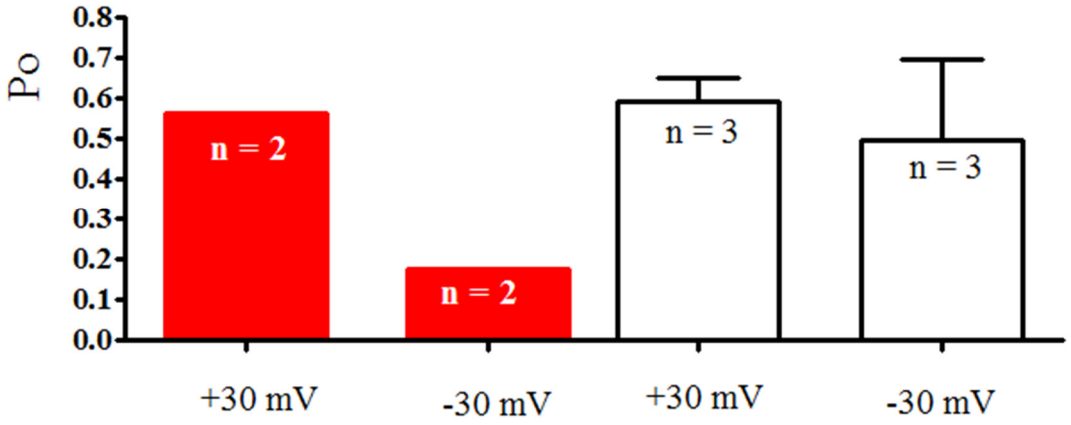


Figure 4.22 The voltage-dependence of the SR K^+ channels when four channels were gating in the bilayer
The Po of WT (red) and TRIC-A KO (white) when 4 channels were in the bilayer is illustrated. The mean data are presented for WT and mean ± SD for TRIC-A KO.

4.3.7 Is the cooperative nature of the SR K^+ channels altered in preps that contain TRIC-A K^+ channels?

In Figure 4.23, we compared the Po of the SR K^+ channels from WT (red) and TRIC-A KO (white) tissue when one, two, three or four channels were gating in the bilayer at ± 30 mV. The figure illustrates that the single-channel properties of the SR K^+ channels from WT and TRIC-A KO are similar. The channels from both preparations have similar conductance,

voltage-sensitivity and contribution of Po_{FULL} to Po_{TOTAL}. In addition, in this chapter, I have demonstrated that the SR K^+ channels from both WT and TRIC-A KO tissue seem to gate in a cooperative manner. Only the average Po for the WT channels at -30 mV with four channels in the bilayer appears to be lower than might be expected. Since only 2 experiments were included, we conclude that there is not enough evidence to discern a difference. Therefore, we decided to combine the channels from TRIC-A KO and WT, as shown in Figure 4.24.

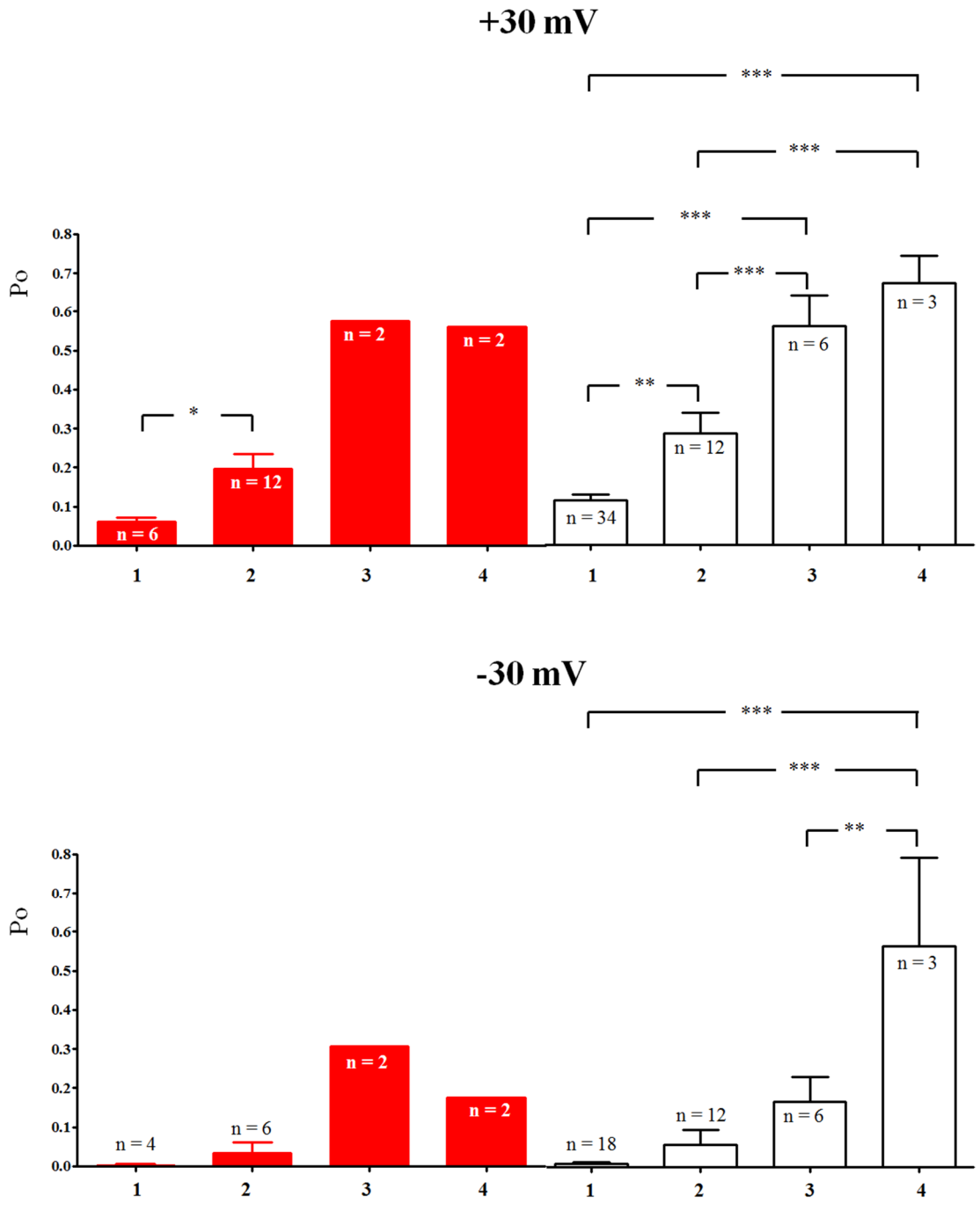
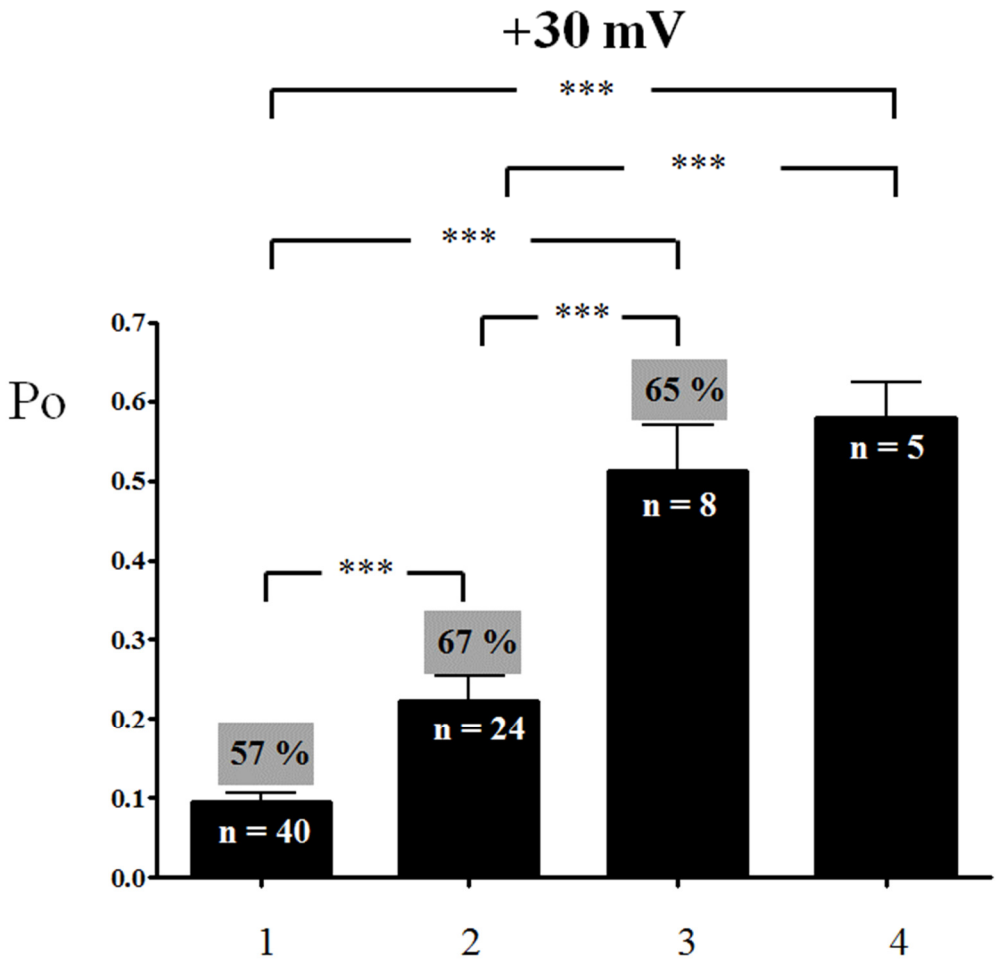


Figure 4.23 SR K^+ channels from WT tissue also gate in a cooperative manner
The Po of the SR K^+ channel from WT (red) and TRIC-A KO (white) increase as the number of channels in the bilayer increases. Mean values are shown with n values labelled within the bars. Error bars are SEM when $n \geq 4$ (*p<0.05, **p<0.01, ***p<0.001).


+30 mV
Po
***
***
***
***
***
0.7
0.6
0.5
0.4
0.3
0.2
0.1
0.0
65 %
n = 5
n = 8
67 %
n = 24
57 %
n = 40
1
2
3
4

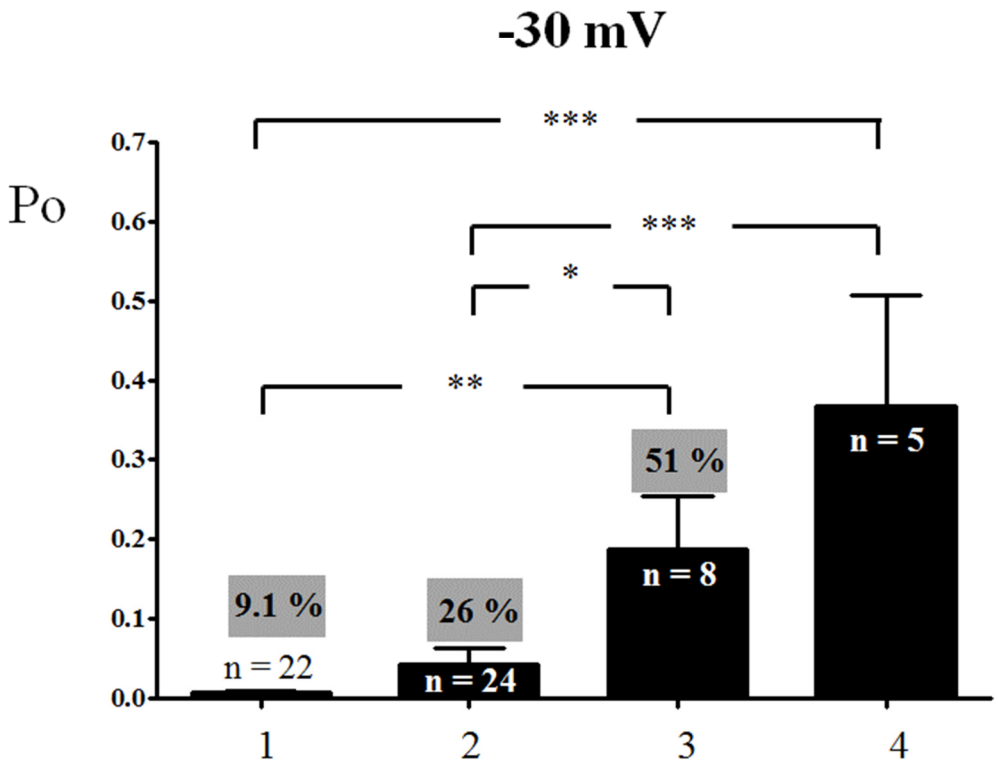

-30 mV
Po
***
***
*
**
0.7
0.6
0.5
0.4
0.3
0.2
0.1
0.0
51 %
n = 5
n = 8
9.1 %
n = 22
26 %
n = 24
1
2
3
4

Figure 4.24 Combining data from TRIC-A KO and WT tissue to determine SR K^+ channel cooperativity
The bar charts show Po of the SR K^+ channels (black columns) as the number of channels present in the bilayer increases. The number of channels in the bilayer are shown underneath each column and the n numbers are indicated within each column. The contribution of Po_{FULL} to Po_{TOTAL} is highlighted in the grey box above each column. The data are presented as mean ± SEM (*p<0.05, **p<0.01, ***p<0.001)

The contribution of Po_{FULL} to Po_{TOTAL} remains relatively constant at +30 mV as the number of channels in the bilayer increases. However, at -30 mV, the contribution of Po_{FULL} to Po_{TOTAL} increases markedly as the number of channels in the bilayer increases. This may reflect the basic gating behaviour of the SR K^+ channels described in Chapter 3 of this thesis.

4.3.8 SR K^+ channels deviate from the binomial distribution prediction

In this chapter, we have illustrated (Figure 4.24) that the Po of the SR K^+ channels increased as the number of channels present in the bilayer increased, suggesting that the channels gate in a cooperative, non-independent fashion. To investigate this further, we preformed binomial distribution analysis using the Po measurements from combined WT and TRIC-A KO single-channel experiments where only one SR K^+ channel was gating in the bilayer (0.09 ± 0.01 at +30 mV and 0.007 ± 0.003 at -30 mV). As illustrated in Figure 4.25 if four identical SR K^+ channels were gating in the bilayer, we used binomial analysis to predict the probability of events in the closed (level 0) and the four full open levels (1-4) if each channel gated independently. We then compared the binomial prediction to our experimental data when we actually did observe four SR K^+ channels gating in the bilayer (n=5, SEM). In the binomial prediction, at +30 mV, if 4 identical SR K^+ channels were gating in the bilayer each with a Po of approximately 0.1, the level that represents all four SR K^+ channels being closed would be observed most frequently, followed by the level that represents one open SR K^+ channel. This is the opposite of what we observed in our

experimental data, with no effects to the level that represents all four SR K^+ channels being closed (hence the use of 1 mM cytosolic decamethonium to induce closing events). On the other hand, at -30 mV, if 4 identical SR K^+ channels were gating in the bilayer with a Po of approximately 0.01, the level that represents all four SR K^+ channels being closed would be observed most frequently, and opening events would be rare. Again, this is not what we observed in our experimental recordings, as we had many full open bursts even at negative holding potentials.

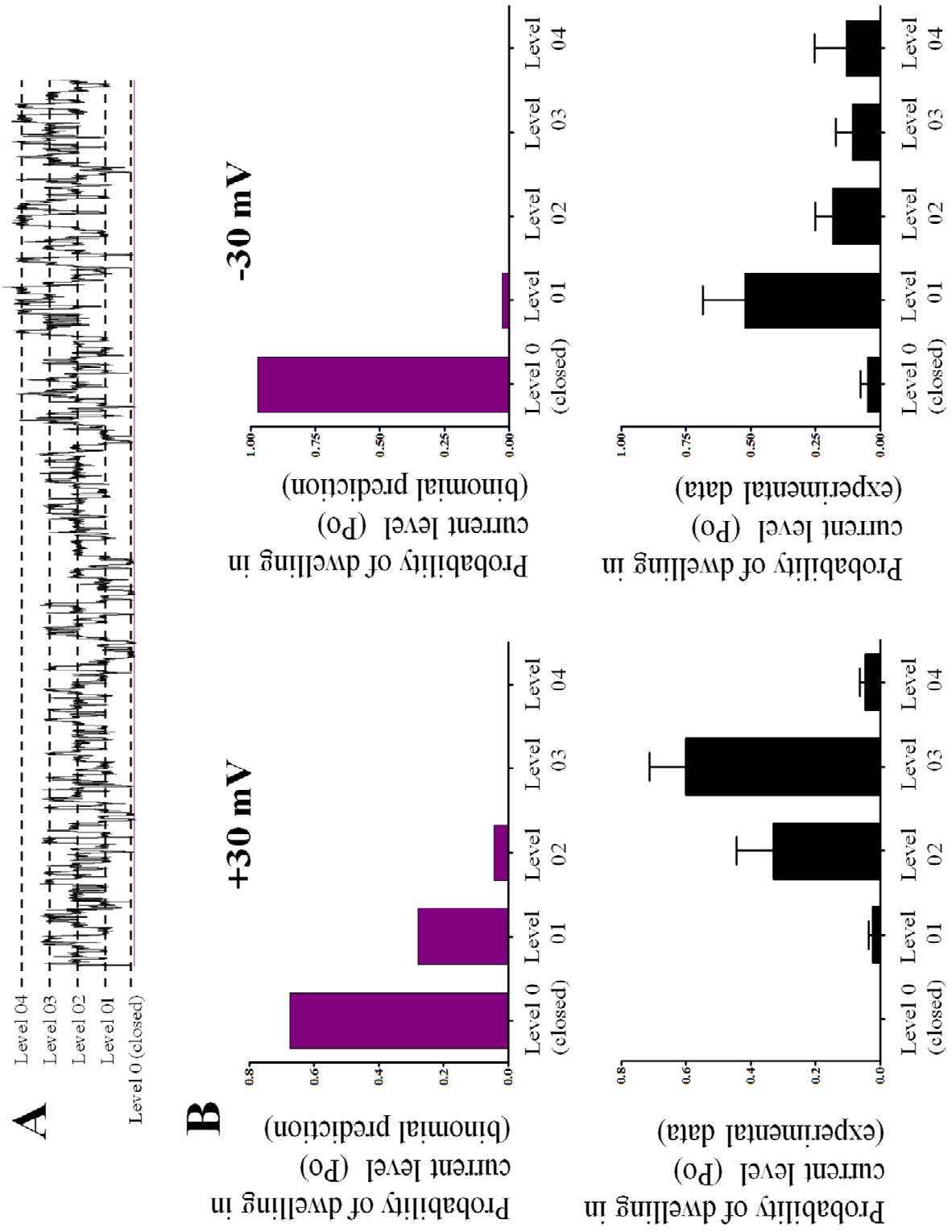


Figure 4.25 The gating of multiple SR K^+ channels in the bilayer deviates from the binomial distribution prediction

When four channels are present in the bilayer, as illustrated in A (+30 mV) there are five possible current levels that may be observed. Levels include the level where all four channels are closed (level 0) and the levels when one (level 01), two (level 02), three (level 03) or four (level 04) channels are open. In B, the bar charts illustrate the distributions of the probability of current amplitudes (levels) occurrence, predicted from binomial distribution analysis that would arise if four identical and independent SR K^+ channels were

present in the bilayer (purple). This was calculated from the Po for single channels (0.09 ± 0.01 at +30 mV and 0.007 ± 0.003 at -30 mV).Our experimental data, when four SR K^+ channels were in the bilayer, is shown underneath (in black) for visual comparison. Each level (level 0 – level 04) corresponds to the levels outlined in A. The experimental data are presented as mean ± SEM for n = 5.

4.4 Summary and Discussion

The objective of this study was to investigate if the single-channel properties of the SR K^+ channels from TRIC-A KO and WT tissue were altered when more than one channel was present in the bilayer. In experimental recordings where we observed multiple SR K^+ channels gating, we therefore explored the possibility that the channels may not be gating independently, and thus, may instead be gating in a cooperative manner.

4.4.1 The Po of the SR K^+ channels increases as the number of channels gating in the bilayer increases

Irrespective of whether we incorporated the LSR from TRIC-A KO or WT tissue into artificial bilayers, we found that there was correlation between the number of SR K^+ channels that were present in the bilayer and the gating of each channel in that experiment. As illustrated in Figure 4.24, as the number of channels in the bilayer increased, the average Po of each SR K^+ channel also increased. In addition, we found that the contribution of the full open state increased as the number of channels in the bilayer increased. The changes in the basic biophysical properties that were observed when there was more than one SR K^+ channel gating bilayer seemed be more pronounced at -30 mV. For example, when only a single-channel was present in the bilayer, we rarely observed events to the full open channel state, and in addition, the contribution of Po_{FULL} to Po_{TOTAL} was only ~ 10%. However, when three SR K^+ channels were gating in the bilayer, the Po_{FULL} increased markedly, accompanied by an increase in contribution of Po_{FULL} to Po_{TOTAL} (51 %). Under our experimental conditions, we have never recorded a single-channel experiment, when only one SR K^+ channel was present in the bilayer that displayed such a high Po_{FULL} and contribution of Po_{FULL} to Po_{TOTAL}.

At +30 mV, as the number of channels in the bilayer increased, Po increased in a non-linear manner, as illustrated in Figure 4.26. The average Po of each SR K^+ channel appeared to plateau in experiments where three and four channels were gating in the bilayer. It may be that four SR K^+ channels are required for each channel to gate with a maximum Po (of approximately 0.6). This may be due to a particular channel arrangement or cluster of SR K^+ channels. Another possibility is that the SR K^+ channels may regulate each other in *pairs*. As illustrated in Figure 4.26 there appears to be a steep increase in Po when three channels were in the bilayer compared to the Po when two channels were in the bilayer. This increment in Po is markedly steeper than the Po change that was observed going from one to two channels in the bilayer and from three to four channels in the bilayer. It could be that increasing the number of channels in the bilayer from an odd number to an even number (1 channel to 2 channels and from 3 channels to 4 channels) has less of an effect on channel gating than increasing the number of channels from an even number to an odd number (2 channels to 3 channels). Further experiments are necessary to investigate whether another steep increment in Po would occur in experiments where there are five channels present (increasing number of channels from an even number to an odd number) followed by another 'plateau' feature when 6 SR K channels are present (increasing number of channels from an odd number to an even number). At -30 mV, the increase in channel Po as the number of channels in the bilayer are increased seems to follow a more linear pattern. However, the error bars are significantly large at -30 mV compared to +30 mV, and therefore, more experiments will be required to determine if the Po at -30 mV plateaus.

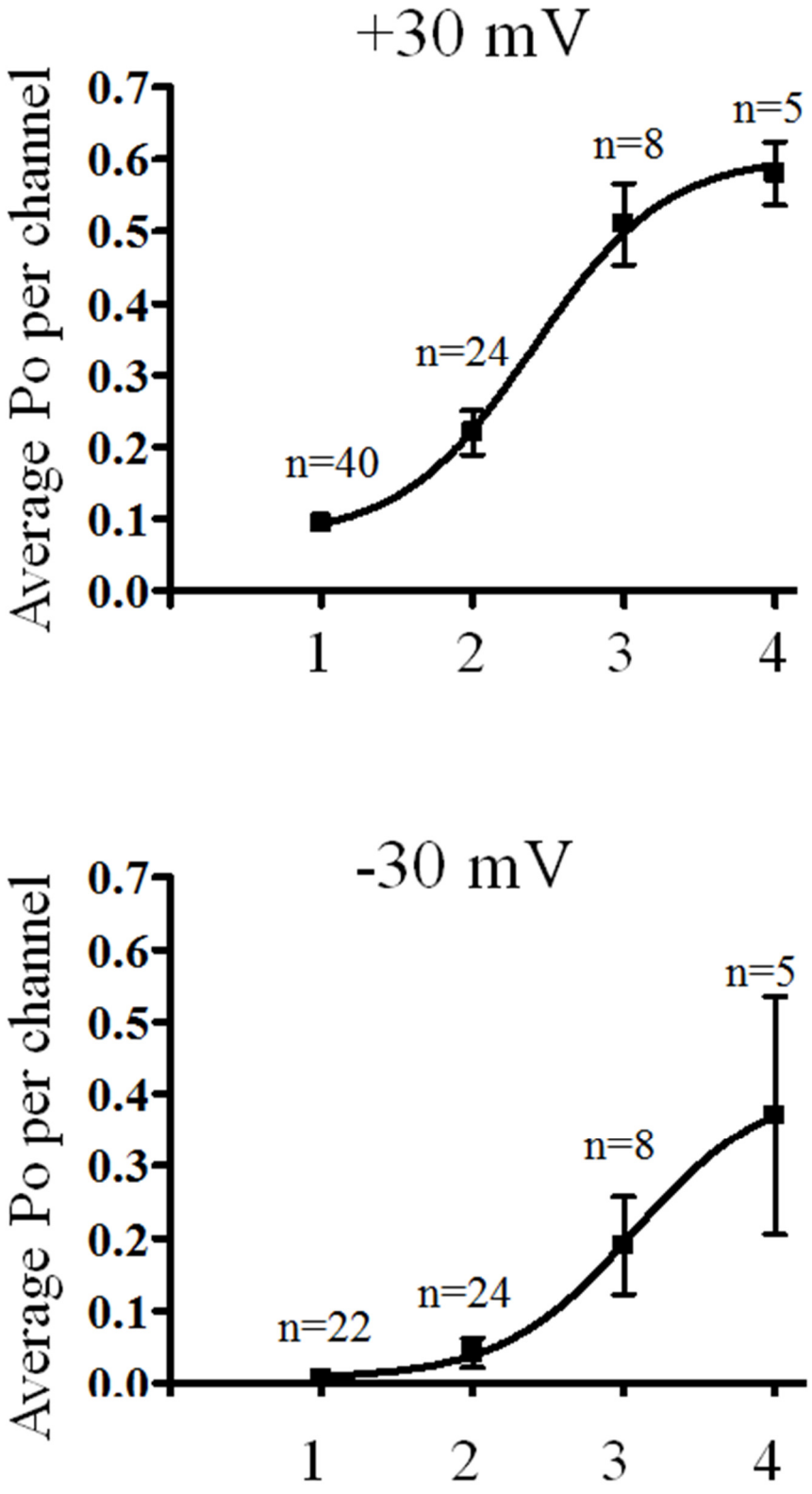


Figure 4.26 The average Po of the SR K^+ channels increases in a non-linear manner as the number of channels in the bilayer increases.

The average Po of each SR K^+ channel as the number of channels in the bilayer increases is shown. Data are presented as mean SEM. Where error bars are not visible, they lie within the symbol. N values are illustrated above each appropriate Po value.

4.4.2 Po-voltage relationships when more than one channel is in the bilayer

Irrespective of the number of channels in the bilayer, the Po was always slightly higher at +30 mV compared to -30 mV in both TRIC-A KO and WT preparations. However, as the number of channels in the bilayer increased, the Po at +30 mV increased and the Po at -30 mV increased, and thus, it appeared that the voltage-dependence was decreased.

I considered if it was possible that the cooperativity observed with increased channel number was caused by a shift to the left of the voltage-dependence of gating. Po tends to plateau at + 20 mV when only one channel is gating in the bilayer. However, I have shown that this feature is still retained when multiple SR K^+ channels are present in the bilayer (Figure 4.16) so that, even if the curve was shifted to the left, we would still observe a plateau between 20 mV and 50 mV. In addition, simply shifting the Po-voltage relationship to the left does not account for the increase in average Po that is observed when multiple channels are present in the bilayer. I therefore suggest that while cooperativity between the channels does alter the voltage-dependence of the channels, another mechanism must also be required to induce the large increases in channel Po that are observed.

4.4.3 The gating of the SR K^+ channels deviates from the binomial statistical prediction

In our experimental recordings when there were four SR K^+ channels gating in the bilayer, we examined the distribution of the probabilities of the amplitude levels that we observed, ranging from the fully closed level to the level where four SR K^+ channels were open. At +30 mV, the probability of dwelling in the amplitudes that corresponded to two and three open SR K^+ channels was higher than the probability of dwelling in the other amplitudes.

In addition, we rarely observed periods where all four SR K^+ channels were closed at the same time. In contrast, at -30 mV the probability of dwelling in the amplitude that corresponded to one SR K^+ channel was much higher than the probability of dwelling in other amplitudes. The remaining amplitudes appeared to have a similar probability of occurring. To determine the 'expected' distribution that would arise if we had four independent SR K^+ channels in the bilayer, we preformed binomial distribution analysis, using our Po calculations when only one single channel was in the bilayer (Po at +30 mV = 0.094 ± 0.012, n=40, and Po at -30 mV = 0.006 ± 0.003, n=22). As illustrated in Figure 4.25, the distributions of the observed levels from our experimental data did not coincide with the outcome predicted by the binomial distribution analysis. One possibility that could account for the differences between our experimental data and our predicted data might be a heterogeneity in SR K^+ channel Po. However, based on our single-channel recordings where only one SR K^+ channel was present in the bilayer, we did not observe any channels with high Po. A second possibility could be that we performed our binomial distribution analysis based on an incorrect Po estimate for a single SR K^+ channel. In this chapter, and in publications from this laboratory (126, 127) , when only one SR K^+ channel was gating in the bilayer, the Po appeared to be consistently low (n=40 single-channel recordings from 8 preparations), even when maximally activated at positive holding potentials. Our Po measurements appear lower than those that have been reported by other groups (139, 140) , and so, in Figure 4.27, the binomial analysis was repeated using a higher Po value to determine whether a higher Po value could fit our experimental data. We used the average Po obtained at ± 30 mV when there were four SR K^+ channels gating in the bilayer (0.58 ± 0.044 at +30 mV and 0.37 ± 0.14). As illustrated in Figure 4.27, when the binomial prediction analysis is repeated using a higher Po value, the predicted distribution of levels that would be observed when 4 independent channels were gating in the bilayer still does

not fit our experimental data at both +30 mV and -30 mV. We can hypothesise, therefore, that the reason why our initial binomial distribution prediction (that was calculating our experimental data where only one SR K^+ channel was gating in the bilayer) did not fit our experimental data (where we had 4 SR K^+ channels gating in the bilayer) was *not* due to to our single-channel Po measurements being too low or incorrectly calculated.

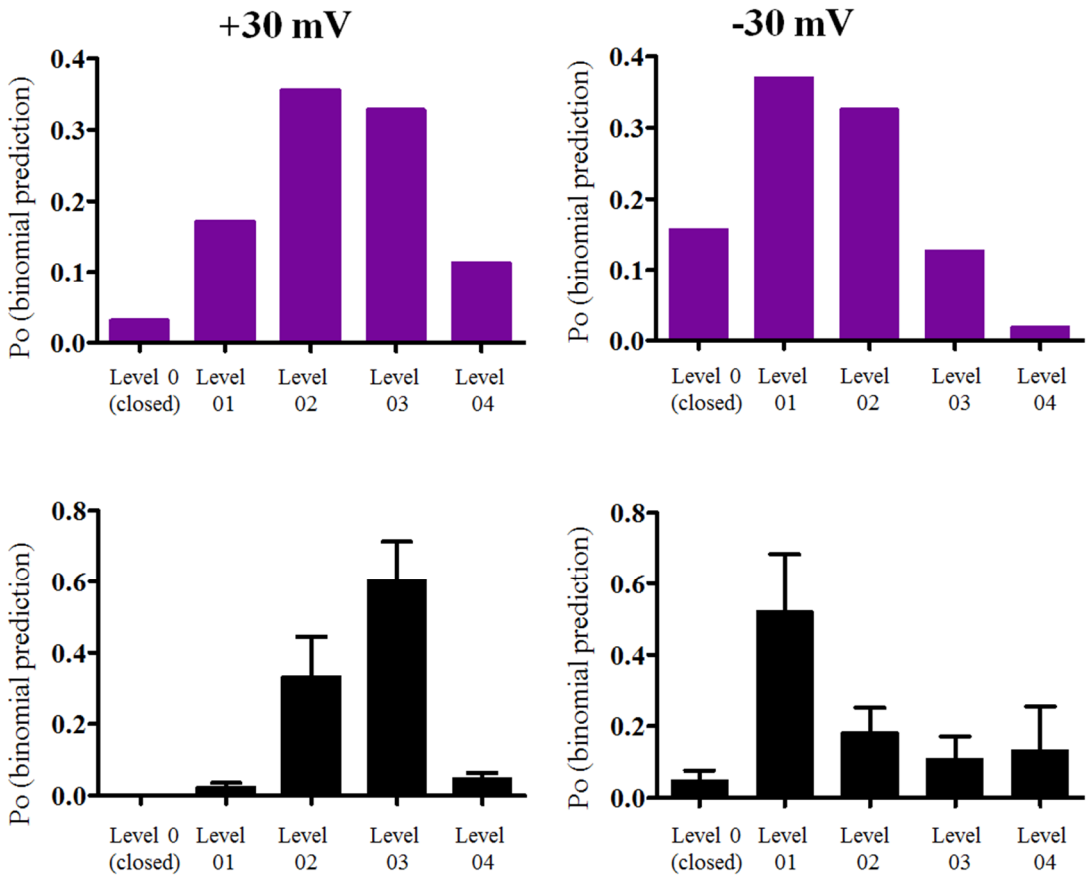


Figure 4.27 The binomial distribution prediction for SR K^+ channels with a higher Po than our single-channel experiments
The purple bar charts illustrate the distributions of the probability of current amplitudes (levels) occurring from binomial distribution statistics that would arise if 4 identical and independent SR K^+ channels were present in the bilayer. Our experimental data, when four SR K^+ channels were in the bilayer, is shown underneath (in black) for visual comparison. Level 0 indicates the zero current level (all 4 SR K^+ channels closed, and level 01–04 indicates the levels of 1-4 open SR K^+ channels , respectively.

Labarca *et al* (1980) (135) first questioned the capability of the SR K^+ channels to gate in a non-independent manner. From their experimental data, when four SR K^+ channels were gating in the bilayer, the probability distribution of the observed levels were shown alongside the predicted values from the binomial statistics. Comparison of their data at +40 mV, with my data at +30 mV shows that the probability of dwelling in the amplitudes that corresponded to one and two open SR K^+ channels was higher than the probability of dwelling in the other amplitudes, and so, the data appears to fit with our observed data at +30 mV.

However, in contrast to what is reported in this thesis, Labarca *et al* (1980) (135) suggested that their experimental data agreed with the binomial prediction and thus, when multiple SR K^+ channels were gating together in a bilayer, they suggested that channels were gating in an independent manner.

However, it should be noted that in this paper, the single-channel Po value was estimated from experiments where >1,000 ion-channels were gating in the bilayer and not from experiments where a single SR K^+ channel was gating. While we can draw similarities between the distribution of observed levels reported in Labarca *et al* (1980) (135) at +40 mV from a *single* bilayer where four channels were gating to our experimental data at +30 mV where we had four channels gating we question the accuracy of their single-channel Po estimate.

4.4.4 Decamethonium block of the SR K^+ channel

In this study, we used decamethonium to distinguish between current fluctuations from open ion-channels and a leak in the bilayer in recordings where the zero current level was not observed. Decamethonium induced channel closings that enabled us to count the channels in the bilayer. The channel closings are thought to represent the rapid transitions

between the fully open and blocked state of the channel, when the drug is thought to bind inside the pore, thus inhibiting K^+ flux (97, 120). We demonstrated that cytosolic decamethonium reduced the Po of the SR K^+ channel at +30 mV. This was expected, as by holding the bilayer at + 30 mV, we essentially applied a driving force that could drive decamethonium, a positively charged drug, into the pore of the channel. The reduction in Po at +30 mV was associated with an apparent reduction in the mean open time of the full open state. At -30mV, we still observed an increase in the blocking events in the presence of decamethonium, coupled with an observed trend towards a decrease in mean open time. The results presented in this thesis are slightly different to those reported by Coronado *et al* (1980) (120) when the effect of luminal decamethonium was investigated on the gating of the skeletal SR K^+ channel. They described the blocking events as being voltage-dependent, in that, the block was only observed at voltages that would drive the drug from the luminal channel side into the pore. However, they never explored decamethonium block from the cytosolic side of the channel. It is likely that decamethonium binds to two different sites, one with access from the cytosolic side and one with access from the luminal side. Tomlins *et al* (1984) (97) subsequently described decamethonium block of the cardiac isoform. When decamethonium was added to both sides of the channel, they reported that there were more closings events at negative holding potentials (potentials that would drive decamethonium into luminal sites within the channel pore) compared to positive holding potentials. Based on the data presented in this chapter, if cytosolic decamethonium can induce closing events even at unfavourable voltages (-30 mV) as well as expected voltages (+30 mV), then perhaps this would explain why Tomlins *et al* (1984) (97) observed more block at negative holding potentials, due to a combination of cytosolic and luminal block. However, additional experiments are necessary to determine the differences between block of decamethonium from the cytosolic and the luminal side of the channel. It is also worth

noting that although we have only provided a brief analysis in this thesis, this is the first report describing decamethonium block of SR K^+ channels from TRIC-A KO tissue, and thus, it is possible that the SR K^+ channels from TRIC-A KO and WT differ in their responses to decamethonium.

5 Does cooperativity between RyRs and SR K^+ channels exist?

5.1 Introduction

In Chapter 4, I have demonstrated that the single-channel gating properties of the SR K^+ channels were markedly affected by the number of channels that were present in the bilayer, indicating that the channels were not gating independently. The Po of each SR K^+ channel increased as the number of channels in the bilayer increased, suggesting that the channels may gate in a cooperative manner. This 'non-independent' gating behaviour was confirmed as the data deviated from binomial distribution predictions. We do not know if the cooperative gating that was observed was a result of a specific physical interaction between SR K^+ channels or whether it was due another reason such as concerted channel activation induced by changes in membrane tension resulting from the opening of a channel.

As discussed previously, RyRs can gate in coupled manner, with synchronous opening and closing events that are observable at the single-channel level (65, 110). Coupled RyR gating may be, in part, due to a physical RyR-RyR interaction, as coupled gating events of purified RyR1 was only found to occur in fractions with a coefficient of sedimentation $\geq$ 60 S, which represents RyR dimers or large structures (110). Coupled gating was not observed when the purified RyR1 from the 30 S fraction was reconstituted (110).

The aim of this chapter is to investigate if any of the gating features of the SR K^+ channels that have been described in Chapter 3 and Chapter 4 of this thesis are altered when a RyR is also gating in the bilayer. To increase the probability of fusing an SR vesical that contains both an SR K^+ channel and a RyR, the HSR was used for these experiments. In addition, these particular experiments would provide an opportunity for me to study the gating of a RyR when there is also an SR K^+ channel in the bilayer. The results from this chapter will assist in determining how the SR ion-channels may communicate with each other in order to fine tune highly regulated Ca^{2+} movements that are required for normal function.

5.2 Methods

5.2.1 Incorporation of SR vesicles containing an SR K^+ channel and a RyR

To increase the possibility of incorporating an SR vesicle that contained both a RyR and an SR K^+ channel, we used the HSR fraction. As a lab, we intend to compare the differences between WT and TRIC-A KO tissue since it has been suggested that TRIC-A may associate with RyR whereas TRIC-B may be more likely to localise with IP_3R (137). I primarily studied the TRIC-A KO tissue but others in the group are now studying WT tissue in more detail. The current fluctuations that were observed in symmetrical in 210 mM KPIPES, pH 7.2 were recorded.

5.2.2 Distinguishing the current-fluctuations due to RyR from those of an SR K^+ channel

The single-channel properties of a RyR can be distinguished from those of the SR K^+ channel when both channels are gating together in symmetrical K^+ solutions. A RyR and an SR K^+ channel from TRIC-A KO tissue are shown gating simultaneously in Figure 5.1 to visually highlight the differences in the biophysical properties. The first, most obvious difference between the two channels is the current amplitude of the open states. In 210 mM symmetrical K^+ the RyR has a larger current amplitude than the SR K^+ channel at any holding potential. As illustrated in Figure 3.2 , the conductance of the full open state of the SR K^+ channel is approximately 210 pS. However, as illustrated in a representative example, in Figure 5.1, the single-channel conductance of RyR is approximately 780 pS, which is in agreement with previous publications (74, 79, 80).

The corresponding single-channel conductances are shown in Figure 5.1. As described in this thesis, the SR K^+ channel gates to sub-conductance open states in addition to the main 200 pS level, while the RyR usually gates to a single main conductance level (74, 79, 80).

Finally, the typical gating behaviour of each channel is completely different. Representative openings from SR K^+ channels consist of long-lived dwellings in the full open channel level (in addition to sub-conductance gating events). In contrast, with cytosolic contaminant Ca^{2+} (10 μM) as the sole activator, typical openings of skeletal RyR are extremely short-lived (74, 79, 80). Thus, considering the differences outlined above, it was possible to visually distinguish the openings of a RyR (presumably RyR1 since this is the most common isoform in mammalian skeletal muscle) from the openings of an SR K^+ channel when both channels were simultaneously gating in an experimental recording.

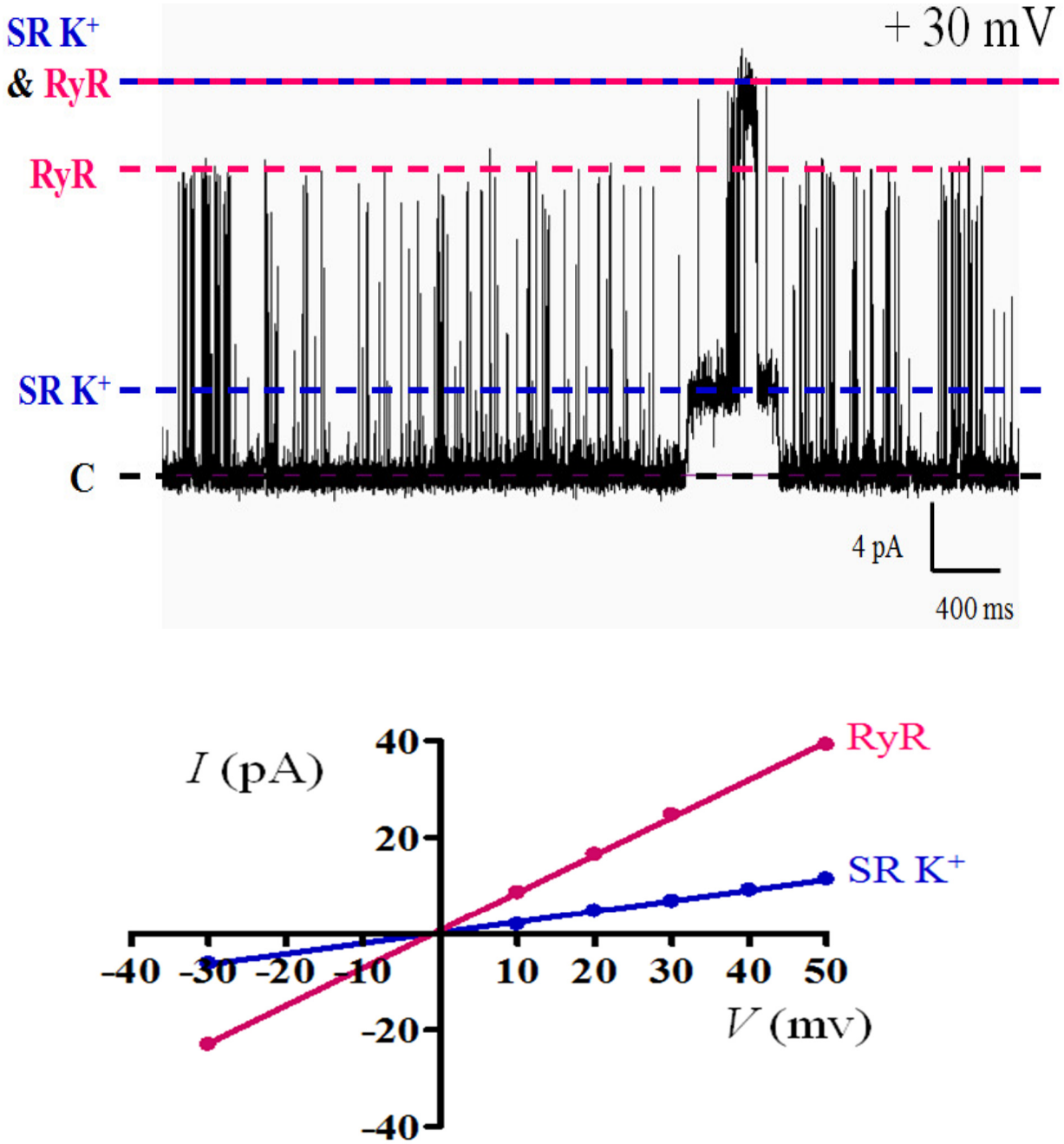


Figure 5.1 The current fluctuations that are observed when both an SR K^+ channel and a RyR are gating in the bilayer.

A representative single-channel trace at +30 mV when an SR K^+ channel and a RyR from TRIC-A KO tissue were simultaneously gating in 210 mM KPIPES, pH 7.2 is shown above. The fully open levels of the SR K^+ channel and RyR are labelled and illustrated by the blue and pink dashed lines, respectively. The current amplitude level produced when both channels are simultaneously open is indicated by the multi-coloured (blue and pink) dashed line. C illustrates the zero current level. The trace was low pass filtered at 1 kHz. Below, the current voltage relationship for the SR K^+ channel and the RyR that was obtained from a single experiment where both channels were gating in the bilayer is shown.

5.2.3 Choosing an optimal filtering level to analyse the current fluctuations when both a RyR and an SR K^+ channel were gating in the bilayer

As discussed in this thesis, and in publications from this laboratory, when analysing the single-channel properties of the SR K^+ channel, a cut off filter of 1 kHz is sufficient to remove high frequency noise but retain obvious gating properties of the SR K^+ channel (101, 126, 127). However, when the single-channel properties of RyR are examined with K^+ as the permeant ion, due to the favourable signal to noise ratio and because of the very short-lived openings, traces are usually filtered between 2 and 5 kHz to ensure that the openings are resolved (79, 80). Therefore, when there was an SR K^+ channel and a RyR present in the bilayer, the first difficulty was deciding on a suitable filtering level. To begin, traces were visualised with a cut-off filter of 1 kHz (as shown in Figure 5.1). However, at a filtering level of 1 kHz, many short-lived openings were observed that appeared to be RyR-like events but they were slightly truncated in current amplitude. When the cut off frequency of the filter was increased from 1 kHz to 4 kHz, a proportion of the truncated, short-lived events (that could have been due to an SR K^+ or a RyR channel) appeared to have a larger current amplitude, as illustrated in Figure 5.2. Therefore, to discern which filtering level was most suitable for our analysis, in addition to visually inspecting each trace at 1 kHz and 4 kHz, we compared the overall Po of the RyR and the SR K^+ channel at 1 kHz and 4 kHz.

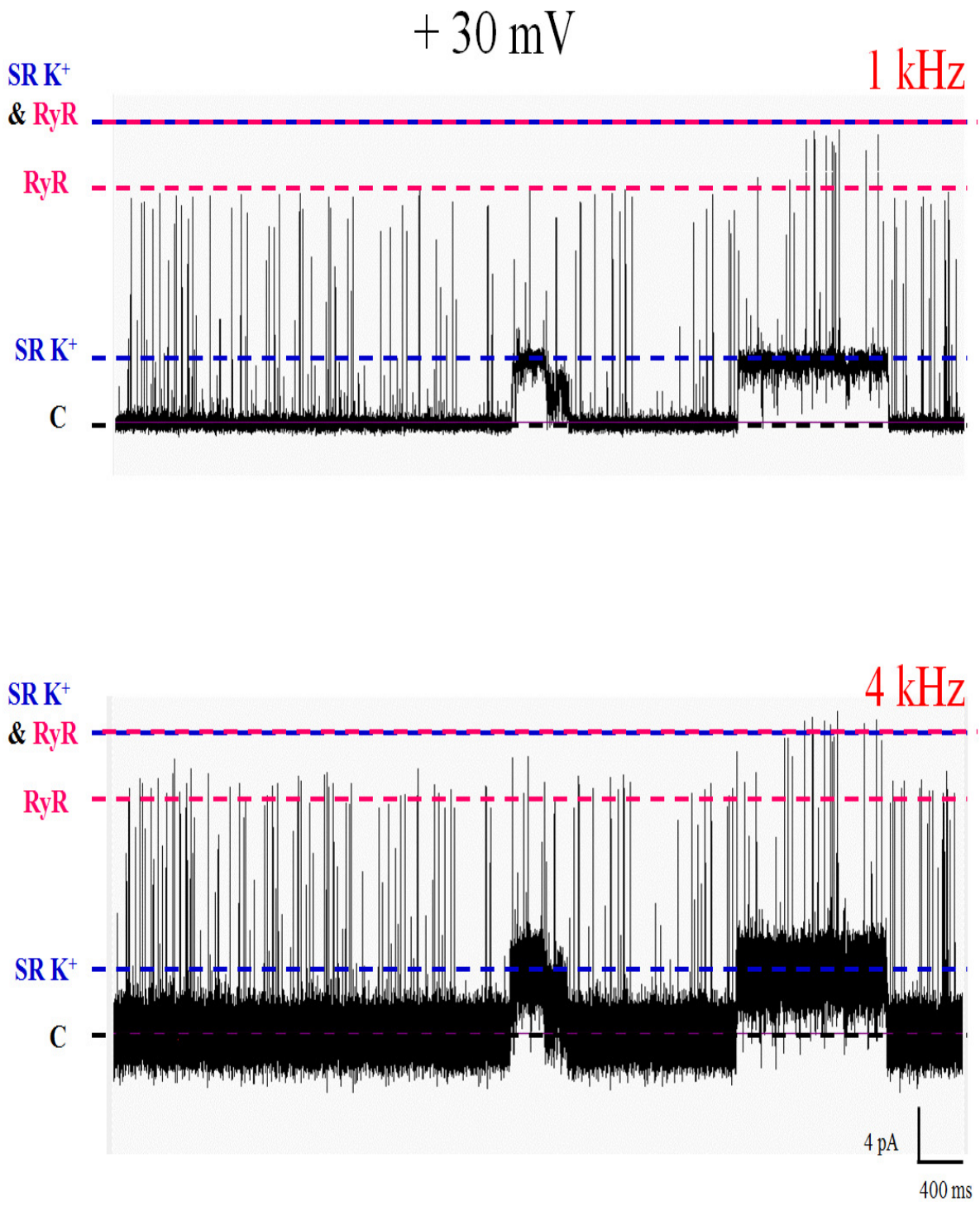


Figure 5.2 The effect of filtering on the current-fluctuations observed when both SR K^+ channel and RyR channel current-fluctuations are observed simultaneously.
A representative single-channel trace at +30 mV at a filtering level of 1 kHz (above) and 4 kHz (below) illustrates the current fluctuations that were observed when an SR K^+ channel and a RyR from TRIC-A KO tissue were simultaneously gating in 210 mM KPIPES, pH 7.2. The fully open levels of the SR K^+ channel and RyR are labelled and illustrated by the blue and pink dashed lines, respectively. The current amplitude level produced when both channels are simultaneously open is indicated by the multi-coloured (blue and pink) dashed line. C illustrates the zero current level

5.2.4 Idealisation of traces that contained a RyR and an SR K^+ channel

In order to construct a simple Markov model in QuB that would distinguish between RyR events and SR K^+ channel events, we excluded the sub-conducting open states of the SR K^+ channel. In the recordings that contained one SR K^+ channel and one RyR, irrespective of the filtering level that was applied, we constructed a 4 state Markov model. Each state of the Markov model and the corresponding level on the single-channel recording that was assigned to that state is summarised in Table 5-1.

STATE IN QUB MODEL	LEVEL ON RECORDING
1	Zero current level
2	SR K^+ channel full open level
3	RyR open level
4	Level when SR K^+ and RyR were both open

Table 5-1 The 4 state Markov model used to idealise experiments containing one SR K^+ channel and one RyR
The corresponding level observed on the single-channel trace is shown on the right of each model level.

The single-channel current levels were highlighted on the recording in QuB and the parameters of the highlighted sections were applied to the corresponding states of the model according to Table 5-1. The traces were idealised according to the method outlined in section 2.6.2. The resulting idealised conductance level sequence was displayed along with the currents, for a visual assessment of the detection accuracy.

In recordings when there were 2 SR K^+ channels present (in addition to a RyR), we added an additional state to the model that corresponded to the amplitude observed when 2 SR K^+ channels were opening together. In the 3 recordings that contained 2 SR K^+ channels and a RyR, all three channels were never observed to open simultaneously.

5.2.5 Separating the Po of the SR K channel from the Po of the RyR

As outlined above, by visual inspection of the traces we could differentiate between the full openings of the SR K^+ channel and the openings of a RyR. Traces were idealised where a RyR and an SR K^+ channel were simultaneously gating. However, we wanted to separate Po of the RyR from the Po of the SR K^+ channel. Po was calculated using the following equation

$$\mathbf{Po} = \frac{\mathbf{T_{openRyR}} + \mathbf{T_{openBOTH}}}{\mathbf{T_{total}}}$$

Equation 22

where $T_{openRyR}$ and $T_{openBOTH}$ correspond to the time that the RyR was open alone (from zero current level) and the time that both the SR K^+ channel and the RyR were open together. T_{TOTAL} corresponds to length of the recording.

Similarly, the SR K^+ channel Po was calculated using the following equation

$$\mathbf{Po} = \frac{\mathbf{T_{openSRK}} + \mathbf{T_{openBOTH}}}{\mathbf{T_{total}}}$$

Equation 23

where $T_{openSRK}$ and $T_{openBOTH}$ correspond to the time that the SR K^+ channel was open alone (from zero current level) and the time that both the SR K^+ channel and the RyR were open together. T_{TOTAL} corresponds to length of the recording.

To investigate whether filtering at 1 kHz or 4 kHz was more effective at separating the RyR events from the SR K^+ channel events, I compared the Po of the RyR and the Po of the SR K^+ channel were compared when the traces were filtered at 1 kHz and at 4 kHz. As illustrated in Figure 5.3 there was no observable difference in Po of the SR K^+ channel when filtered at 1 kHz or 4 kHz, however, there was a small, but significant difference in the Po of the RyR when filtered at 1 kHz compared to 4 kHz. In addition to Po analysis, each trace was visually inspected and, at 1 kHz, numerous short-lived RyR-like events were assigned to the SR K^+ channel conductance level. When the filtering level was increased from 1 kHz to 4 kHz, these particular events increased in current amplitude, and many of the events were reclassified as RyR events. I concluded that by filtering at 1 kHz, we were truncating numerous RyR events and thus, they were misclassified as SR K^+ channel events. Based on the results shown in Figure 5.3 and, in addition, after visual inspection of each trace (as shown in Figure 5.2), I proceeded with a cut off frequency of 4 kHz for the remainder of this study.

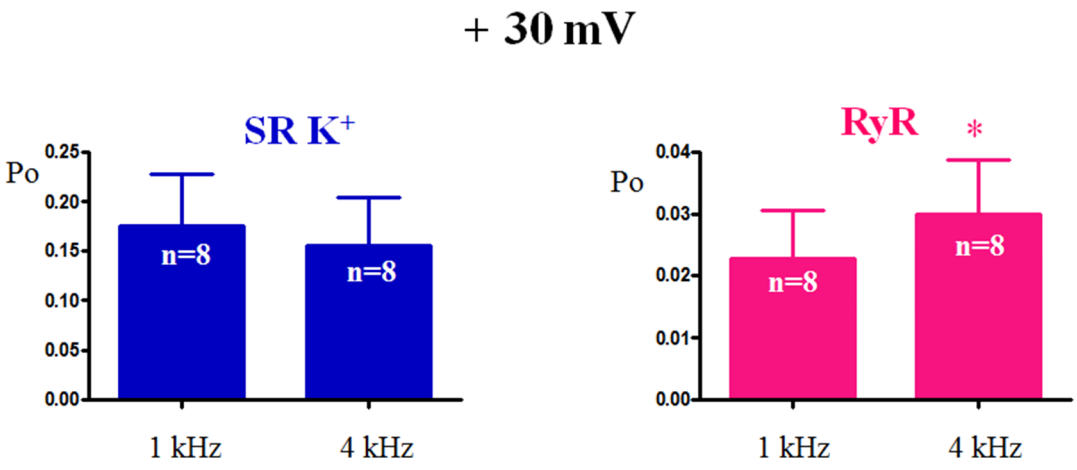


Figure 5.3 Comparison of the Po of the SR K^+ and RyR channels at filtering levels of 1 kHz and 4 kHz

The bar chart illustrates Po of the SR K^+ channel (blue) and the RyR (pink) at filtering levels of 1 kHz and 4 kHz. The data is presented as mean ± SEM for n=8 recordings that contained both an SR K^+ channel and a RyR (*p<0.05).

5.3 Results

5.3.1 Are the biophysical properties of the SR K^+ channels altered when there is a RyR present in the bilayer?

Voltage-dependence

As illustrated in this thesis, when SR K^+ channels are reconstituted into artificial membranes, the gating is voltage dependent with the Po higher at +30 mV compared to -30 mV. In our experimental recordings where a RyR and an SR K^+ channel were both present in the bilayer, we investigated whether the voltage-dependent gating feature of the SR K^+ channel was altered. The mean data, shown in Figure 5.4, illustrates that the SR K^+ channels were still voltage-dependent when there was a RyR also present in the bilayer.

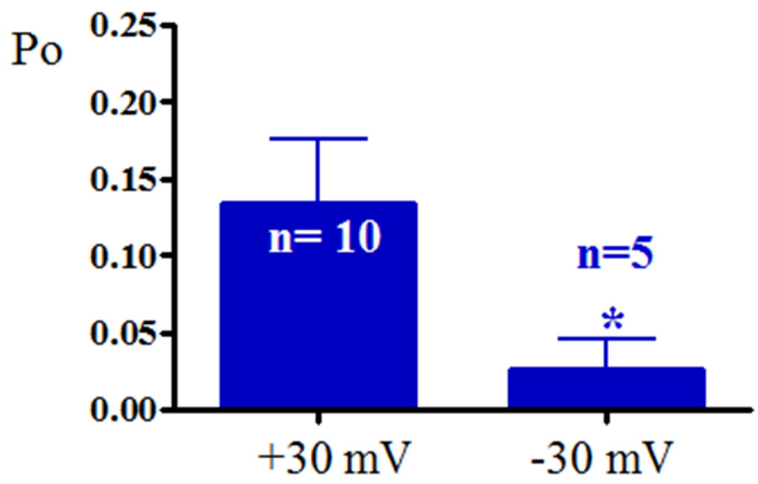


Figure 5.4 SR K^+ channels are voltage-dependent when a RyR is also gating in the bilayer

In experiments where an SR K^+ channel and a RyR were both gating in the bilayer, the Po of the SR K^+ channel at ± 30 mV is shown. Data are presented as mean ± SEM (*p<0.05).

Cooperative gating

In addition to the voltage regulation of SR K^+ channel gating, in this thesis we have demonstrated that the activity of the SR K^+ channel is affected by the number of channels

that are present in the bilayer. In the 10 recordings that contained an SR K^+ channel and a RyR gating in the bilayer, 7 out of 10 experiments contained one SR K^+ channel (and one RyR) and the remaining 3 out of 10 experiments contained 2 SR K^+ channels (and one RyR). We separated the experiments based on the number of SR K^+ channels that were present, and we compared the mean Po values of the SR K^+ channel, as illustrated in Figure 5.5. The mean data suggest that the cooperative nature of the SR K^+ channels is not affected by the presence of a RyR in the bilayer.

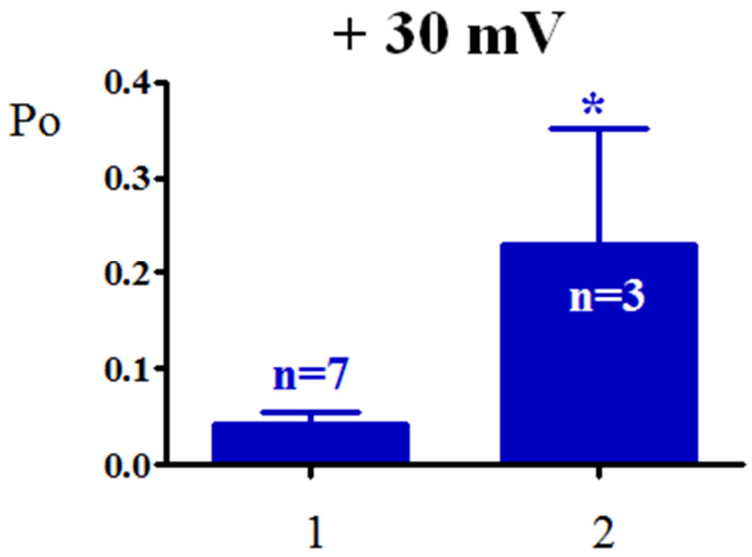


Figure 5.5 SR K^+ channels retain their cooperative gating behaviour when there is also a RyR present in the bilayer.
The Po of the SR K^+ is shown when there were one (1) or two (2) channels, in addition to a RyR, gating in the bilayer. Mean values are shown with n values labelled within the bars. Error bars are SEM when n ≥ 4 (*p<0.05).

How do the values presented in this chapter compare to our recordings where there is no RyR present?

It was difficult to compare the experiments that we obtained where a SR K^+ channel was gating alone in the bilayer to the experiments where an SR K^+ was gating in addition to a RyR. For example, when an SR K^+ channel was gating alone in the bilayer, a filter of 1

kHz was applied to analyse the the single channel gating properties. On the other hand, in the experiments where an SR K^+ was gating in addition to a RyR, a 4 kHz filter was applied. In this chapter, I have illustrated that altering the filtering level does not appear to have a significant effect on the gross Po value calculated from the gating of the SR K^+ channels when there was also a RyR present in the bilayer. However, in addition to changing filtering levels, we also used a different Markov model to idealise the recordings. When a SR K^+ channel was gating alone in the bilayer a 3 state Markov model was used that accounted for the sub-conductance levels in addition to the full open channel level. However, in experiments where an SR K^+ was gating in addition to a RyR, we used a simplified 2 state Markov model to idealise the recording.

Nevertheless, as illustrated in Figure 5.6, we compared the Po_{TOTAL} (white bars) *and* the Po_{FULL} (black bars) of the SR K^+ channels when there was no RyR present in the bilayer to the Po values of the SR K^+ channel when there was also an RyR present in the bilayer (blue bars).

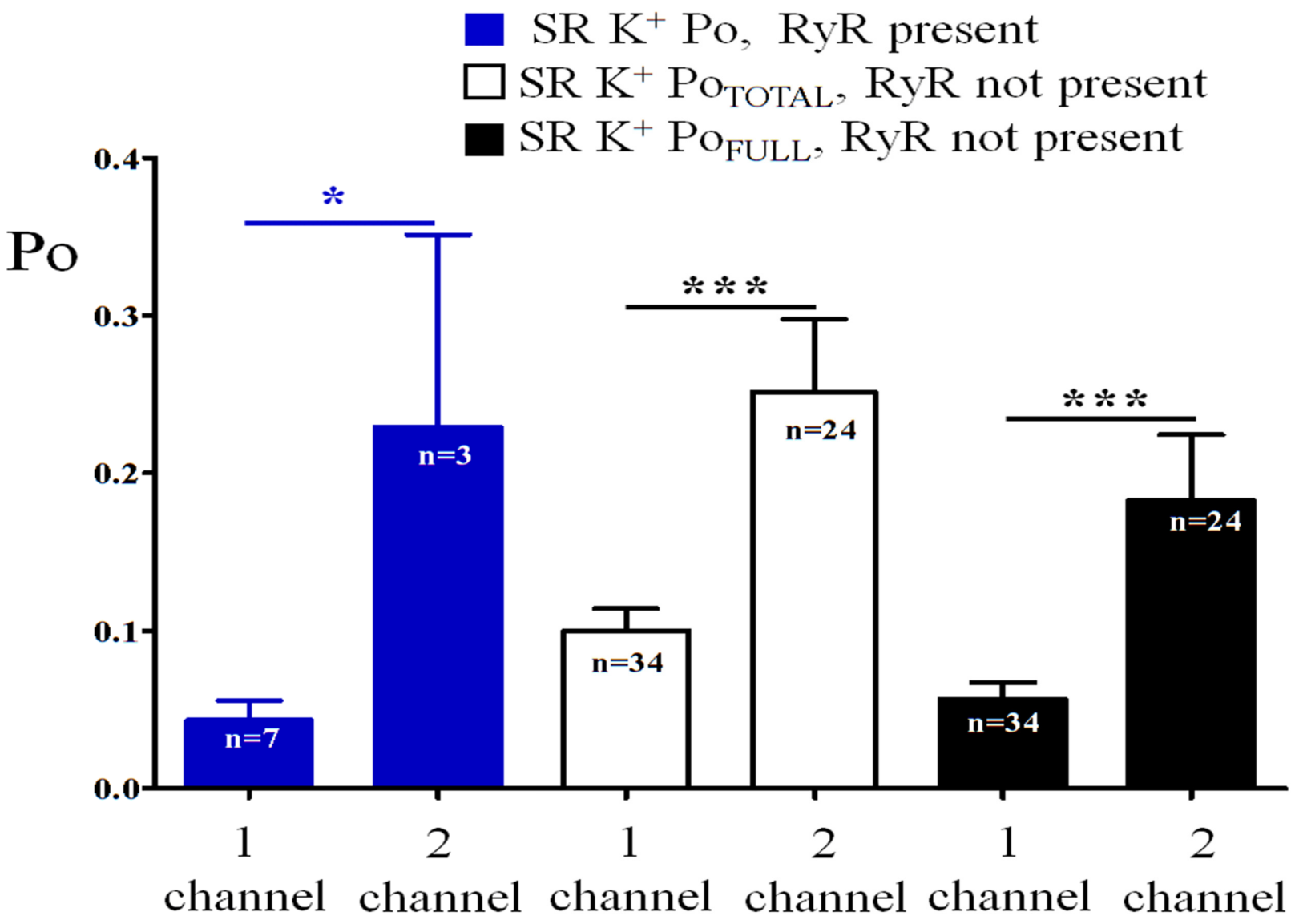

SR K+ Po, RyR present
SR K+ PoTOTAL, RyR not present
SR K+ POFULL, RyR not present
Po
0.4
0.3
0.2
0.1
0.0
*
***
***
n=3
n=7
n=34
n=24
n=34
n=24
1 channel
2 channel
1 channel
2 channel
1 channel
2 channel

Figure 5.6 Comparison of the gating of the SR K^+ channel when a RyR was present in the bilayer

In experiments where an SR K^+ channel and a RyR were both gating in the bilayer, we compared the Po values (blue) to the Po of the SR K^+ channel when there was no RyR in the bilayer. The Po_{TOTAL} is shown in white and the Po_{FULL} is shown in black. The data are presented as Mean ± SEM and the n numbers are illustrated in each column.

5.3.2 Does the conformation of the SR K^+ channel (open or closed) affect the gating properties of RyR?

In addition to the overall Po of the RyR in experiments when there was also an SR K^+ channel in the bilayer, we wanted to investigate if the RyR events that occurred from the zero current level were any different to the RyR events that occurred when an SR K^+ channel was also open. Therefore, in experiments when we had both a RyR and SR K^+ channel present in the bilayer, we separated the RyR events that occurred from the zero current level (SR K^+ channel closed) from the events that occurred when the SR K channel was open. By separating the data, we could calculate the Po of the RyR when the SR K^+ channel was closed, and the Po of RyR when the the SR K^+ channel was open. The mean data, shown in Figure 5.7, illustrates that the gating of RyR did not appear to be influenced by the open state of the SR K^+ channel. Panel B compares the mean open duration of RyR events opening from the zero current level (SR K^+ channel closed) to those RyR events that occurred when an SR K channel was open. In this study, we only analysed events at +30 mV, as the SR K^+ channel was practically closed at -30 mV.

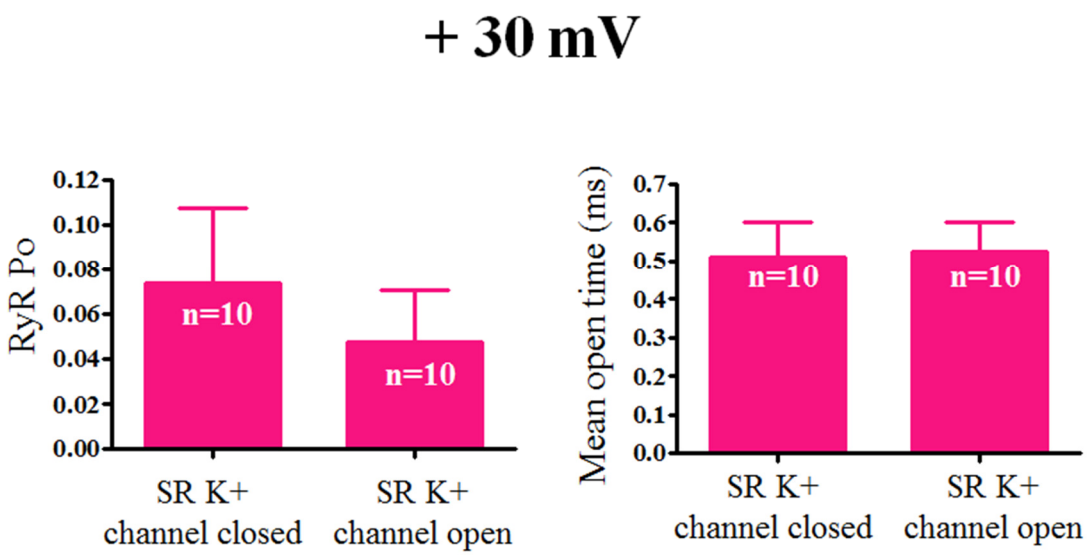


Figure 5.7 The effect of SR K^+ channel gating on RyR function
The bar chart on the left illustrates the Po of the RyR calculated from segments of the recording when the SR K^+ channel was either closed or open. On the left, the mean open time of the RyR is shown. The data are presented as mean ± SEM for n=10 recordings that contained both an SR K^+ channel and a RyR present in the bilayer.

5.3.3 The gating of a RyR *without* an SR K^+ channel gating in the bilayer

It was difficult to observe the gating of a RyR without the presence of a SR K^+ channel when the HSR vesicles from TRIC-A KO tissue were incorporated into artificial bilayers. Usually, when the single-channel properties of a RyR is studied with K^+ as the permeant ion, the RyR from the HSR is purified using a combination of detergent solubilisation and linear sucrose gradients to separate the RyR channels from the SR K^+ and SR Cl^- channels. However. I recorded one experiment that contained a single RyR gating without an SR K^+ channel present in the bilayer. The gating that was observed is illustrated in Figure 5.8. There were no obvious differences in the gating of the RyR in this experiment when compared to the the gating of the RyR channels when SR K^+ channels were also gating in the bilayer. The Po of this RyR and the mean open time are compared to the individual

values for the RyR where SR K^+ channels were present (see Figure 5.8). More data is required to determine if the gating of RyR is affected by SR K^+ channels.

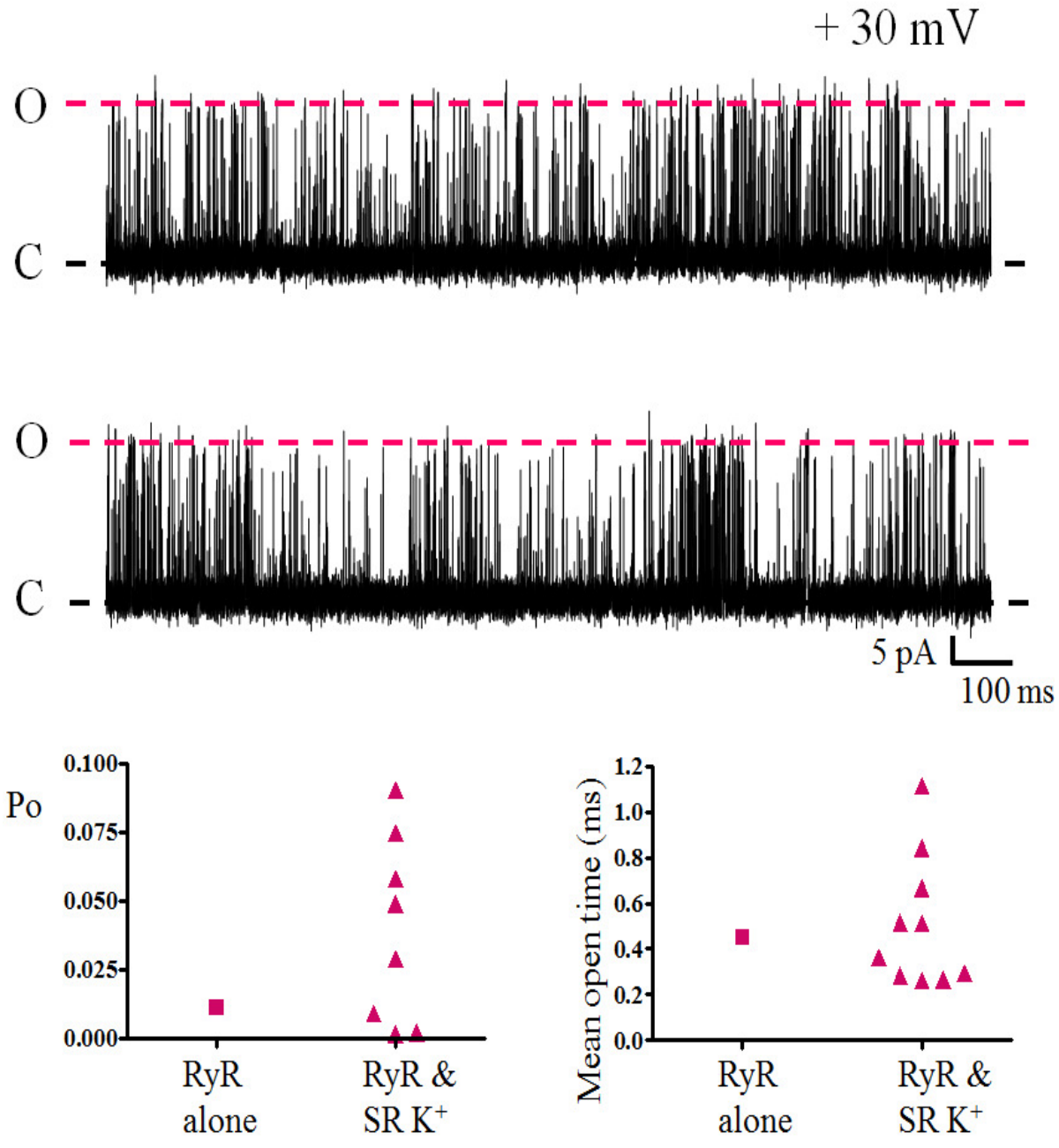


Figure 5.8 Single-channel current fluctuations observed when only a RyR was gating in the bilayer.
The traces show the single-channel activity at +30 mV traces). O and C indicate the full open and closed levels, respectively. The recording was low pass filtered at 4 kHz.

5.4 Summary

The aim of this study was to investigate if the single-channel properties of the SR K^+ channel or of the RyR were altered when both channels were gating together in a bilayer.

5.4.1 SR K^+ channels retain their biophysical properties when a RyR is gating in the bilayer

In this thesis, I have demonstrated that the gating of SR K^+ channels derived from TRIC-A KO tissue are voltage-dependent, with the Po at +30 mV being markedly higher than the Po at -30 mV. In this chapter, I have also shown that when a RyR and a SR K^+ channel were both present in the bilayer, the gating of the SR K^+ channel was still voltage-dependent (the Po at +30 mV was higher than the Po at -30 mV). In addition to voltage regulation of SR K^+ channel activity, in Chapter 4, a novel regulatory mechanism of channel gating was described. The channels appeared to gate cooperatively when multiple SR K^+ channels were gating in the bilayer. In this chapter, I also described how the cooperative gating behaviour of the SR K^+ channels still remains when a RyR is also gating in the bilayer. In experiments when there were 2 SR K^+ channels (in addition to a RyR) present in the bilayer, the average Po of each SR K^+ channel was significantly higher than the Po of the SR K^+ channel in experiments that contained one SR K^+ channel (in addition to a RyR). The Po values of the SR K^+ channels in this chapter (when there is also a RyR present in the bilayer) are similar to the Po values outlined in this thesis when only SR K^+ channel gating in the bilayer (see Figure 5.6). However, as both sets of experiments were analysed with different filtering levels and different models in QuB, a direct comparison of the gating of the SR K^+ channel with and without a RyR in the bilayer is inappropriate. Increasing n values for experiments where an SR K^+ channel is gating in addition to a RyR and analysing single SR K^+ channels (where there is no RyR gating) with a simplified 2 state Markov model

(with a filter cut of of 4 kHz) are some of the experiments that are required to make a direct comparison.

The results presented in this chapter allow speculation about the mechanisms that may be responsible for the cooperative gating of SR K^+ channels. One possible explanation for cooperative gating that has been documented in the literature, is that channels possess mechanosensitive properties (141-143). For example, when a channel opens in the bilayer, changes in membrane tension may occur from ion-channel conformational movements, which are detected by neighbouring channels, inducing conformational changes in those channels that cause openings. Evidence in this chapter suggests that a membrane mediated force may not be the underlying factor that governs cooperative gating when multiple SR K^+ channels are present in the bilayer. If the gating of the SR K^+ channel was sensitive to changes in membrane tension (caused by ion-channel open and closing events), then we would expect the SR K^+ channel to sense changes in membrane tension that are produced by the RyR gating movements. In recordings where both an SR K^+ channel and a RyR are present, we might expect the SR K^+ channel to have a higher Po than the value we calculated in chapter 3 where a single SR K^+ channel was gating in the bilayer. This is not the case. It is possible, of course, that RyR and SR K^+ channel movements produce different distortions within the membrane, or that, in our bilayers, the RyR channels just happen to be located in a different region of the bilayer.

5.4.2 RyR gating when an SR K^+ channel is also in the bilayer

We examined whether the RyR events that occurred when the SR K^+ channel was in the closed confirmation were any different to the RyR events that occurred when the SR K^+ channel was in the full open channel conformation. Whether the SR K^+ channel was open or closed had no observable effect on the Po or the mean open time of the RyR. However,

hypothetically if the RyR and the SR K^+ channel were to influence each other in some way at the single-channel level, then it is plausible that the difference may only be uncovered by comparing the gating of the RyR when it is is the only channel present in the bilayer and the gating of the RyR when there is also an SR K^+ channel present. I recorded one experiment where a single RyR was gating without a SR K^+ in the bilayer. Although the Po of this RyR appeared to be similar to the properties of the RyRs when an SR K^+ was present in the bilayer (see Figure 5.8), further experiments are required to investigate any potential differences further.

6 Investigating the pH sensitivity of the SR K^+ channel

6.1 Introduction

Miller demonstrated that the native SR K^+ current that was observed when massive numbers of SR K^+ channels were fused to artificial bilayers was both voltage and pH sensitive (87). The voltage-dependence of these K^+ currents were characterised and it was illustrated that the channels involved were more open at +30 mV compared to -30 mV (87). In addition, Miller illustrated that at a pH of 5.5, the macroscopic K^+ current from incorporated SR was inhibited by 95 % at a fixed voltage (87). In a later paper, Labarca *et al* (1980) (135) revisited the pH sensitivity of the macroscopic K^+ currents from SR when the activity was recorded over a range of holding voltages at pH 6, pH 7, and pH 9 . They concluded that the current-voltage relationship curve of the SR K^+ current shifted to the right as the pH is lowered and the gating charge was relatively unaffected (135). In 1985, Bell (144) suggested that protons decrease the single-channel conductance of the SR K^+ channel by competing with the K^+ binding site within the pore. In this paper, single-channel experiments were reported to be used for analysis however, no single-channel traces were shown (144).

As described previously, it is thought that the SR K^+ channel current fluctuations arise form discrete openings from TRIC-A and TRIC-B channels (101). In chapter 1, I have illustrated that the SR K^+ channels from WT and TRIC-A KO tissue display similar voltage-dependent gating behaviour, with channels being more open at +30 mV compared to -30 mV. The aim of this chapter, is to investigate the pH sensitivity of single SR K^+ channels derived from TRIC-A KO and WT tissue.

6.2 Methods

6.2.1 Mean open and closed durations

Although measurements of Po can tell us about overall changes in ion-channel gating, it is only a simplified approximation of the channel behaviour. As discussed previously, lifetime analysis can extract further details about the gating of the channel by investigating durations of closed and open events. Since most experiments contained more than one SR K^+ channel gating in the bilayer, lifetime analysis could not be performed. However, an alternative approach was used to measure the mean durations in the fully open channel level of the SR K^+ channel, and the duration of the sojourns between these events, as outlined below.

6.2.1.1 Measurement of full open burst length

In this thesis, we define the burst length as the dwell time in the full open channel level. Recordings were idealised as explained in section 2.6.2.2. In the recordings (that often contained more than one channel in the bilayer), single SR K^+ channel open bursts (where only one SR K^+ channel was gating) were selected within traces and these openings were analysed individually. The prerequisite for selecting openings was that they had to dwell in the full open channel level for a duration of at least 20 ms. Upon closer inspection of the idealisation, it was noted that, during long-lived sojourns in the full open channel level, there were many very short-lived transitions to lower conductance levels, which resulted in the idealisation of the full open channel level being segmented (illustrated in Figure 6.1, panel B). Segmentation of the full open channel level durations would mask any changes in the duration of full open bursts (as illustrated in Figure 3.8 where increments of voltage appeared to have no effect on the duration of the full open channel level bursts). Thus, every data point within each open burst was reviewed. Any rapid transitions to lower

conductance levels, or, any transition to the closed level that was < 20 ms, were reassigned as events in the full open channel level. This analysis was done by hand in the QuB software. After the idealisation was adjusted, each individual opening burst was reanalysed to determine the mean open time in of the full open channel level as illustrated in panel C.

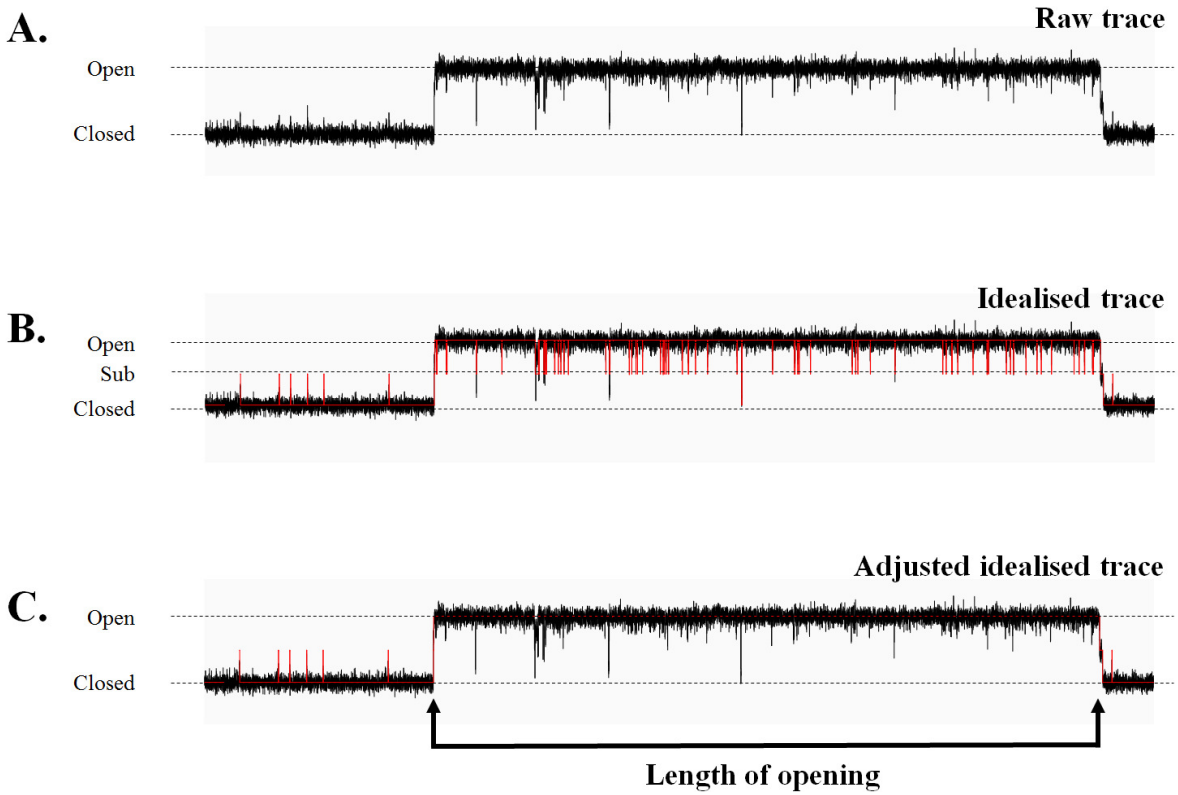


Figure 6.1 Single-channel mean open time measurements using SKM idealisation
A. The top trace shows a typical single SR K^+ channel recording after filtering at 1 kHz. The closed and the full open channel levels are indicated by the dotted lines. **B.** The result of the SKM idealisation is shown. **C.** Events to lower conductance levels that occurred from the full open channel level were removed from the idealisation. The arrows indicate the duration of the opening burst.

6.2.1.2 Measurement of interburst interval length

The mean duration in the closed state (zero current level) was measured in experiments that contained only one single SR K^+ channel gating in the bilayer. The recordings were idealised according to section 2.6.2.2. The length of the closings that occurred between the full open channel bursts were measured. These closings were referred to as the interburst intervals. After closer evaluation of the idealisation, we noticed that during long periods where the channel was closed, we observed many very short-lived transitions to sub-conductance levels, which resulted in the idealisation of the closed state being segmented into smaller durations. Therefore, using a similar approach to that used to measure the mean open duration, every data point was reviewed, and, any rapid transitions to sub conductance levels that occurred from the long dwell times in the closed state were reassigned as events in the closed state. This analysis was done by hand in the QuB software and is illustrated in Figure 6.2. Each closing event was separately reanalysed after the idealisation was adjusted to determine the mean closed time of the interburst interval as illustrated in panel C.

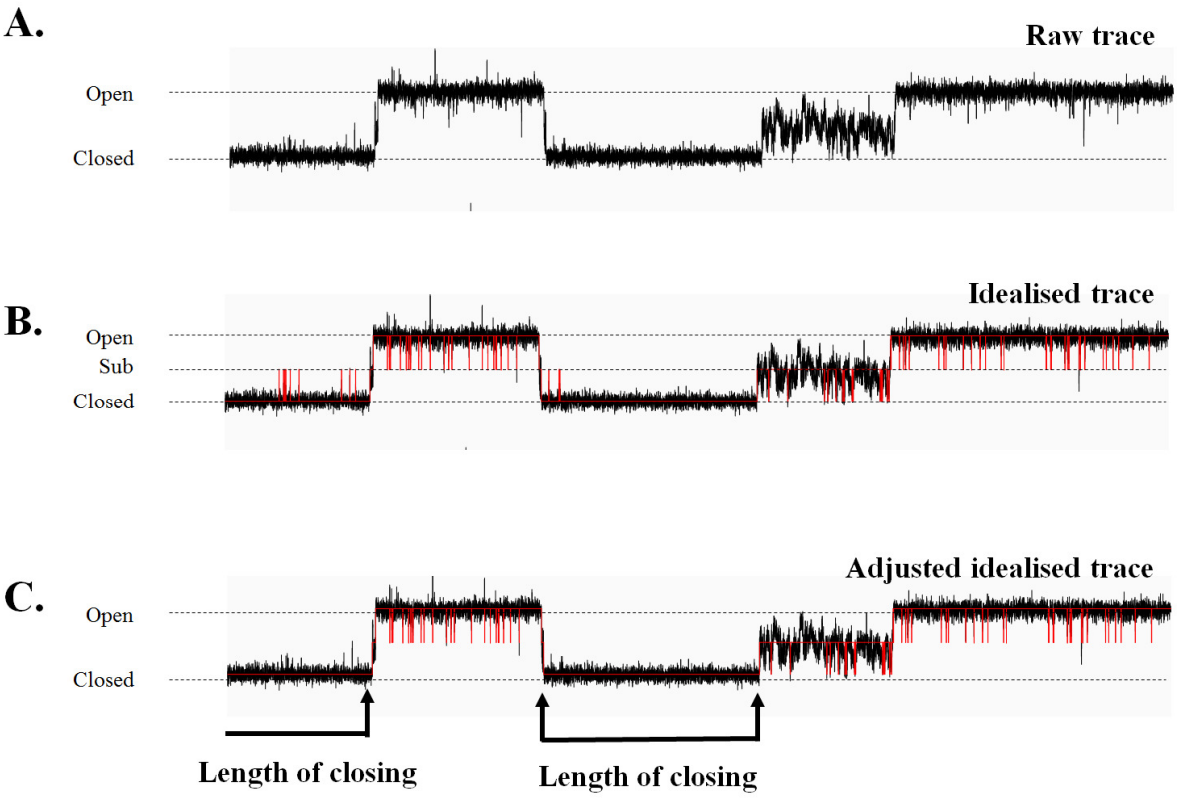


Figure 6.2 Single-channel mean closed time measurements using SKM idealisation
A. The top trace shows a typical single SR K^+ channel recording after filtering at 1 kHz. The closed and the full open channel levels are indicated by the dotted lines. **B.** The result of the SKM idealisation is shown in B. The 'merged' sub-conductance level is indicated with a dotted line. Events to sub-conductance levels that occurred from the closed level were removed from the idealisation. The arrows indicate where the length of the closings were measured.

6.3 Results

6.3.1 Contribution by other members of the lab to experiments described in this chapter.

Some experiments that are included in the mean data were performed by Dr. Elisa Venturi and Dr. Elena Galfre. Their contribution to the mean data is indicated under the each figure.

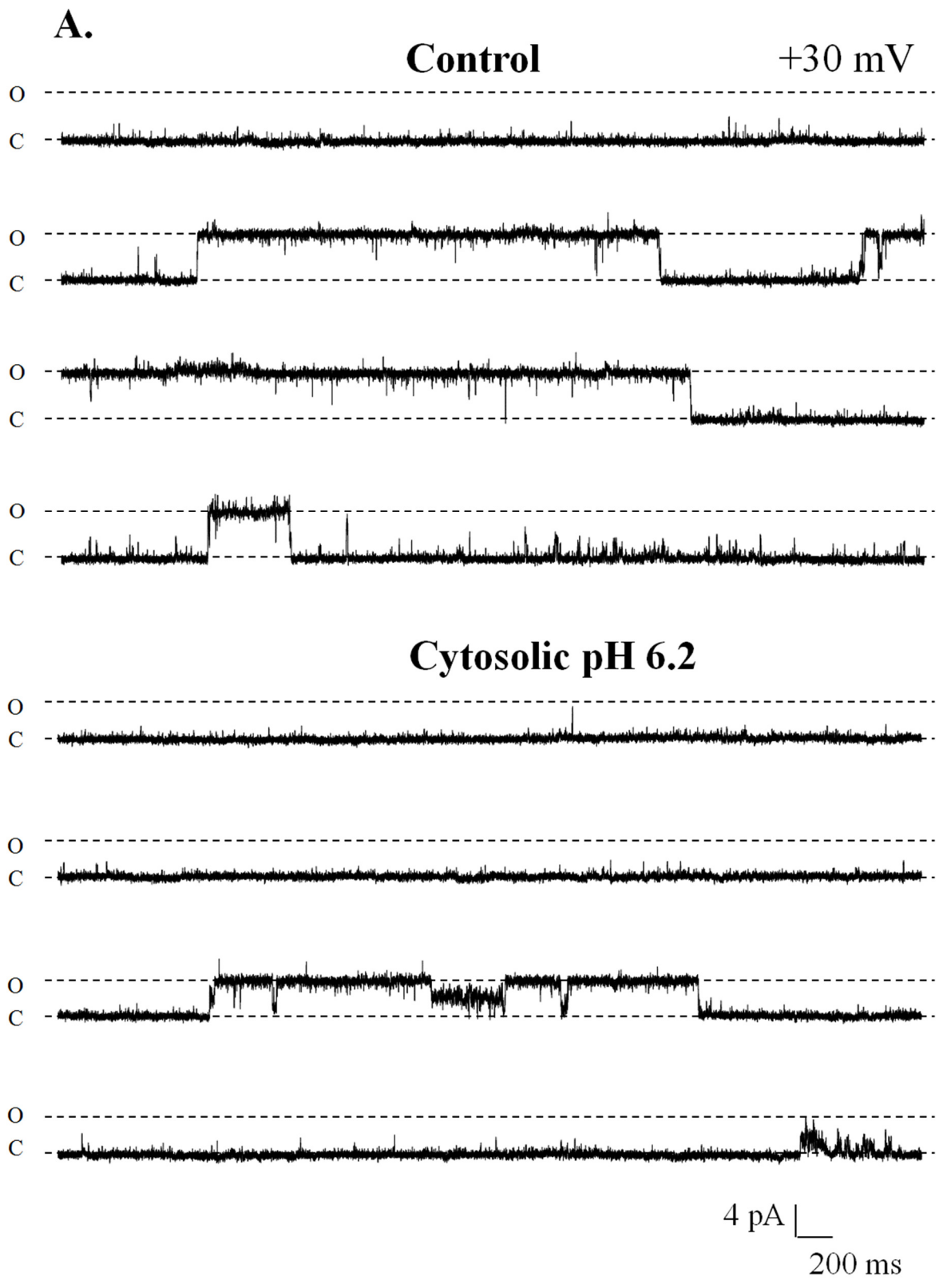
6.3.2 Composition of the buffers used in this chapter

A solution of 210 mM KOH was adjusted to the appropriate pH (pH 6.2, pH 7.2 or pH 9.2) with piperazine-N,N′-bis(2-ethanesulfonic *acid*) (PIPES).

6.3.3 Effect of cytosolic pH 6.2 on SR K^+ channels from TRIC-A KO

6.3.3.1 Effect of cytosolic pH 6.2 on SR K^+ channel gating

After monitoring the gating activity of SR K^+ channels from TRIC-A KO skeletal muscle in control solution (210 mM KPIPES, pH 7.2), the cytosolic side of the channel was perfused with 210 mM KPIPES, pH 6.2. Figure 6.3 shows recordings from a typical experiment.


A.
Control
+30 mV
O
C
Cytosolic pH 6.2
4 pA
200 ms

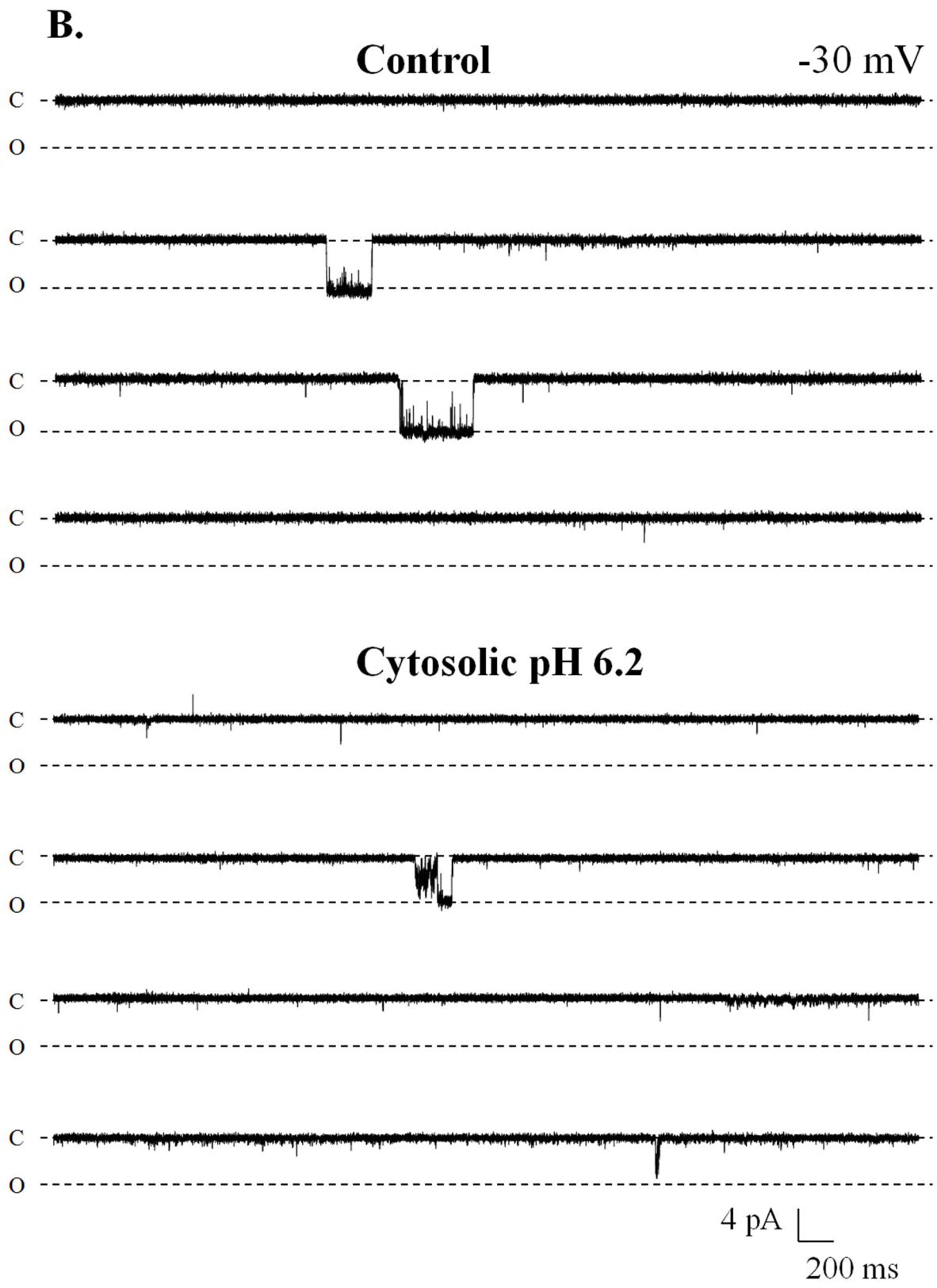


Figure 6.3. The effect of cytosolic pH 6.2 on SR K^+ channel gating.
The traces show the single-channel activity of the SR K^+ channel, from TRIC-A KO skeletal muscle, before (top traces) and after (bottom traces) the cytosolic side of the channel was perfused with 210 mM KPIPES, pH 6.2. O and C indicate the open and closed channel levels, respectively. The recording was low pass filtered at 1 kHz.

The bar charts in Figure 6.4 illustrate the mean Po at +30 mV before and after the cytosolic side of the channel was perfused with 210 mM KPIPES, pH 6.2. Acidic pH, on the cytosolic side of the SR K^+ channel, reduced Po. Po_{FULL} was decreased, however, PoSUB was unchanged.

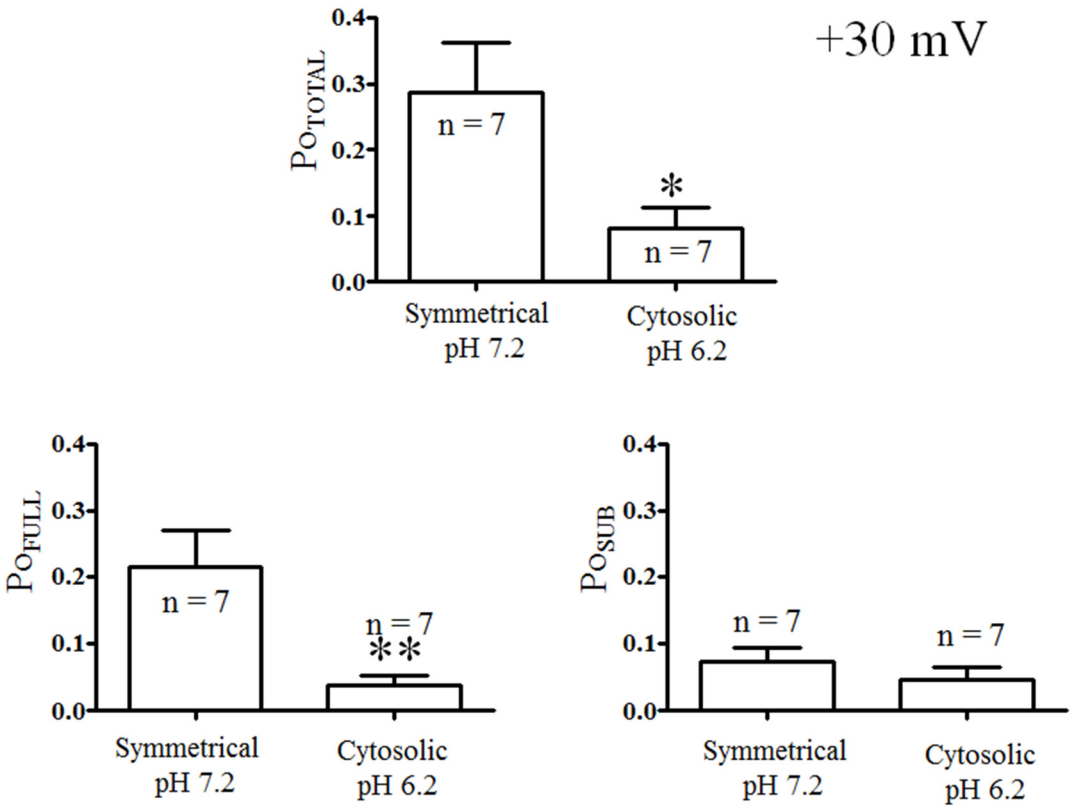


Figure 6.4 The effect of cytosolic pH 6.2 on SR K^+ channel Po at +30 mV.
The bar charts show the decrease in SR K^+ channel Po after the cytosolic side of the channel was perfused with pH 6.2 (*p<0.05, **p<0.01). Data are presented as mean ± SEM.

In cytosolic pH 6.2, the contribution of Po_{FULL} to Po_{TOTAL} decreased, indicating, that an opening of the SR K^+ channel in acidic pH is more likely to be to a sub-conductance state than the full open channel level. This is shown in Figure 6.5.

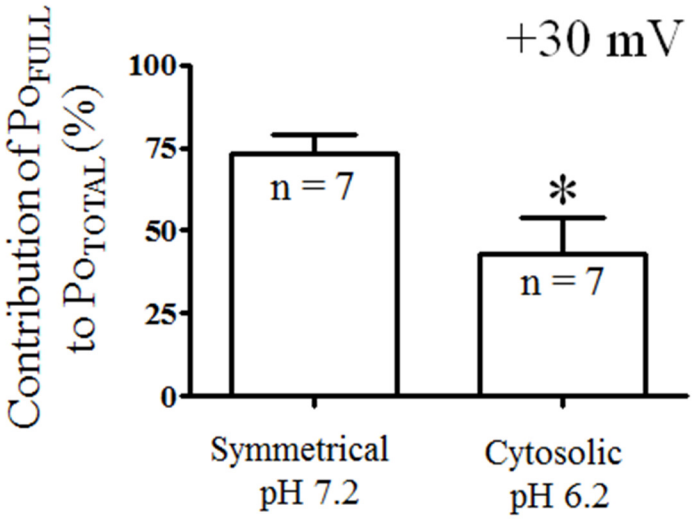


Figure 6.5. The effect of cytosolic pH 6.2 on the contribution of Po_{FULL} to Po_{TOTAL} at + 30 mV.
Data are presented as mean ± SEM.

At -30 mV, there were no significant changes in SR K^+ channel Po at cytosolic pH 6.2, as shown in Figure 6.6. No changes in Po_{FULL} or Po_{SUB} or in the contribution of Po_{FULL} to Po_{TOTAL} were observed.

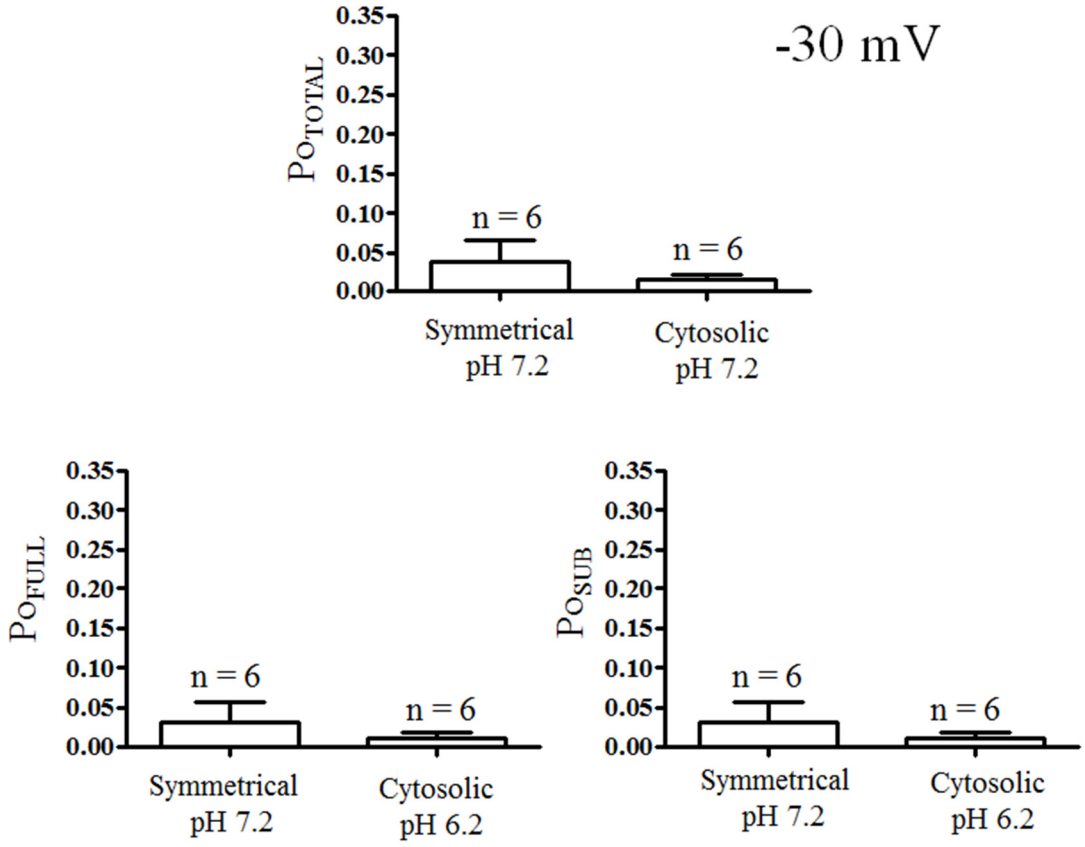


Figure 6.6. The effect of cytosolic pH 6.2 on SR K^+ channel Po at -30 mV.

Data are presented as mean ± SEM.

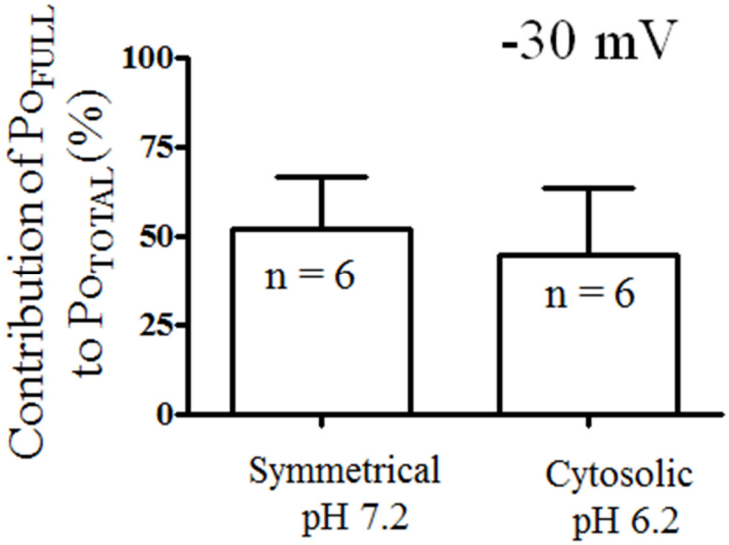


Figure 6.7 The effect of cytosolic pH 6.2 on the contribution of Po_{FULL} to the overall Po at - 30 mV. Mean values ± SEM are shown

It is worth noting that, although the mean data shown in Figure 6.6 suggests that cytosolic pH 6.2 has no effect on Po at -30 mV, 5 out of the 6 recordings did not have many (if any) openings to the full open channel level at -30 mV under control conditions due to the voltage-dependent nature of the channel. However, in one experiment, at -30 mV, the Po was 0.17 in pH 7.2 and decreased to 0.04 in cytosolic pH 6.2. Thus, it is likely that any significant reduction in Po was masked by the very low number of channel openings at -30 mV in control conditions.

6.3.3.2 Investigating the time-dependence of the effect of cytosolic pH 6.2 on SR K^+ channel function

The time dependence of the effect cytosolic pH 6.2 on SR K^+ channel gating was investigated. At +30 mV, each recording was split into 10 s segments, and the Po of each segment was calculated. The mean data shown in Figure 6.8 suggests that the effect of acidic pH on SR K^+ channel gating occurred immediately after the solution was perfused with pH 6.2.

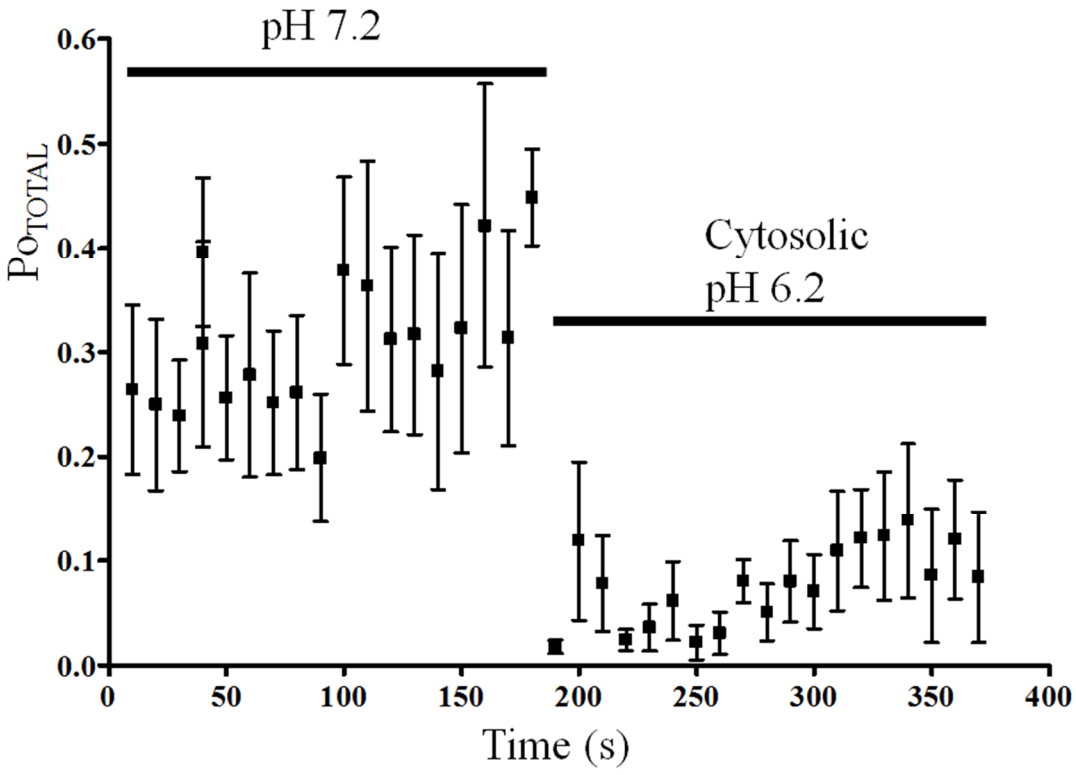


Figure 6.8 Time course of cytosolic pH 6.2 inhibition of the SR K channel.
Mean Po values were calculated in 10 s segments and plotted against the time (s). The black horizontal bars indicate when the pH of the recording solution was changed. Data are presented as mean ± SEM for n=7. Holding potential was +30 mV.

6.3.3.3 The effect of cytosolic pH 6.2 on the mean open time of the full open state

The underlying mechanism of action of cytosolic pH 6.2 on SR K^+ channel gating was investigated by looking at the durations of the sojourns to the full open channel state according to the protocol outlined in section 6.2.1.1 . In 6/7 experiments, although 5 recordings contained more than one channel in the bilayer, the duration of openings when only one channel was open were analysed individually (section 6.2.1.1.) In total, from 6 recordings, 45 openings were measured in symmetrical pH 7.2 and 30 openings were measured in cytosolic pH 6.2. The decrease in channel Po at +30 mV was associated with a decrease in the mean open duration of the full open conductance level. This is illustrated in Figure 6.9.

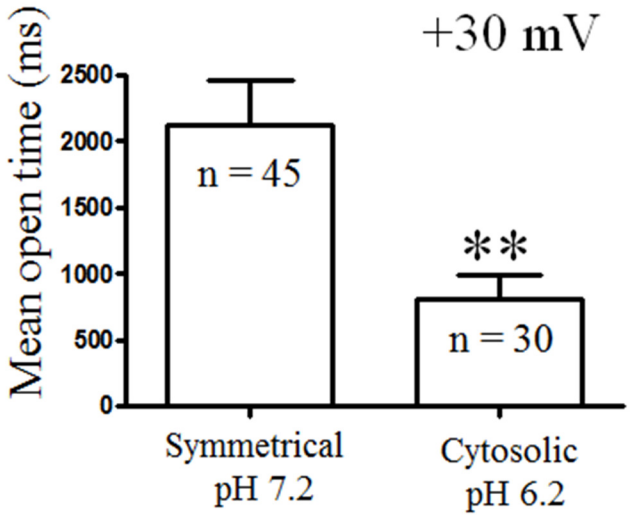


Figure 6.9 Effect of cytosolic pH 6.2 on the SR K^+ channel mean open time at +30 mV.
The decrease in the mean open time of the full open state of the SR K^+ channel is shown at +30 mV. Data are presented as mean ± SEM and the number of individual openings measured is shown in each column (**p<0.01).

At -30 mV, only four openings to the full open channel level were observed (from two experiments) in cytosolic pH 6.2. Nevertheless, in the two experiments, the individual open durations of the full open channel level in control conditions and when the cytosolic side of the channel was perfused with pH 6.2 were compared. In total, from the 2 recordings

that contained openings at -30 mV, 15 openings in symmetrical pH 7.2 and 4 openings in cytosolic pH 6.2 were measured. The individual data points are shown in Figure 6.10. Although the n numbers are too low to perform any statistical analysis, it appears that the mean open duration of the full open channel level was unaffected at -30 mV.

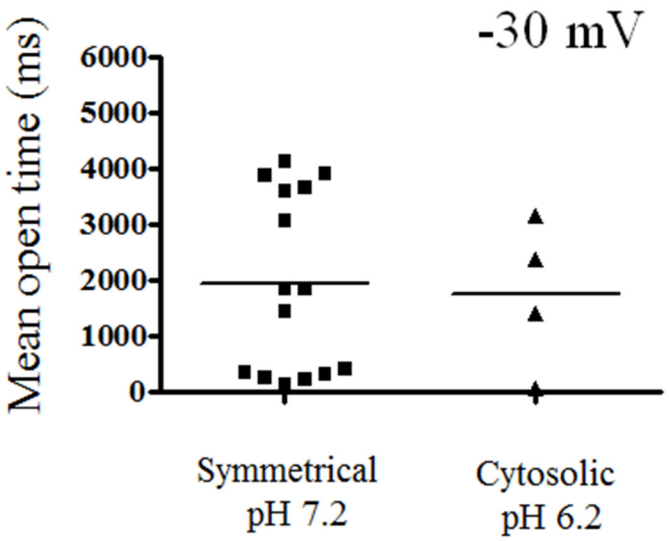


Figure 6.10 Effect of cytosolic pH 6.2 on the mean open time of the full open state at -30 mV. The open times, measured from individual openings is shown.

6.3.3.4 Effect of cytosolic pH 6.2 on mean open channel noise in the full open state

The open channel noise of the full open state was compared from the data shown in Figure 6.9, in pH 7.2 and after the cytosolic pH was changed to pH 6.2 by comparing the standard deviation of the open channel level in QuB. As shown in Figure 6.11, the decrease in mean open time was not associated with any change in open channel noise of the full open state.

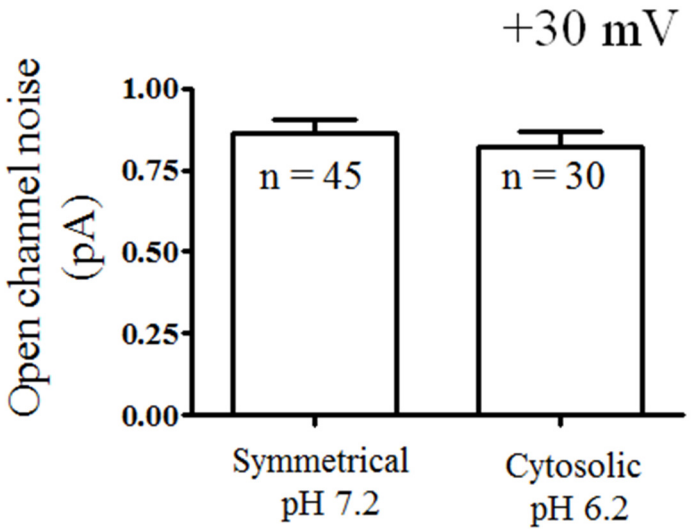


Figure 6.11 Effect of cytosolic pH 6.2 on the open channel noise of the full open state at +30 mV.
Mean ± SEM is shown

6.3.3.5 Effect of cytosolic pH on the frequency of openings to the full open channel level at +30 mV

In the one recording that had a single SR K^+ channel gating in the bilayer, the durations of the closings in between the openings that reached the fully open channel level were measured (as explained in section **Error! Reference source not found.**.) The data are shown in Table 6-1

Mean closed duration (ms)	
pH 7.2	**Cytosolic pH 6.2**
7229	22743

Table 6-1. Closed time durations at +30 mV
The table shows the mean closed duration in symmetrical pH 7.2 and in cytosolic pH 6.2 for the one experiment with a single K^+ channel in the bilayer.

Although there was only one experiment, and no statistical analysis was performed, I can hypothesise that the reduction in Po in cytosolic pH 6.2 at + 30 mV was due to both a decrease in the duration of openings to the fully open channel level and a decrease in frequency of openings to the fully open channel level.

At -30 mV, the only recording that had one SR K^+ channel in the bilayer was very voltage-dependent, and no openings to the fully open channel level were observed, so closed durations could not be measured. However, to speculate whether the frequency of openings to the full open channel state was altered at -30 mV, the number of full open bursts at -30 mV in symmetrical pH 7.2 and when the cytosolic side of the channel was changed to pH 6.2 were manually counted in 6 recordings. As illustrated in Figure 6.12, the apparent decrease in SR K^+ channel Po appeared to be associated with a possible decrease in the frequency of openings.

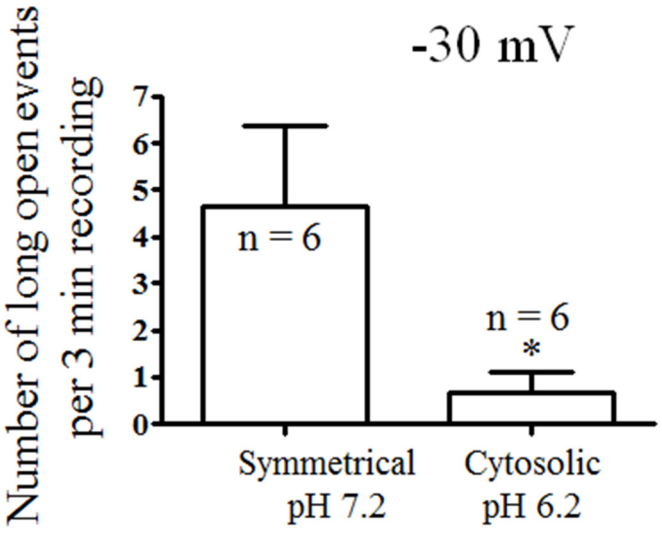


Figure 6.12 Effect of cytosolic pH 6.2 on the frequency of full open level bursts at -30 mV
Data is shown as mean ± SEM for 6 recordings (*p<0.05)

6.3.3.6 Effect of cytosolic pH 6.2 on SR K^+ channel conductance

The single-channel current amplitude of the full open channel level was measured under control conditions (symmetrical 210 mM KPIPES, pH 7.2), and, when the cytosolic side of the channel was perfused with 210 mM KPIPES, pH 6.2. The membrane potential was held at ± 30 mV. The mean data derived from the measurements of the single-channel current amplitude in symmetrical pH 7.2 and after perfusion to cytosolic pH 6.2 are shown in Figure 6.13 As illustrated in panel A., the current amplitude of the full open channel

level at +30 mV decreased significantly (n=9, ***p<0.001). The current amplitude of the channel at -30 mV remained unchanged. In order to investigate this further, more experiments were performed at different holding potentials in symmetrical pH 7.2 and after the cytosolic side of the channel was perfused with pH 6.2. The resulting current-voltage relationships are shown in panel B. In cytosolic pH 6.2, there was an observed reduction in the conductance of the SR K^+ channel at positive holding potentials, but no change at negative holding potentials (n=3, SD).

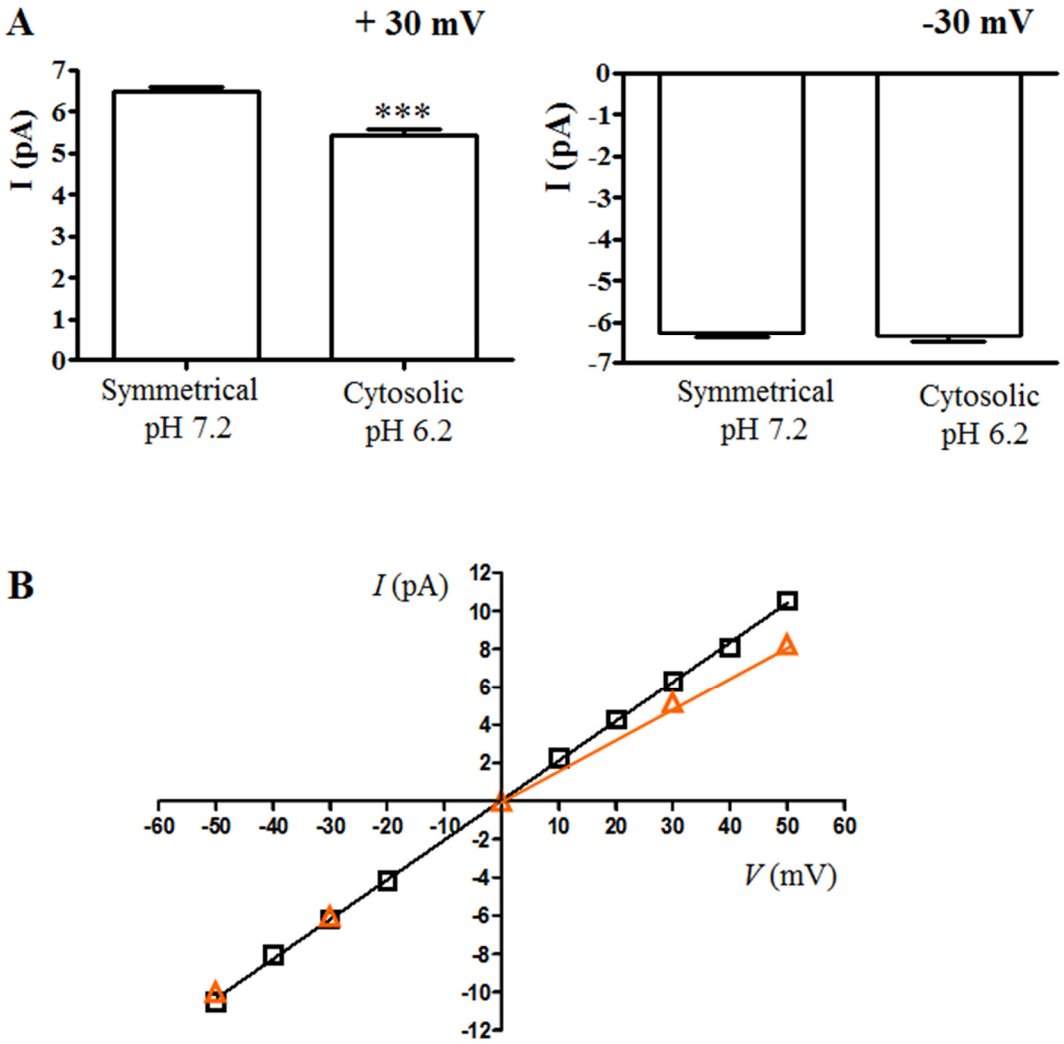


Figure 6.13. Effect of cytosolic pH 6.2 on the conductance of the SR K^+ channel.
A. Bar charts illustrate the mean current amplitude at ±30 mV in control (symmetrical 210 mM KPIPES pH 7.2) and after the cytosolic side of the channel was perfused with 210 mM

KPIPES, pH 6.2 (n=10, ***p<0.001). **B.** Current-voltage relationships comparing control conditions (black squares) and after the cytosolic side of the channel was perfused with 210 mM KPIPES pH 6.2 (orange triangles). Mean ± values SD are shown (n=3).

6.3.3.7 Investigating whether cytosolic pH 6.2 altered the properties of the merged sub-conductance level

The properties of the merged sub-conductance level were investigated to determine if they were altered when the pH of the cytosolic side of the channel was lowered to 6.2. To do so, the idealised data points from each trace from QuB were exported to excel. The events were grouped in excel based on the level of Model M2 that they had been assigned to (closed level, merged sub-conductance level and full open channel level). For each trace, the mean amplitude of the merged sub-conductance level was calculated and was expressed as a % of the mean amplitude of the full open channel state. As shown in Figure 6.14 (A), no statistical difference was found when the experiments in symmetrical pH 7.2 and the corresponding traces in cytosolic pH 6.2 were compared (n=6, SEM). The noise of the merged sub-conductance level (equivalent to the standard deviation in QuB) was also compared in pH 7.2 and cytosolic pH 6.2, as shown in B. No change in the noise of the merged conductance level was observed (n=6, SEM).

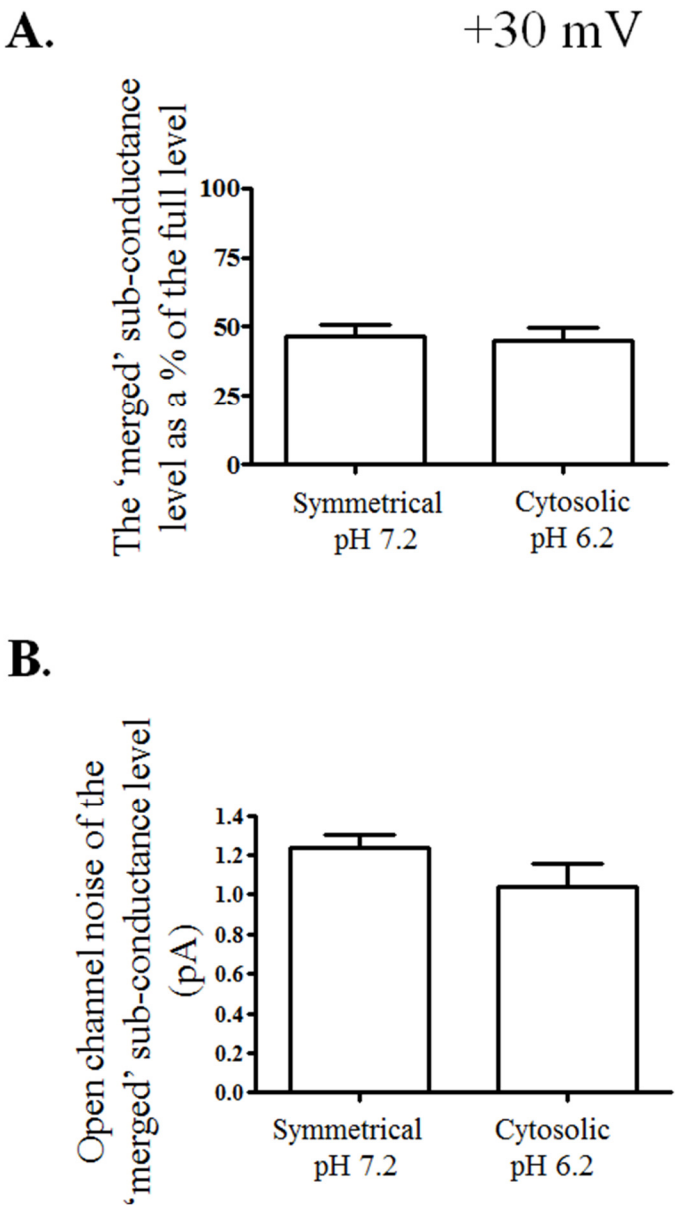


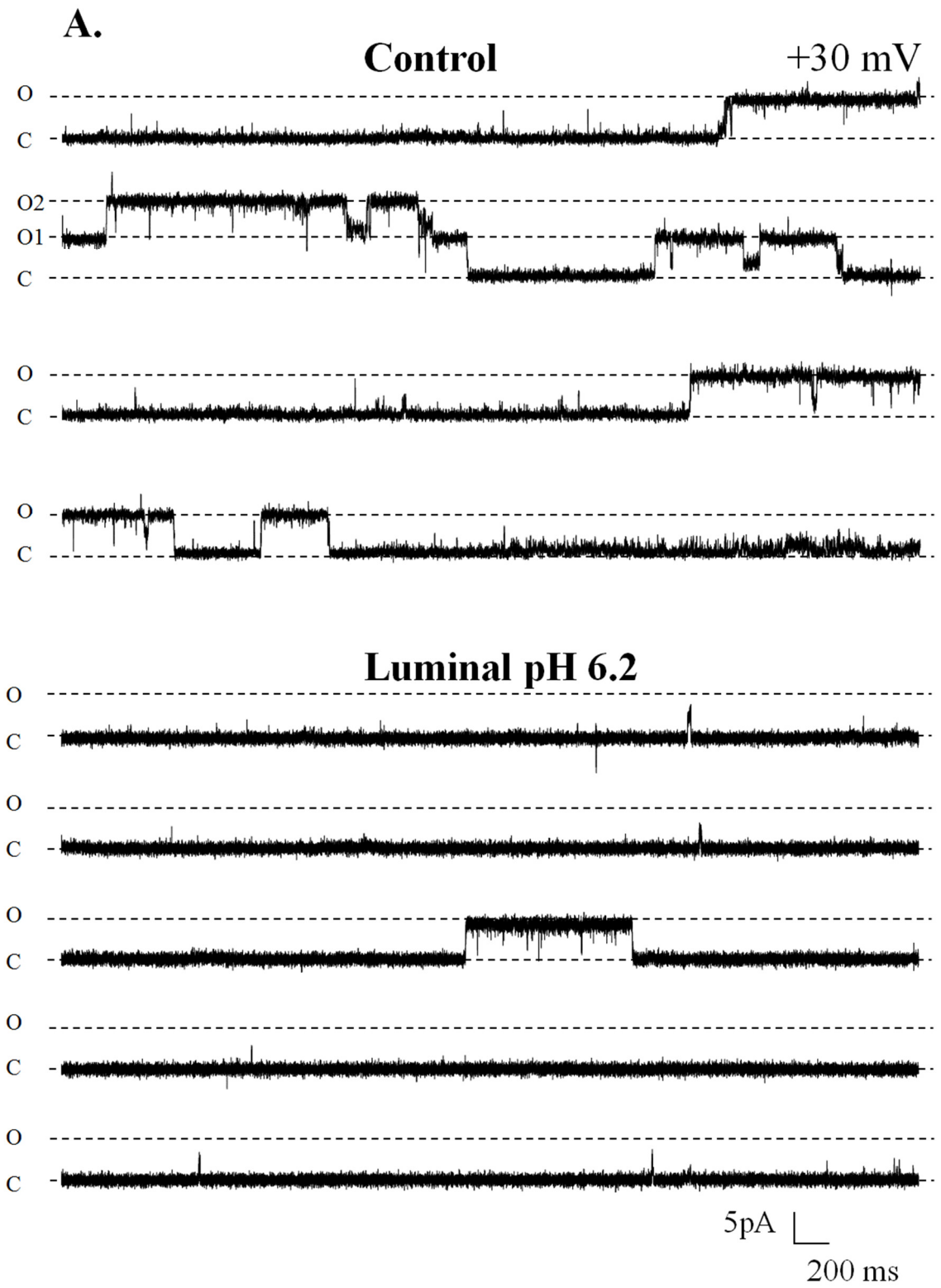
Figure 6.14 The effect of cytosolic pH 6.2 on the parameters of the merged sub-conductance level at +30 mV.

A. When the pH of the solution on the cytosolic side of the channel was lowered from from pH 7.2 to 6.2, the mean amplitude of the merged sub-conductance level remained at ~50 % of the full open channel level amplitude. In addition, no change in the open channel noise of the merged sub-conductance (B) in cytosolic pH 6.2 was observed.

6.3.4 Effect of luminal pH 6.2 on SR K^+ channels from TRIC-A KO

6.3.4.1 Effect of luminal pH 6.2 on SR K^+ channel gating

Similar experiments were performed to investigate whether reducing the luminal pH from 7.2 to 6.2, could also affect channel function. After monitoring the gating of SR K^+ channels from TRIC-A KO under control conditions (symmetrical 210 mM KPIPES pH 7.2), the luminal side of the channel was perfused with a solution containing 210 mM KPIPES, pH 6.2. Figure 6.15 shows recordings from a typical experiment.


A.
Control
+30 mV
O
C
O2
O1
C
O
C
O
C
Luminal pH 6.2
O
C
O
C
O
C
O
C
O
C
5pA
200 ms

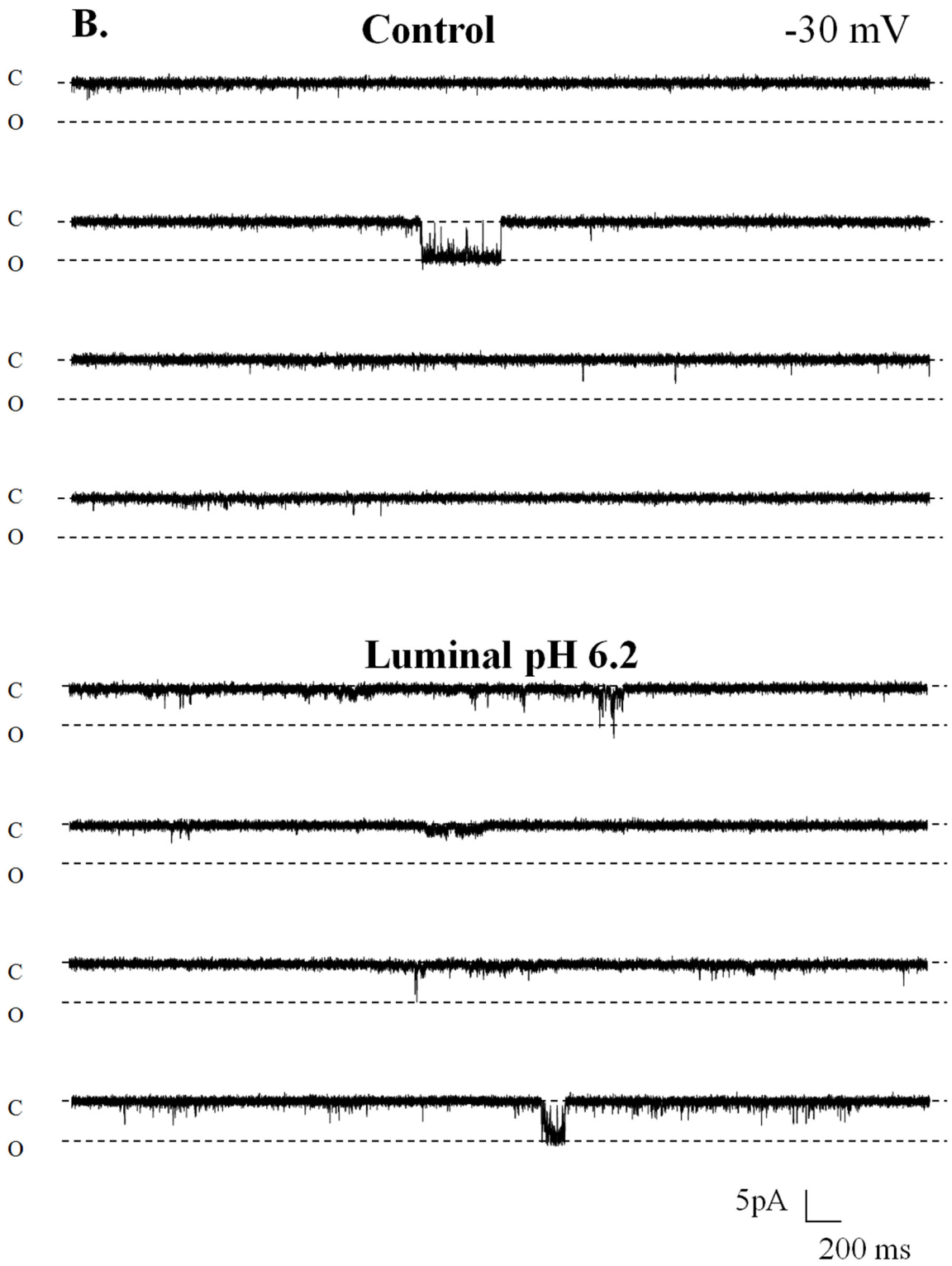


Figure 6.15 The effect of luminal pH 6.2 on SR K^+ channel gating.
A representative single-channel trace at +30 mV (A) and -30 mV (B) showing the effect of luminal acidic pH on SR K^+ channel gating. The traces show the single-channel activity before (top traces) and after (bottom traces) the luminal side of the channel was perfused with 210 mM KPIPES, pH 6.2. O1 and O2 indicate the channel levels for one and two SR

K^+ channels opening, respectively, and C indicates the zero current level. The recording was low pass filtered at 1 KHz. This experiment was recorded by Dr. Elisa Venturi.

Figure 6.16 illustrates the mean Po at +30 mV before and after the luminal side of the channel was perfused with solutions at pH 6.2. Acidic pH, on the luminal side of the SR K^+ channel, did not alter channel Po_{TOTAL}, Po_{FULL} or Po_{SUB} (n=4, SEM).

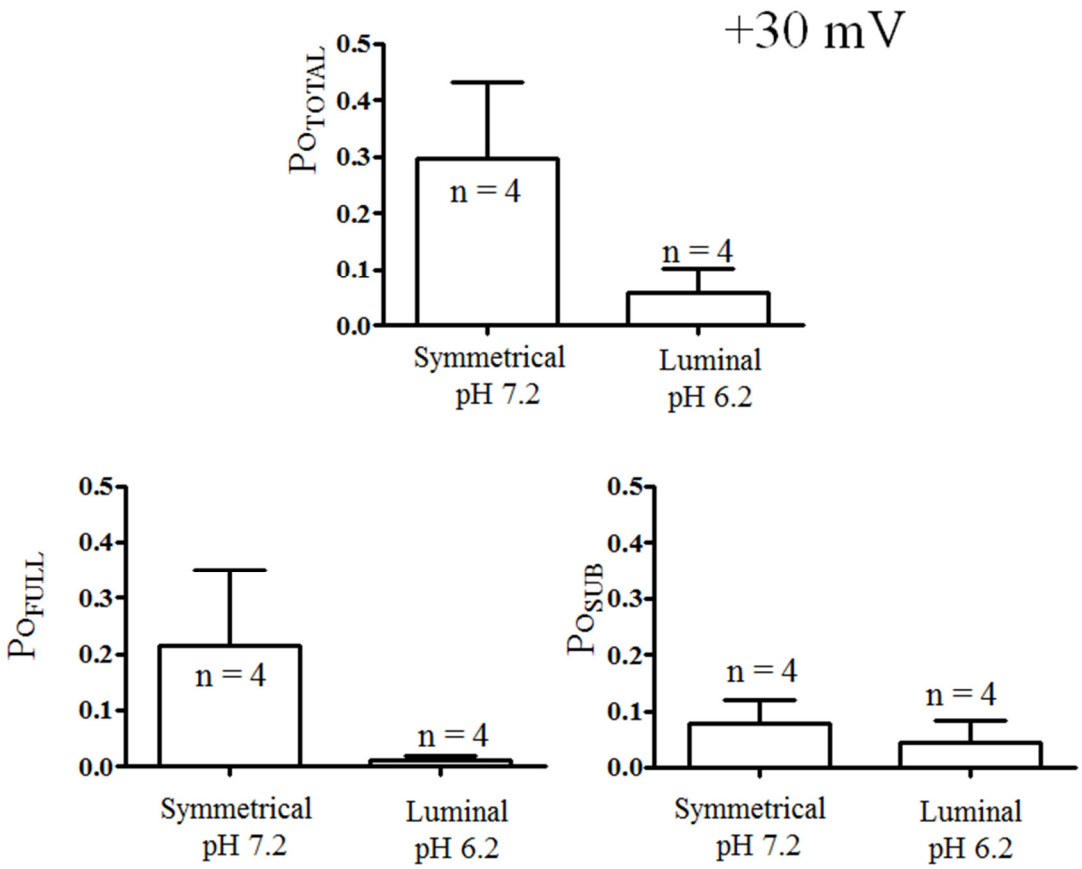


Figure 6.16 . The effect of luminal pH 6.2 on SR K^+ channel Po at +30 mV.
Data is presented as Mean ± SEM. This set of experiments was recorded by Dr. Elisa Venturi and Dr. Elena Galfrè, and the data was analysed by myself.

There was no difference in the contribution of Po_{FULL} to Po_{TOTAL} in luminal pH 6.2, as, illustrated in Figure 6.17.

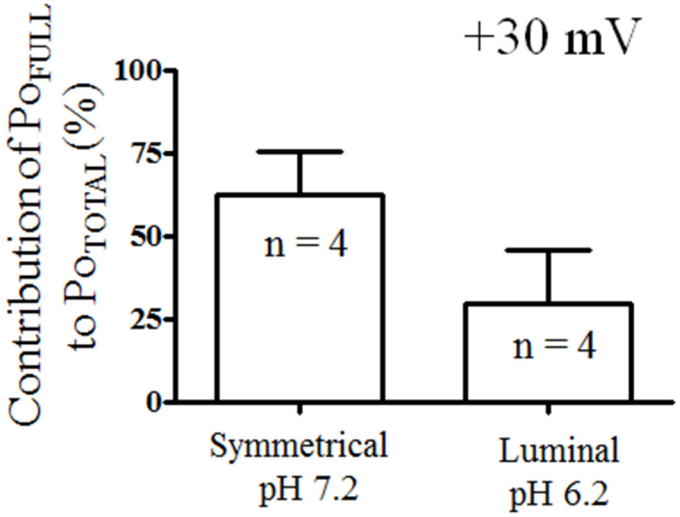


Figure 6.17 The effect of luminal pH 6.2 on the contribution of Po_{FULL} to Po_{TOTAL} at + 30 mV.
Data are presented as Mean ± SEM. The data was recorded by Dr. Elisa Venturi and Dr. Elena Galfrè, and was analysed by myself.

At -30 mV, there were also no significant changes in SR K^+ channel Po, as illustrated in Figure 6.18. Only 1/4 experiments exhibited gating to amplitudes expected for the full open channel level at -30 mV.

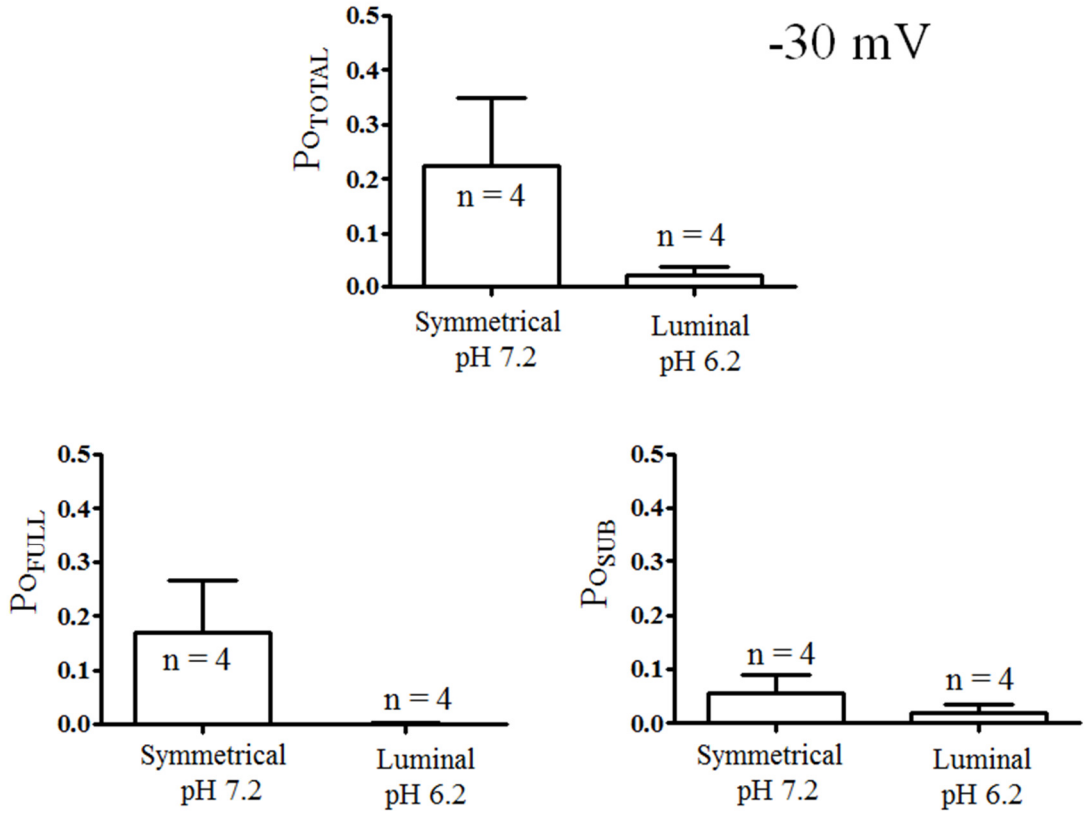


Figure 6.18. The effects of luminal pH 6.2 on SR K^+ channel Po at -30 mV.
The data are presented as Mean ± SEM. This set of experiments was performed by Dr. Elisa Venturi and Dr. Elena Galfrè, and were analysed by myself.

There was no change in the contribution of Po_{FULL} to Po_{TOTAL} in luminal pH 6.2, as shown in Figure 6.19.

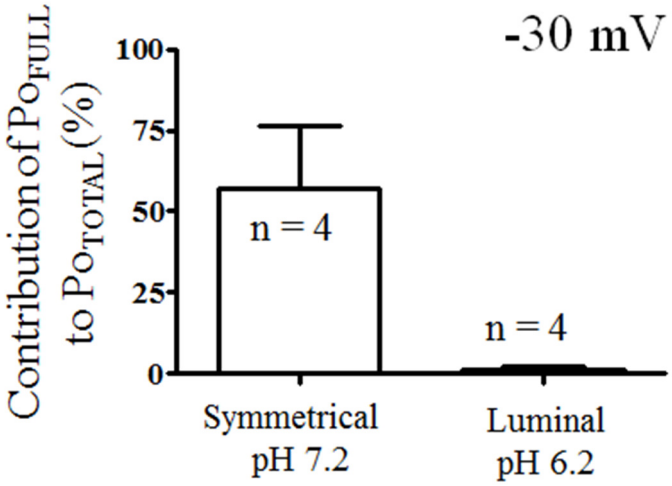


Figure 6.19. The effects of luminal pH 6.2 on the contribution of Po_{FULL} to Po_{TOTAL} at -30 mV.
The data are presented as Mean ± SEM. This set of experiments was performed by Elisa Venturi, Elena Galfrè and myself. All analysis was done by myself.

6.3.4.2 Investigating the time-dependence of the effect of luminal pH 6.2 on SR K^+ channel function

The time-dependence of luminal pH 6.2 was investigated. Each recording was split into 10 s segments, and the Po of each segment was calculated. The mean data shown in Figure 6.20 suggests that the effect of luminal pH 6.2 on SR K^+ channel gating occurred immediately after the solution was perfused with pH 6.2 at +30 mV.

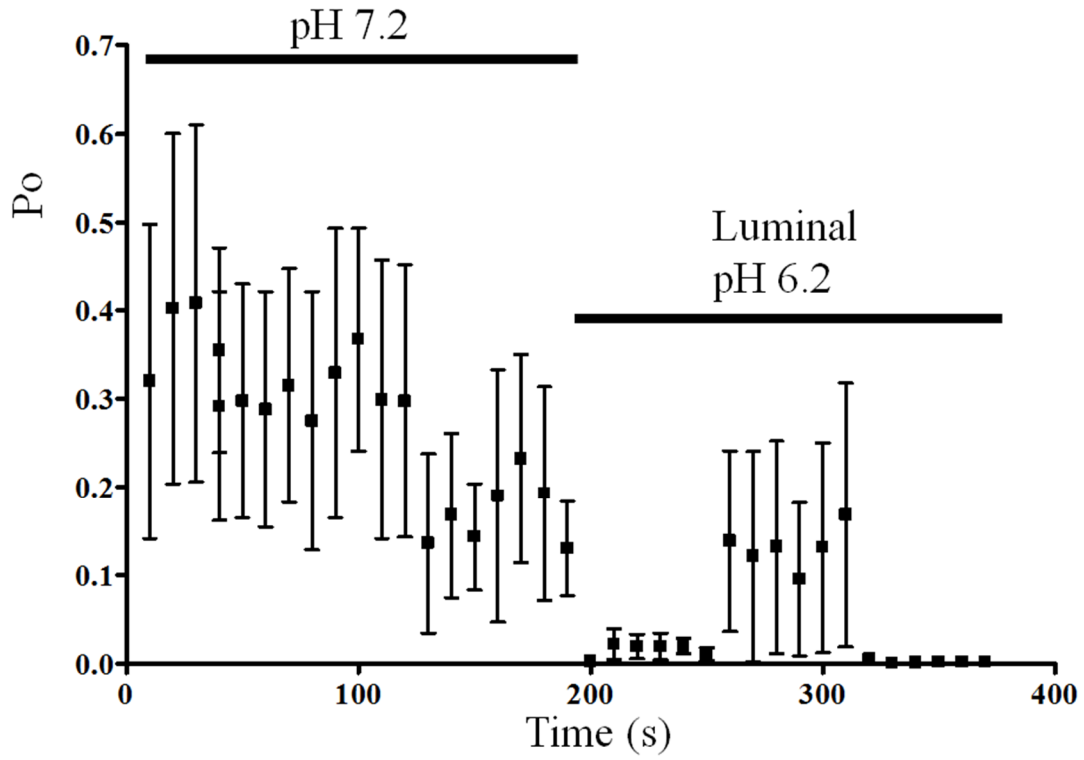


Figure 6.20 Time course of luminal pH 6.2 inhibition of the SR K^+ channel.
Mean Po values were calculated in 10 s segments and plotted against the time (s). The black bars indicate when the recording solution was changed. Data are presented as mean ± SEM for n=7. Holding potential was +30 mV. This set of experiments was performed by Elisa Venturi, Elena Galfrè and myself. All analysis was done by myself.

6.3.4.3 The effect of luminal pH 6.2 on mean open duration of the full open level

The underlying mechanism of action of luminal pH 6.2 on SR K^+ channel gating was investigated by looking at the durations of the sojourns in the full open channel level according to the protocol outlined in section 6.2.1.1. In 3/4 experiments, although 2 of these recordings contained more than one channel gating in the bilayer, individual openings, where only one full open state was observed, were analysed. In total, from 3 recordings, 38 openings were measured in symmetrical pH 7.2 and 6 openings in luminal pH 6.2. The decrease in channel Po at +30 mV was not associated with any change in the durations of the openings to the full open channel level. The mean data are shown in Figure 6.21.

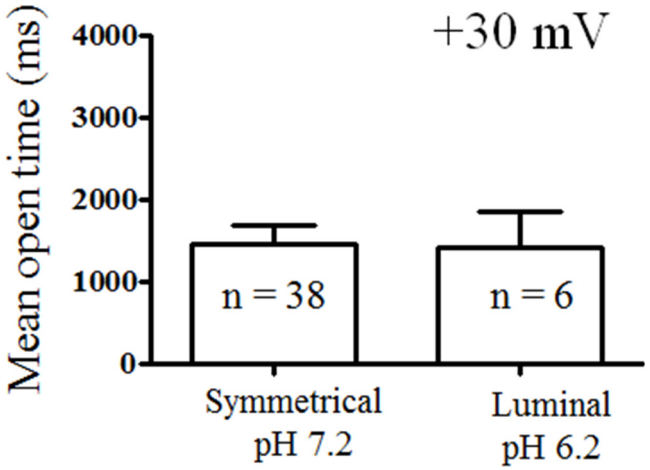


Figure 6.21 Effect of luminal pH 6.2 on the mean open time of the full open channel level at +30 mV. The mean open time was measured from 38 individual openings in pH 7.2 and 6 individual openings in luminal pH 6.2 from 3 experiments.

At -30 mV, only three openings (from one experiments) in luminal pH 6.2 were observed. To give an indication whether the mean open time was affected, the individual open durations of the full open channel level in control conditions and when the cytosolic side of the channel was perfused with pH 6.2 were compared. From the one recording, 22 openings in symmetrical pH 7.2 and 3 openings in luminal pH 6.2 were measured, and the individual data points are shown in Figure 6.22. Although the n numbers are too low to perform any statistical analysis, it appears that the mean open duration of the full open channel level may be reduced at -30 mV.

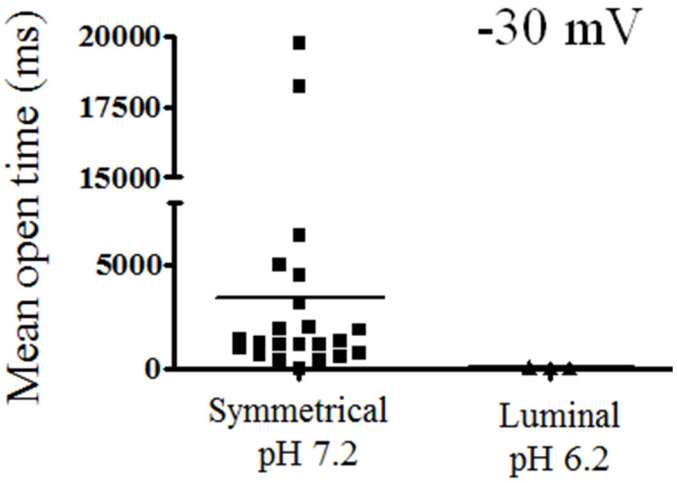


Figure 6.22 Effect of luminal pH 6.2 on the mean open time of the full open channel level at -30 mV.
Individual durations in the full open channel level are shown for n=1 experiment.

6.3.4.4 Effect of luminal pH on the frequency of openings to the full open channel level

Since the observed decrease in Po when the luminal side of the channel was changed to pH 6.2 was not associated with a decreased in the durations in the full open channel level at +30 mV, the recording containing only one active channel was analysed to determine if I could uncover clues to the mechanism behind the decrease in Po. The durations of the closings between the openings that reached the fully open channel level were measured, as explained in section **Error! Reference source not found.**. The data is shown in the table below

Mean closed duration (ms)	
pH 7.2	**Luminal pH 6.2**
9656	68783

Table 6-2 Mean closed duration +30 mV.
It appears that the mean closed time increases in luminal pH 6.2, suggesting a decrease in the frequency of openings to the full open channel level (n=1).

Although there was only one recording, and no statistical analysis was performed, I can hypothesise that the reduction in Po in luminal pH 6.2 at + 30 mV was due to a decrease in frequency of openings to the fully open channel level, while the durations in the fully open channel remained the same.

At -30 mV, the only recording that had one SR K^+ channel in the bilayer was very voltage-dependent, and no openings to the fully open channel level were observed, so closed durations could not me measured. The number of open bursts at -30 mV in symmetrical pH 7.2 and when the luminal side of the channel was changed to pH 6.2 were manually counted. As illustrated in Figure 6.23, the apparent decrease in SR K^+ channel Po was associated with a possible decrease in the frequency of openings.

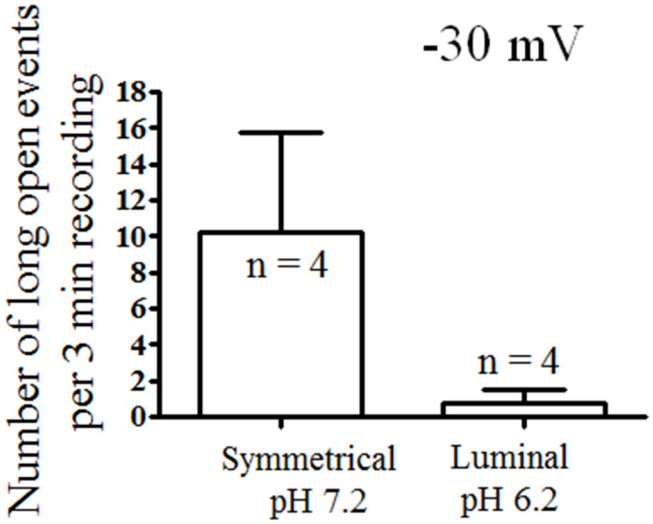


Figure 6.23 Effect of luminal pH 6.2 on frequency of full open bursts at -30 mV
Data is presented as Mean ± SEM.

6.3.4.5 Effect of luminal pH 6.2 on SR K^+ conductance

The single-channel current amplitude of the SR K^+ channel was measured under control conditions (symmetrical 210 mM KPIPES, pH 7.2) and when the luminal side of the channel was perfused with 210 mM KPIPES, pH 6.2. The mean data are shown in Figure 6.24. At +30 mV, there was no change in the current amplitude of the full open channel level of the SR K^+ channel when the luminal side of the channel was perfused with pH 6.2. At -30 mV, although only one experiment contained measureable openings in the full open channel level in luminal pH 6.2, it appears that the unitary current amplitude was decreased in that one experiment.

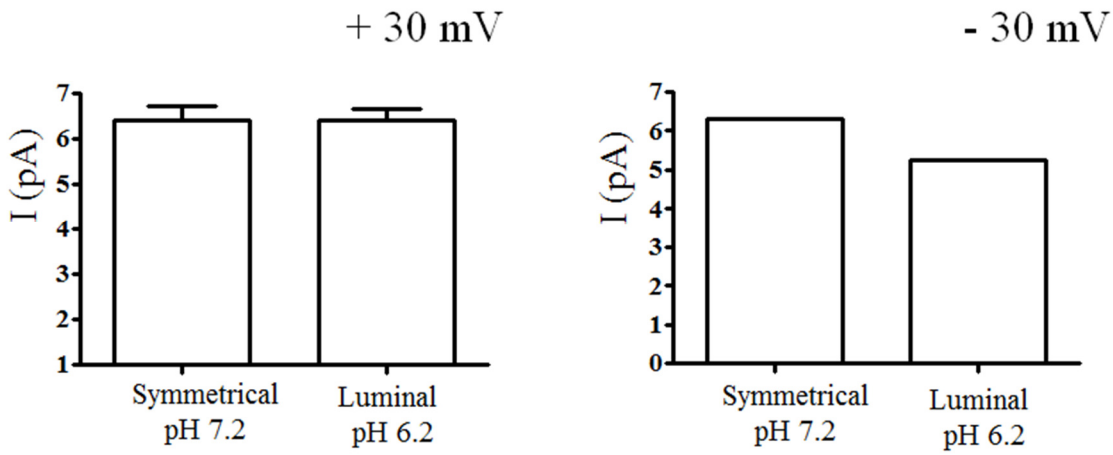


Figure 6.24. Effect of luminal pH 6.2 on the unitary conductance of the SR K^+ channel.
The bar charts show the mean current amplitude value at +30 mV and -30mV in control (symmetrical 210 mM KPIPES pH 7.2) and when the luminal side of the channel was perfused with 210 mM KPIPES pH 6.2. This set of experiments was performed by Elisa Venturi, Elena Galfrè and myself. All analysis was done by myself.

6.3.5 Effect of pH 6.2 on SR K^+ channels from WT tissue

As I described in chapter 3, when incorporated into artificial bilayers, and gating in 210 mM KPIPES, pH 7.2, there seems to be no obvious difference in the single-channel properties of the SR K^+ channels from TRIC-A KO and WT skeletal muscle. Since consistent decrease in Po of the SR K^+ channels from TRIC-A KO tissue in pH 6.2 was observed, I investigated if a similar effect occurred when WT LSR was incorporated into artificial bilayers. After monitoring the gating activity of SR K^+ channels from WT skeletal muscle in control solutions (symmetrical 210 mM KPIPES, pH 7.2), both chambers were perfused with 210 mM KPIPES, pH 6.2. Figure 6.25 illustrates the mean Po at +30 mV. Symmetrical pH 6.2, reduced the overall Po (n=3, $*p<0.05$) and Po_{FULL} (n=3 $**p<0.01$), but had no significant effect on Po_{SUB}.

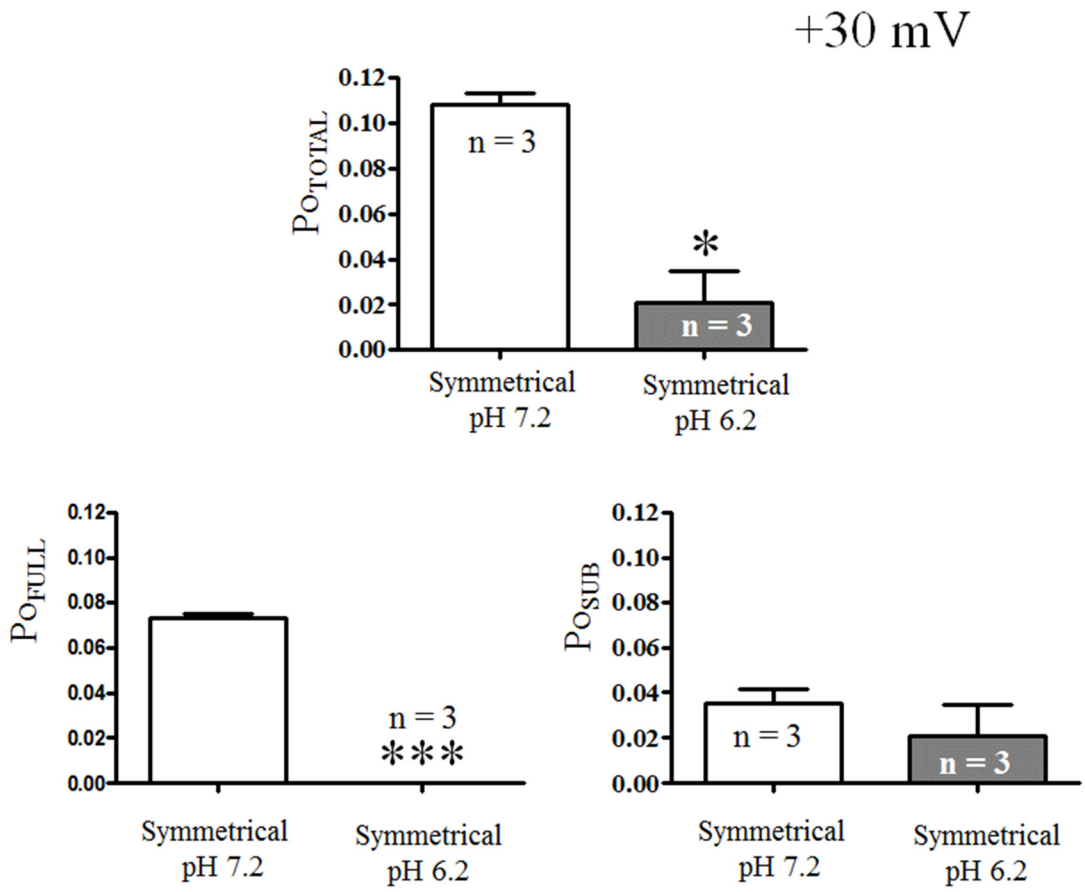


Figure 6.25 Effect of pH 6.2 on SR K^+ channel gating from WT tissue
Bar charts are used to show SR K^+ channel Po after both sides of the channel were perfused with pH 6.2 (***p<0.001, *p<0.05). The data are presented as Mean ± SD.

In pH 6.2, at +30 mV, the contribution of $P_{O_{FULL}}$ to $P_{O_{TOTAL}}$ decreased, indicating, that an opening of the SR K^+ channel in acidic pH was more likely to be in a sub-conductance state than the full open channel level.

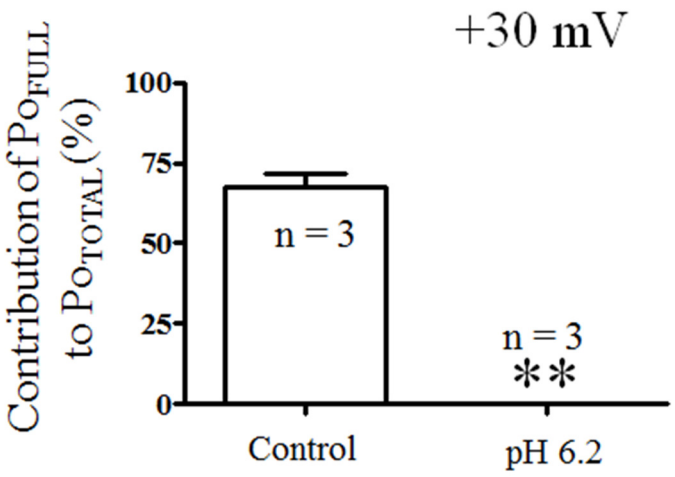


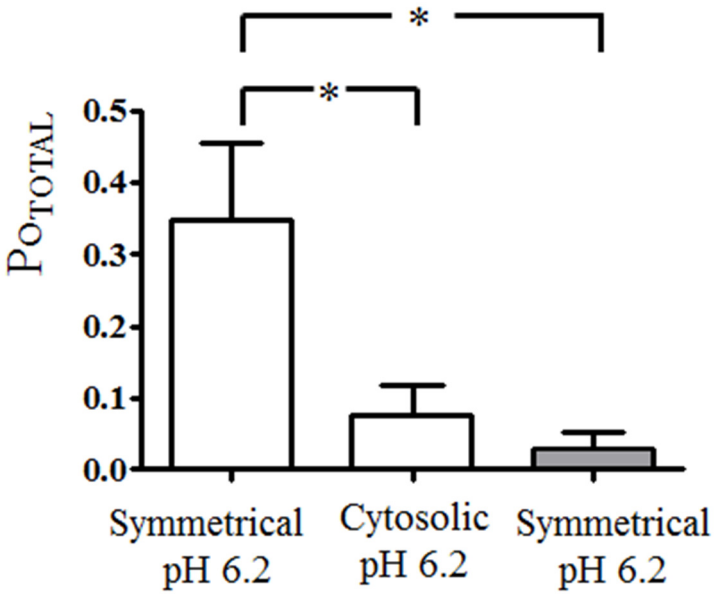
Figure 6.26 The effect of pH 6.2 on the contribution Po_{FULL} to Po_{TOTAL} at + 30 mV.
The data are presented as Mean ± SD (**p<0.01).

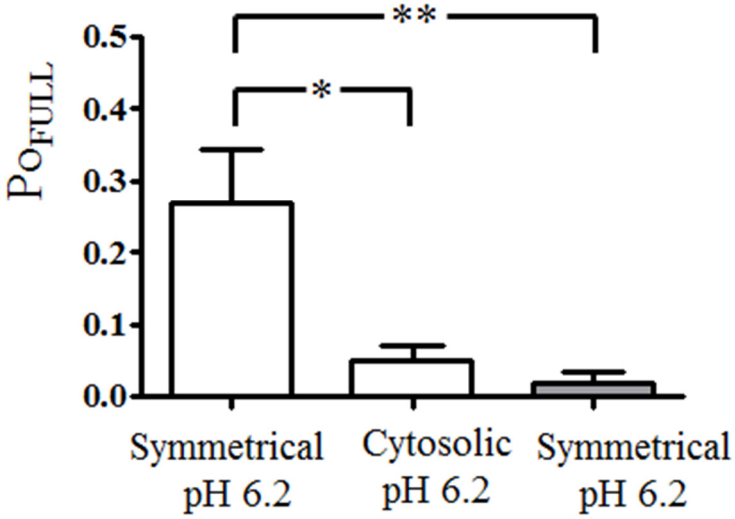
6.3.6 Effect of symmetrical pH 6.2 on SR K^+ channel gating

6.3.6.1 Are their distinct sites on the cytosolic and luminal side of the SR K^+ channel that are sensitive to acidic pH?

Since a decrease in Po was observed when the cytosolic or luminal face of the channel was perfused with pH 6.2, we wanted to investigate whether subsequent perfusion of both sides of the channel had any additional or additive effect on SR K^+ channel gating. Since the SR K^+ channels from WT and TRIC-A KO appeared to have similar sensitivity, the Po values were combined. In 5 experiments where the cytosolic side of the channel was first perfused with pH 6.2, the luminal side of the channel was subsequently perfused with pH 6.2. Mean data at +30 mV are shown in bar charts in Figure 6.27.

Po decreased when the cytosolic side of the channel was perfused with pH 6.2 and did not significantly decrease further when both sides of the chamber were perfused with symmetrical 210 mM KPIPES pH 6.2 (n=5 *p<0.05). When the Po was split into Po_{FULL} and Po_{SUB}, Po_{FULL} significantly decreased (n=5 **p<0.01), while Po_{SUB} remained unchanged.


*
*
$P_{O_{TOTAL}}$
0.5
0.4
0.3
0.2
0.1
0.0
Symmetrical pH 6.2
Cytosolic pH 6.2
Symmetrical pH 6.2


**
*
$P_{O_{FULL}}$
0.5
0.4
0.3
0.2
0.1
0.0
Symmetrical pH 6.2
Cytosolic pH 6.2
Symmetrical pH 6.2

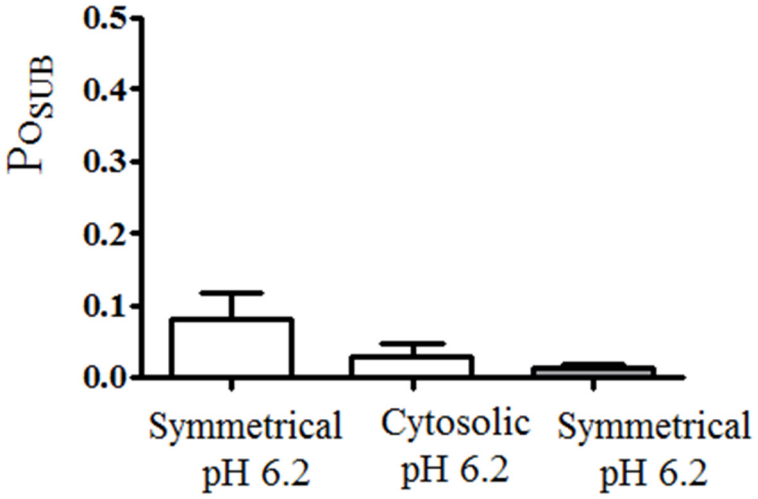
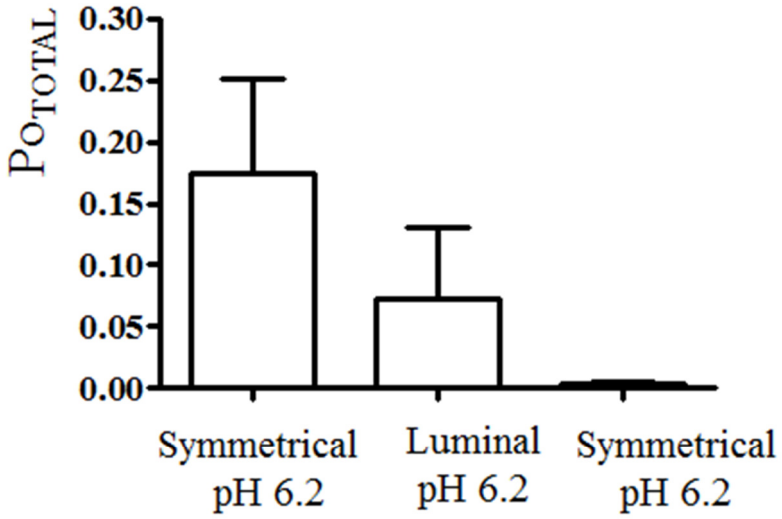
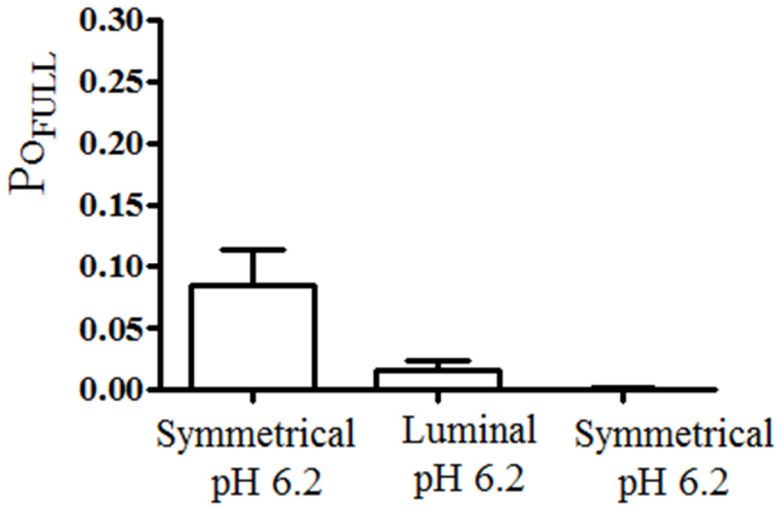

$P_{O_{SUB}}$
0.5
0.4
0.3
0.2
0.1
0.0
Symmetrical pH 6.2
Cytosolic pH 6.2
Symmetrical pH 6.2

Figure 6.27. Effect of subsequent perfusion of both chambers with pH 6.2 (Cytosolic side first) at +30 mV.
Bar charts are used to show the decrease in SR K^+ channel Po after the cytosolic side, and subsequently, the luminal side, was perfused with pH 6.2 (*p<0.05, **p<0.001). The data are presented as Mean ± SEM for 5 experiments.

Additionally, in 3/4 experiments where the luminal side of the channel was first perfused with pH 6.2, the cytosolic side was subsequently perfused. There was no significant changes in $P_{O_{TOTAL}}$, $P_{O_{FULL}}$ or $P_{O_{SUB}}$ when the luminal and subsequently the cytosolic sides of the channel was perfused. Mean data are shown in bar charts in Figure 6.28.


$P_{O_{TOTAL}}$
0.30
0.25
0.20
0.15
0.10
0.05
0.00
Symmetrical pH 6.2
Luminal pH 6.2
Symmetrical pH 6.2


$P_{O_{FULL}}$
0.30
0.25
0.20
0.15
0.10
0.05
0.00
Symmetrical pH 6.2
Luminal pH 6.2
Symmetrical pH 6.2

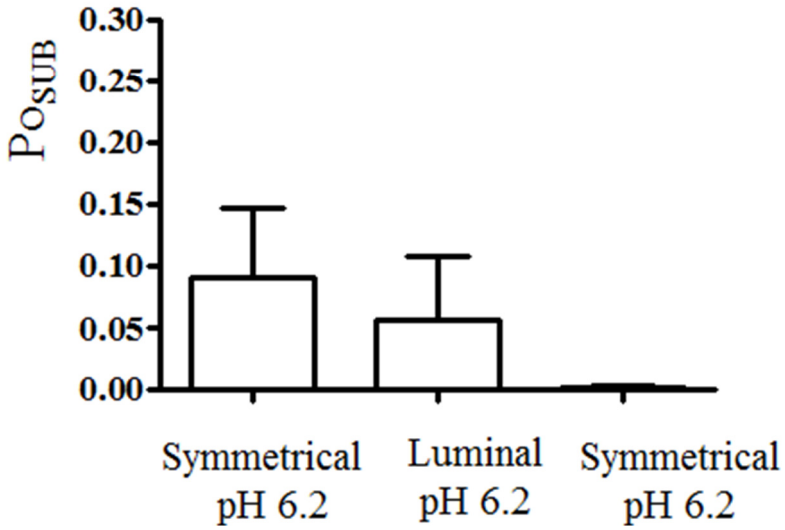

$P_{O_{SUB}}$
0.30
0.25
0.20
0.15
0.10
0.05
0.00
Symmetrical pH 6.2
Luminal pH 6.2
Symmetrical pH 6.2

Figure 6.28. Effect of subsequent perfusion of both chambers with pH 6.2 (Luminal side first) at +30 mV.
Bar charts are used to show the decrease in SR K^+ channel Po after the luminal side, and subsequently, the cytosolic side, was perfused with pH 6.2. The data is presented as Mean ± SD for 3 experiments. This set of experiments was performed by Dr. Elisa Venturi and Dr. Elena Galfrè and analysed by myself.

From the data above, it appeared that at +30 mV, a change in cytosolic pH to 6.2 had a greater effect on Po than a change in luminal pH. Based on the analysis at +30 mV, in cytosolic pH 6.2, the decrease in Po seemed to be due to a combined effect of a decrease in the duration and the frequency of openings to the full open channel level. On the other hand, at +30 mV, in luminal pH 6.2, the decrease in Po appears to be only due to a decrease in the frequency of openings to the full channel level.

In this thesis, I have found that the Po of the SR K^+ channel is quite variable, and in addition, the Po can be affected by the number of channels gating in the bilayer. To overcome the variably in channel Po, and to investigate whether the effect of cytosolic pH 6.2 was greater at +30 mV, mean data from Figure 6.27 and Figure 6.28 were expressed as a % change of control Po, as shown in Figure 6.29.

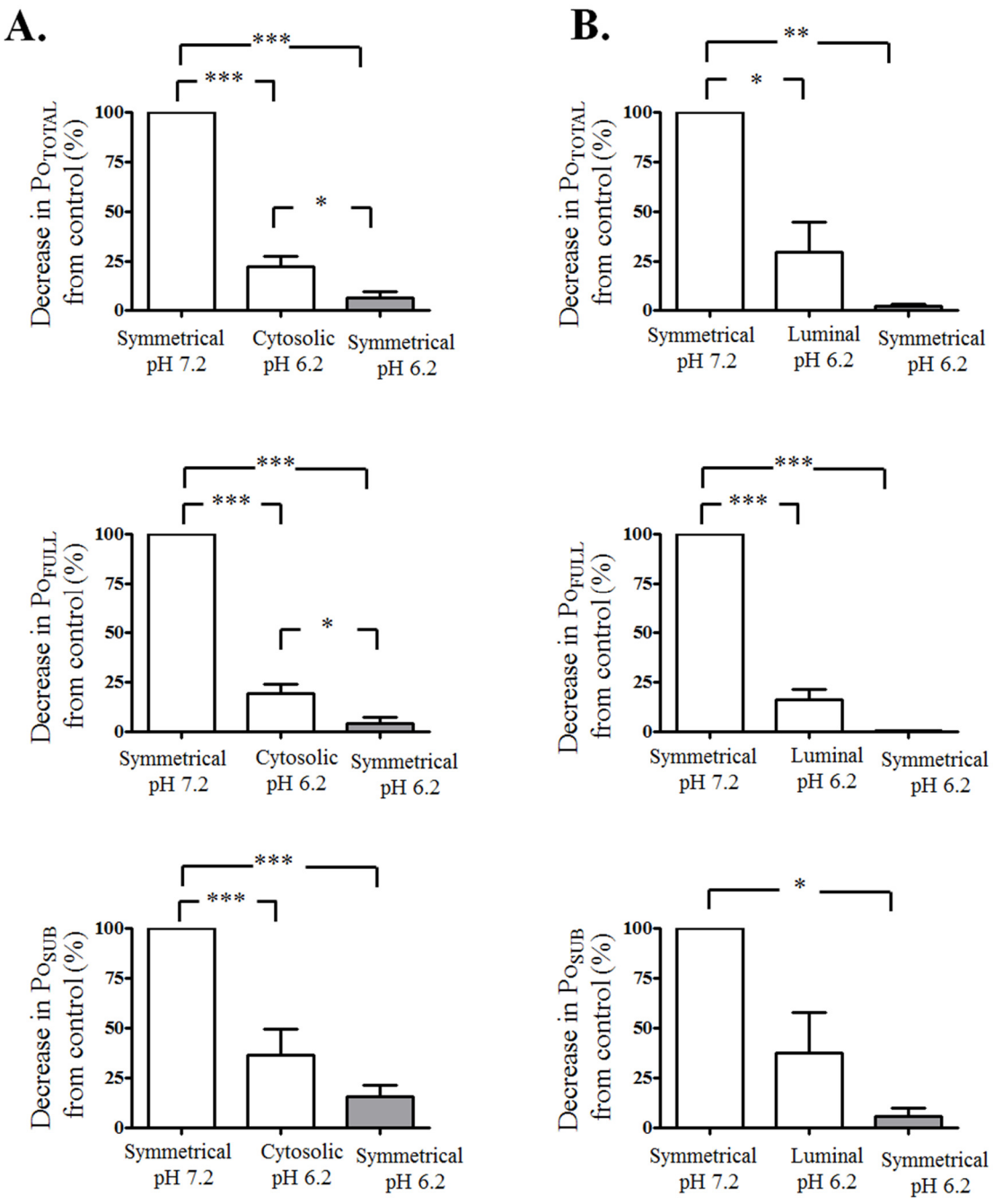


Figure 6.29 Effect of subsequent perfusion of both chambers with pH 6.2
The mean data from Figure 6.27 and Figure 6.28 expressed as a % of control (symmetrical pH 7.2) in A and B, respectively. The values are summarised in Table 6-3

	Cytosolic pH 6.2	Symmetrical pH 6.2	Luminal pH 6.2	Symmetrical pH 6.2
P_{OTOTAL}	22 ± 5.4	6.4 ± 3.1	29 ± 15	2.2 ± 1.2
P_{OFULL}	19 ± 4.9	4.2 ± 3.3	16 ± 5.3	0.40 ± 0.39
P_{OSUB}	37 ± 13	16 ± 5.8	38 ± 20	6.0 ± 4.1

Table 6-3. The mean data illustrating the decrease in Po in pH 6.2 as a % of control (symmetrical pH 7.2)

We wanted to investigate whether at +30 mV, in luminal pH 6.2, when the decrease in Po seemed to be due to a decrease in frequency of openings to the full open channel level, if the cytosolic chamber was then perfused with pH 6.2, would a decrease in duration of openings to the full open channel level be observed. Only one recording had measureable openings in control, luminal pH 6.2 and symmetrical pH 6.2. The mean open time of the fully open channel level was measured from individual openings as described earlier. The individual measurements are shown in Figure 6.30.

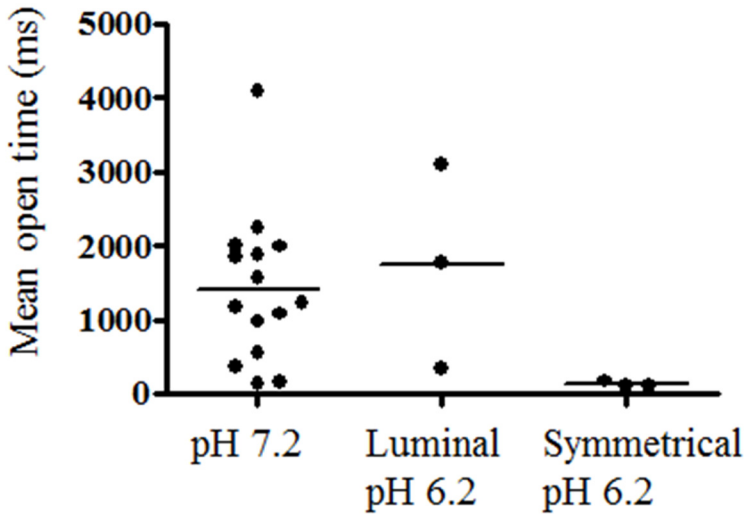


Figure 6.30 Effect of pH 6.2 on the mean open time of the full open channel level at +30 mV.

The chart shows the mean open duration of the full open level pH 7.2, in luminal pH 6.2, and symmetrical pH 6.2 (n=1)

Although there was only one recording, and no statistical analysis was performed, the results suggest that, at +30 mV, in luminal pH 6.2, the decrease in Po was due to a decrease in the frequency of openings to the full open channel level, due to a luminal proton binding site on the channel. Furthermore, in symmetrical pH 6.2, the further decrease in Po was due to the additional combination of a decrease in both the frequency and duration of openings to the full open channel level mediated by a cytosolic proton binding site on the channel.

6.3.6.2 The gating properties of the SR K^+ channel in symmetrical pH 6.2

Figure 6.31 shows a representative trace of the SR K^+ channel gating in symmetrical 210 mM KPIPES pH 7.2, and, when both chambers of the bilayer were subsequently perfused with 210 mM KPIPES pH 6.2. Experiments were combined regardless of whether the cytosolic or luminal side of the channel was perfused first (The 5 experiments where the cytosolic side of the channel was perfused first were combined with the 3 experiments where the luminal side of the channel was perfused first).

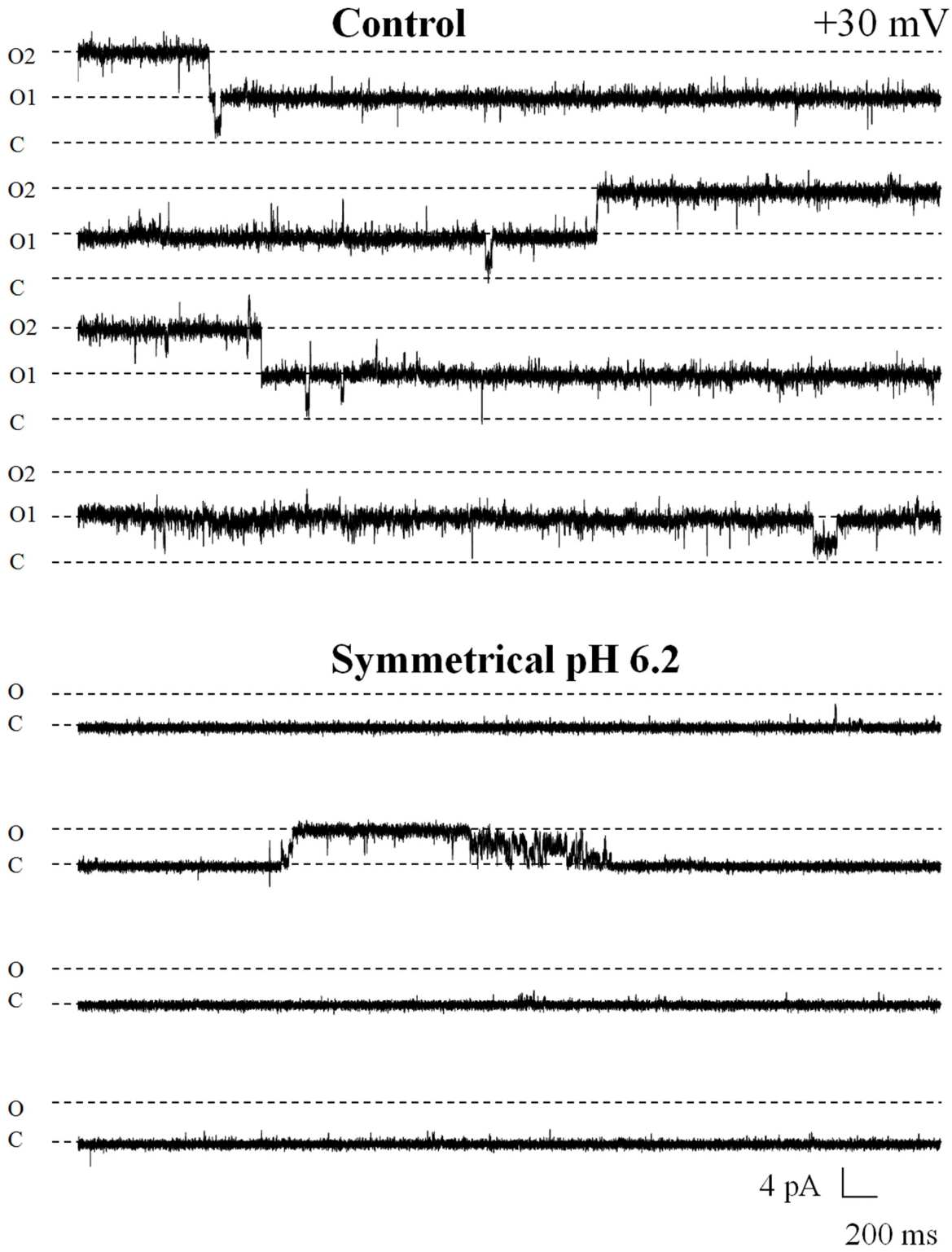


Figure 6.31. The effect of pH 6.2 on SR K^+ channel gating.
The traces show the single-channel activity before (top traces) and after (bottom traces) both chambers were perfused with 210 mM KPIPES, pH 6.2. O1 and O2 indicate the full open level of the first and second SR K+ channel, respectively, and, C indicates the zero current level. The recording was low pass filtered at 1 kHz.

The bar charts in Figure 6.32 illustrate the mean Po of the SR K^+ channels at +30 mV before and after both sides of the channel were perfused with pH 6.2. Po was significantly reduced in symmetrical pH 6.2 (n=8, $^{**}p<0.01$). Po_{FULL} and Po_{SUB} both significantly decreased (Figure 6.32).

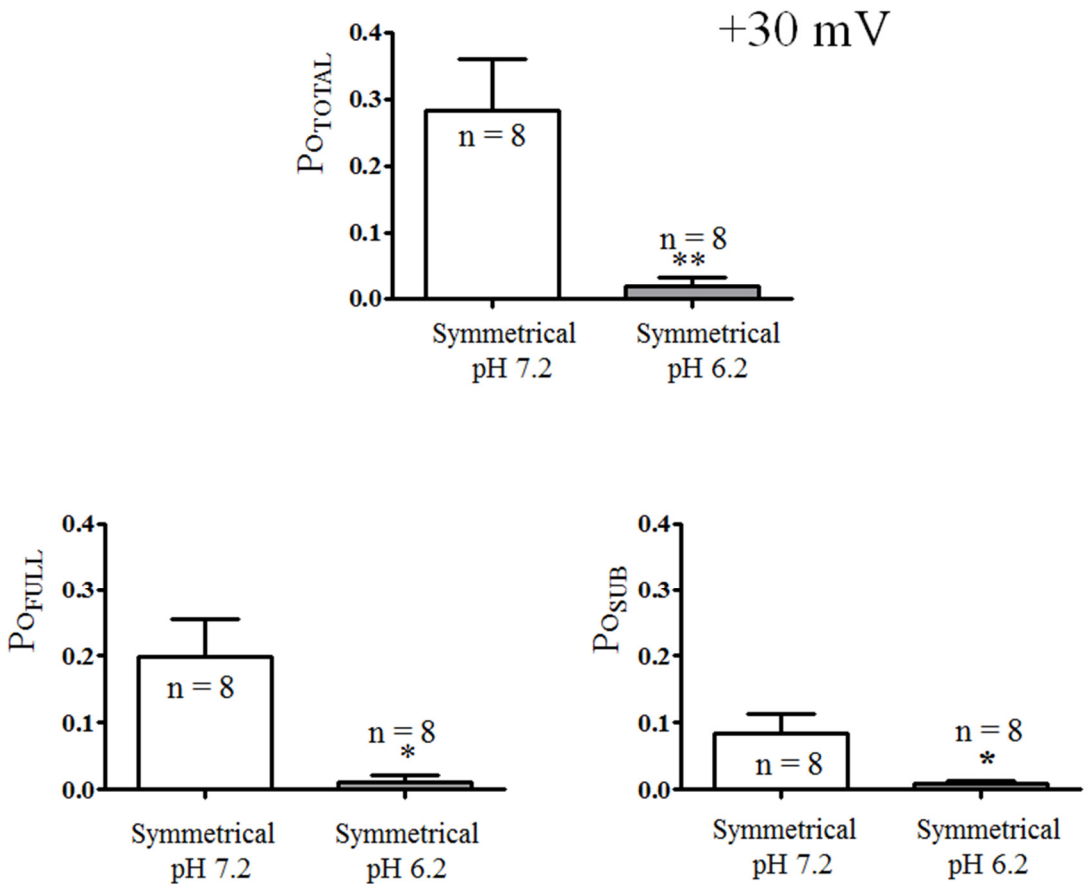


Figure 6.32. Effect of symmetrical pH 6.2 on SR K^+ channel Po at +30 mV.
The bar charts show the Po of the SR K^+ channel in symmetrical solutions of 210 mM, pH 7.2 and subsequently when both chambers were perfused with 210 mM KPIPES, pH 6.2. The data are presented as Mean ± SEM. This set of experiments was performed by myself, Dr. Elisa Venturi, Dr. Elena Galfrè.

Furthermore, the contribution of Po_{FULL} to Po_{TOTAL} was markedly reduced at +30 mV (n=8, $^{**}p<0.01$).

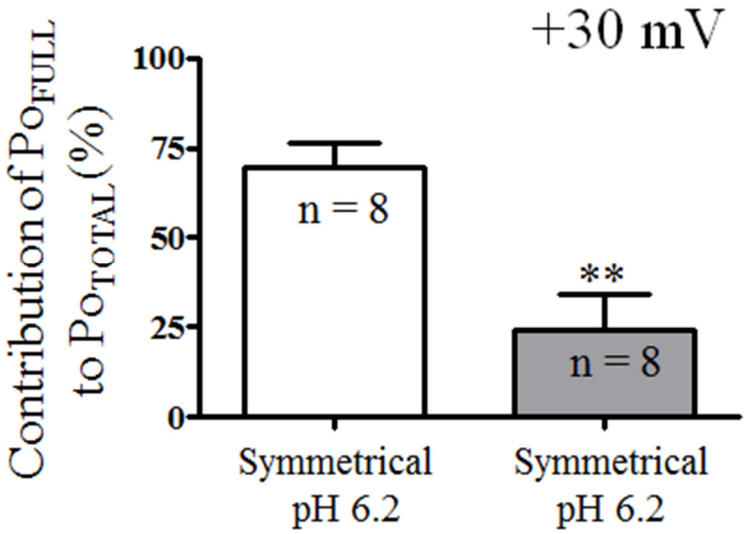


Figure 6.33 The effects of symmetrical pH 6.2 on the contribution of the full open channel level at + 30 mV.
The data are presented as Mean ± SEM (**p<0.01). This set of experiments was performed by myself, Dr. Elisa Venturi and Dr. Elena Galfrè.

At -30 mV, there are no significant changes in SR K^+ channel Po. The mean data is expressed as bar charts in Figure 6.34.

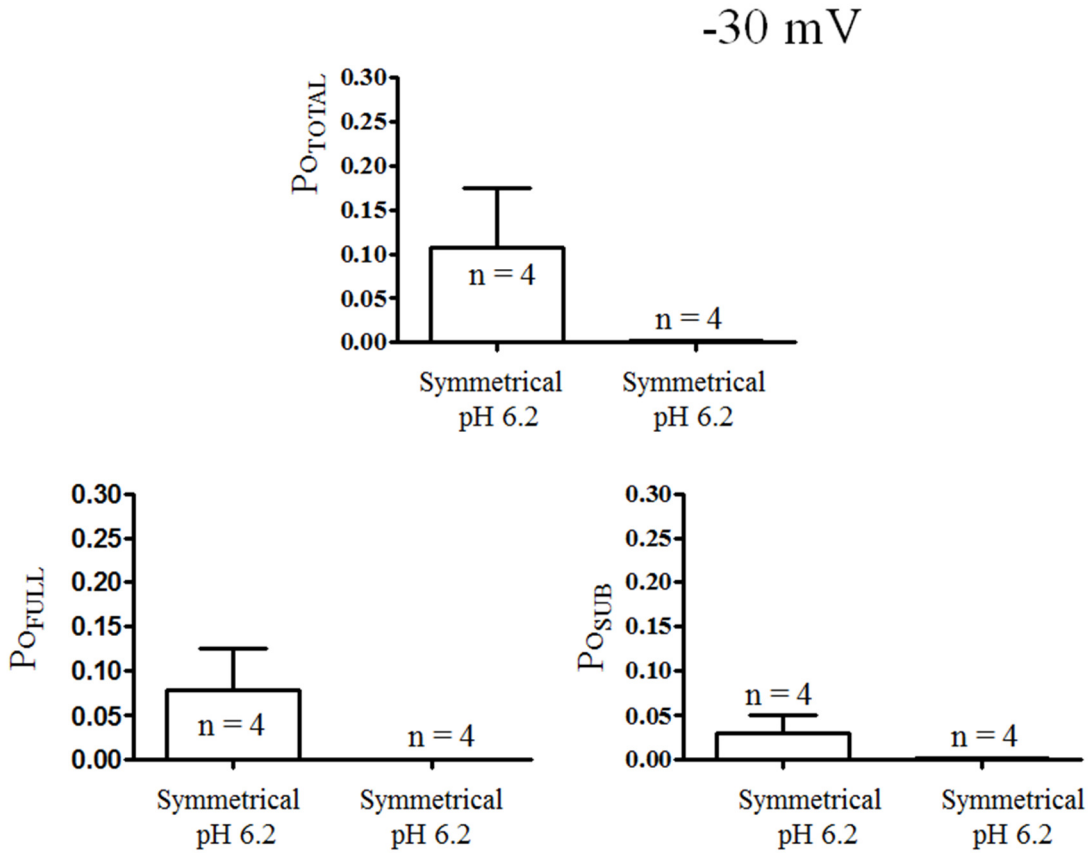


Figure 6.34 Effect of symmetrical pH 6.2 on SR K_+ channel Po at -30 mV.

The bar charts show show the decrease in SR K^+ channel Po in symmetrical pH 6.2. The data is presented as Mean ± SEM. This set of experiments was performed by myself, Dr. Elisa Venturi and Dr. Elena Galfrè.

6.3.6.3 The conductance of the SR K^+ channel in symmetrical pH 6.2

Experiments were performed at different holding potentials in symmetrical 210 mM KPIPES, pH and when both chambers were subsequently perfused with a solution containing 210 mM KPIPES pH 6.2. The current-voltage relationship for the full open channel level of the SR K^+ channel in pH 7.2 and cytosolic pH 6.2 is shown in Figure 6.35. The data were fitted by linear regression and the estimated conductance for the channel in symmetrical pH 7.2 and symmetrical pH 6.2 were compared. As shown, there was a significant reduction in the conductance of the full open channel level in symmetrical 210 mM pH 6.2.

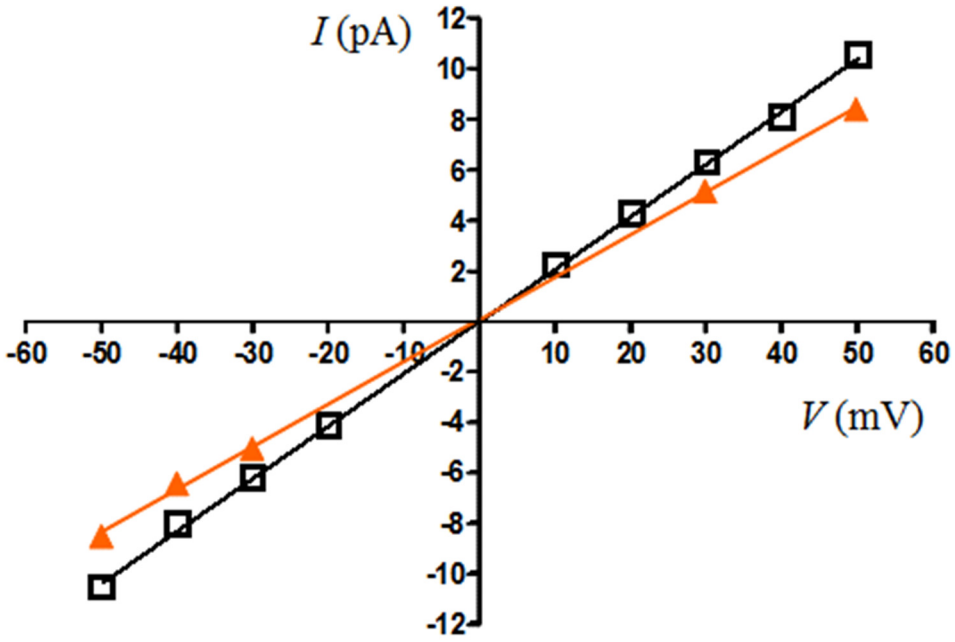


Figure 6.35. Effect of symmetrical pH 6.2 on SR K^+ channel conductance.
Comparison of the current-voltage relationship of an SR K^+ channel under control condition (black line) and post perfusion in symmetrical pH 6.2 (orange line). Data are

fitted by linear regression. The conductance in symmetrical pH 7.2 was 207 ± 0.02 pS and 169 ± 0.03 pS in symmetrical pH 6.2 (n=3-10). This set of experiments was performed by myself, Dr. Elisa Venturi and Dr. Elena Galfrè.

6.3.7 Effect of pH 9.2 on SR K^+ channel function

Since acidic pH, decreased the Po of the SR K^+ channel, we wanted to investigate whether alkaline pH, on the cytosolic or luminal side of the channel could also modulate channel gating. After the SR K^+ channel was recorded gating in control conditions (210 mM KPIPES pH 7.2), the cytosolic side of the channel was perfused with 210 mM KPIPES, pH 9.2. In the majority of experiments, when the cytosolic (or luminal) side of the channel was perfused with pH 9.2, a large, variable and unidentifiable current appeared in the bilayer. This current was unanalysable at the single-channel level. It seemed, that if more than one SR K^+ channel was gating in the bilayer, this phenomenon was observed. An example is shown in Figure 6.36 when the cytosolic side of the channel was perfused with 210 mM KPIPES, pH 9.2. Noise analysis was done to illustrate the changes in current throughout the experiment. To look into this further, firstly, the effect of pH 9.2 was tested on the stability of the artificial membrane, and secondly, very low Po channels were deliberately chosen, which often did not gate to the full open channel level to see if an increment in activity could be measured.

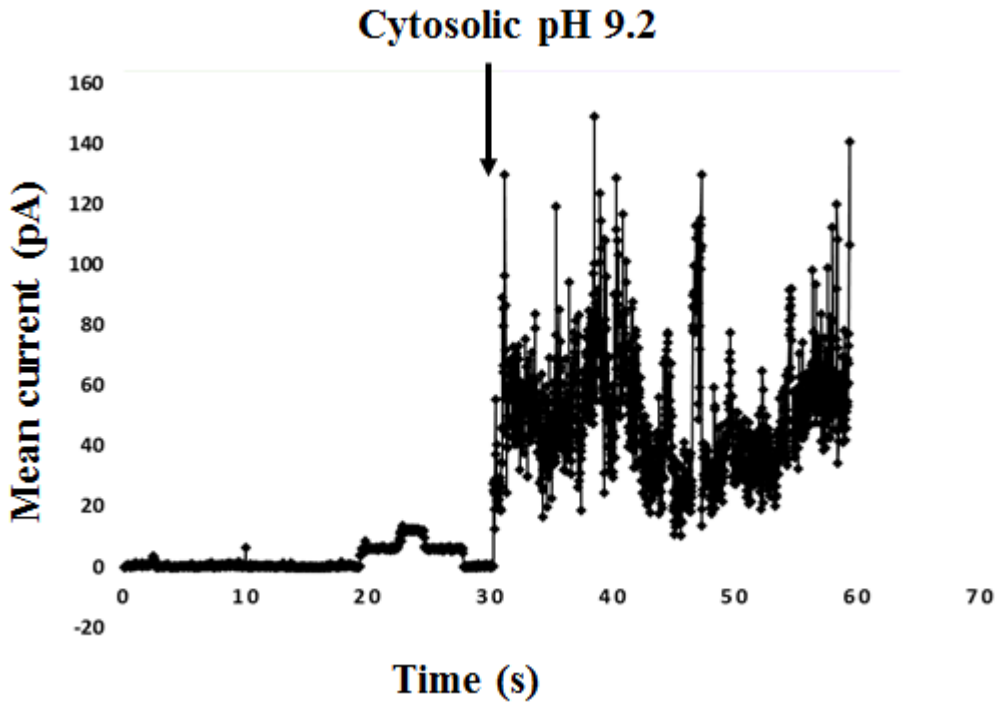


Figure 6.36. A representative example of the 'unanalysable' current observed in pH 9.2.
Noise analysis of a typical experiment before and after the cytosolic side of the channel was perfused with 210 mM KPIPES, pH 9.2. An arrow indicates when the cytosolic chamber was perfused. The recording was low pass filtered at 1 KHz.

6.3.7.1 The effect of alkaline pH 9.2 on the stability of the artificial membrane

A bilayer was painted in 210 mM KPIPES, pH 7.2, and both chambers were perfused with 210 mM KPIPES pH 9.2. In 4/4 control experiments, there was no observed change in the bilayer properties, such as changes in membrane capacitance measurements or peak to peak baseline noise. In addition, no large variable currents were observed.

6.3.7.2 Effect of cytosolic pH 9.2 on SR K^+ channel gating

After the SR K^+ channel was recorded gating in control conditions (symmetrical 210 mM KPIPES pH 7.2), the cytosolic side of the channel was perfused with 210 mM KPIPES, pH 9.2. Figure 6.37 shows a typical experiment.

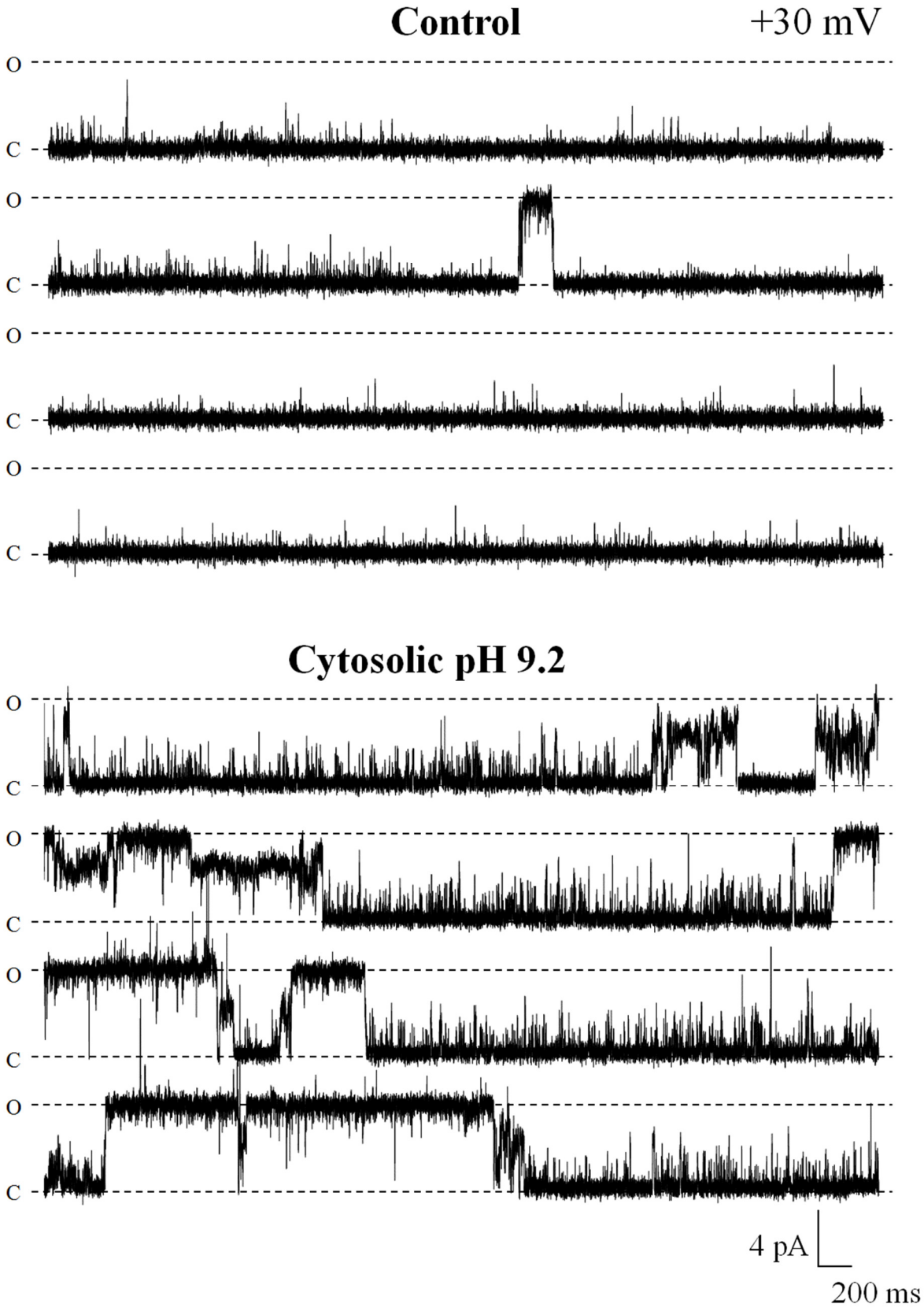


Figure 6.37. Effect of cytosolic pH 9.2 on SR K^+ channel gating.
The traces show the single-channel activity before (top traces) and after (bottom traces) the cytosolic side of the channel was perfused with 210 mM KPIPES, pH 9.2. O and C indicate the open and closed levels, respectively. The recording was low pass filtered at 1 kHz.

The bar charts in Figure 6.38 illustrate the mean Po at +30 mV before and after the cytosolic side of the channel was perfused with 210 mM KPIPES, pH 9.2. Alkaline pH, on the cytosolic side of the SR K^+ channel, increased the Po_{TOTAL} (n=3, $^{**}p<0.01$). When Po_{TOTAL} was separated into Po_{FULL} and Po_{SUB}, the effect of alkaline pH was not significant (n=3, SD).

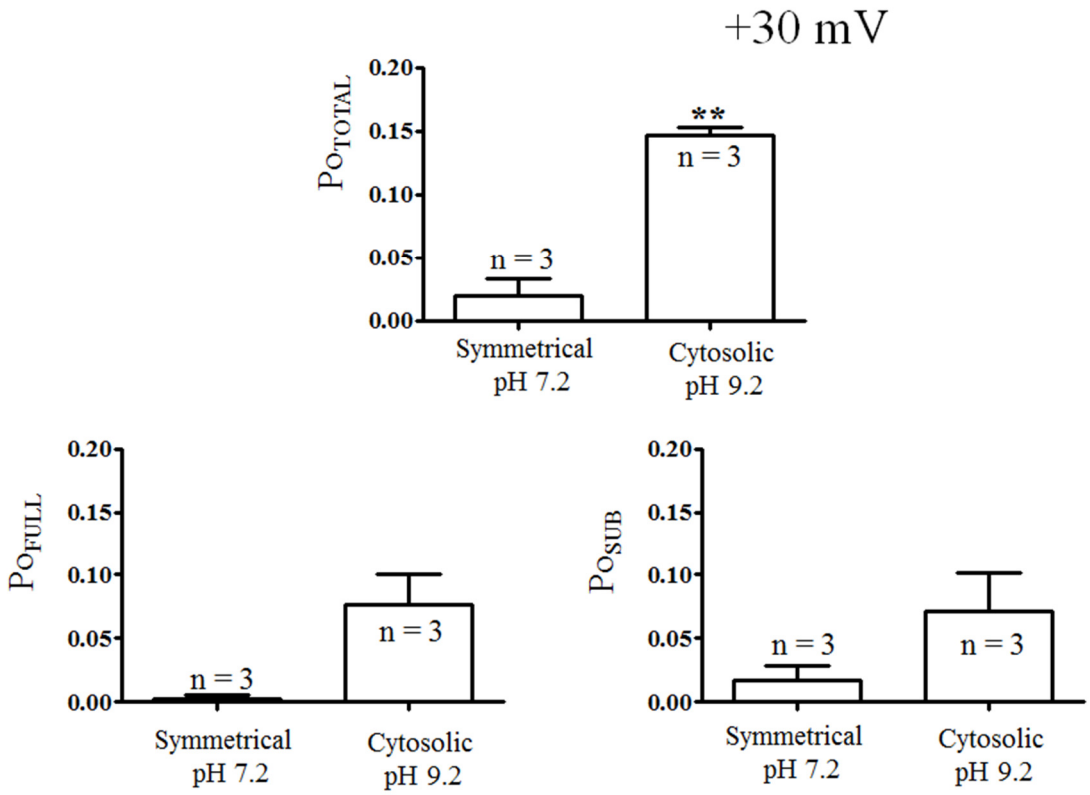


Figure 6.38. The effects of cytosolic pH 9.2 on SR K^+ channel Po.
Bar charts show that, pH 9.2, on the cytosolic side of the SR K^+ channel, increased the Po ($^{**}p<0.01$). The data are presented as Mean ± SD.

There was no significant change in the contribution of Po_{FULL} to Po_{TOTAL} in alkaline (n=3, SD). The mean data is shown in Figure 6.39.

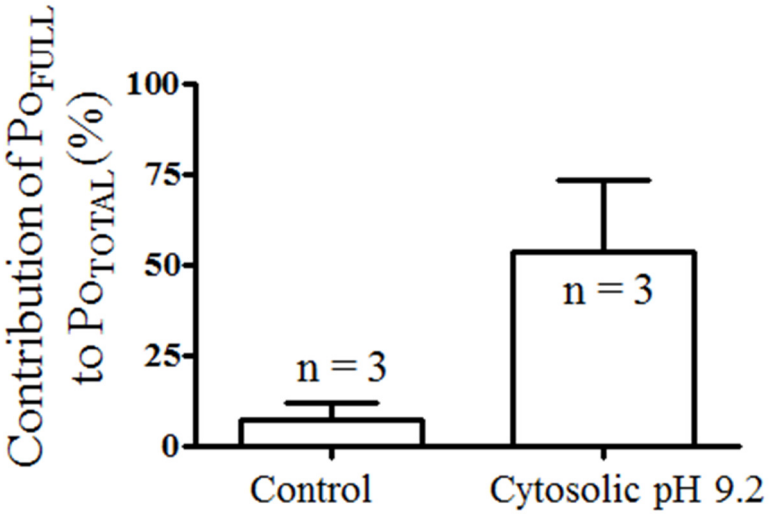


Figure 6.39 The effects of cytosolic pH 9.2 on the contribution of Po_{FULL} to Po_{TOTAL} + 30 mV. The data are presented as Mean ± SD.

6.3.7.3 The effect of cytosolic pH on the mean open duration of the full open channel level.

The underlying mechanism of action of cytosolic pH 9.2 on SR K^+ channel gating was investigated by looking at the durations of the sojourns in the full open channel level according to the protocol outlined in section 6.2.1.1 . Because we purposely chose channels that had a very low Po, we only had one experiment that had an opening at +30 mV. Nevertheless, we decide to measure the mean open time of the full open channel level using the protocol outlined in Section 6.2.1.1. The individual data points are illustrated in Figure 6.40.

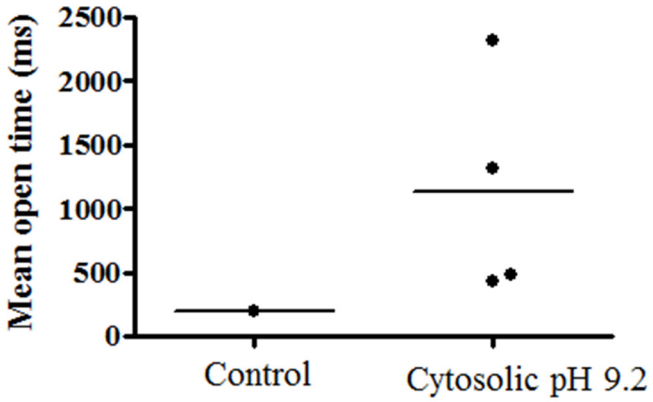


Figure 6.40 Effect of cytosolic pH 9.2 on the mean open time of the full open channel level at +30 mV.
Individual full open times are shown for one experiment.

6.3.8 Effect of luminal pH 9.2 on SR K^+ channel function

6.3.8.1 Effect of luminal pH 9.2 on SR K^+ channel gating

After monitoring the gating activity of SR K^+ channels at ± 30 mV under control conditions (210 mM KPIPES pH 7.2), the luminal side of the channel was perfused with 210 mM KPIPES, pH 9.2. Figure 6.41 shows a typical experiment.

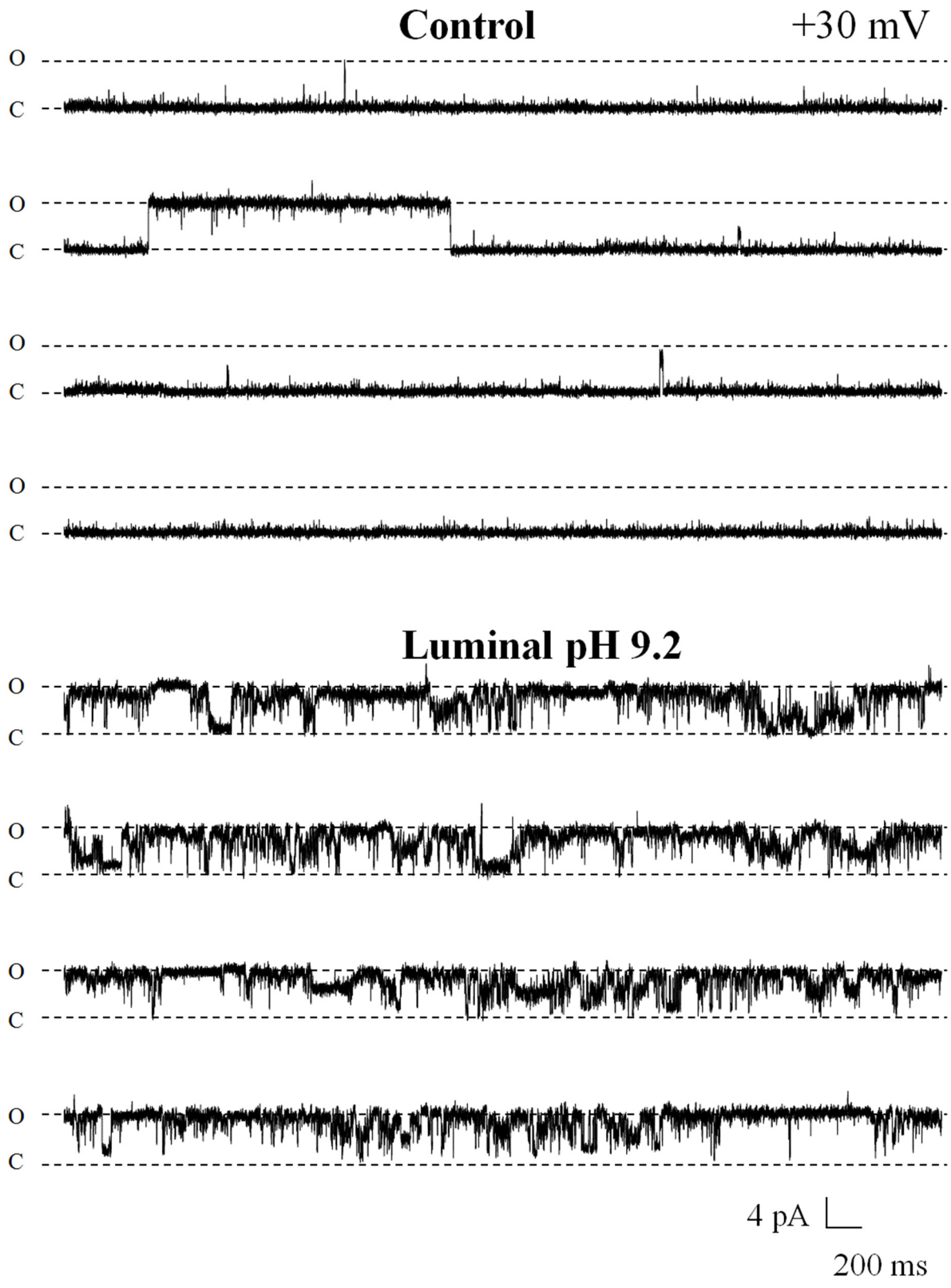


Figure 6.41 Effect of luminal pH 9.2 on SR K^+ channel gating.
The traces show the single-channel activity before (top traces) and after (bottom traces) the luminal side of the channel was perfused with 210 mM KPIPES, pH 9.2. O and C indicate

the open and closed levels, respectively. The recording was low pass filtered at 1 KHz. This experiment was recorded by Dr. Elisa Venturi.

The bar charts in Figure 6.42 illustrates the mean Po at +30 mV before and after the luminal side of the channel was perfused with 210 mM KPIPES, pH 9.2. Alkaline pH, on the luminal side of the SR K^+ channel, did not significantly increase channel Po (n=3, SD).

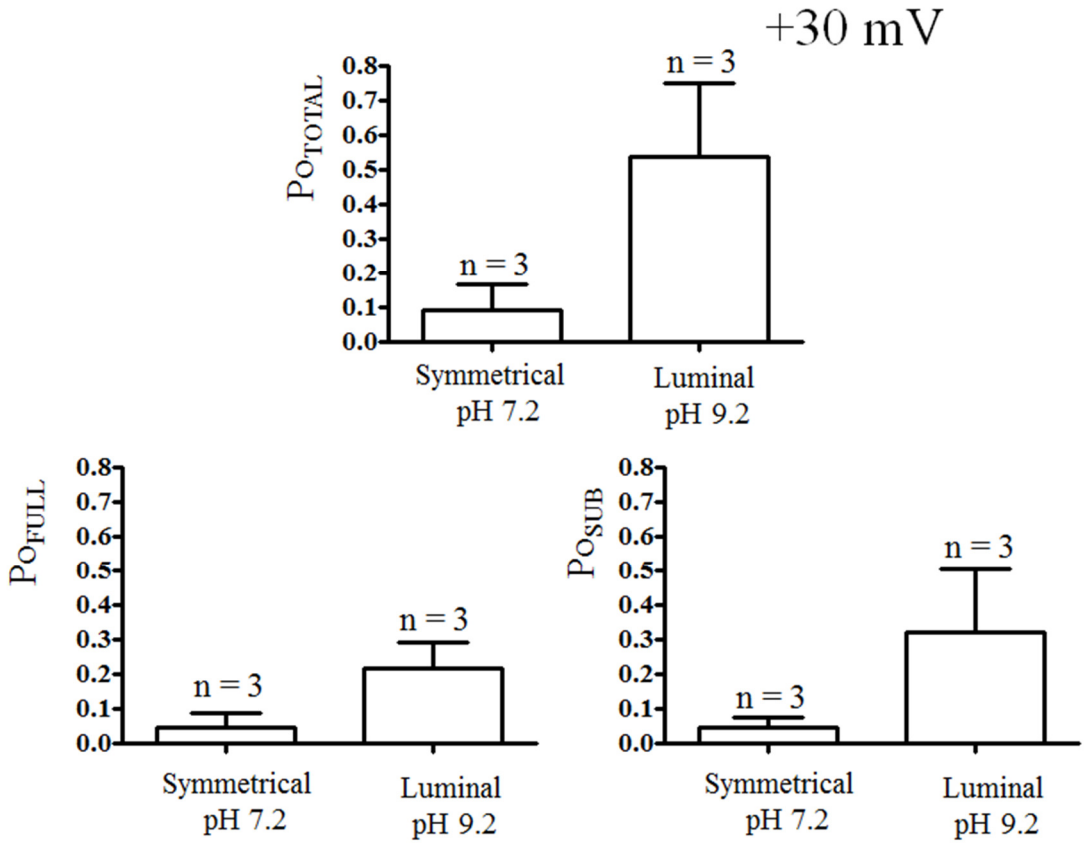


Figure 6.42 The effect of luminal pH 9.2 on SR K^+ channel Po.
Bar charts are used to show the change in SR K^+ channel Po after the luminal side was perfused with pH 9.2. The data are presented as Mean ± SD. This set of experiments was performed by Dr. Elisa Venturi and Dr. Elena Galfrè and analysed by myself.

There was a no significant difference in the contribution of PoFULL to PoTOTAL in alkaline pH 9.2. This data are shown in Figure 6.43.

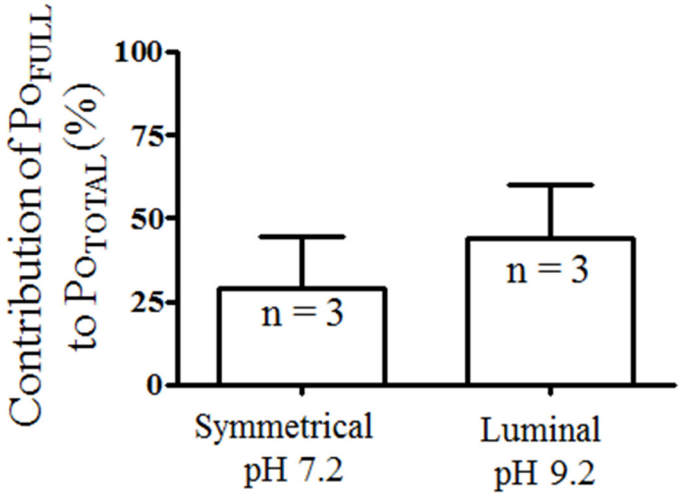


Figure 6.43 The effects of luminal pH 9.2 on the contribution of Po_{FULL} to Po_{TOTAL} at + 30 mV. The data is presented as Mean ± SD. This set of experiments was performed by Dr. Elisa Venturi and Dr. Elena Galfrè and analysed by myself.

6.3.8.2 Effect of cytosolic or luminal pH 9.2 on the SR K^+ channel conductance

There appeared to be no effect of alkaline pH on the conductance of the SR K^+ channel, however, we have only measured unitary conductance at +30 mV in pH 7.2 and in pH 9.2.

6.3.9 Comparison of the gating of the SR K^+ channel in pH 6.2 and pH 9.2

As I have discussed in chapter 4, when more than one SR K^+ channel is gating in the bilayer, the channels appear to gate in a cooperative manner with a higher Po value than the values observed when only a single SR K^+ channel was gating. To compare the Po over a range of pHs (6.2, 7.2 and 9.2) the variability in control data (because we had different number of channels gating in each control experiment) would mask the effect of changing pH. For this reason, I have expressed the mean data at pH 6.2 and pH 9.2 as an increase in Po above control. In this comparison, I have split the data into symmetrical pH 6.2 (both sides of the channel perfused), asymmetrical pH 6.2 (1 side of the channel perfused with pH 6.2) and asymmetrical pH 9.2 (1 side of the channel perfused with pH 9.2). The mean data are shown in Figure 6.44.

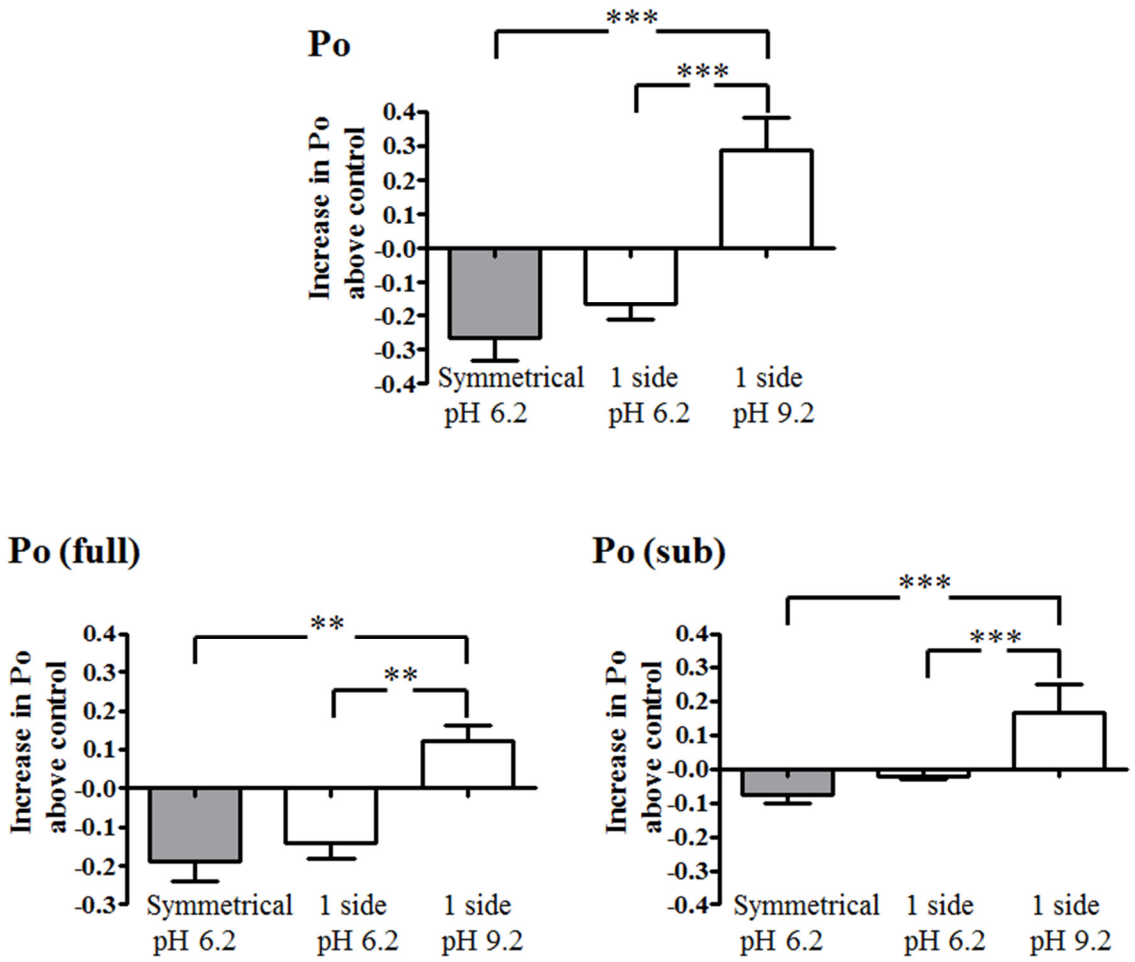


Figure 6.44 Combined effect of cytosolic or luminal pH change on SR K^+ channel gating.

The bar charts show the effects of pH 6.2 and pH 9.2 on SR K^+ channel Po. Cytosolic and luminal pH change were grouped together. For each channel, the control Po was subtracted from the Po when the pH was changed. The error bars show the mean values ± SEM (n=6-17).

6.4 Discussion

The objective of this study was to investigate if the SR K^+ channels from TRIC-A KO and WT tissue were sensitive to changes in cytosolic and luminal pH. Although the effects of pH on SR K^+ currents in bilayers has been reported in the literature, this study provides the first detailed analysis of the mechanisms that underlie proton inhibition of the SR K^+ channel at the single-channel level.

6.4.1 The SR K^+ channel has more than one proton binding site

I have demonstrated that protons, on the cytosolic or on the luminal side of the SR K^+ channel decreased Po at +30 mV and at -30 mV. Furthermore, I have illustrated that the underlying mechanisms that mediate the decrease in channel Po in acidic conditions are different at +30 mV compared to -30 mV. The effect of protons on the gating of the SR K^+ channel at +30 mV can be summarised by the kinetic scheme as illustrated in Figure 6.45. In cytosolic pH 6.2, at +30 mV, the decrease in Po was associated with a decrease in the duration and the frequency of full open channel bursts (as indicated by the red symbols and arrows in Figure 6.45), whereas, at -30 mV, the decrease in Po was associated only with a decrease in the frequency of full open bursts. On the other hand, in luminal pH 6.2, at +30 mV, the decrease in Po was associated with a decrease in the frequency of full open channel bursts (as indicated by the red symbols and arrows in Figure 6.45) whereas at -30 mV, the decrease in Po appeared to be associated with a decrease in the frequency and the duration of full open bursts.

The analysis that is presented in this chapter provides information about the transitions *to* the full open channel level (which we know from Figure 3.9 are most likely from a sub-conductance state) and the transitions *from* the full open channel (which we know from Figure 3.9 are most likely to a sub-conductance state). As illustrated in Figure 6.29, in

cytosolic or luminal acidic conditions, we observed a significant decrease in the sub-conductance gating events. In our simplified kinetic scheme in Figure 6.45, if we only observe changes in transitions *to* and *from* the full open channel level to a sub-conductance state (red arrows), we would not observe significant decrease in Po_{SUB}. Therefore, it is likely that the transitions between the sub-conductance levels and the closed level are also altered in a similar fashion to the transitions between the sub-conductance levels and the full open channel level in acidic pH (blue arrows and symbols in Figure 6.45).

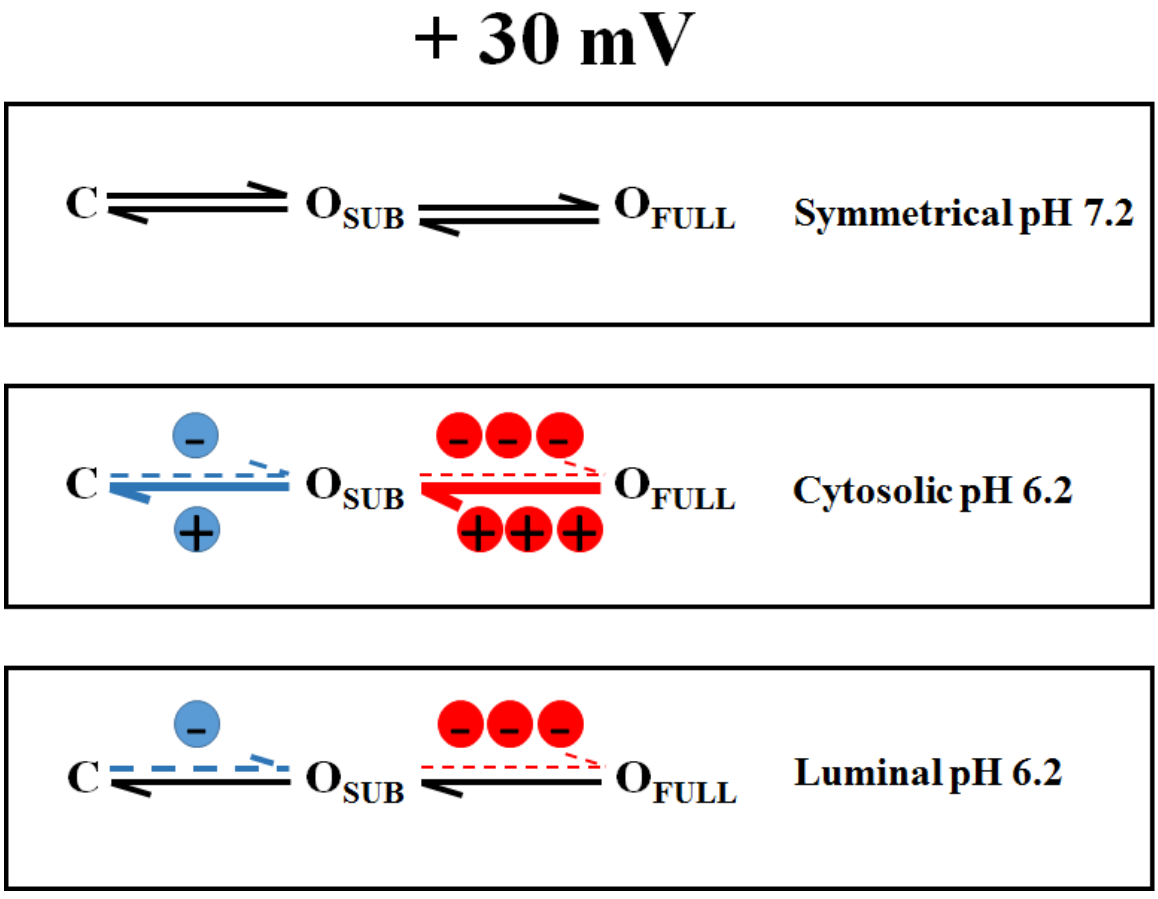


Figure 6.45 A simplified kinetic scheme illustrating the mechanisms underlying cytosolic or luminal pH 6.2 at +30 mV.
In cytosolic pH 6.2, there was a decrease in frequency of openings to the full open channel level from the lower conductance levels (sub-conductance levels and closed level), indicated by the blue and red dashed arrows. In addition, we observed an increase in transitions from the full open channel level to lower conductance levels (sub-conductance

levels and closed level), indicated by the blue and red thick arrows. In luminal pH 6.2, there is a decrease in the frequency of openings to the full open channel level from lower conductance levels (sub-conductance levels and closed level), indicated by the blue and red dashed arrows.

We can speculate about the location of the proton binding sites on the SR K^+ channel. For example, when the pH was lowered from pH 7.2 to 6.2 on the cytosolic or the luminal side of the SR K^+ channel, a decrease in the frequency of the full open bursts was observed, irrespective of the holding potential applied, and thus, we can postulate that the proton binding site that mediates this effect does not lie within the pore region of the channel since it appears that open channels are not required before the effect takes place. However, in the same conditions, a decrease in the duration of the full open bursts was only observed at holding potentials that would drive protons into the pore of the SR K^+ channel and thus, this additional proton binding site is likely to be located within the pore region of the SR K^+ channel. The decrease in the duration of full open bursts was coupled with a decrease in the unitary conductance of the channel which could suggest that proton binding within the pore of the channel causes block of K^+ current. We believe that this reduction in the conductance of the full open state is not a change in channel gating behaviour such that the channel is opening to a sub-conductance level in preference to the full open state. This is because the open channel noise of the reduced current amplitude in pH 6.2 was similar to the measurement at pH 7.2, rather than nosier as seen in the merged sub-conductance level. Additionally, the parameters of the merged sub-conductance level were identical in pH 6.2 compared to the parameters in pH 7.2.

I have illustrated that when the pH on the cytosolic or the luminal side of the SR K^+ channel is lowered from pH 7.2 to pH 6.2 and subsequently, when the remaining side of the channel is lowered to pH 6.2, the effect of symmetrical protons on the gating of the channel was

additive. We believe that this additive effect illustrates the existence of distinct proton binding states that are present on the cytosolic and on the luminal side of the SR K^+ channel.

Therefore, given the results outlined above, it appears that there are at least four proton binding sites on the SR K^+ channel, two on the cytosolic side of the channel (one within the pore region accessible from the cytosolic side) and two on the luminal side of the channel (with one within the pore region accessible from the luminal side).

It would be nice to look at voltage-dependent block in more detail by measuring conductance and gating over a range of voltages as this could provide much insight into blocking mechanisms. However, this type of experiment is far too time consuming to be the subject of a PhD because it is very difficult to obtain SR K^+ channel openings at negative holding potentials.

6.4.2 Alkaline pH increases SR K^+ channel activity

It was more difficult to obtain long-lasting, high-quality, single-channel recordings in alkaline (pH 9.2) solutions as we often observed a large unidentified current that was unanalysable at the single-channel level (see Figure 6.36). However, by purposefully selecting channels that had an extremely low Po in pH 7.2, I have illustrated that increasing the cytosolic or luminal pH to 9.2 resulted in a marked increase the Po of the SR K^+ channel from TRIC-A KO tissue. In this set of experiments, it was extremely difficult to speculate about the mechanisms that may underlie the pronounced increase in channel activity as many of the control experiments did not contain many opening events in pH 7.2. In one experiment there was one full open burst in pH 7.2 and thus, I have illustrated that cytosolic pH 9.2 appeared to increase the duration of the full open bursts. In addition, considering we only observed openings when we raised the pH of the recording solutions (due to the low Po at pH 7.2), we can speculate that pH 9.2 increased the frequency of openings.

It may be that the changes observed in the frequency/duration of the full open bursts occur in the sequential order pH 6.2 < pH 7.2 < pH 9.2, however, it is worth noting that each experiment in this chapter contains a different number of channels in the bilayer (with acidic experiments containing >1 channel gating and alkaline experiments containing 1 channel gating). We have demonstrated that SR K^+ channel gate in a cooperative manner, however we do not know if this increase in SR K^+ Po that is observed when more than one channel is in the bilayer is mediated by an increase in the frequency and/or the duration of full open bursts.

6.4.3 Mechanisms underlying the effects of changing pH on SR K^+ channel gating

It is difficult to determine where the pH sensors of the SR K^+ channel may lie, or which amino acids may be responsible for mediating the pH sensitive change in ion-channel gating or conductance. Nevertheless, it is important to consider how the amino acids that constitute the SR K^+ channel may be altered in response to changes in pH. This is necessary to try and postulate which residues might be responsible for producing the dramatic changes in the gating properties as the pH is altered.

An amino acid is a simple organic compound that contains an amino functional group (-NH_2), a carboxyl functional group (-COOH), and a side-chain group that is specific to each amino acid (represented as the R-group), as illustrated in Figure 6.46. Each amino acid side group can gain a H^+ (and exist in the protonated state) or lose a H^+ (and exist in the deprotonated state) depending on the pH. The carboxyl group, as the name suggests (carboxylic acid) is a strong acid and thus, this side group has a low pKa (1.83 to 2.83). The carboxyl group exists in the protonated state (COOH) when the pH < the negative log of the acid dissociation constant (pKa) and exists in the deprotonated (COO^-) state when the pH > pKa. On the other hand, the amino group is a strong base and a very weak acid and therefore has a higher pKa (8.8 -10.6). The amino group exists in the protonated state

(NH_3^+) when the pH < pKa and in the deprotonated state (NH_2) when the pH > pKa. Therefore, at pH 7.2, we can assume for all 20 amino acids, the carboxyl group will exist in the deprotonated state and the amino group will exist in the protonated state (as illustrated by Figure 6.46). In addition, at pH 7.2, of the 20 common amino acids, five have a charged side chain (R-group) that results in a net overall charge. Aspartic acid (Asp, D) and glutamic acid (Glu, E) are the two amino acids that have an acidic side chain and are negatively charged at pH 7. In addition, lysine (Lys, K) and arginine (Arg, R) have a basic side chain and are positively charged at pH 7. However, it is thought that at pH 7, histidine residues are only 10% protonated and therefore have only a very slight positive charge (compared to arginine and lysine).

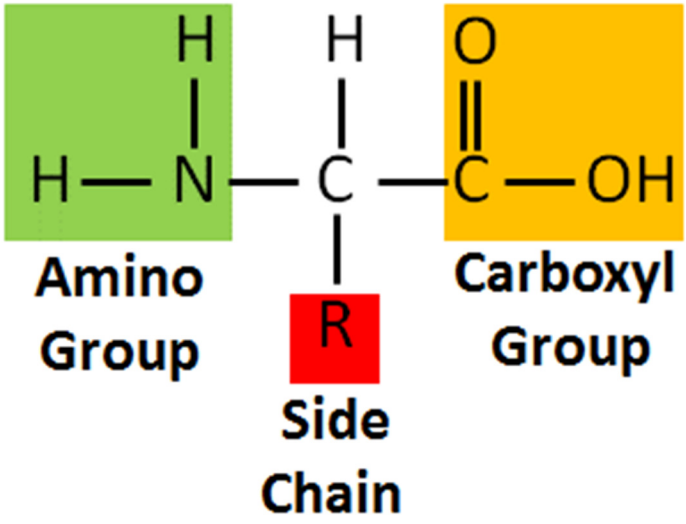


Figure 6.46 Simplified schematic of the structure an amino acid

In this chapter, I have either raised (pH 9.2) or lowered (pH 6.2) the the pH of the recoding solution from pH 7.2 and thus, it is important to determine if this pH range will alter the properties of the 5 charged amino acids. When the pH is lowered from pH 7.2 to pH 6.2,

there is no change in the overall net charge of these 5 charged amino acids, based on the overall isoelectric point (pI) of each amino acid (pI of histidine is 7.59, pI of arginine is 10.76, pI of lysine is 9.74, pI of aspartic acid is 2.77 and pI of glutamic acid is 3.22). However, when we look at the individual pKa values of the carboxyl group, amine group and the side-chain group, the side chain of histidine is an imidazole, with a pKa of 6.5 -6.9. Therefore, at pH 6.2, this imidazole side-chain will have become protonated at this pH value, leading to histidine residues carrying an increased net positive charge.

On the other hand, when the pH was raised from pH 7.2 to pH 9.2, the amine group of histidine, arginine and lysine would become deprotonated (NH_3^+ to NH_2) because the pH is raised above the pKa for that side group (pKa values of 9.17, 9.04 and 8.95, respectively). Arginine and Lysine, both of which were positively charged at pH 7.2, will now both have a neutral overall net charge, whereas histidine which is considered slightly positively charged at pH 7.2 will have a net overall negative charge at pH 9.2.

Based on the information above, histidine could potentially be responsible for mediating the changes in SR K^+ channel behaviour observed at acidic pH (pH 6.2), whereas, histidine, arginine and/or lysine could be responsible for the altered gating in alkaline pH. It may be possible that histidine alone may be responsible for the changes in SR K^+ channel gating at pH 6.2 and at pH 9.2, for example, protonation of the histidine (imidazole) side-chain at acidic pH (pH 6.2) and deprotonation of the amine side-chain at alkaline pH (pH 9.2). There are many reports in the literature stating that single histidine residues are pH sensors for a number of ion-channels (145-147).

Since the majority of the data presented in this thesis was derived from TRIC-A KO tissue, and therefore, I have highlighted residues that would have an overall net charge at pH 7.2 on mouse TRIC-B in Figure 6.47.

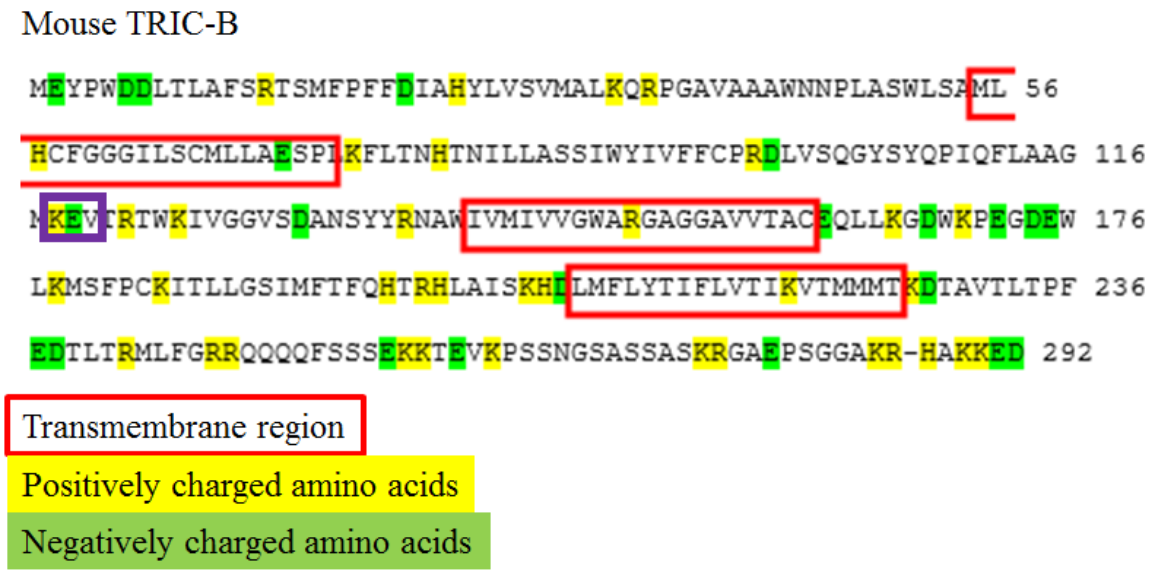


Figure 6.47 Amino acid sequence for mouse TRIC-B proteins
The three transmembrane domains identified by the hydropathicity analysis by Yawaza *et al* (2007) (100) are indicated by the red boxes. The highly conserved KEV motif is marked by a purple box. Positively charged amino acids (lysine (Lys, K), arginine (Arg, R) and histidine (His, H) are highlighted in yellow and negatively charged amino acids (aspartic acid (Asp, D) and glutamic acid (Glu, E) are highlighted in green.

6.4.4 Future work

The optimal experiment to test the hypothesis that histidine residues underlie the pH sensitivity of the SR K^+ channel would be to generate a mutant SR K^+ channel where one or multiple histidine residue is substituted by a neutrally charged amino acid, such as an alanine residue and then incorporate the mutant channels into bilayers to determine if the pH sensitivity is altered. However, as I will discuss in Chapter 7, we are currently trying to improve the protocol used to purify TRIC proteins and thus, we need to optimise the protocol for control channels before we begin to make mutants. Another possible experiment would be to use a histidine specific covalent modifier diethylpyrocarbonate (DEPC) to determine if histidine residues are responsible for the pH sensitivity of the SR K^+ channel. However, in addition to covalently modifying histidine residues, it can also

modulate lysine, cysteine and tyrosine residues (148) and therefore, this may not be an ideal experiment to target histidine residues.

7 Investigating the single-channel properties of purified TRIC-A channels

7.1 Introduction

In this thesis, the SR was isolated from TRIC-A KO and WT tissue and fused to artificial bilayers and K^+ was used as the permeant ion and the current-fluctuations that were observed were characterised. The single-channel properties of the SR K^+ channels that were observed from both preparations displayed similar biophysical properties. In addition, the SR K^+ channels from both preparations demonstrated cooperative gating behaviour when more than one SR K^+ channel was gating in the bilayer. I noticed, however, that single channels were present in the bilayer in only 21 % (n = 6) of experiments from WT tissue whereas 64 % (n = 34) of experiments from TRIC-A KO tissue had single channels. The TRIC-A KO mouse was used to study the SR K^+ channels remaining after the TRIC-A gene was deleted however, as described earlier, purified TRIC-channels are required to study each isoform in isolation and to relate the function to the channel structure.

Native SR preparations are easier to work with compared to purified ion-channels. The biophysical properties of native SR ion-channels have been studied at the single-channel level in this laboratory for >20 years. The procedure used to isolate the SR has been optimised to ensure a high yield of functional ion-channels is achieved with each preparation. In addition, the conditions that are used for fusing SR vesicles into bilayers have been developed in order to increase the probability of fusing the channel of interest.

Reconstitution of purified functional ion-channels is significantly more difficult than fusion of vesicles containing native channels, however, we are still at the early stages of optimising the purification procedure. Incorporation of ion-channels from our purified preparations are rare (in comparison to native SR incorporations) and often perfusion of the chambers is difficult, most likely because of the instability of the bilayers after addition of proteoliposomes that contain detergent molecules. However, the major advantage of

purified ion-channels is that molecular identity of the ion-channel under investigation is known.

As part of a larger study, we are actively trying to develop a method to purify functional TRIC-channels suitable for reconstitution experiments. The current-fluctuations that were observed when purified TRIC-A and TRIC-B were incorporated into planar lipid bilayers (Pitt *et al* (2010)) (101) used DDM detergent and the proteins were expressed in yeast. In recording solutions of 210 mM K^+ PIPES, TRIC-A was observed to exhibit a full open channel conductance of 192 pS, whereas TRIC-B appeared to gate to a full open conductance of 138 pS (101). Both purified TRIC-A and TRIC-B gated in a voltage-dependent manner, with the Po at +30 mV being higher than the Po at -30 mV. The TRIC proteins in this study were purified using 1% DDM as the detergent (101). In a later paper, Venturi *et al* (2013) (126) suggested that the full open channel conductance of native TRIC-B was approximately 200 pS (similar to the full open channel conductance of purified TRIC-A) and that it may be possible that the gating of the channels were altered by the detergent molecules that surround the proteins. In addition to the problems that are associated with purifying proteins from E.coli and yeast, it is possible that proteins purified from E.coli/yeast could be misfolded, which could lead to alterations in normal channel gating behaviour.

As a lab, we are actively trying to optimise the purification procedure of TRIC-proteins for single-channel reconstitution experiments. Since one of the main disadvantages of the yeast purification method is the requirement for detergent, we explored purification methods that have very little or no detergent. My role in this study was to investigate if the wheat germ cell free system could be used to purify functional TRIC proteins that are suitable for single-channel reconstitution.

7.2 Methods

TRIC-A was purified using the Wheat Germ cell-free system in the laboratory of Hiroshi Takeshima. The presence of purified TRIC-A was confirmed by western blot and the proteins were shipped on dry ice to Oxford for single-channel reconstitution experiments. Below, I will briefly summarise the key stages in the procedure of purifying TRIC-proteins using the Wheat Germ cell-free system.

7.2.1 Preparation of liposomes for protein purification

A mixture of 1-Palmitoyl-2-oleoyl-*sn*-glycero-3-phosphoethanolamine (POPE) and 1-Palmitoyl-2-oleoyl-*sn*-glycero-3-phosphocholine (POPC) was used to make liposomes for TRIC-protein purification. POPE and POPC were stored in chloroform at -80ºC. 3.5 mg of POPE and 1.25 mg of POPC were placed in a vial and the chloroform was evaporated using N_2 gas. 500 µl of 1 x SUB-AMX (translational buffer, see below) was added to the lipids to yield a final concentration of 10 mg / ml. The lipid solution was vortexed and sonicated for 3 min and extruded 21 times through a 0.1 µm filter to ensure liposomes were equal in size.

7.2.2 Wheat Germ cell-free protein synthesis kit

WEPRO 7240 (Cell Free Sciences, Japan) is a high yield, general purpose protein synthesis kit used to purify TRIC-proteins. The kit contains all the transcription and translation reagents for wheat germ cell-free protein synthesis. Also included in the kit were the transcription buffer and SUB-AMIX SGC translation buffer. The contents of the kit are summarised in Table 7-1

Reagents	Specification	Volume
WEPRO7240	240 OD	2 mL
SUB-AMIX SGC (S1～S4)	Set of 4 parts, 40x each	1.1 mL x 4
SP6 RNA Polymerase	80,000 units/mL	0.03 mL
RNase Inhibitor	80,000 units/mL	0.03 mL
NTP Mix	25 mM	0.2 mL
5x Transcription Buffer	5x	0.4 mL
Creatine Kinase	20 mg/mL	0.02 mL

Table 7-1. List of reagents included in the WEPRO7240

7.2.3 Transcription of plasmid DNA

The first step in the purification of TRIC-proteins using the wheat germ system was transcription, a process by which information in a strand of DNA is copied into a new molecule of messenger RNA (mRNA). Transcription is carried out by an enzyme called RNA polymerase and a number of accessory proteins called transcription factors (149). For transcription using the wheat germ system, a transcription solution mix was made using the reagents outlined in Table 7-2. All reagents were defrosted slowly on ice before use. Once the transcription mix was complete, the reaction was incubated at 37 ºC for 6 hr. After incubation, the mRNA quality was checked by agarose gel electrophoresis.

Reagent	Final concentration
Nuclease free water	86.25 µl
5x Transcription Buffer LM	30 µl
NTP mix (25 mM)	15 µl

RNase Inhibitor (80 U/µl)	1.875 µl
SP6 RNA Polymerase (80 U/ µl)	1.875 µl
pEU-mTRIC-A or -mTRIC-B (1 µg/ul)	15 µl

Table 7-2 Reagents used for the transcription mixture for the wheat germ cell free system

7.2.4 Translation

Translation is the process by which the protein is synthesised from the information contained in a molecule of mRNA. After the 6 hr transcription reaction was complete, the tube was slowly cooled down to room temperature. For translation, the novel bilayer-based cell-free protein synthesis system, published in Sawasaki *et al* (2002) was used (150). This method is based on a bilayer diffusion system that enables the continuous supply of substrates, together with the continuous removal of small by-products, through a phase between the translation mixture and substrate mixture. Using a multiwell plate, the substrate mixture was layered on top of the translation mixture using a pipette. The upper later (substrate mixture) consisted of 5.5 ml of SUB-AMIX SGC translational buffer. The SUB-AMIX SGC translational buffer consisted of < 30 % w/w 2-[-4-(2-Hydroxyethyl)-1-piperazinyl]ethanesulfonic Acid, < 30 % w/w Disodium Creatinephosphate Tetrahydrate, < 5 % w/w DTT, < 5 % w/w Magnesium Acetate Tetrahydrate, < 40 % w/w Potassium Acetate. The lower layer (translation mixture) had a total volume of 500 µl and consisted of the transcription reaction mixture (150 µl), SUB-AMIX SGC (174 µl), Creatine kinase (1 µl pf a 20 mg/ml stock), liposomes (125 µl of a 10 ml/mg stock) and WEPRO 7240 (125 µl). After the layers in every well were completed, the plate was sealed with parafilm and incubated for 20 hr at 15 ºC. After translation, the bilayer reaction was gently mixed using a pipette.

7.2.5 Purification of proteoliposomes

The contents of the multi well plate were added to 40 % accudenz centrifugation medium to yield a total volume of 12 ml. 4 ml of this solution was added to the bottom of a 12 ml centrifuge tube. 6.5 ml of 1.2 M sucrose dissolved in sucrose buffer (10 mM Hepes-NaOH, pH 7.4, 150 mM NaCl, 1 mM DTT, 1 mM $MgCl_2$) was slowly layered on top of each fraction. 1.4 ml of 0.3 M sucrose dissolved in the sucrose buffer was added to the top of the tube as illustrated in Figure 7.1. The tubes were centrifuged at 189,000 x g in a Beckman SW-41 rotor for 5 hr. After centrifugation, the proteoliposome band was at the interface between the 0.3 M and 1.2 M sucrose gradients as shown in Figure 7.1 . The band containing the proteoliposomes was isolated, aliquoted, and stored at -80 ºC.

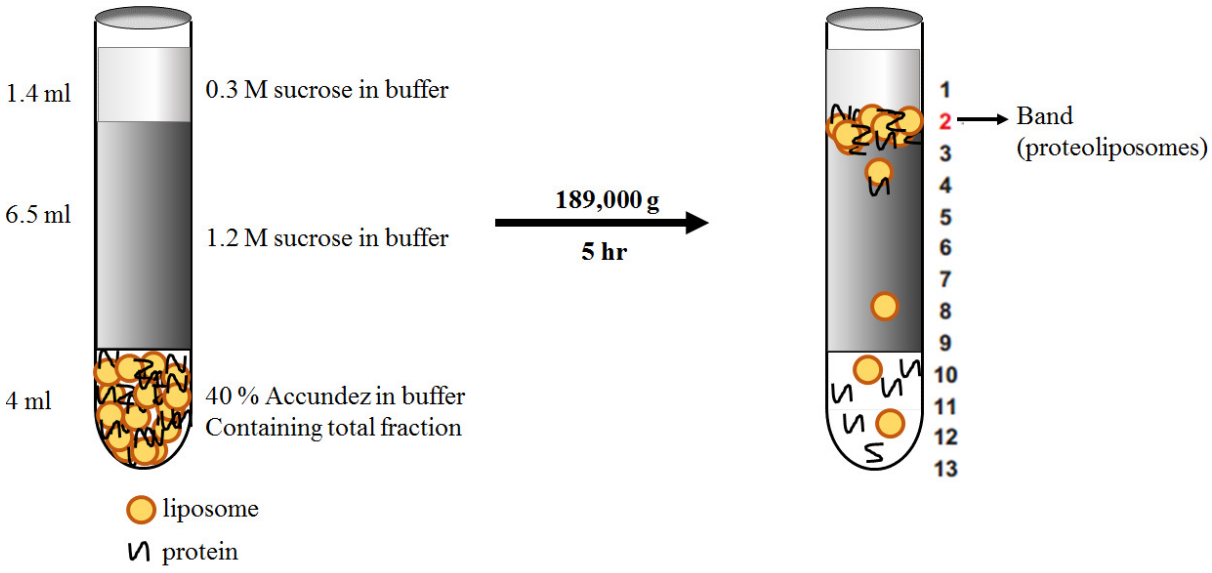


Figure 7.1 Purification of the proteoliposomes containing TRIC-proteins
On the left, the sucrose gradient was prepared on top of the proteoliposome mix. After centrifugation, on the right, the interface between the 1.2 M sucrose and 0.3 M sucrose contained the purified sample.

7.2.6 Immunoblotting

Immunoblotting of purified TRIC-A protein was done in the laboratory of Hiroshi Takeshima in Japan. In brief, protein samples were separated by SDS-PAGE on a 4-20 % precast gel (Biorad, Hertfordshire, UK) and transferred to a nitrocellulose membrane (Biorad, Hertfordshire, UK) using a mini trans blot cell (Biorad, Hertfordshire, UK). The transfer was performed at 150 mA for 1 hr, in a Transfer buffer (25 mM Tris, 192 mM glycine). The membrane was then incubated in a Blocking buffer (5 % milk, 50 mM Tris-HCl pH 7.4, 15 mM NaCl, 1 % tween-20) at 21 °C. After 1 hr the Blocking buffer was replaced with a fresh buffer containing a polyclonal primary anti-TRIC-A antibody ((1:500) developed by the Takeshima laboratory) and incubated for 2 hr at 21 °C. Prior to incubation with the secondary antibody, the membrane was washed twice with a buffer containing 50 mM Tris-HCl pH 7.4, 15 mM NaCl, and 1 % tween-20, to remove traces of unbound antibody.

The horseradish peroxidase linked anti-rabbit IgG ((1:5000) GE-Healthcare, Buckinghamshire, UK) was diluted in the Blocking buffer and incubated with the membrane for 1 hr. At the end of the incubation, an Enhanced Chemiluminescence (ECL) detection reagent (GE-Healthcare, Buckinghamshire, UK) was added to cover the entire surface of the membrane and incubated for five min. The signal was visualised by chemiluminescence.

7.2.7 Solubilisation of native SR

To study the single-channel gating of RyR with K^+ as the permeant ion (usually 210 mM KCl), the RyR needs to be separated from the SR K^+ channels and the SR Cl^- channels (74). The first step in purification of the RyR is to solubilise the HSR in detergent, and then spin the solubilised HSR on a linear sucrose gradient (74). The band containing RyR channels

is identified using [3H] ryanodine in a radio ligand binding assay. The detergent is then removed via dialysis and the resulting proteoliposomes containing RyR channels can be used for single-channel reconstitution analysis (74). In this thesis, we have modified the protocol to purify RyR channels to study the gating of solubilised SR K^+ channels.

SR was solubilised by incubating SR membranes (2 mg protein/ml) with 0.5 % CHAPS and 0.25 % phosphatidylcholine (PC) in solubilisation solution (see Table 7-3) for 45 min on ice. The non-solubilised material was removed by centrifugation at 15,000 × *g* for 30 min. The resulting supernatant was aliquoted and incorporated into bilayers. The CHAPS detergent was not removed by dialysis.

Reagent	Final concentration
NaCl	1 M
EGTA	0.1 mM
$CaCl_2$	0.15 mM
PIPES	25 mM
DTT	2.5 mM
NaOH	pH 7.2

Table 7-3 Reagents used for solubilisation of native SR vesicles

7.3 Results

7.3.1 Confirmation of TRIC-A synthesised by the Wheat Germ cell-free system

The procedures used to confirm the presence of TRIC-A proteins were performed in the Takeshima lab. The purified TRIC-A was analysed by SDS-PAGE and the resulting coomassie gel is shown in panel A in Figure 7.2. The immunoblot analysis is showed in panel B.

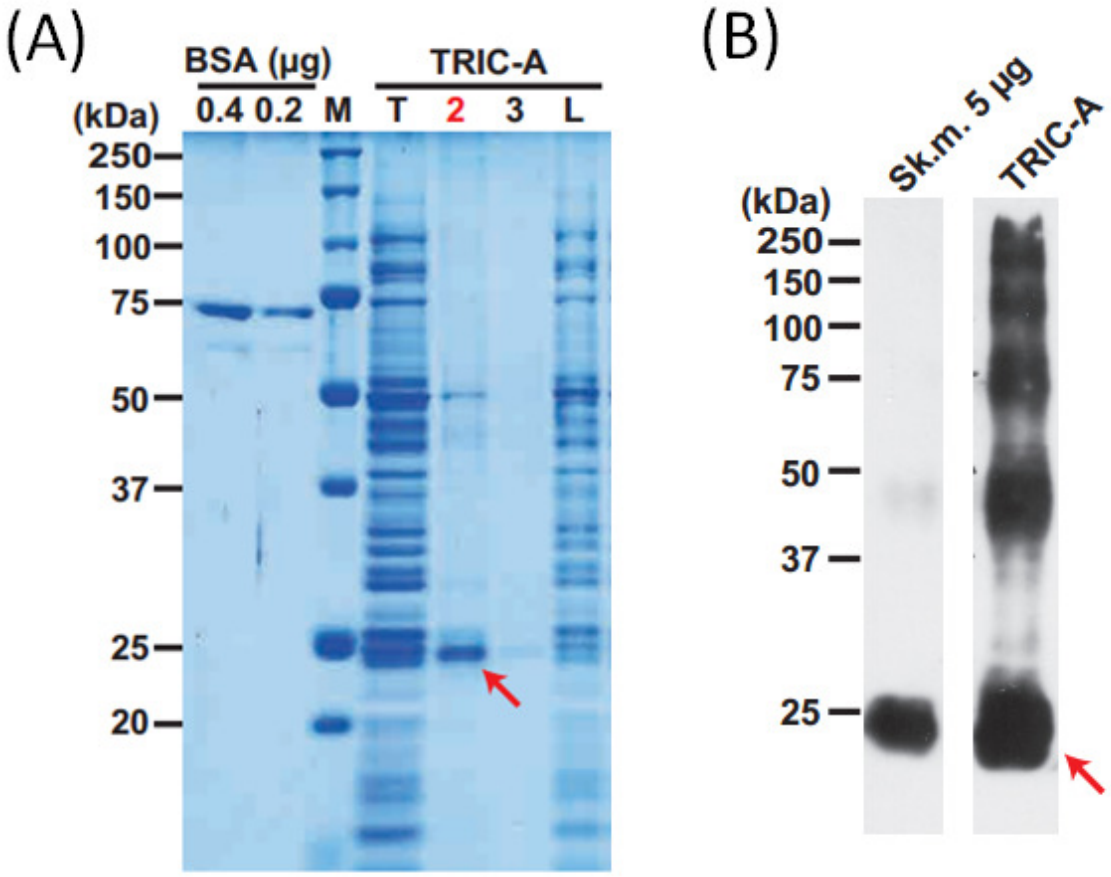


Figure 7.2 Purification of TRIC-A using the Wheat Germ cell-free system
A. Gel electrophoresis of the purified TRIC-A synthesised using the Wheat Germ cell-free system. Protein were separated on a 12% SDS-polyacrylamide gel and stained with Coomassie blue. Size markers are indicated in kDa and the migration position of TRIC-A is marked by an arrowhead. T represents the total fraction (5 µl / lane), 2 and 3 represent the 2nd and 3rd fraction (both 5 µl / lane) and L represents a sample taken from a lower fraction (5 µl / lane). B. Immunoblot analysis. The expression of TRIC-A was confirmed by western blot analysis. Molecular weights are shown on the left. Lane 1 shows TRIC-A proteins present in Mouse skeletal muscle (5 µg / lane) and lane 2 confirms the presence of

TRIC-A in the TRIC-A purified preparation (5 µl / lane). The procedures above were performed by Tsunaki Iida in the Takeshima lab**.**

7.3.2 Purified TRIC-A single-channel currents

I investigated the current fluctuations that were observed when purified TRIC-A was incorporated into artificial bilayers. Initially the recording solutions were identical to those used to study native SR K^+ channels from TRIC-A KO and WT tissue (210 mM KPIPES, pH 7.2). To facilitate incorporation of proteoliposomes containing TRIC-A channels, I added 200 µl of 3 M KCl to the cytosolic chamber.

7.3.2.1 Single-channel currents from purified TRIC-A

Representative single-channel events that were observed when purified TRIC-A was incorporated into the bilayer is illustrated in Figure 7.3. Frequently, while still in the high KCl gradient (used to facilitate incorporation), I observed current-fluctuations that appeared to be channel-like. However, the Po was relatively low and often the channel only opened at one holding potential and thus, the channel conductance could not be calculated. In addition, when the KCl gradient was removed, often there was no activity or the bilayer broke during perfusion.

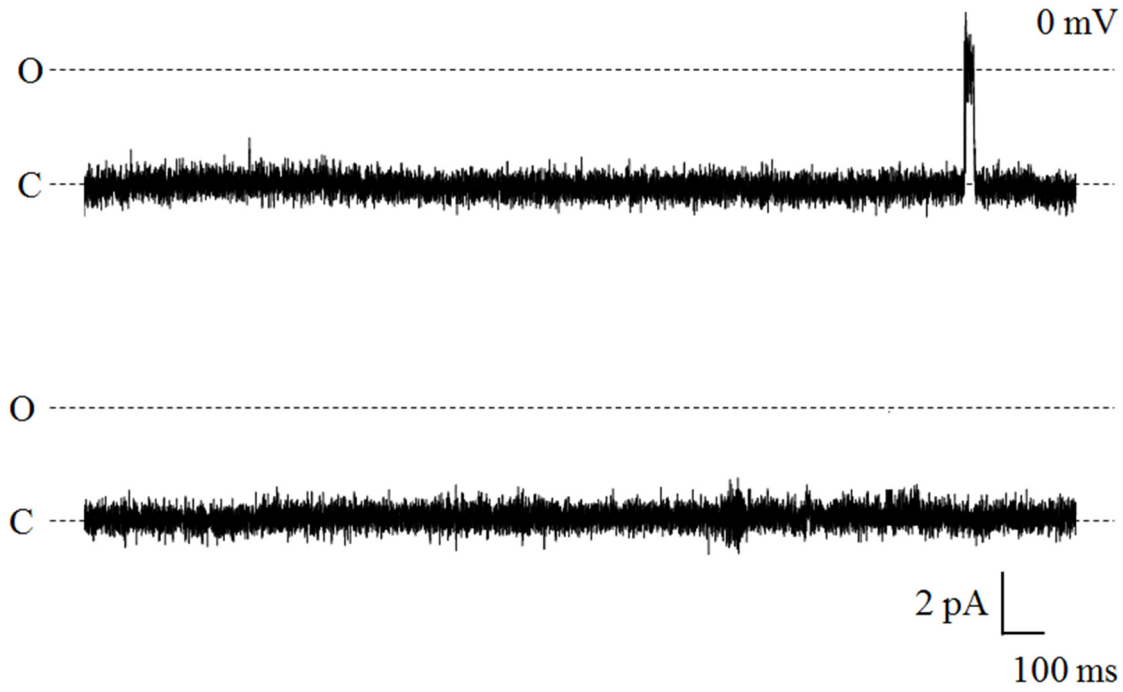


Figure 7.3 A typical opening observed from a purified TRIC-A channel
A representative trace at 0 mV when a purified TRIC-A K^+ channel was gating in the bilayer in 810 mM cytosolic K^+ and 210 mM luminal K^+ is shown. C and O represent the closed and open channel respectively. The recording was low pass filtered at 1 KHz. This trace is representative of 5 recordings from 2 wheat germ TRIC-A preparations.

Due to the low Po of purified TRIC-A, I changed my recording parameters to try and increase the Po of the channels to enable me to study the properties observed. Based on the native SR K^+ channel experiments that I presented in Chapter 6, I attempted to incorporate purified TRIC-A in alkaline solutions (210 mM KPIPES pH 9.2) in the hope that the channels would open for longer. In addition, I incubated the purified TRIC-A in a phosphorylation mixture (10 U Protein kinase A (PKA) /10 U Protein kinase C (PKC) /3 mM ATP/1 mM free Mg^{2+}) to investigate if that would increase the probability of observing a channel with a higher Po. By changing the recording parameters, I was able to visualise single-channel gating events and analyse the biophysical properties. As each single-

channel recording had slightly different recording parameters, it was inappropriate to mean the data, and thus, I will present each individual recording separately.

Investigating TRIC-A incorporation and gating after incubation with kinases and using alkaline solutions

The single-channel current fluctuations that were observed when purified TRIC-A was incubated in the phosphorylation mixture and incorporated into artificial membranes is illustrated in Figure 7.4.

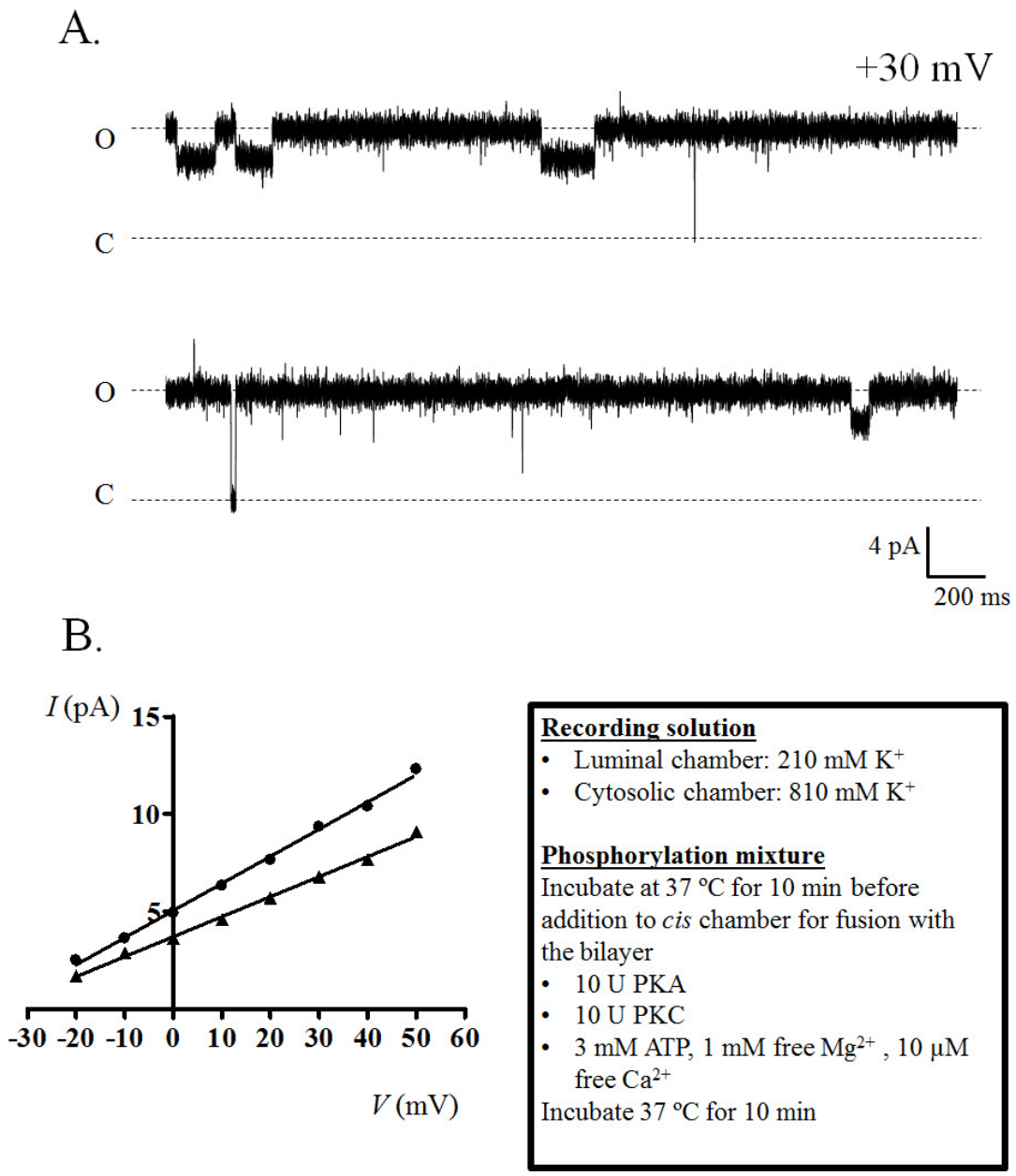


Figure 7.4 TRIC-A gating in alkaline recording solutions after incubation in phosphorylation mixture

In A, the trace shows an example of the single-channel activity observed from incorporation of the purified TRIC-A in 210 mM KPIPES, pH 9.2 with a 200 µl 3M KCl gradient added to the cytosolic chamber. O and C indicate the open and closed channel levels, respectively. The recording was low pass filtered at 1 kHz. In B, the current-voltage relationship of the full open state (circles) and the sub-conductance state (triangles) yields a conductance of 139 pS and 103 pS respectively. The reversal potential of – 36 mV indicates that this channel is ideally selective for K^+ and not Cl^-.

Incorporating liposomes containing purified TRIC-A into bilayers using alkaline solutions

When we incubated TRIC-A in a phosphorylating mixture and incorporated purified TRIC-A into artificial membranes, the Po of the channel was extremely high, with very few closing events. In addition, the conductance of the full open state was lower than expected and thus, I removed the phosphorylation step from future experiments. The single-channel current fluctuations that were observed when purified TRIC-A incorporated into artificial membranes in alkaline recording solutions (210 mM KPIPES, pH 9.2) is illustrated in Figure 7.5.

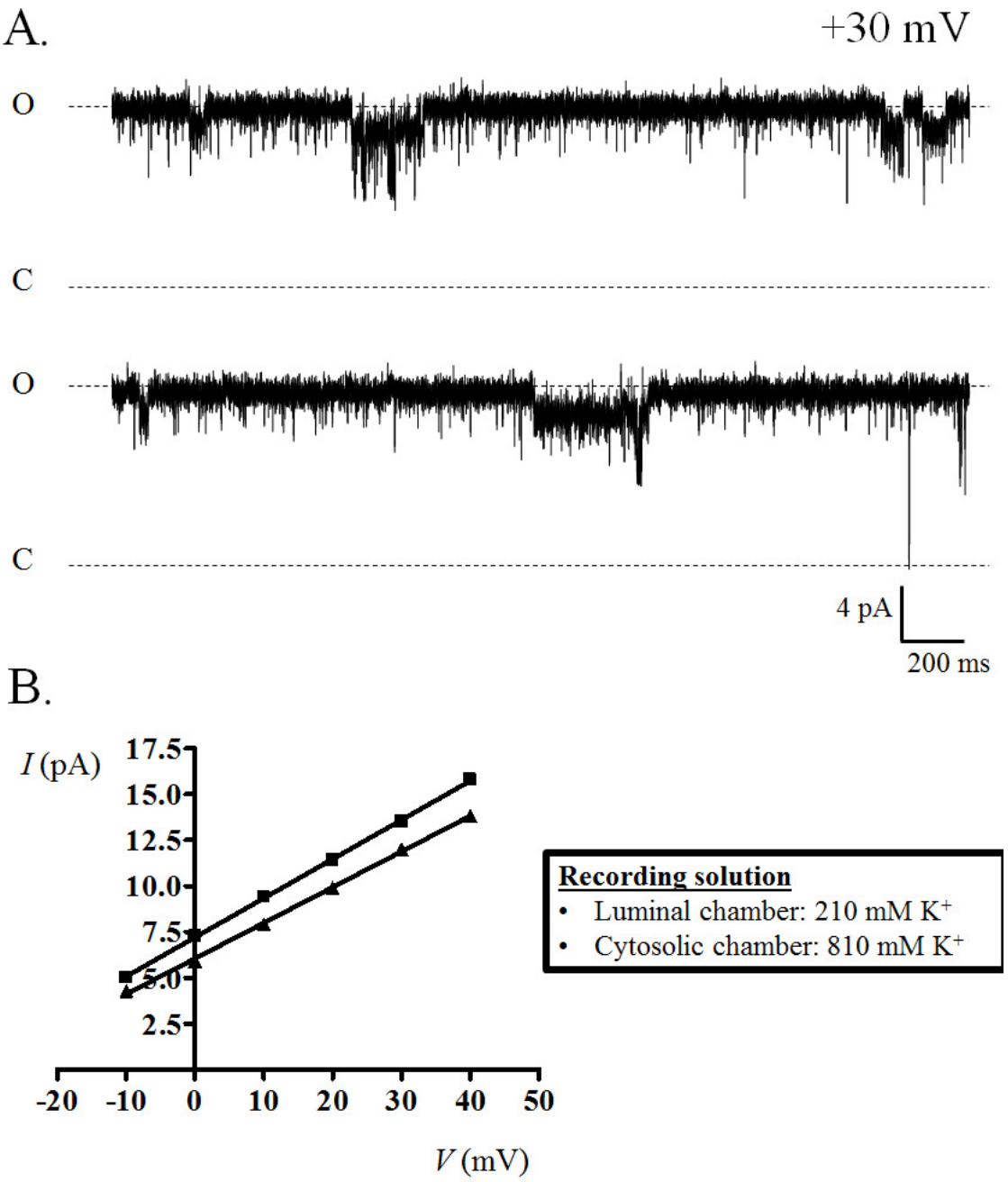


Figure 7.5 TRIC-A gating in alkaline solutions
In A, the traces show the single-channel activity of purified TRIC-A in 210 mM KPIPES, pH 9.2. A 200 µl 3M KCl gradient was added to the cytosolic chamber. O and C indicate the open and closed channel levels, respectively. The recording was low pass filtered at 1 kHz. In B, the current-voltage relationship of the full open state (circles) and the sub-conductance state (triangles) yields a conductance of 213 pS and 194 pS respectively. The reversal potential of – 33 mV indicates that this channel is ideally selective for K^+ and not Cl^-.

7.3.3 Recording native SR K^+ channels in gradient conditions

Although we observed some K^+ channel current fluctuations when purified TRIC-A was incorporated into artificial bilayers, the gating that we observed did not resemble the gating characteristics of the SR K^+ channels that have been described in earlier chapters of this thesis. It was very difficult draw comparisons between the gating of purified TRIC-A that were only recorded in gradient conditions (810 mM cytosolic K+/ 210 mM luminal K^+), and the gating of the SR K^+ channel that was recorded in symmetrical 210 mM KPIPES, pH 7.2. Therefore, to see if a high KCl gradient alters native SR K^+ channel activity, I recorded SR K^+ channels from WT mouse skeletal muscle in similar recording solutions to those that were used for recording purified TRIC-A channels. Representative gating behaviour is shown in Figure 7.6. All three recordings from WT skeletal muscle that were recorded in gradient conditions had a very high Po with only very brief closing events. In addition, any sub-conductance gating that was observed was mostly to the levels close to the full open channel level.

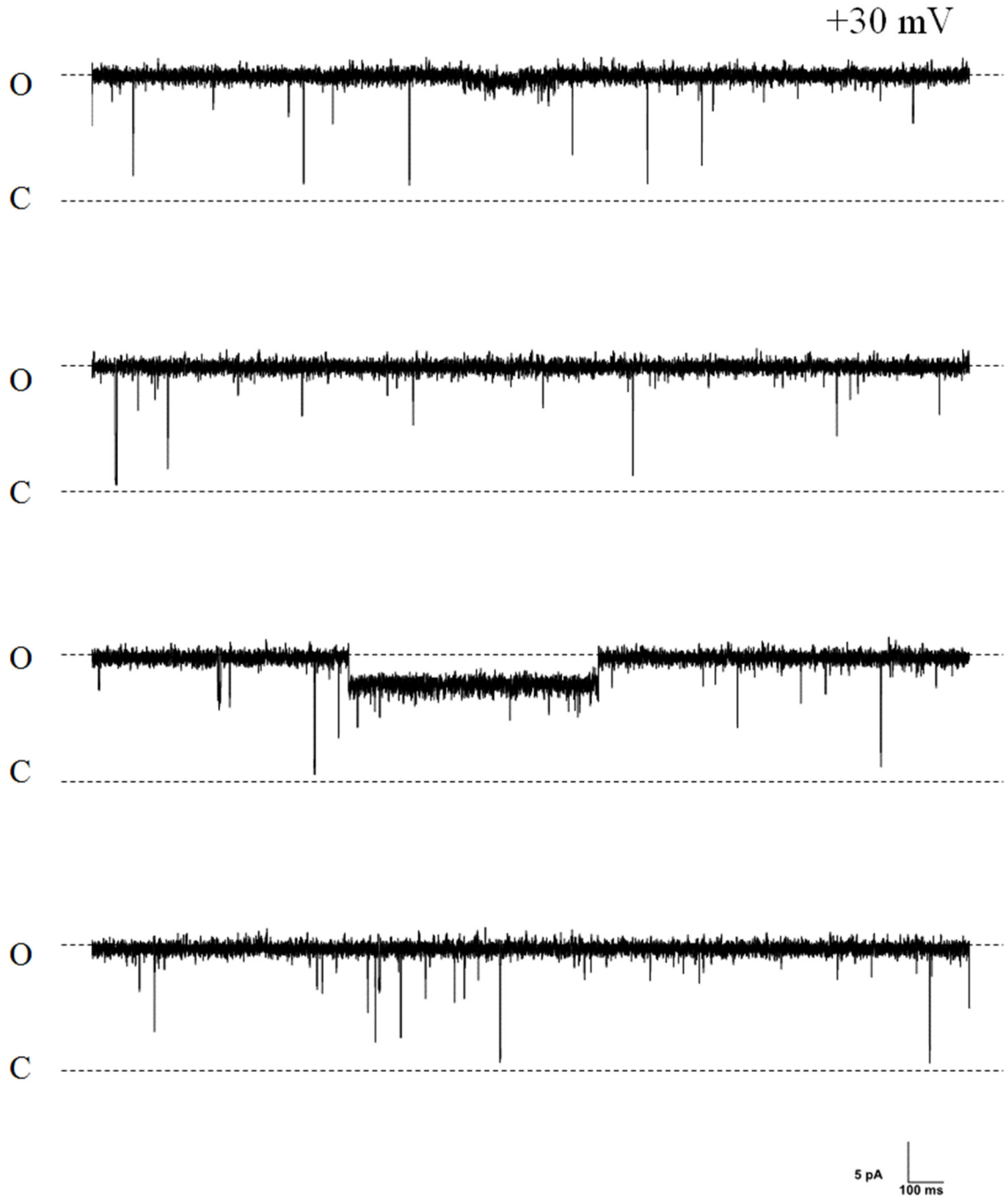


Figure 7.6 Representative openings of native SR K^+ channels from WT tissue in gradient conditions
The traces show the single-channel activity at +30 mV. O and C indicate the full open and closed levels, respectively. The recording was low pass filtered at 1 KHz.

Although the native SR K^+ channels, when gating in gradient conditions displayed a similar style of gating, the conductance of the channels varied slightly as illustrated in Figure 7.7. However, the reversal potentials (ERev) for each channel was close to the expected value for K^+ (-34 mV), indicating that channels were ideally selective for K and not Cl^-.

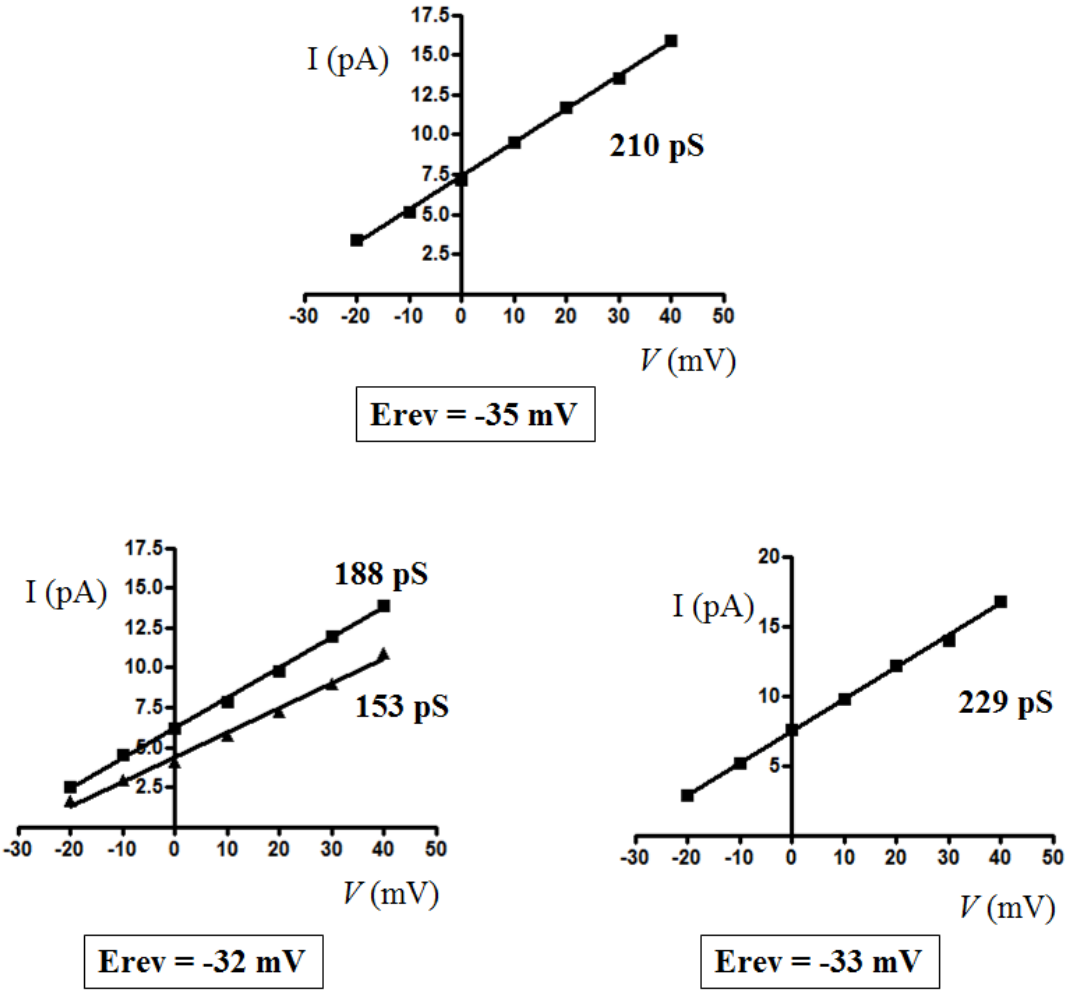
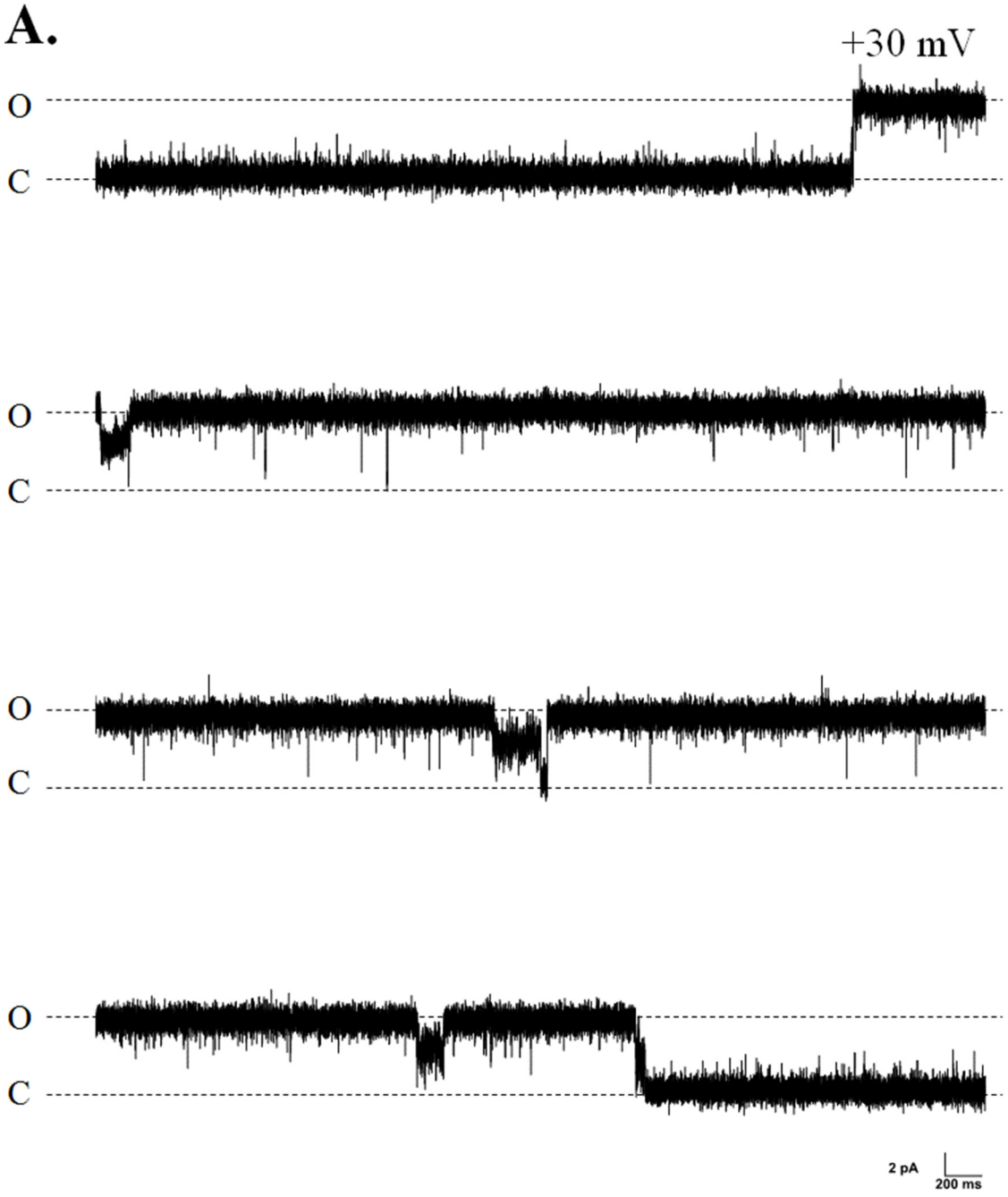


Figure 7.7 Current-voltage relationships of SR K^+ channels recorded in gradient conditions.
The conductance of each recording is shown next to the current-voltage plot. The reversal potential of each channel indicated that the channels were ideally selective for K^+ and not for Cl^-.

7.3.4 The effect of detergent on SR K^+ channel function

When the biophysical properties of purified TRIC-channels were initially studied (Pitt *et al* (2010) (101), 1% DDM was used to purify the proteins from yeast. It has been documented that detergent can alter the properties of ion-channels (74, 151-153). For example, in this laboratory we use the detergent 3-[(3-Cholamidopropyl)dimethylammonio]-1-propanesulfonate (CHAPS) to purify RyR from native HSR. After purification, when proteoliposomes containing RyR are reconstituted into artificial membranes, the RyR channel gating observed can sometimes be insensitive to Ca^{2+} (even when the RyR was purified from a Ca^{2+}-sensitive preparation) or can gate into multiple sub-conductance states not normally observed in native channels. Therefore, to try and understand the effect of detergent on the SR K^+ channel, we incorporated solubilised LSR into artificial membranes. Due to the large volumes of material required for solubilisation, we used rabbit skeletal muscle instead of mouse skeletal muscle (as one solubilisation protocol would use nearly an entire mouse preparation). We solubilised rabbit skeletal at a concentration of 2 mg / ml as outlined in Section 7.2.7 Representative gating of the SR K^+ channels from solubilised skeletal LSR is illustrated in Figure 7.8.


A.
+30 mV
O
C
O
C
O
C
O
C
2 pA
200 ms

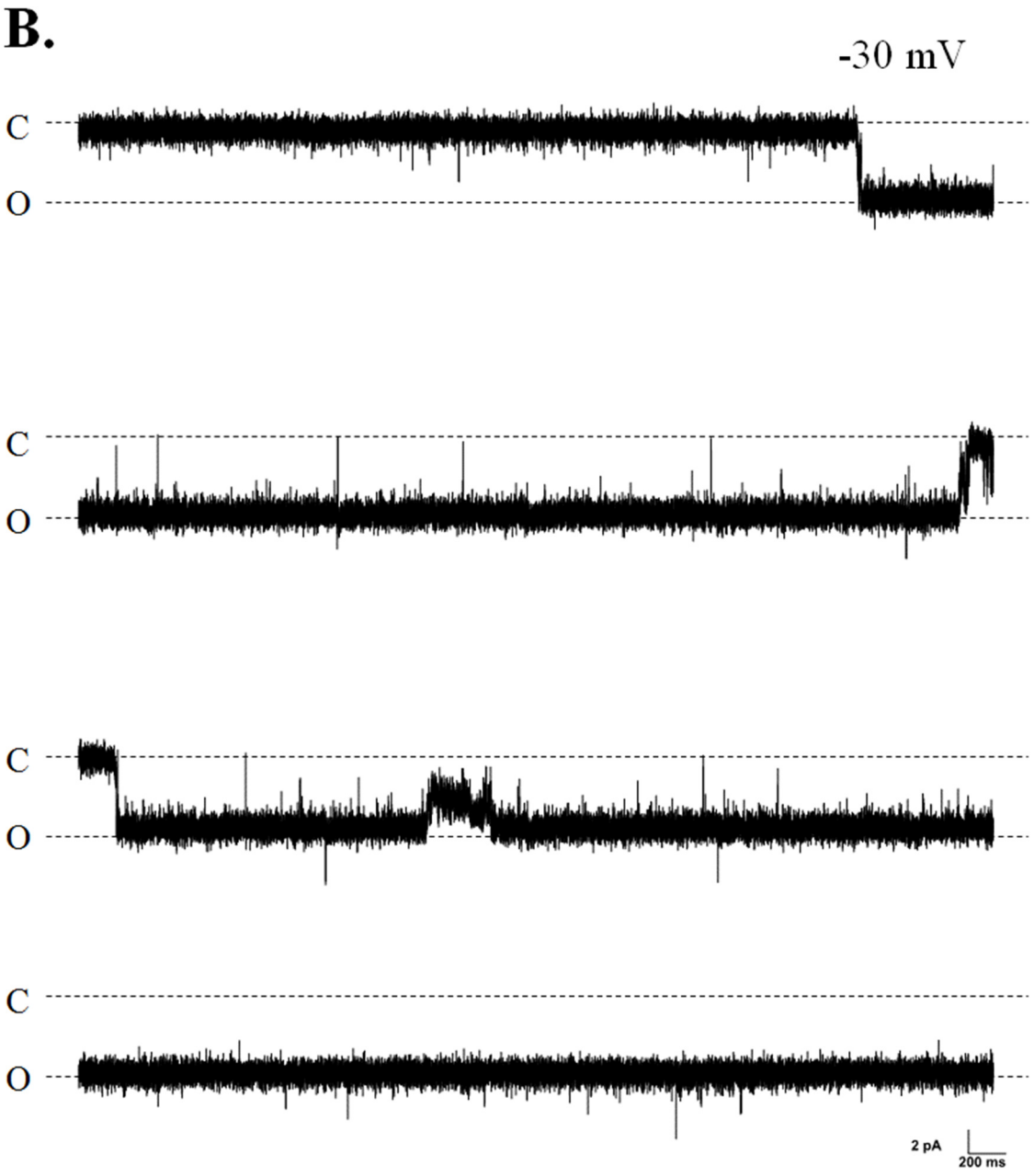


Figure 7.8 Representative trace illustrating the typical gating properties of the K^+ channels observed after incorporation of solubilised LSR into a bilayer.
The traces show the single-channel activity at +30 mV (top traces) and at -30 mV (bottom traces) of a typical experiment. O and C indicate the full open and closed levels, respectively. The recording was low pass filtered at 1 KHz.

7.3.4.1 The voltage-dependence of the solubilised LSR K^+ channels

The mean data shown in Figure 7.9 highlights the voltage-dependence of the SR K^+ channels from solubilised rabbit skeletal LSR. All 5 recordings were voltage-independent; the Po at +30 mV was the same (or slightly lower) than the Po at -30 mV.

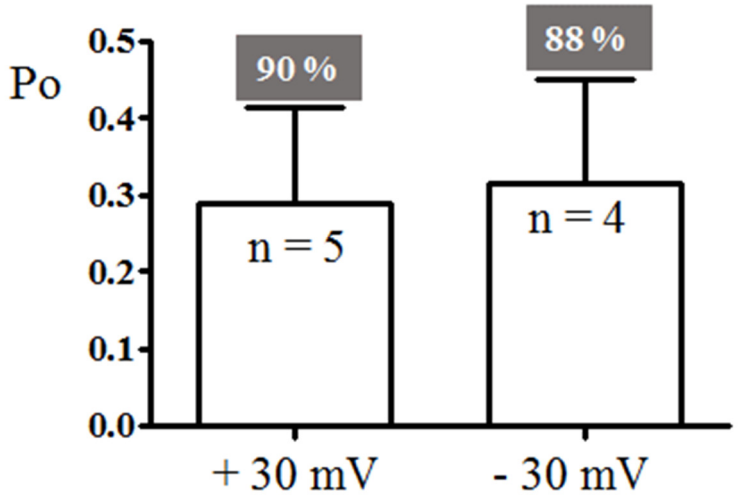


Figure 7.9 The SR K^+ channels from solubilised LSR are voltage-independent
The Po of the SR K^+ channel at holding potentials of +30 mV and -30 mV is shown. The contribution of Po_{FULL} to Po_{TOTAL} is indicated in the grey box above each column.

7.4 Discussion

The objective of this study was to investigate if the wheat germ cell free purification system could be used to purify functional TRIC-channels. Purified TRIC-A proteins were incorporated into artificial bilayers and the single-channel current fluctuations that were observed were characterised.

7.4.1 Purified TRIC-A single-channel current fluctuations

The Po of the purified TRIC-A channels were extremely low, and therefore, a current-voltage plot could not be obtained. At 0 mV, however, in our experimental solutions, the upward current deflections that were observed were indicative of predominately cation currents. In Chapter 6, I have illustrated that the Po of the SR K^+ channel was significantly increased by changing the pH of the recording solution from pH 7.2 to pH 9.2 and therefore, I changed the pH of the solutions used for incorporating purified TRIC-A channels to pH 9.2.

Using ScanProsite analysis tool in ExPASy (www.expasy.org/tools), we detected possible PKA and CK2 phosphorylation sites (see Figure 7.10) and thus, I incubated the purified TRIC-A protein in a phosphorylation mixture (154, 155) to investigate if it would increase the chances of observing longer open events. In the two recordings that were obtained, purified TRIC-A gating was only recorded in gradient conditions (810 mM K^+ on the cytosolic side of the channel and 210 mM K^+ on the luminal side of the channel). Although Po analysis was not calculated, the Po of both the channels in both experiments appeared to be very high with few closing events (see Figure 7.4 and Figure 7.5). In both experiments, there was a prominent sub-conductance gating level that was close in amplitude to the observed full open channel level.



Figure 7.10 Amino acid sequence alignments and conserved motifs for mouse, rabbit and human TRIC-A proteins and for mouse and human TRIC-B proteins.
The three transmembrane domains identified by the hydropathicity analysis by Yawaza *et al* (2007) (100) are indicated by the red boxes. The highly conserved KEV motif is marked by a green box and asterisks. Possible PKC (pink boxes) and Casein Kinase 2 (CK2) (orange boxes) phosphorylation sites, detected by the ScanProsite analysis tool in ExPASy (www.expasy.org/tools) are also indicated.

7.4.1.1 Can TRIC-A gate like TRIC-B?

As discussed previously, in symmetrical 210 mM K^+, purified TRIC-A was reported to exhibit a full open channel conductance of 192 pS and purified TRIC-B was reported to exhibit a full open channel conductance of 138 pS (101). The TRIC-B full open channel

conductance was later revisited when Venturi *et al* (2013) (126) suggested that the conductance of the native TRIC-B channel was similar to the conductance of purified TRIC-A (approximately 200 pS) and it was postulated that the purified TRIC-B channels that were reported by Pitt *et al* (2010) (101) were damaged from the purification procedure. In this chapter, I have obtained two single-channel TRIC-A conductances. In 210 mM KPIPES, pH 9.2, I recorded a TRIC-A channel with a full open channel conductance of 213 pS and a sub-conductance level conductance of 194 pS (see Figure 7.5). Both of these measurements are similar to those reported in Pitt *et al* (2010) (101). However, in the second experiment, I recorded a TRIC-A channel with a full open channel level conductance of 138 pS and a sub-conductance level conductance of 103 pS (see Figure 7.4). The full open channel level conductance observed in this experiment for purified TRIC-A is almost identical to the TRIC-B full open channel conductance that was reported by Pitt *et al* (2010) (101). The decrease in TRIC-A conductance that was observed in this experiment may be due to one of the phosphorylating agents causing the channel to gate in sub-conducting levels only. However, it may also be possible that TRIC-A can gate in a TRIC-B like manner and *vice versa*, which adds to the complexity of characterising both isoforms. Further experiments are needed to quantify this observation.

7.4.2 The gating of native SR K^+ channels is altered in gradient conductions

The native SR^+ channels from mouse WT skeletal muscle that were recorded in gradient conditions (810 mM K^+ on the cytosolic side of the channel and 210 mM K^+ on the luminal side of the channel) displayed different biophysical gating characteristics to those that have been described in Chapter 3 (in symmetrical 210 mM K^+). The channels that were observed appeared to gate with an extremely high Po (although the Po was not calculated) and closing events were rare. In addition, the channels gated to sub-conductance levels that

were closest to the full open channel level as illustrated in Figure 7.8. Further experiments are required to determine if the high cytosolic [K^+] in the gradient conditions alters the gating of the SR K^+ channel or whether the addition of 500 mM cytosolic Cl^- (due to adding 200 µL 3M KCl) is responsible for the altered biophysical properties.

7.4.3 CHAPS detergent alters the gating of the native SR K^+ channel

Our results have demonstrated that the voltage-dependence of the SR K^+ channel was markedly altered when the native LSR was solubilised with 1 % CHAPS and subsequently fused with artificial bilayers. All five recordings displayed voltage-independent gating behaviour, with the Po at +30 mV being similar to the Po at -30 mV (see Figure 7.9). The voltage-dependence of native (not solubilised) SR K^+ channels from rabbit skeletal muscle have been previously reported in the literature by our group (3, 101) and several other studies (82, 85, 88) and is similar to the voltage-dependence of the mouse skeletal muscle that I have reported in this thesis. It is unlikely that the solubilised SR K^+ channels simply fused to the bilayer in the opposite orientation. If this was the case, very little activity would be observed at +30 mV and channel openings observed at -30 mV. It is also unlikely that we are simply observing the voltage-insensitive high Po SR K^+ channels that were described in Chapter 3. These voltage-insensitive native SR K^+ channels gated predominately in sub-conductance open states (see Figure 3.13), whereas the voltage-insensitive solubilised SR K^+ channels appeared to gate primarily in the full open channel level (see Figure 7.9). The voltage-insensitive solubilised SR K^+ channels were analysed using a simplified 2 state Markov Model so we cannot quantify the contribution of Po_{FULL} to Po_{SUB}.

This is not the first report of the gating characteristics of the rabbit skeletal SR K^+ channels from solubilised SR. Tomlins *et al* (1986) solubilised SR membranes and reconstituted the

solubilised ion-channels into liposomes for patch-clamp (90). In contrast to what we describe in this thesis, Tomlins *et al* (1986) (90) reported that the gating of the SR K^+ channels from solubilised SR were still voltage sensitive when reconstituted into liposomes. They concluded that the SR K^+ channels fused with the liposomes in a fixed orientation, with the cytosolic side of the channel facing the patch pipette and the luminal side of the channel facing the recording chamber (90). To successfully incorporate functional SR K^+ channels into liposomes, Tomlins *et al* (1986) (90) dialysed away the detergent that was used to solubilise the HSR membranes whereas in this thesis, we have not dialysed the detergent away. Further experiments are required to determine whether the presence of the detergent molecules alter the voltage-dependence of channels and if subsequent dialysis of the samples restores the voltage-dependent feature. Recent functional investigation of voltage-gated channels in membranes have reported that lipids may modulate the gating of certain channels through close association with voltage sensor domains (156, 157). Hypothetically, if this was the case for the SR K^+ channel, then perhaps the presence of detergent molecules prevents lipid interactions with the voltage sensor. Another possibility is that detergent molecules change the membrane properties of the bilayer inducing conformational changes in the SR K^+ channel.

7.5 Future work

The use of purified TRIC channels is necessary to characterise their biophysical properties and to investigate their structure-function relationships. For example, TRIC- channels that contain mutations in residues that might be involved in the pore forming region or responsible for the voltage-dependence of these channels can be generated and purified for the subsequent investigation of their single-channel properties in bilayer experiments. My data on the TRIC-A channels purified using the wheat germ system have shown that the purification procedure may be inadequate to obtain completely functional channels that

could be studied after bilayer reconstitution. Therefore, improvements in the protocol used to isolate recombinant channels are needed.

A large variety of recombinant ion-channels, including RyR channels, are generally expressed in mammalian expression systems such as human embryonic kidney epithelial cells (HEK 293) and Chinese ovary cells (CHO) for functional studies (131, 132, 158, 159). At the moment, our laboratory are growing sufficient HEK 293 and Chinese hamster ovary (CHO) cells that are overexpressing TRIC-A/TRIC-B proteins with a His-tag (6xHis) inserted at the C-terminal. The TRIC-channels can be isolated using a Ni-affinity chromatography and subsequently eluted for single-channel reconstitution experiments. Once a stable production of fully functional recombinant TRIC protein is achieved, several mutants can be generated for investigating the structure-function relationship of TRIC channels.

8 Conclusion

This thesis has focused on the biophysical properties of the K^+-selective ion-channels that are located on the SR of cardiac and skeletal muscle cells. These K^+ channels are thought to support SR Ca^{2+} movements by providing a counter current of ions necessary to maintain the SR membrane potential close to 0 mV at all times and to ensure that monovalent cation concentrations across the SR are equilibrated. It has been suggested suggested that TRIC-A and TRIC-B are the SR K^+ channels. In this thesis, I have predominately focused on the biophysical properties of the SR K^+ channels from TRIC-A KO tissue to investigate whether TRIC-B exhibited unique properties different to those of the SR K^+ channels from native WT SR. I have demonstrated, however, that the channels from TRIC-A KO tissue displayed similar gating behaviour, including voltage-dependence and conductance to those from WT tissue.

In Chapter 4, I demonstrated that when more than one SR K^+ channel from TRIC-A KO tissue was gating in the bilayer, the channels gated in a cooperative manner, deviating from binomial predictions. The Po of each SR K^+ channel increased as the number of channels gating in the bilayer increased. In addition, I have illustrated that this cooperative gating feature is also present in the SR K^+ channels from WT tissue.

Both the TRIC-channels and the RyRs have a higher abundance in the HSR compared to the LSR and I therefore fused the HSR to artificial bilayers and experiments where both an SR K^+ channel and a RyR were simultaneously gating. I separated the SR K^+ channel events from the RyR events when both channels were gating simultaneously to monitor Po in both species of channel. I found that when an RyR was present in the bilayer in addition to an SR K^+ channel, the SR K^+ channel retained the single-channel properties that were described in earlier chapters. This is the first report to characterise the properties of two distinct species of SR channel gating simultaneously in a bilayer. These experiments, along

with further experiments underway in this laboratory will be important for establishing any inter-channel relationships that may exist between the different ion-channels of the SR and which may be important for SR Ca^{2+}-release.

I have also demonstrated that the SR K^+ channels from WT and TRIC-A KO tissue are sensitive to changes in cytosolic and luminal pH. Acidic pH (pH 6.2) on the cytosolic side of the SR K^+ channel decreased channel Po and single-channel conductance, whereas alkaline pH (pH 9.2) on the cytosolic or luminal side of the channel increased Po, without altering conductance. Although sensitivity to pH has been previously reported (87, 135), these experiments were based on bilayers containing >1,000 SR K^+ channels. The study described here provides the first detailed analysis of the mechanisms that underlie pH sensitivity of the SR K^+ channel at the single-channel level.

As part of a larger study, as a laboratory we are trying to optimise the procedures for purifying TRIC-proteins. I therefore have investigated if the Wheat germ cell-free system could be used to purify functional TRIC-A channels. I incorporated purified TRIC-A into bilayers and recorded the single-channel current fluctuations that were observed. My data on the recombinant TRIC-A channels have shown that the purification procedure was inadequate to obtain completely functional channels that could be studied after bilayer reconstitution. In addition, in this chapter, I have illustrated that CHAPS detergent modifies the voltage-sensitivity of the native SR K^+ channels. This observation may be important for comparing the current-fluctuations from purified TRIC-channels to the native SR K^+ channel in future studies.

In conclusion, the SR consists of a variety of distinct ion-channels, transporters and associated proteins that regulate physiological intracellular Ca^{2+}-release during cardiac and skeletal muscle contraction. Understanding the properties of all of the ionic fluxes that take

place across the SR during Ca^{2+} movements and how these fluxes can modulate RyR-mediated Ca^{2+}-release under normal conditions is crucial to determining how these processes may become dysregulated in pathophysiological states.

So far, I have found that only voltage and pH are able to radically alter the gating properties of SR K^+ channels. SR K^+ channels gate in a cooperative manner and I believe that this will be proved to be key to their ability to respond to signals within the SR. However, the mechanism of cooperative gating is not known, and it it also not known whether voltage, pH or ligands affects the ability of the SR K^+ channels to gate in a cooperative manner.

References

1. Schneider MF, Chandler WK. Voltage dependent charge movement in skeletal muscle: a possible step in excitation-contraction coupling. Nature. 1973;242:244-6.

2. Endo M. Calcium release from the sarcoplasmic reticulum. Physiol Rev. 1977;57:71-108.

3. Caputo C. Excitation and Contraction Processes in Muscle. Annu Rev Biophys Bioeng. 1978;7(1):63-83.

4. Melzer W, Herrmann-Frank A, L ttgau HC. The role of Ca^{2+} ions in excitation-contraction coupling of skeletal muscle fibres. Biochimica et Biophysica Acta. 1995;1241:59-116.

5. Berchtold MW, Brinkmeier H, Müntener M. Calcium Ion in Skeletal Muscle: Its Crucial Role for Muscle Function, Plasticity, and Disease. Physiol Rev. 2000;80(3):1215-65.

6. Fabiato A, Fabiato F. Contractions induced by a calcium-triggered release of calcium from the sarcoplasmic reticulum of single skinned cardiac cells. J Physiol. 1975;249:469-95.

7. Bers DM. Excitation-contraction coupling and cardiac contractile force. Dordrecht: Kluwer; 1991.

8. Franzini-Armstrong C. Structure of sarcoplasmic reticulum. Fed Proc. 1980;39:2403-9.

9. Peachey LD. The sarcoplasmic reticulum and transverse tubules of the frog's sartorius. The Journal of Cell Biology. 1965;25(3):209-31.

10. Volpe P, Villa A, Damiani E, Sharp AH, Podini P, Snyder SH, et al. Heterogeneity of microsomal Ca^{2+} stores in chicken Purkinje neurons. EMBO Journal. 1991;10:3183-9.

11. Franzini-Armstrong C, Jorgensen AO. Structure and development of E-C coupling units in skeletal muscle. Annu Rev Physiol. 1994;56:509-34.

12. Saito A, Seiler S, Chu A, Fleischer S. Preparation and morphology of sarcoplasmic reticulum terminal cisternae from rabbit skeletal muscle. JCell Biol. 1984;99:875-85.

13. Costello B, Chadwick C, Saito A, Chu A, Maurer A, Fleischer S. Characterization of the junctional face membrane from terminal cisternae of sarcoplasmic reticulum. JCell Biol. 1986;103:741-53.

14. Treves S, Vukcevic M, Maj M, Thurnheer R, Mosca B, Zorzato F. Minor sarcoplasmic reticulum membrane components that modulate excitation–

contraction coupling in striated muscles. The Journal of Physiology. 2009;587(13):3071-9.

15. Caswell AH, Brunschwig JP. Identification and extraction of proteins that compose the triad junction of skeletal muscle. JCell Biol. 1984;99:929-39.

16. Franzini-Armstrong C, Nunzi G. Junctional feet and particles in the triads of a fast-twitch muscle fibre. J Muscle Res Cell Motil. 1983;4:233-52.

17. Jewett PH, Leonard SD, Sommer JR. Chicken cardiac muscle: Its Elusive Extended Junctional Sarcoplasmic Reticulum and Sarcoplasmic Reticulum Fenestrations. The Journal of Cell Biology. 1973;56(2):595-600.

18. Sommer JR, Johnson EA. Comparative ultrastructure of cardiac cell membrane specializations. A review. Am J Cardiol.25(2):184-94.

19. Sommer JR, Waugh RA. The ultrastructure of the mammalian cardiac muscle cell--with special emphasis on the tubular membrane systems. A review. The American Journal of Pathology. 1976;82(1):192-232.

20. Forbes MS, Hawkey LA, Sperelakis N. The transverse-axial tubular system (TATS) of mouse myocardium: its morphology in the developing and adult animal. Am J Anat. 1984;170(2):143-62.

21. Komazaki S, Ito K, Takeshima H, Nakamura H. Deficiency of triad formation in developing skeletal muscle cells lacking junctophilin type 1. FEBS Lett.524(1):225-9.

22. Ito K, Komazaki S, Sasamoto K, Yoshida M, Nishi M, Kitamura K, et al. Deficiency of triad junction and contraction in mutant skeletal muscle lacking junctophilin type 1. The Journal of Cell Biology. 2001;154(5):1059-68.

23. Nishi M, Hashimoto K, Kuriyama K, Komazaki S, Kano M, Shibata S, et al. Motor Discoordination in Mutant Mice Lacking Junctophilin Type 3. Biochem Biophys Res Commun. 2002;292(2):318-24.

24. Caswell AH, Brandt NR, Brunschwig JP, Purkerson S. Localization and partial characterization of the oligomeric disulfide-linked molecular weight 95 000 protein (triadin) which binds the ryanodine and dihydropyridine receptors in skeletal muscle triadic vesicles. Biochemistry (Mosc). 1991;30:7507-13.

25. Knollmann BC. New roles of calsequestrin and triadin in cardiac muscle. The Journal of Physiology. 2009;587(13):3081-7.

26. Chopra N, Yang T, Asghari P, Moore ED, Huke S, Akin B, et al. Ablation of triadin causes loss of cardiac Ca^{2+} release units, impaired excitation–contraction coupling, and cardiac arrhythmias. Proceedings of the National Academy of Sciences. 2009;106(18):7636-41.

27. Shimuta M, Komazaki S, Nishi M, Iino M, Nakagawara K-i, Takeshima H. Structure and expression of mitsugumin29 gene1. FEBS Lett.431(2):263-7.

28. Takeshima H, Shimuta M, Komazaki S, Ohmi K, Nishi M, Iino M, et al. Mitsugumin29, a novel synaptophysin family member from the triad junction in skeletal muscle. Biochem J. 1998;331:317-22.

29. Brotto MAP, Nagaraj RY, Brotto LS, Takeshima H, Ma J, Nosek TM. Defective maintenance of intracellular Ca^{2+} homeostasis is linked to increased muscle fatigability in the MG29 null mice. Cell Res. 2004;14(5):373-8.

30. Franzini-Armstrong C, Protasi F. Ryanodine receptors of striated muscles: A complex channel capable of multiple interactions. Physiol Rev. 1997;77:699-729.

31. Fabiato A. Simulated calcium current can both cause calcium loading in and trigger the calcium release from the sarcoplasmic reticulum of a skinned cardiac Purkinje cell. J Gen Physiol. 1985;85:291-320.

32. Rich TL, Langer GA, Klassen MG. Two components of coupling calcium in single ventricular cell of rabbits and rats. Am J Physiol. 1988;254:H937-H46.

33. Meissner G. Isolation and characterization of two types of sarcoplasmic reticulum vesicles. Biochimica et Biophysica Acta (BBA) - Biomembranes. 1975;389:51-68.

34. Kawamoto RM, Brunschwig JP, Kim KC, Caswell AH. Isolation, characterization and localization of the spanning protein from skeletal muscle triads. JCell Biol. 1986;103:1405-14.

35. Takeshima H, Nishimura S, Matsumoto T, Ishida H, Kangawa K, Minamino N, et al. Primary structure and expression from complementary DNA of skeletal muscle ryanodine receptor. Nature. 1989;339:439-45.

36. Nabauer M, Callewaert G, Cleemann L, Morad M. Regulation of calcium release is gated by calcium current, not gating charge, in cardiac myocytes. Science. 1989;244:800-3.

37. Nabauer M, Ellis-Davies GC, Kaplan JH, Morad M. Modulation of Ca^{2+} channel selectivity and cardiac contraction by photorelease of Ca^{2+}. Am J Physiol. 1989;256:H916-H20.

38. Sham JS, Cleemann L, Morad M. Functional coupling of Ca^{2+} channels and ryanodine receptors in cardiac myocytes. Proc Natl Acad Sci U S A. 1995;92(1):121-5.

39. Bers DM. Cardiac excitation-contraction coupling. Nature. 2002;415:198-205.

40. Fabiato A. Calcium-induced release of calcium from the cardiac sarcoplasmic reticulum. Am J Physiol. 1983;245:C1-C14.

41. Tanabe T, Beam KG, Powell JA, Numa S. Restoration of excitation-contraction coupling and slow calcium current in dysgenic muscle by dihydropyridine receptor complementary DNA. Nature. 1988;336:134-9.

42. Flucher BE, Takekura H, Franzini-Armstrong C. Development of the excitation-contraction coupling apparatus in skeletal muscle: Association of sarcoplasmic reticulum and transverse tubules with myofibrils. Dev Biol. 1993;160:135-47.

43. Rios E, Pizarro G. Voltage sensor of excitation-contraction coupling in skeletal muscle. Physiol Rev. 1991;71:849-907.

44. Rios E, Ma JJ, Gonzalez A. The mechanical hypothesis of excitation-contraction (EC) coupling in skeletal muscle. J Muscle Res Cell Motil. 1991;12:127-35.

45. Ildefonse M, Jacquemond V, Rougier O, Renaud JF, Fosset M, Lazdunski M. Excitation contraction coupling in skeletal muscle: Evidence for a role of slow Ca^{2+} channels using Ca^{2+} channel activators and inhibitors in the dihydropyridine series. Biochem Biophys Res Commun. 1985;129(3):904-9.

46. Block BA, Imagawa T, Campbell KP, Franzini-Armstrong C. Structural evidence for direct interaction between the molecular components of the transverse tubule/sarcoplasmic reticulum junction in skeletal muscle. JCell Biol. 1988;107:2587-600.

47. Dally S, Corvazier E, Bredoux R, Bobe R, Enouf J. Multiple and diverse coexpression, location, and regulation of additional SERCA2 and SERCA3 isoforms in nonfailing and failing human heart. J Mol Cell Cardiol.48(4):633-44.

48. Periasamy M, Bhupathy P, Babu GJ. Regulation of sarcoplasmic reticulum Ca^{2+} ATPase pump expression and its relevance to cardiac muscle physiology and pathology. Cardiovasc Res. 2008;77(2):265-73.

49. Blaustein MP, Lederer WJ. Sodium calcium exchange: Its physiological implications. Physiol Rev. 1999;79:763-854.

50. Terracciano CMN, De Souza AI, Philipson KD, MacLeod KT. Na^{+} $-Ca^{2+}$ exchange and sarcoplasmic reticular Ca^{2+} regulation in ventricular myocytes from transgenic mice overexpressing the Na^{+} $-Ca^{2+}$ exchanger. The Journal of Physiology. 1998;512(Pt 3):651-67.

51. Carafoli E. Calcium pump of the plasma membrane. Physiol Rev. 1991;71:129-53.

52. Strehler EE, Zacharias DA. Role of Alternative Splicing in Generating Isoform Diversity Among Plasma Membrane Calcium Pumps. Physiol Rev. 2001;81(1):21-50.

53. Inui M, Saito A, Fleischer S. Isolation of the ryanodine receptor from cardiac sarcoplasmic reticulum and identity with the feet structures: J.Biol.Chem.; 1987. 15637-42 p.

54. Inui M, Saito A, Fleischer S. Purification of the ryanodine receptor and identity with feet structures of junctional terminal cisternae of sarcoplasmic reticulum from fast skeletal muscle. JBiolChem. 1987;262:1740-7.

55. Ferguson DG, Schwartz HW, Franzini-Armstrong C. Subunit structure of junctional feet in triads of skeletal muscle: A freeze-drying, rotary-shadowing study. JCell Biol. 1984;99:1735-42.

56. Protasi F, Takekura H, Wang Y, Chen SR, Meissner G, Allen PD, et al. RYR1 and RYR3 have different roles in the assembly of calcium release units of skeletal muscle. Biophys J. 2000;79:2494-508.

57. Yin C-C, Blayney LM, Anthony Lai F. Physical Coupling between Ryanodine Receptor–Calcium Release Channels. J Mol Biol. 2005;349(3):538-46.

58. Stern MD, Song LS, Cheng H, Sham JSK, Yang HT, Boheler KR, et al. Local Control Models of Cardiac Excitation-Contraction Coupling. A Possible Role for Allosteric Interactions between Ryanodine Receptors. J Gen Physiol. 1999;113:469-89.

59. Yin CC, Lai FA. Intrinsic lattice formation by the ryanodine receptor calcium-release channel. NatCell Biol. 2000;2:669-71.

60. Franzini-Armstrong C, Protasi F, Ramesh V. Shape, size and distribution of Ca^{2+} release units and couplons in skeletal and cardiac muscles. Biophysical Journal. 1999;77:1528-39.

61. Van Petegem F. Ryanodine Receptors: Allosteric Ion Channel Giants. J Mol Biol. 2015;427(1):31-53.

62. Porta M, Diaz-Sylvester PL, Neumann JT, Escobar AL, Fleischer S, Copello JA. Coupled gating of skeletal muscle ryanodine receptors is modulated by Ca^{2+}, Mg^{2+}, and ATP. American Journal of Physiology - Cell Physiology. 2012;303(6):C682-C97.

63. Marx SO, Ondrias K, Marks AR. Coupled gating between individual skeletal muscle Ca^{2+} release channels (ryanodine receptors). Science. 1998;281:818-21.

64. Franzini-Armstrong C, Protasi F, Ramesh V. Comparative ultrastructure of Ca^{2+} release units in skeletal and cardiac muscle. Annals of the New York Academy of Sciences. 1998;853:20-30.

65. Marx SO, Gaburjakova J, Gaburjakova M, Henrikson C, Ondrias K, Marks AR. Coupled gating between cardiac calcium release channels (ryanodine receptors). Circ Res. 2001;88(11):1151-8. Epub 2001/06/09.

66. Nakai J, Imagawa T, Hakamata Y, Shigekawa M, Takeshima H, Numa S. Primary structure and functional expression from cDNA of the cardiac ryanodine receptor/calcium release channel. FEBS Lett. 1990;271:169-77.

67. Hakamata Y, Nakai J, Takeshima H, Imoto K. Primary structure and distribution of a novel ryanodine receptor/calcium release channel from rabbit brain. FEBS Lett. 1992;312:229-35.

68. Rousseau E, Smith JS, Meissner G. Ryanodine modifies conductance and gating behaviour of single Ca^{2+} release channel. American Journal of Physiology. 1987;253:C364-8.

69. Holmberg SRM, Williams AJ. The cardiac sarcoplasmic reticulum calcium-release channel: modulation of ryanodine binding and single-channel activity. Biochim Biophys Acta. 1990;1022:187-93.

70. Tunwell REA, Wickenden C, Bertrand BMA, Shevchenko VI, Walsh MB, Allen PD, et al. The human cardiac muscle ryanodine receptor-calcium release channel: Identification, primary structure and topological analysis. Biochem J. 1996;318:477-87.

71. Otsu K, Willard HF, MacLennan DH. Molecular cloning of cDNA encoding the Ca^{2+} release channel (ryanodine receptor) of rabbit cardiac sarcoplasmic reticulum. Biophysical Journal. 1990;57:503a.

72. Wagenknecht T, Samso M. Three-dimensional reconstruction of ryanodine receptors. Front Biosci. 2002;1(7):d1464-74.

73. Smith JS, Coronado R, Meissner G. Sarcoplasmic reticulum contains adenine nucleotide-activated calcium channels. Nature. 1985;316:446-9.

74. Lindsay ARG, Williams AJ. Functional characterisation of the ryanodine receptor purified from sheep cardiac muscle sarcoplasmic reticulum. Biochim Biophys Acta. 1991;1064:89-102.

75. Lindsay ARG, Manning SD, Williams AJ. Monovalent cation conductance in the ryanodine receptor-channel of sheep cardiac muscle sarcoplasmic reticulum. J Physiol. 1991;439:463-80.

76. Williams AJ. Ion conduction and discrimination in the sarcoplasmic reticulum ryanodine receptor/calcium-release channel. J Muscle Res Cell Motil. 1992;13:7-26.

77. Tinker A, Lindsay ARG, Williams AJ. A model for ionic conduction in the ryanodine receptor-channel of sheep cardiac muscle sarcoplasmic reticulum. J Gen Physiol. 1992;100:495-517.

78. Tinker A, Williams AJ. Divalent cation conduction in the ryanodine receptor-channel of sheep cardiac muscle sarcoplasmic reticulum. J Gen Physiol. 1992;100:479-93.

79. Sitsapesan R, Williams AJ. Gating of the native and purified cardiac SR Ca^{2+} -release channel with monovalent cations as permeant species. Biophysical Journal. 1994;67:1484-94.

80. Hill AP, Sitsapesan R. DIDS modifies the conductance, gating, and inactivation mechanisms of the cardiac ryanodine receptor. Biophys J. 2002;82:3037-47.

81. McKinley D, Meissner G. Evidence for a K^+ , Na^+ permeable channel in sarcoplasmic reticulum. Journal of Membrane Biology. 1978;44:159-86.

82. Coronado R, Rosenberg RL, Miller C. Ionic selectivity, saturation, and block in a K^+-selective channel from sarcoplasmic reticulum. Journal of General Physiology. 1980;76:425-46.

83. Adrian RH, Peachey LD. Reconstruction of the action potential of frog sartorius muscle. The Journal of Physiology. 1973;235(1):103-31.

84. Vergara J, Bezanilla F, Salzberg BM. Nile blue fluorescence signals from cut single muscle fibers under voltage or current clamp conditions. The Journal of General Physiology. 1978;72(6):775-800.

85. Labarca P, Miller C. A K^+-selective, three-state channel from fragmented sarcoplasmic reticulum of frog leg muscle. Journal of Membrane Biology. 1981;61:31-8.

86. Meissner G. Monovalent ion and calcium ion fluxes in sarcoplasmic reticulum. Mol Cell Biochem. 1983;55(1):65-82.

87. Miller C. Voltage-gated cation conductance channel from fragmented sarcoplasmic reticulum: Steady-state electrical properties. J Membr Biol. 1978;40:1-23.

88. Coronado R, Miller C. Conduction and block by organic cations in a K^+ -selective channel from sarcoplasmic reticulum incorporated into planar phospholipid bilayers. Journal of General Physiology. 1982;79:529-47.

89. Hill JA, Jr., Coronado R, Strauss HC. Potassium channel of cardiac sarcoplasmic reticulum is a multi-ion channel. Biophysical Journal. 1989;55:35-45.

90. Tomlins B, Williams AJ. Solubilisation and reconstitution of the rabbit skeletal muscle sarcoplasmic reticulum K^+ channel into liposomes suitable for patch clamp studies. Pflügers Archiv - European Journal of Physiology. 1986;407:341-7.

91. Gray MA, Tomlins B, Montgomery RAP, Williams AJ. Structural aspects of the sarcoplasmic reticulum K^+ channel revealed by gallamine block. Biophysical Journal. 1988;54:233-9.

92. Williams AJ, Tomlins B. Solubilization and reconstitution of the K^+ -selective channel of rabbit skeletal muscle sarcoplasmic reticulum. Biochemical Society Transactions. 1985;13:1247-8.

93. Fox JA. Conductance and selectivity properties of a substate of the rabbit sarcoplasmic reticulum channel. Biophys J. 1985;47:573-6.

94. Coronado R, Miller C. Voltage-dependent caesium blockade of a cation channel from fragmented sarcoplasmic reticulum. Nature. 1979;280:807-10.

95. Cukierman S, Yellen G, Miller C. The K^+ channel of sarcoplasmic reticulum. A new look at Cs^+ block. Biophysical Journal. 1985;48:477-84.

96. Coronado R, Miller C. Decamethonium and hexamethonium block K^+ channels of sarcoplasmic reticulum. Nature. 1980;288(5790):495-7.

97. Tomlins B, Williams AJ, Montgomery RAP. The characterization of a monovalent cation selective channel of mammalian cardiac muscle sarcoplasmic reticulum. J Membr Biol. 1984;80:191-9.

98. Meissner G, McKinley D. Permeability of canine cardiac sarcoplasmic reticulum vesicles to K^+ ,Na^+ ,H^+ and Cl^-. JBiolChem. 1982;257:7704-11.

99. Nishi M, Komazaki S, Iino M, Kangawa K, Takeshima H. Mitsugumin23, a novel transmembrane protein on endoplasmic reticulum and nuclear membranes. FEBS Lett. 1998;432:191-6.

100. Yazawa M, Ferrante C, Feng J, Mio K, Ogura T, Zhang M, et al. TRIC channels are essential for Ca^{2+} handling in intracellular stores. Nature. 2007;448:78-82.

101. Pitt SJ, Park KH, Nishi M, Urashima T, Aoki S, Yamazaki D, et al. Charade of the SR K^+-Channel: Two Ion-Channels, TRIC-A and TRIC-B, Masquerade as a Single K^+-Channel. Biophys J. 2010;99:417-26.

102. Hals GD, Stein PG, Palade PT. Single channel characteristics of a high conductance anion channel in "sarcoballs". The Journal of General Physiology. 1989;93(3):385-410.

103. Holmberg SRM, Williams AJ. Single channel recordings from human cardiac sarcoplasmic reticulum. Circ Res. 1989;65:1445-9.

104. Rousseau E. Single chloride-selective channel from cardiac sarcoplasmic reticulum studied in planar lipid bilayers. J Membrain Biol. 1989;110(1):39-47.

105. Ide T, Sakamoto H, Morita T, Taguchi T, Kasai M. Purification of a Cl - - channel protein of sarcoplasmic reticulum by assaying the channel activity in the planar lipid bilayer system. Biochemical and Biophysical Research Communications. 1991;176:38-44.

106. Townsend C, Rosenberg RL. Characterization of a chloride channel reconstituted from cardiac sarcoplasmic reticulum. J Membr Biol. 1995;147:121-36.

107. Decrouy A, Juteau M, Rousseau E. Examination of the role of phosphorylation and phospholamban in the regulation of the cardiac sarcoplasmic reticulum Cl - channel. Journal of Membrane Biology. 1995;146:315-26.

108. Kourie JI, Laver DR, Ahern GP, Dulhunty AF. A calcium-activated chloride channel in sarcoplasmic reticulum vesicles from rabbit skeletal muscle. Am J Physiol. 1996;270:C1675-C86.

109. Kourie JI, Laver DR, Junankar PR, Gage PW, Dulhunty AF. Characteristics of two types of chloride channel in sarcoplasmic reticulum vesicles from rabbit skeletal muscle. Biophys J. 1996;70:202-21.

110. Divangahi M, Balghi H, Danialou G, Comtois AS, Demoule A, Ernest S, et al. Lack of CFTR in Skeletal Muscle Predisposes to Muscle Wasting and Diaphragm Muscle Pump Failure in Cystic Fibrosis Mice. PLoS Genet. 2009;5(7):e1000586.

111. Sheppard DN, Welsh MJ. Structure and Function of the CFTR Chloride Channel. Physiol Rev. 1999;79(1):S23-S45.

112. Shoshan-Barmatz V, Hadad N, Feng W, Shafir I, Orr I, Varsanyi M, et al. VDAC/porin is present in sarcoplasmic reticulum from skeletal muscle. FEBS Lett. 1996;386:205-10.

113. Zhao X, Yamazaki D, Park KH, Komazaki S, Tjondrokoesoemo A, Nishi M, et al. Ca^{2+} overload and sarcoplasmic reticulum instability in tric-a null skeletal muscle. J Biol Chem. 2010;285(48):37370-6.

114. Yamazaki D, Komazaki S, Nakanishi H, Mishima A, Nishi M, Yazawa M, et al. Essential role of the TRIC-B channel in Ca^{2+} handling of alveolar epithelial cells and in perinatal lung maturation. Development. 2009;136:2355-61.

115. Takeshima H, Komazaki S, Hirose K, Nishi M, Noda T, Lino M. Embryonic lethality and abnormal cardiac myocytes in mice lacking ryanodine receptor type 2. EMBO J. 1998;17:3309-16.

116. Yamazaki D, Tao S, Takeshima H. [TRIC channel and hypertension]. Clin Calcium. 2013;23(4):543-50.

117. Yamazaki D, Tabara Y, Kita S, Hanada H, Komazaki S, Naitou D, et al. TRIC-A Channels in Vascular Smooth Muscle Contribute to Blood Pressure Maintenance. Cell Metab.14(2):231-41.

118. Jones LR, Besch HR, Jr., Fleming JW, McConnaughey MM, Watanabe AM. Separation of vesicles of cardiac sarcolemma from vesicles of cardiac sarcoplasmic reticulum. Comparative biochemical analysis of component activities. J Biol Chem. 1979;254(2):530-9.

119. Mueller P, Rudin DO, Tien HT, Wescott WC. Resconstitution of excitable cell membrane structure in vitro. Circulation. 1962;26:1167-71.

120. Parsegian VA. Ion membrane interactions as structural forces. Ann N Y Acad Sci. 1975;264(1):161-74.

121. Andrews DM, Manev ED, Haydon DA. Composition and energy relationships for some thin lipid films, and the chain conformation in monolayers at liquid-liquid interfaces. Special Discussions of the Faraday Society. 1970;1(0):46-56.

122. Miller C. Ion channel structure and function. Science. 1992;258:240-1.

123. Nyquist H. Certain Topics in Telegraph Transmission Theory. American Institute of Electrical Engineers, Transactions of the. 1928;47(2):617-44.

124. Shannon CE. A Mathematical Theory of Communication. Bell System Technical Journal. 1948;27(3):379-423.

125. Chapman ML, VanDongen HMA, Vandongen AMJ. Activation-dependent subconductance levels in the drk1 K channel suggest a subunit basis for ion permeation and gating. Biophys J. 1997;72:708-19.

126. Venturi E, Matyjaszkiewicz A, Pitt S, Tsaneva-Atanasova K, Nishi M, Yamazaki D, et al. TRIC-B channels display labile gating: evidence from the TRIC-A knockout mouse model. Pflugers Arch - Eur J Physiol. 2013;465(8):1135-48.

127. Matyjaszkiewicz A, Venturi E, O'Brien F, Iida T, Nishi M, Takeshima H, et al. Subconductance Gating and Voltage Sensitivity of Sarcoplasmic Reticulum K^+ Channels: A Modeling Approach. Biophys J.109(2):265-76.

128. Sigworth FJ, Sine SM. Data transformations for improved display and fitting of single-channel dwell time histograms. Biophys J. 1987;52:1047-54.

129. Colquhoun D, Hawkes AG. The principles of the stochastic interpretation of Ion-channel mechanisms. In: Sakmann B, Neher E, editors. Single-channel recording. New York & London: Plenum; 1983. p. 135-75.

130. Horne R, Lange K. Estimating kinetic constants from single channel data. Biophys J. 1983;43:207-23.

131. Martel J, Dupuis G, Deschenes P, Payet MD. The sensitivity of the human Kv1.3 (hKv1.3) lymphocyte K^+ channel to regulation by PKA and PKC is partially lost in HEK 293 host cells. J Membr Biol. 1998;161(2):183-96.

132. Wu LM, Orikabe M, Hirano Y, Kawano S, Hiraoka M. Effects of Na^+ channel blocker, pilsicainide, on HERG current expressed in HEK-293 cells. J Cardiovasc Pharmacol. 2003;42(3):410-8.

133. Hille B. Ionic channels of excitable membranes. Sunderland, MA.: Sinauer; 1984.

134. Tammaro P, Smith AL, Crowley BL, Smirnov SV. Modulation of the voltage-dependent K^+ current by intracellular Mg^{2+} in rat aortic smooth muscle cells. Cardiovasc Res. 2005;65(2):387-96.

135. Labarca P, Coronado R, Miller C. Thermodynamic and kinetic studies of the gating behavior of a K^+-selective channel from the sarcoplasmic reticulum membrane. JGenPhysiol. 1980;76:397-24.

136. Venturi E, Mio K, Nishi M, Ogura T, Moriya T, Pitt SJ, et al. Mitsugumin 23 forms a massive bowl-shaped assembly and cation-conducting channel. Biochemistry (Mosc). 2011;50(13):2623-32. Epub 2011/03/09.

137. Zhou X, Lin P, Yamazaki D, Park KH, Komazaki S, Chen SRW, et al. TRIC Channels and Sarcoplasmic/Endoplasmic Reticulum Calcium Homeostasis. Circ Res. 2014;114(4):706-16.

138. Ding S, Sachs F. Evidence for non-independent gating of P_2X_2 receptors expressed in Xenopus oocytes. BMC Neurosci. 2002;3(1):17.

139. Picher M, Decrouy A, Rousseau E. Conducting and voltage-dependent behaviors of potassium ion channels reconstituted from diaphragm sarcoplasmic reticulum: Comparison with the cardiac isoform. Biochim Biophys Acta. 1996;1279:93-103.

140. Guo T, Nani A, Shonts S, Perryman M, Chen H, Shannon T, et al. Sarcoplasmic Reticulum K^+ (TRIC) Channel Does Not Carry Essential Countercurrent during Ca^{2+} Release. Biophys J.105(5):1151-60.

141. Dekker JP, Yellen G. Cooperative Gating between Single HCN Pacemaker Channels. The Journal of General Physiology. 2006;128(5):561-7.

142. Silberberg SD, Magleby KL. Voltage-induced slow activation and deactivation of mechanosensitive channels in Xenopus oocytes. J Physiol. 1997;505(Pt 3):551-69.

143. Gil Z, Magleby KL, Silberberg SD. Membrane-pipette interactions underlie delayed voltage activation of mechanosensitive channels in Xenopus oocytes. Biophys J. 1999;76(6):3118-27.

144. Bell J. Protons decrease the single channel conductance of the sarcoplasmic reticulum K^+ channel in neutral and negatively charged bilayers. Biophys J. 1985;48(2):349-53.

145. Takeuchi K, Takahashi H, Kawano S, Shimada I. Identification and characterization of the slowly exchanging pH-dependent conformational rearrangement in KcsA. J Biol Chem. 2007;282(20):15179-86.

146. Thompson AN, Posson DJ, Parsa PV, Nimigean CM. Molecular mechanism of pH sensing in KcsA potassium channels. Proc Natl Acad Sci U S A. 2008;105(19):6900-5.

147. Zúñiga L, Márquez V, González-Nilo FD, Chipot C, Cid LP, Sepúlveda FV, et al. Gating of a pH-Sensitive K2P Potassium Channel by an Electrostatic Effect of Basic Sensor Residues on the Selectivity Filter. PLoS ONE. 2011;6(1):e16141.

148. Hnízda A, Šantrůček J, Šanda M, Strohalm M, Kodíček M. Reactivity of histidine and lysine side-chains with diethylpyrocarbonate — A method to identify surface exposed residues in proteins. J Biochem Biophys Methods. 2008;70(6):1091-7.

149. Carter R, Drouin G. The Evolutionary Rates of Eukaryotic RNA Polymerases and of Their Transcription Factors Are Affected by the Level of Concerted Evolution of the Genes They Transcribe. Mol Biol Evol. 2009;26(11):2515-20.

150. Sawasaki T, Hasegawa Y, Morishita R, Seki M, Shinozaki K, Endo Y. Genome-scale, biochemical annotation method based on the wheat germ cell-free protein synthesis system. Phytochemistry. 2004;65(11):1549-55.

151. Lai FA, Erickson HP, Rousseau E, Liu QY, Meissner G. Purification and reconstitution of the Ca release channel from skeletal muscle. Nature. 1988;331:315-9.

152. Liu QY, Lai FA, Rousseau E, Jones RV, Meissner G. Multiple conductance states of the purified calcium release channel complex from skeletal sarcoplasmic reticulum. Biophys J. 1989;55:415-24.

153. Williams AJ, Tinker A, Lindsay ARG. Ion conduction and discrimination in the cardiac ryanodine receptor-channel. J Mol Cell Cardiol. 1992;24,SIV:S23.

154. Carter S, Pitt SJ, Colyer J, Sitsapesan R. Ca^{2+}-dependent phosphorylation of RyR2 can uncouple channel gating from direct cytosolic Ca^{2+} regulation. J Membr Biol. 2011;240(1):21-33. Epub 2011/01/29.

155. Carter S, Colyer J, Sitsapesan R. Maximum Phosphorylation of the Cardiac Ryanodine Receptor at Serine-2809 by Protein Kinase A Produces Unique Modifications to Channel Gating and Conductance Not Observed at Lower Levels of Phosphorylation. Circ Res. 2006;98:1506-13.

156. Sands ZA, Sansom MS. How does a voltage sensor interact with a lipid bilayer? Simulations of a potassium channel domain. Structure. 2007;15(2):235-44.

157. Mokrab Y, Sansom MSP. Interaction of Diverse Voltage Sensor Homologs with Lipid Bilayers Revealed by Self-Assembly Simulations. Biophys J. 2011;100(4):875-84.

158. Treves S, Larini F, Menegazzi P, Steinberg TH, Koval M, Vilsen B, et al. Alteration of intracellular Ca^{2+} transients in COS-7 cells transfected with the cDNA encoding skeletal-muscle ryanodine receptor carrying a mutation associated with malignant hyperthermia. Biochemical Journal. 1994;301:661-5.

159. Rossi D, Simeoni I, Micheli M, Bootman M, Lipp P, Allen PD, et al. RyR1 and RyR3 isoforms provide distinct intracellular Ca^{2+} signals in HEK 293 cells. J Cell Sci. 2002;115(Pt 12):2497-504.